9. Noble Metal Nanoparticles

Theruvakkattil S. Sreeprasad, Thalappil Pradeep

Noble metal nanoparticles in general and their gold and silver analogs in particular are attracting huge interest from the scientific community owing to their fabulous properties and diversity of applications. Mankind has been fascinated by gold and silver since prehistoric times, and applications of their nanoparticles have attracted attention for millennia, although understanding phenomena at the nanoscale is very recent. Nanoscale analogs are being explored due to their unusual functional attributes quite unlike the bulk. As research in this area moves forward, scientists are discovering novel application possibilities. Tunability of properties by varying size, shape, composition, or local environment presents them with unusual capabilities. By manipulating the chemical composition of the materials at the nanoscale, their electrical, chemical, optical, and other properties can be manipulated precisely. In this chapter, an overview of their history, diversity, strategies of synthesis, and optical properties is presented. The specialized methods employed for synthesis of anisotropic nanosystems are also discussed. Approaches to modulate the properties of these systems postsynthetically either through chemical reactions or by the formation of superstructures via assembly are also covered. Methodologies for fabricating functionalized nanomaterials are also discussed. Various proposed applications of such materials are pointed out. A glimpse into a newly emerging category of noble metal nanosystems called quantum clusters is also given.

R. Vajtai (Ed.), *Springer Handbook of Nanomaterials*, DOI 10.1007/978-3-642-20595-8_9,
© Springer-Verlag Berlin Heidelberg 2013

Noble metals are those metals which are resistant to corrosion and oxidation in moist air. The list contains ruthenium, rhodium, palladium, silver, osmium, iridium, platinum, and gold, in order of atomic number. Many of them are also precious as they are of poor abundance in the Earth's crust. Noble metal nanoparticles (NPs), especially of gold (Au) and silver (Ag), have been intensely explored by the scientific community owing to their spectacular properties. The *noble* nature of these NPs compared with other NPs, for example, transition metal NPs such as iron, nickel, or cobalt, as well as their lesser cytotoxicity make them attractive candidates for biological and environmental applications. A large proportion of the study of noble metal NPs is done with Au and Ag NPs. Therefore, Au and Ag NPs can be taken as examples to demonstrate the relevance and diversity of the area of NPs in general.

9.1 Historical Perspective of Gold and Silver NPs

From time immemorial, three metals, namely gold, silver, and copper, were used extensively by mankind. In fact, it is certain that these were the metals first used by human beings, since they are found in the native state. Even before the invention of gold coins in Egypt around 3400 BC, these metals were used as primitive money, hence the name *coinage metals*. The origin of the names *gold* and *silver* has long history. Different words are used in different languages to represent gold. Most of them simply mean *yellow* (*metal*), which comes from its appearance; for example, the Latin name *aurum* means yellow. This word is believed to have been coined from the ancient Roman word *aurora* or *ausosa*, meaning morning glow. The word is said to have its origin in the Sanskrit word *hari*, meaning *yellow*. In Slavic languages, gold was referred to as *золото* (*zlato*), having connections with the Indo-European word *sol* (sun). The present-day name *gold* is believed to have Germanic origin (*goud* in Dutch). The root of the word *gold* is believed to be from *gelwa*, meaning again yellow, which is connected to the Sanskrit word *jval*, meaning *to shine*. Hence, the word *gold* really means *the yellow shining metal*. Silver also has a rich history and it is also known by different names. It has different but very similar names in Dutch (*zilver*), German (*Silber*), and Anglo-Saxon (*seolfor*). In Greek, silver is known as *argyros* and in Latin as *argentums*, which in turn are closely related. The Italian (*argento*) and French (*argent*) names are also similar. However, the Spanish use a totally different name for silver: *plata*.

Gold and silver NPs have a rich history in science, where they were used for both esthetic and medicinal purposes [9.1]. A mixture of gold salts with molten glass was used by medieval artisans to produce tiny gold colloids having a rich ruby color, and their varieties were exploited for coloration of glass, ceramics, and pottery. The great alchemist and founder of modern medicine, Paracelsus (1493–1541), developed many highly successful treatments from metallic minerals, including gold. In China, people cook their rice with a gold coin in order to help replenish gold in their bodies. Colloidal gold has been incorporated into glasses and vases to give them color. The oldest of these is the fourth century AD Lycurgus cup made by the Romans (one piece is kept in the British Museum in London) (Fig. 9.1). The cup appears red in transmitted light (if a light source is held within the cup) and appears green in reflected light (if the light source is outside). Modern chemical analysis shows that the glass is not much different from that used today. However, it contains very small amounts of gold (about 40 ppm) and silver (about 300 ppm) in the form of mixed Au-Ag NPs of approximately 70 nm diameter. *Purple of Cassius*, a pink pigment commonly used in the seventeenth century, is also now known to be a combination of gold particles and tin dioxide.

The Egyptians used gold for mental, bodily, and spiritual purification [9.2], and the medicinal use of gold can be traced back to China in 2500 BC. In ancient times, Egyptians used gold in dentistry as well. In the Indian medical system called *Ayurveda*, gold is used in several preparations. One popular preparation is called *Saraswatharishtam*, prescribed for memory enhancement. Gold is also added in certain medicinal preparations for babies, in order to enhance their mental capability. All these preparations use finely ground gold along with herbs.

The curative power of gold is well documented from antiquity. Until the Middle Ages, gold was used as a cure for various diseases such as heart and venereal problems, dysentery, epilepsy, and tumors, as documented in a book written by Francisci Antonii in 1618 [9.1]. The use of *soluble gold* for diagnosis of syphilis is also documented [9.1]. In his book of 1676,

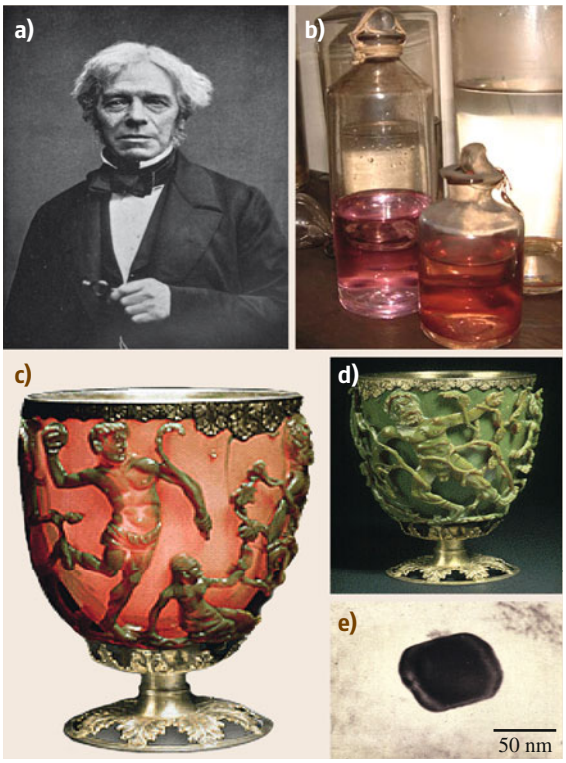

Fig. 9.1 **(a)** Michael Faraday (after [9.3]). **(b)** Faraday's gold preserved at the Royal Institution of Great Britain (after [9.4]). **(c,d)** The Lycurgus cup made from glass appears red in transmitted light and green in reflected light (after [9.5]). **(e)** The 70 nm Au-Ag alloy NPs found in the glass of the Lycurgus cup, as seen in a transmission electron micrograph (after [9.5])

Johann Kunckels mentioned a form of gold which he addressed as *drinkable gold that contains metallic gold in a neutral, slightly pink solution that exerts curative properties for several diseases* [9.1]. In this book, he even foresaw the possibility of the existence of gold in a form that is not visible to the human eye. It was also reported in 1718 by Hans Heinrich that the stability of *drinkable gold* can be increased by a special combination with boiled starch [9.1].

During this period, gold was used for coloring fabrics as well. In 1794 Mrs. Fuhlame reported that she had dyed silk with colloidal gold, which is documented in her book *An Essay on Combustion with a View to a New Art of Dying and Painting*. The different colors exhibited by different *drinkable gold preparations* were explained by Jeremias Benjamin Richters in 1818 [9.1]. He hypothesized that *pink or purple solutions contain gold in the finest degree of subdivision, whereas yellow solutions are found when these fine particles have aggregated* [9.1].

Systematic chemical synthesis of colloidal NPs was pioneered by Michael Faraday in 1857, when he observed the formation of a pure form of deep-red-colored colloidal gold by the reduction of an aqueous solution of chloroaurate ($AuCl_4^-$) using phosphorus in CS_2 in a two-phase system [9.6] (the word *colloid* itself was nonexistent at the time of Faraday's work). This is considered to have been a major step in the development of nanotechnology. He found that colloidal gold had special optical and electrical properties. In this study, he also investigated the optical properties of thin films prepared from dried colloidal solutions. He observed a reversible color change from bluish-purple to green upon pressurizing the films. In 1861, *Graham* coined the word *colloid* from the French word *colle* [9.7]. Following Faraday, a large number of experimental methods have been reported for synthesis of gold NPs (GNPs). This is dealt with in a separate section.

Similar to gold, silver has also been used for thousands of years in various fields. As explained earlier, it is Au-Ag NPs which are responsible for the color of the Lycurgus cup. However, the major use of silver historically was in the medicinal field and as an antimicrobial/disinfectant agent. Silver vessels were used to keep water and other liquids fresh by the Greeks [9.8]. The writings of *Herodotus*, the Greek philosopher and historian, date the use of silver to before the birth of Christ [9.9]. Silver urns were used for storage of wine to prevent spoilage in the Roman Empire. A similar use of silver is mentioned in ancient Egyptian writings also. Although most ancient civilizations were not fully aware of the antibacterial properties of silver, it was widely accepted that addition of silver to water would increase clarity, reduce odor, and improve the taste as well [9.10]. In ancient civilizations (especially the Greek and Roman Empires), Ag was used for various applications because of its well-known medical, preservative, and restorative powers [9.8, 10]. The germicidal power of silver was also known during these times [9.11]. Before modern germicides and antibiotics were discovered, the old civilizations understood that disease-causing pathogens would not survive in the presence of silver. Hence, silver was used in dishware, drinking vessels, and eating utensils [9.11]. Rich families of those periods stored and ate their food from silver vessels to prevent bacteria from growing. This is perhaps the reason for the phrase, *born with a silver spoon*, indicating traditional wealth. Vikings had knowledge

of the antialgal effects of silver. They applied strings of silver and copper below the water-line on the hull of their ships to prevent growth of algae and barnacles. The same methodology is used on modern ships as well [9.12].

Hippocrates, the father of modern medicine, promoted the use of silver by writing about the beneficial healing and antidisease properties of silver in his book [9.13]; he also recommended the use of finely powdered silver formulations for various ailment conditions such as ulcers and wounds [9.14]. Alexander the Great was advised by Aristotle to boil and store water in silver vessels to eradicate waterborne diseases [9.15]. Ancient Indian civilizations also had knowledge of the medicinal powers of silver. In Ayurvedic medicine, silver was used (in small amounts) as a tonic and rejuvenating agent for patients incapacitated by age or disease. Silver was also used as an eyedrop for ophthalmic problems [9.16], for various infections [9.17], and sometimes internally for diseases such as gonorrhea, epilepsy, common cold, and tropical sprue [9.11, 18]. Colloidal silver preparations (CSP) were used to treat or prevent gonorrhea and gonorrheal conjunctivitis [9.19]. It was also used in pure silver tongue scrapers as part of dental maintenance and for other oral disease conditions. Silver was widely used for the treatment of heart problems, blood purification, and other conditions, especially in the Middle East. Silver needles have been used for acupuncture by physicians of Chinese medicine over the years.

Silver also found applications in many other medical therapies and devices, including bone prostheses, ophthalmic surgery, treatments for venereal disease, and veterinary medicine [9.10]. The use of silver pins to fuse bones, silver wire to suture wounds, silver powder on ulcerations, and silver foil to protect wounds against infection was reported by ancient surgeons. In Egypt, skeletons where silver pins were used to repair bones via surgical procedures were found to support this [9.15]. As early as the late thirteenth century, it is reported that Lanfranc utilized silver tubes for introduction of food beyond fistula [9.20]. However, Paracelsus is credited to be the pioneer of the use of metals for medical applications. In his hermetic and alchemical writings, he associated silver with the development of brain activities. In 1617 Fabricius of Aquapendente, used a small silver tube to feed patients suffering from tetanus [9.21]. In 1884, Crede, a German obstetrician, popularized administering 1% silver nitrate solution to newborns to prevent ophthalmia neonatorum [9.22, 23]. It is also documented that he even used finely divided silver powder also for medical applications in 1896, which can be considered as the first proper medicinal use of colloidal silver [9.24, 25]. It is also documented that, during the mid-nineteenth century, silver wire structures were used to reduce septic complications [9.20]. Even in the late eighteenth century, William Halsted used silver wire for hernia operations and silver foil to prevent wound-related infections [9.26]. It is documented that, during the late 1800s and early 1900s, silver was frequently used as a medicine. During ancient times, it was understood that several metal salts and compounds have strong germicidal properties. However, it was also proved that silver alone has both strong germicidal properties and low or no toxicity to humans, which increased the use of silver-based preparations. The colloidal state is known to be the most effective form among other formulations because colloidal silver does not have the caustic properties of salts (such as $AgNO_3$) and it also demonstrated a high level of activity at very low concentrations [9.24]. Although it was established that colloidal silver was superior in this regard, the use of silver nitrate continued for a long time [9.24].

Scientific and methodological study of the antibacterial effects of metals against bacteria and lower life forms was carried out by Ravelin (1869) and in a more detailed manner by Karl Wilhelm von Nägeli, a Swiss botanist who discovered chromosomes (he named them *cytoblasts*) [9.13]. *Nägeli* reported that even low concentrations (9.2×10^{-9} and 5.5×10^{-6} M) of extremely fine silver, copper, as well as other metal hydrosols have toxic effects on *Spirogyra* and *Aspergillus niger* spores, respectively. The term *oligodynamic effect* was coined by him to explain this phenomenon [9.13]. In early twentieth century the germicidal properties of colloidal silver were popularized by Henry Crookes. He even stated in his book [9.11, 24] that:

> *silver in the colloidal state is highly germicidal, quite harmless to humans and absolutely nontoxic. Rather than in a chemical compound, the silver in the colloidal state may be applied in a much more concentrated form, with correspondingly better results. All virus, fungus, bacterium, streptococcus, staphylococcus, and other pathogenic organisms are killed in three or four minutes upon contact. There are no side effects whatsoever from the highest concentrations.*

Long before the introduction of antibiotics, colloidal silver had been known and used as a bactericide for at least 1200 years [9.15]. Also, it is reported that in

World War I, when antibiotics has not yet been discovered, silver formulations were used to prevent and treat infections, as antiseptics [9.27], as eyedrops to prevent conjunctivitis, etc. Silver compounds were used in dermatology to treat certain skin conditions, such as corns and warts [9.28]. In the early 1900s, silver foil dressings were used for wounds. These dressings were used extensively until just after World War II and were listed in the Physician's Desk Reference until 1955 [9.27]. However, with the introduction of antibiotics in the 1940s, the use of silver as an antimicrobial agent diminished. Still, silver holds an edge over antibiotics, since bacteria do not generally develop resistance to silver unless they have a very thick wall that does not absorb it [9.10].

In 1889, *Frens* and *Overbeek* [9.29] and *Lea* [9.30] accomplished a major landmark in chemistry by preparing silver colloid for the first time through reduction of silver nitrate using ferrous sulfate and consequent protection of colloidal particles with citrate ions. A huge interest in colloidal silver followed this, and a large number of researchers worked on the antibacterial properties of silver in the early twentieth century. Research work was initiated to use silver for water purification as well. In 1928, Katadyn of Switzerland developed a silver-impregnated ceramic gravity-fed water filter termed *Katadyn silver*. This was utilized as an antibacterial water filter in remote areas where clean water was not readily available by various agencies and militaries around the world [9.31]. In another instance, in a Federal Bureau of Investigation (FBI) declassified document 100-93211.247 dated December 21, 1949 and declassified on September 9, 2004, the use of silver for converting sea water to fresh water is quoted. This document illustrates that during World War II the US Navy used the services of Alexander Goetz, then Associate Professor of Physics at the California Institute of Technology, for generating drinking water. The document says *he helped perfect the process for converting sea water into fresh water by the use of silverized carbon pellets* [9.32]. Throughout the twentieth century, the popularity of silver salts continued to grow and several silver-based products were also commercialized (Katadyn, Argyrol, Movidyn, Tetrasil, Alagon, etc.) [9.33]. Silver in the supported form was also used to disinfect water. Zero-valent silver was immobilized on activated carbon in 1966 by *Renn* for disinfection of water [9.34]. Silver has also been used in space programs since the Apollo missions to sterilize recycled water. The same practice continues, and silver ion-exchange materials are still being used in space stations and space shuttles to recycle water.

As this historical perspective illustrates, gold and silver have been used for a large number of applications in several fields. However, until the last century, most applications were restricted to their medicinal value or antimicrobial activity. Catalysis is another area where silver found application in the early twentieth century. A few examples where noble metals were used as catalysts include silver-based catalysis of methanol to formaldehyde [9.35] and ethylene to ethylene oxide [9.36].

9.2 Diverse Nanostructures

The size and shape-dependent variation in properties of matter at the nanoscale is one of the most fascinating aspects of nanoscience. Hence, various parameters which directly affect the intrinsic properties of such materials [9.37–40] must be thoroughly understood. Nanomaterials can be broadly classified into four groups depending upon the confinement: (a) zero-dimensional (0-D), (b) one-dimensional (1-D), (c) two-dimensional (2-D), and (d) three-dimensional (3-D) nanomaterials. Similarly, based on geometry, they can be classified into isotropic and anisotropic NPs.

Gold and silver nanosystems are interesting because of the diversity that they exhibit. They are found in different shapes. Spherical NPs, quantum dots, and the newest excitement in the subnano regime called *quantum clusters* are all included in isotropic nanosystems, since they have no specific direction of growth and no difference in properties in different directions. They are generally considered to be 0-D nanosystems. However, materials of 1-D and 2-D NPs, and most 3-D nanosystems, which usually have a specific direction of growth and confinement of electronic motion along specific axes, are included in anisotropic NPs. Anisotropic NPs comprise a plethora of nanostructures such as nanorods (NRs) [9.41–43], nanowires (NWs) [9.44–46], nanotubes [9.47] (which can be collectively termed as 1-D); triangles [9.48, 49], plates and sheets [9.50, 51], ribbons or helices [9.52, 53], nanobelts [9.54, 55], nanocombs [9.56], nanorattles [9.57] etc. (belonging to 2-D), and pyramids [9.58, 59], stars [9.60, 61], flowers [9.62–65], multipods [9.66, 67], nanourchins [9.68, 69], tad-

poles [9.70, 71], nanocages [9.72, 73], nanorice [9.74, 75], nanocorn [9.76], nanoboxes [9.77, 78], nanocubes [9.79], triangular nanoframes [9.80], nanodumbbells [9.81], etc. (belonging to 3-D).

Noble metal nanosystems are attracting intense research efforts due to their diverse properties and exceptional tunability in properties. The size, surface, and shape dependence of the physical, optical, and electronic properties of anisotropic nanomaterials make them fascinating components in modern materials research. These properties of these systems are dealt with in a separate section. However, the most important step in utilizing these properties is to synthesize these materials with precise control over their size and shape. Specialized synthetic strategies are needed to make them with precise control over size and shape. These synthetic methods, at least in some cases, should have the flexibility to be expanded for possible commercial exploitation, if suitable applications are found. In this section, the most common methods used for synthesis of noble metal nanomaterials are briefly discussed.

9.2.1 Physical and Chemical Methods

General methods of synthesis can be broadly divided into two categories: physical and chemical routes. In the former approach, bulk material or constituents of the desired nanomaterial are taken and formulate systematic conditions by which nanomaterials are formed. Since the methods of synthesis start from bulk materials, they are called *top-down* approaches. This method includes the following techniques:

1. High-energy ball milling: Nanoscale powders are produced by milling bulk materials.
2. Wire explosion: Used to produce conducting nanomaterials such as metals. A sudden high current pulse is supplied resulting in an explosion.
3. Arc discharge: Alternating current (AC) or direct current (DC) arcs are used to evaporate materials.
4. Inert-gas condensation: Particle growth is achieved by condensing evaporated atoms in a matrix.
5. Laser ablation: High-energy laser to induce evaporation.
6. Ion sputtering: Impact using high energy ions (usually rare gases) cause evaporation.

By controlling the environment in which evaporation happens, we can control the composition of the resulting material. For example, if evaporation of metals occurs in the presence of oxygen, oxides can be produced. These methods can effectively manufacture large quantities of materials. However, these methods can only produce materials with large particle size variation.

In chemical methods, which will be described in more detail later, a range of techniques is used. In all of these, nanomaterials are made starting from atoms generated from ions, in solution, and are assembled to make nanomaterials. As the synthesis initiates from atoms, these methods are also called *bottom-up* approaches. Several methods come under this category:

1. Chemical reduction: Metal ions are reduced using reducing agents to create atoms.
2. Electrochemical synthesis: Electrochemical reduction or oxidation reactions.
3. Photochemical synthesis: Chemical processes assisted by light.
4. Sonochemical routes: Chemical reaction system done with the aid of ultrasound.
5. Solvothermal synthesis: Chemical processes in a closed system using solvents at lower temperatures.
6. Interfacial synthesis: An organic–aqueous interface is created to make nanomaterials.
7. Micelles and microemulsions: Producing nanomaterials by using oil-in-water or water-in-oil emulsions, or cavities of micelles or reverse micelles.
8. Biological methods: Biomolecules or living cells being used as synthetic reactors.
9. Thermolysis (e.g., pyrolysis, spray pyrolysis) strategies: Reactions in flames and thermal decomposition.
10. Arrested precipitation (mainly for semiconductors and oxides): Desired material is precipitated from an organometallic precursor solution.
11. Hybrid methods: More than one of the methods described above is used in a systematic combination to produce complex structures.
12. Solvated metal atom dispersion (SMAD): Nanoparticles are synthesized from metal vapors deposited in solid matrices of solvents, which upon heating evaporates to create the nanostructure. Synthesis of protected clusters is also possible if a capping agent is present in the solvent used.

Since NPs are made up of atoms, a two-phase colloidal system can be categorized in terms of the dispersed phase and the dispersion medium. The dispersed phase and the dispersion medium can be gas, liquid, or solid, except for the combination *gas in gas*. Therefore, NPs dispersed in an amorphous solid is a colloidal

system and consequently a *nanofluid*. A dispersion of nanomaterials in a fluid medium is generally referred to as *nanofluid*. Here, the fluid is a liquid at ordinary conditions of temperature and pressure, and hence supercritical fluids and gases as the dispersion phase can be omitted. However, it is worth mentioning that the synthesis of NPs in media such as solid matrices [9.82] and supercritical fluids [9.83] is a highly advanced research area. From the historical perspective discussed above, it is also important to remember that some of the early applications of NPs were in the form of particles embedded in glasses. Supercritical fluids are attracting a great deal of interest currently. Generally these fluids are mostly termed as colloids. The nanomaterials so prepared can be in the form of a fluid or solid. In many cases, applications of these materials will be in the form of solutions or dispersions, called nanofluids. They may also be used as powders, often referred to as nanomaterials. Particle films, pastes, emulsions, and many other forms may also be used.

9.2.2 General Issues of Concern

For devising a synthetic strategy, several factors of interest should be taken into account.

Thermal Stability

NPs being metastable systems will transform to stable materials having global energy minima in the free energy landscape. Thus, they will transform back to the bulk form at infinite time. Mostly, the time involved has no practical consequence. For example, *Faraday*'s colloids, made in 1856 (and reported in 1857), are still stable [9.6]. In other words, even though the bulk metal is more stable, the comparison is similar to that comparing the stability of graphite in comparison with diamond. Although diamond is metastable, it will not become graphite at normal conditions of temperature and pressure even in a millennium. Diamond-to-graphite transformation kinetics is very slow and hence insignificant under normal conditions. The situation of NPs in suitable media is analogous and is referred to as *kinetic stability*.

Dispersibility in Diverse Media

An NP usually has two entities: a core, which can be ceramic, metallic, or polymeric, and a thin shell, which also can be ionic, molecular, polymeric, ceramic, or metallic (Fig. 9.2). For this review, the core is always a noble metal which governs the properties of the NPs. The shell which is usually used to provide a protective

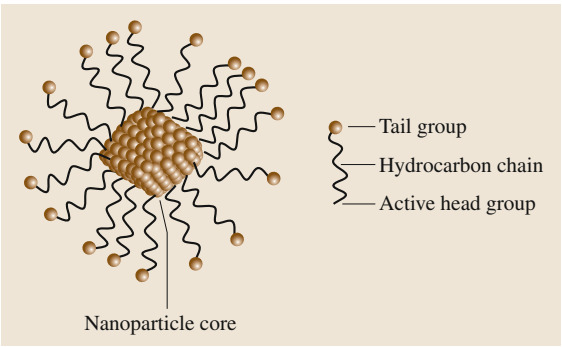

Fig. 9.2 Schematic of an NP with metallic core and organic shell. The shell may also be an extended solid such as SiO_2

layer is important in a number of applications such as those utilizing the luminescence of the particles. Moreover, the chemical nature of the shell determines the dispersibility of a NP.

Generally, the molecular shell will have a characteristic chemical affinity to the core due to its specific atoms or groups. In the case of a metal NP such as gold, for example, the metal can bind with a sulfur atom of the thiolate (−SR) group, a common protecting ligand, to form a protecting shell. Such a bond present on the surface of the NP is termed a protective monolayer or capping layer, and the NP is called a protected or capped NP. The chemical link so formed renders thermal stability to the system. The weaker the bond, the more easily it desorbs from the surface of the NP and hence the NP will be less stable. Therefore, the binding between metal and the active head group binding on the ligand is an important parameter influencing the thermal stability of the nanosystem.

It must be emphasized that the shell need not be a molecule. In specific examples, the shell will be an inherent part of the core, like in the case of silica NPs. Here, the surface will have a layer of hydroxyl groups and hence the particles can be easily suspended in water. A hydrocarbon monolayer in contrast can disperse the particle in organic solvents. In a similar manner, Au NPs can be made hydrophilic or hydrophobic. For reactive NPs such as copper, the surface is susceptible to oxidation and when the particles are exposed to air, a layer of oxide will form over the surface.

Depending upon the medium, the tail group can change its nature especially for end groups such as −COOH, $-NH_2$, −OH, etc. These groups will change form depending on the pH of the medium. In acidic media, the COOH group, for example (in the case

of a −COOH-terminated monolayer), will not become ionized and will remain as −COOH, whereas in alkaline media it will become transformed into −COO− by losing H^+. These surface charge modifications play an important role in applications such as drug delivery. Sometimes, the pH changes can affect the core as well.

Nanoparticles prepared by diverse routes and covered by a variety of activators and dispersants [9.84] such as laurate salts ($CH_3(CH_2)_{10}COO-X$), oleic acid ($CH_3(CH_2)_7CH=CH(CH_2)_7COOH$), etc., and dispersed in different media such as transformer oil, water, ethylene glycol, etc., were used for early conductivity studies [9.85]. Generally, surface functionalization is done so that the NP surface is friendly to the medium in which NPs are dispersed. The core–shell structure of an NP system is not limited to spherical particles. The very same general structure may be considered for anisotropic structures such as NRs, nanotubes, nanoshells, etc., where a chemically compatible shell is put around the nanosystem to make it go into the solution, biological environment, etc.

Chemical Compatibility and Ease of Surface Manipulation

When NPs of the same core size are considered for several applications, the above parameters attain significance. The synthetic conditions determine the size, shape, and properties of NPs as to be expected from a method producing metastable systems. Kinetically, an NP is always trapped in a local minimum of free energy, and the synthetic parameters are crucial in deciding the final product. Hence, to get uniformly the desired core size, it is essential to follow the same experimental conditions. Usually, this poses limitations in the adaptability of the system to various chemicals and conditions.

Post-synthetically, solvent compatibility can be modulated by changing the monolayer on the NPs. This process is often termed the ligand exchange, in which one monolayer of ligand molecules present on the NP surface are exchanged with another one in the medium. This exchange process usually results in equilibrium between the molecules in the adsorbed and free states. Repetition of this process a few times can complete the exchange process.

Chemical modification of the monolayer is similar to solution chemistry with simple molecules. Utilizing the chemistry of monolayers, suitable post-synthetic changes are made on NPs. For example, by employing functional group chemistry, a given monolayer can be polymerized or can be included into a polymeric matrix. This can be achieved via chemical, thermal, and photochemical processes. In specific cases, post-synthetic modification can result in the entrapment of nanosystems inside the cavity of a large molecule so that the nanosystem can be transferred into a suitable medium. The use of dendrimers and cyclodextrins are examples of this kind of chemistry.

Size Control and Monodispersity

An ideal synthetic strategy should produce particles of a given size distribution through a simple process. A narrow size distribution is always desired. Post-synthetic processes are utilized if a methodology fails to generate particles with a narrow size distribution. This involves selecting particles of interest or converting one system to another. However, post-synthetic methods also have their own advantages and disadvantages.

When a methodology produces of a variety of sizes in the as-synthesized particles, selection of a given size can be done by post-synthetic approaches. Several such processes exist. The first is size exclusion chromatography. Here, the mixture of NPs is passed through a size-selective stationary phase (e.g., a gel) having definite pore sizes. The applied eluent (solvent) elutes the material as a function of size. Agarose and Sephadex are the two common media used. The next method involves solvent-selective precipitation. In this method, by progressively changing the polarity of the medium from low to high, larger particles are forced to precipitate from the mixture. One disadvantage is that the stability of the material in different solvents may vary. However, by repeating this process, precise control over the size of the resulting NP is possible. Digestive ripening is also used to obtain monodisperse samples. In this method, the NP is digested with the protecting agent used during the synthesis at elevated temperatures. Smaller sized particles become consumed during the ripening process. Ostwald ripening or particle coarsening is a similar process where the as-prepared particles are allowed to age for a finite period during which large particles grow at the expense of smaller particles, narrowing the particle size distribution. This may be achieved along with temperature cycling.

9.3 Common Synthetic Routes for the Preparation of Noble Metal NPs

This section outlines the various strategies applied for synthesis of noble metal NPs. The discussion will mostly pertain to conventional spherical NPs. Synthesis of other shapes are extensions of some of these methods and a brief description of some of these will also be provided without going into the details.

9.3.1 Solution Phase Routes by Chemical Reduction

Metal atoms produced by the reduction of metal ions can upon aggregation produce NPs. The growth of these aggregates can be arrested at a desired stage by the use of protecting agents. A general reduction reaction can be represented as

$$M^{n+} + n\,e^- \rightarrow M^0\,. \tag{9.1}$$

Instead of supplying the electron directly, the oxidation of the reducing agent results in the production of electrons bringing about the reductions.

$$Red^{m-} \rightarrow Oxi^{(m-n)-} + n\,e^-\,, \tag{9.2}$$

where the reducing species (reducing agent) having a finite charge loses some specific amount of charge and becomes oxidized. It is important to mention that both the metal and the reductant may not contain any distinct charge and those mentioned are only nominal. The net reaction

$$M^{n+} + Red^{m-} \rightarrow M^0 + Oxi^{(m-n)-} \tag{9.3}$$

and its feasibility depends on the thermodynamics of the process, which in turn is governed by the electrochemical potentials of the corresponding half-cell reactions (standard reduction potentials). The sum of the reduction potentials (with their signs) of reactions (9.1) and (9.2) gives a net positive value, thus the process is thermodynamically feasible. This implies a net negative free energy change of $\Delta G = -nFE$, where ΔG is the free energy change of the reaction (9.3), n is the number of electrons involved, F is the Faraday constant, and E is the electrochemical potential of the reaction (9.3). Since the potential must be taken at the appropriate conditions, E must be considered not E^o. Thermodynamically feasible reactions have negative ΔG.

When the ions present in the solution are in complex form, the reduction potentials are not the only criteria that determine the feasibility of reduction. Ions present in complex form will have different potential compared to bare ions. For example, simple Au^{3+} (as in $[AuCl_4]^-$) can be reduced using mild reducing agents such as carboxylates or alcohols. However, in the presence of excess thiol this is not possible. The formation of metal thiolates makes the reduction of these complexes and reduction will only take place with strong reducing agents such as borohydride. In the presence of gold metal particles, reduction with mild reducing agents is possible, since the reduction occurs on the surface of gold. The reduction of gold ions by ascorbic acid in the presence of gold seeds during the preparation of GNRs (discussed below) is an example.

A molecule or ion itself can act both as the reducing agent and as the capping agent as in the case of citrate, amines, alcohols, thiols, etc. Reduction and the subsequent stabilization action of trisodium citrate for making Au NPs is the best example. In the recent past, several such examples have been reported where a variety of amines, alcohols, thiols, complex ions, etc., were used. Since alcohols are not good protecting agents, polyols containing a larger number of hydroxyl groups per molecule are used, which effectively chelate (multiply coordinate) the metal ions. A summary of the specific reduction processes employed is presented in Table 9.1.

Strong Reducing Agents

Reduction of metals with a large negative reduction potential is very difficult and demands careful control of the reaction conditions. The use of a strong reducing agent can minimize the solvent and other reactants present. For example, the presence of water should be avoided if the reagent is very strong to avoid the following reaction

$$2H_2O + 2e^- \rightarrow H_2 + 2OH^-\,. \tag{9.4}$$

The standard reduction potential of this reaction is -0.828 V. Solvated electrons are the most powerful reducing agents. They can be prepared in the laboratory by dissolving alkali metals in aprotic solvents like diethylether or tetrahydrofuran in the presence of excess complexing agents such as crown ether. The reaction can be depicted as

$$M + 2(15\text{-crown-5}) = M^+(15\text{-crown-5})_2\,e^-\,. \tag{9.5}$$

However, in the presence of smaller amounts of complexing agent, an alkalide (the alkali metal anion) will be formed [9.86],

$$2M + (15\text{-crown-5}) = M^+(15\text{-crown-5})M^-\,. \tag{9.6}$$

Since the thermal stability of the above reagents is less, the reactions should be done at lower tempera-

Table 9.1 Summary of various solution-phase reduction processes employed to make metal NPs

Method	Metal/reducing agent	Example	References
1. $NaBH_4$ route	Metal ion/BH_4^-	Au, Ag	[9.88, 89]
2. Amine route	Metal ion/APS[a], AES[b]	Ag	[9.90]
3. Polyol route	Metal ion/ethylene glycol	Ag, Pd	[9.91]
4. Citrate route	Metal ion/Cit^{3-}	Au, Ag	[9.6, 92]
5. Polyvinylpyrrolidone route	Metal ion/PVP[c]	Pd	[9.93]

[a] APS: 3-aminopropyltrimethoxysilane
[b] AES: 3-(2-aminoethylaminopropyl)trimethoxysilane
[c] PVP: polyvinylpyrrolidone

tures. This approach has been successfully employed for the synthesis of several nanocrystalline metals and alloys [9.87].

Trialkylborohydrides ($ABEt_3H$, A = Li, Na, K) are another class of strong reducing agents. Some methods utilizing aralkyl aluminum as the reducing agent have also been reported. A variety of transition metal NPs have been synthesized through the use of strong reducing agents [9.87, 94].

9.3.2 The Most Common Methods for Gold NPs

Two of the most common methods used for the synthesis of GNPs, namely the citrate route and the Brust method, are described in detail in this section. Other common methods for the preparation of metallic NPs are also briefly discussed.

The Citrate Route

This method also known as the Turkevich method [9.95], is the most used and easy-to-use method for the synthesis of colloidal gold NPs having a mean diameter of ≈ 15 nm. In this approach, the reducing agent used, sodium citrate (other reducing agents, such as amino acids, have also been employed successfully), also acts as the stabilizing agent, reducing Au^{3+} ions to atoms and subsequent aggregation results in the formations of NPs at elevated temperature. The NPs produced via this method are mostly monodisperse and spherical with a diameter of around 10–20 nm. The reduction in the amount of sodium citrate can increase the size of the resulting NPs. In 1973 *Frens* modified this method to obtain Au NPs of predetermined size by varying the trisodium citrate to gold ratio [9.96]. Transmission electron microscopy (TEM) images of the particles obtained by this method are shown in Fig. 9.3.

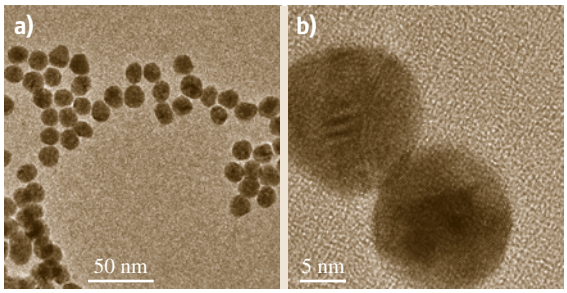

Fig. 9.3a,b TEM images of Au@citrate prepared by the citrate reduction method with average particle diameter of 15 nm. **(a)** low magnification and **(b)** higher magnification, lattice resolved image

Covering citrate-protected particles with various molecules or ceramics such as silica, can enable the NPs to be taken out of the solution, and redispersed. Since these particles can be good starting points for various investigations in biology and materials science, this approach is widely practiced [9.97].

Brust–Schiffrin Reduction

The Brust–Schiffrin method [9.98] involves phase transfer of $[AuCl_4]^-$ from the aqueous phase to the organic phase by a phase-transfer reagent, tetraoctyl ammonium bromide, and subsequent reduction of it at the interface by $NaBH_4$ in the presence of a thiol, resulting in the production of thiolate (RS−)-protected GNPs having a very small core diameter (range 1–5 nm). Variation of the Au/thiol ratio used in the synthesis can bring about a change in core dimension. A smaller Au/thiol ratio (a higher thiol concentration) produces smaller particles. The main advantage of the process is that the synthesized Au NPs can be repeatedly isolated and redispersed in organic solvents without aggregation or decomposition. The NPs can be taken out of the medium and dried, and the powder can be stored for a long time and can again be redispersed. Figure 9.4

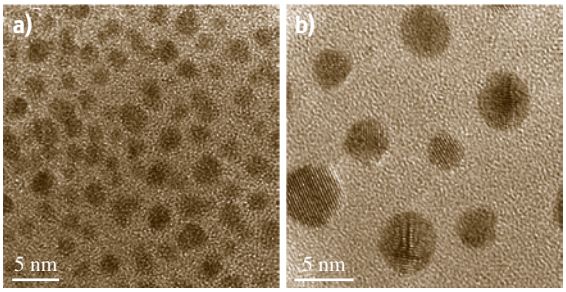

Fig. 9.4a,b Typical TEM images of Au@ODT NPs, prepared by the Brust method. Particles of 3 nm diameter are observed. **(a)** low magnification and **(b)** lattice resolved image showing single crystalline nature of most of the particles (courtesy T. Pradeep)

shows the representative image of NPs obtained in such a synthesis with a 1 : 2 Au : S ratio.

Another main advantage of this approach is that functionalization of the particles formed is feasible by using functionalized thiols during the synthesis. Alternately functionalization can be realized via exchange reaction (described earlier), where one kind of thiol or another ligand is exchanged with that on the NP surface. These NPs, often referred to as monolayer-protected clusters (MPCs), have been extensively reviewed [9.99, 100]. Several ways exist to conduct the synthesis. Using acid [9.101] for phase transfer helps to avoid phase-transfer catalyst impurity in the ensemble. The high degree of monodispersity can induce two-dimensionally-ordered lattices on a TEM grid. Digestive ripening (discussed earlier) [9.102] has been employed to reduce the particle size distribution in the Brust method. After this, the resulting particles with a narrow size distribution arrange to give 2-D and 3-D superstructures [9.103].

Similar superstructures can be produced with silver as well. Here, a variety of reducing agents can be used instead of $NaBH_4$ and the synthesis can be achieved without phase transfer. Several reports exist on the preparation of water-soluble NPs, synthesized using water-soluble thiols such as glutathione [9.104] and mercaptosuccinic acid (MSA) [9.105]. Reduction of the Au–thiolate complex in methanol by $NaBH_4$ in water is the important step during the reaction. The NP being insoluble in methanol precipitates out. This is washed repeatedly using methanol and is redispersed in water. Clusters formed using MSA are known to form well-arranged superlattices (SLs) [9.106]. Glutathione is known to produce a variety of molecular clusters starting from Au_8 to Au_{39}, which can be size separated using polyacrylamide gel electrophoresis (PAGE) [9.107].

Electrochemical Reduction

Chemical reduction is the most extensively investigated and employed method for making nanomaterials. However, various other methods have also been employed for the synthesis of special nanosystems. Electrochemical reduction where the metal is dissolved at the anode and the metal ion formed is reduced at the cathode is one of the prominent ones. To avoid the deposition of the resulting NP on the cathode (leading to electroplating), the process is done in the presence of a stabilizer. Nanoparticles of palladium (Pd) of 4.8 nm diameter have been synthesized by this approach by passing 0.1 mA cm^2 current at 1 V in a 0.1 M tetraoctylammonium bromide (TOAB) solution in 4 : 1 acetonitrile : tetrahydrofuran (THF) mixture [9.108]. The resultant NPs, which precipitated out could be redispersed in THF or toluene. A similar methodology can be used for other metals such as silver [9.109] and also for the preparation of GNRs [9.110].

Radiolytic Reduction

Reduction under various radiations such as visible, ultraviolet (UV), x-rays, and γ-rays is another method for synthesizing NPs. Metal salts solutions are irradiated in presence of stabilizing agents. In photoreduction with gamma rays, various species are generated in the medium, depending on the photon energy absorbed. In an aqueous solution, H_2, $H^\bullet$, H_2O_2, OH, and e^- are produced by radiolysis of water. Nitrous oxide in the medium scavenges the electrons generated, which further generates OH− and $OH^\bullet$ [9.111].

$$N_2O + e^-(aq) + H_2O \rightarrow N_2 + OH^- + OH^\bullet \,. \quad (9.7)$$

Alcohols react with the formed radical according to the following reaction

$$CH_3OH + OH^\bullet \rightarrow H_2O + {}^\bullet CH_2OH \quad (9.8)$$

$$CH_3OH + H^\bullet \rightarrow H_2 + {}^\bullet CH_2OH \,. \quad (9.9)$$

The $^\bullet CH_2OH$ radical in the reaction mixture acts as the reducing agent according to the equation

$$M^{n+} + n\,{}^\bullet CH_2OH \rightarrow M + nCH_2O + nH^+ \,. \quad (9.10)$$

The reduced metal and formaldehyde are the final products of the reaction and if the solvated electron itself can be used, the reduction is more powerful. Nanoparticles of Au [9.112], Ag [9.113], Cu [9.114], and Co [9.115] have been synthesized using this methodology. This approach is especially useful for the preparation of complex structures such as core–shell particles, where a metal core is coated with a shell of another metal. A few examples are Au@Ag [9.116], Au@Pt [9.117],

Pt@Au [9.117], Au@Pb [9.118], etc. Radiolysis is done on a mixture of a metal NP and aqueous metal ion using a ^{60}Co source. The surface of metal NPs become charged due to the transfer of electrons from the generated radicals. These NPs thus reduce the metal ions which are deposited on the surface of the NPs, resulting in core–shell geometry. Using a similar strategy, the size of Au NPs (repeated radiolysis) were modulated [9.119].

Thermal Decomposition of Organometallics

Decomposition of corresponding metal carbonyls by heating in an inert solvent at elevated temperature in the presence of a suitable stabilizing agent is another way to produce metal NPs. For example, heating $Co_2(CO)_8$ in decalin at 130–170 °C can produce Co NPs [9.120]. Usually, nitrogen-containing polymers are used as stabilizers in the reaction. It is known that the stabilizer will form metal cluster macromolecules, where these polymers act as a complexing agent. The particle size can be controlled by varying the functionality of the polymer. Various NPs made up of Fe [9.121], Ni, Cr, Mo, and W [9.122,123], as well as alloy NPs have been prepared by employing different polymers. It is to be noted that the ligands should be selected with care as they should be stable at high temperatures. A new metastable Co phase (ε-Co) obtained through the use of this method has also been reported [9.124]. The stabilizer used in the reaction was trioctylphosphine oxide (TOPO), and in the absence of TOPO this phase was not formed. The formations of various kinetically stabilized shapes have been studied in detail [9.125,126]. Mixtures of carbonyls and other organometallic reagents were used to prepare FePt [9.127] and CoPt [9.128] alloy and core–shell NPs. Thermal decomposition of metalloalkenes is also known to form NPs [9.129, 130]. Various ligands such as 1,5-cyclooctadiene (COD), 1,3,5-cyclooctatriene (COT), dibenzylidene, and cyclooctenyl ($C_8H_{13}-$) have been used in various syntheses. Some examples of NPs synthesized through the use of this approach include Co, Ni, Ru, Pd, and Pt NPs, Co and Ni NRs, and CoPt, CoRu, CoRh, and RuPt nanoalloys.

Microwave-Assisted Synthesis

A microwave-assisted approach has been abundantly employed for the synthesis of a variety of organic and inorganic materials. This method can be utilized for both synthesis and processing aspects [9.131]. This method is less time-consuming and heating is achieved from within. Usually the mixture to be irradiated is placed inside a domestic microwave oven working at a frequency of 2450 MHz and the mixture is stirred. In the case of metals, the metal ion and the reducing agent in a suitable solvent are placed in the oven and especially in the case of Au and Ag, this approach is known to form highly monodisperse NP samples (when compared to thermal reduction) [9.132]. Polyols are one of the most effective reductants for metal ions using microwave irradiation and the process is often referred to as the microwave polyol process [9.133]. Microwave irradiation of a mixture of poly(vinylpyrrolidone) (PVP), ethylene glycol, NaOH, and H_2PtCl_6 in water resulted in the formation of 2–4 nm Pt NPs [9.134]. A similar strategy was employed for the synthesis of 6 nm diameter Ni NPs as well [9.135]. This synthesis methodology can be automated by adapting it to continuous-flow reactors [9.136]. An excellent review on microwave-based methods for NP fabrications is available in the literature [9.137].

Sonolysis

Ultrasound (typically at 20 kHz) irradiation of the reaction mixture is utilized for the synthesis of NPs in this methodology. Here NP formation here is termed cavitation, which involves the implosion of cavities of very small dimensions on nanosecond timescales. This leads to the formation of local hot spots of very high temperature in the range of 5000 K. The reactant (a precursor species like organometallics) becomes trapped in this and is decomposed at this temperature. The products are instantaneously quenched by the surrounding solvent medium, resulting in the formation of amorphous NPs. A variety of transition metal NPs has been synthesized using this strategy [9.138]. Sonolysis of $Fe(CO)_5$ in decane in the presence of oleic acid resulted in the formation of 8 nm oleic acid protected Fe NPs [9.136]. Alloy NPs can be also prepared by this method. This approach has also been reviewed in [9.139].

9.3.3 Specialized Synthetic Strategies – Anisotropic NPs

As discussed earlier, specialized strategies are needed to synthesize nanosystems of various shapes with control over size and shape. Most of these are either an adaptation or modification of the methods described above. However, specific molecular interactions or templates can be used to facilitate shape-selective synthesis. It has been found that metal ions can be reduced via radiolytic [9.140] and photochemical [9.141,142] methods. NPs of various morphologies such as rods, triangles, hexagons, etc., can be generated using the photochem-

ical method [9.141, 142]. Template-assisted [9.143] methods have been used to make 1-D nanostructures with uniform size and controllable physical dimensions. The galvanic displacement reaction [9.144] is another method to make GNPs and their hybrid forms. This method has been widely used to produce nanostructures with different morphologies, including plates, cubic nanoboxes, cubic nanocages, nanorings, nanoboxes, single-walled nanotubes, and multi-walled nanoshells or nanotubes [9.145, 146]. Many other techniques such as sonolysis [9.147], microwave-assisted synthesis [9.148, 149], the hydrothermal method [9.150], etc., are being used to make gold and silver NPs. All the above-mentioned methods come under the category of bottom-up approaches for synthesizing NPs. The following section describes some of the important strategies employed in this regard. Only brief descriptions are given.

Seed-Mediated Growth Method

This is one of the most widely used strategies for the synthesis of anisotropic NPs of gold and silver. It is a modified version of Zsigmondy's *nuclear* method [9.151], which involves two steps. However, the seed-mediated method usually produces larger NPs of size 30–100 nm. This was first demonstrated by *Brown* and *Nathan* [9.152]. The first step involves the synthesis of *seed NPs* by reduction of metal salts in the presence of stabilizing agents. Usually this is carried out by using a strong reducing agent such as sodium borohydride ($NaBH_4$). It must be noted that the seed need not always be a metal NP. Subsequently in the second step growth of seed NPs into the desired shape happens in a growth solution containing excess metal ions, a surfactant or shaping agent, and a mild reducing agent. Here, the reduction of metal salts is facilitated on the surface of the seed NPs, and due to the presence of the surfactant molecules which form suitable templates, the growth happens to yield NPs of the desired morphology.

Murphy et al. devised various strategies based on the seed-mediated growth approach to make NPs of various shapes [9.153, 154]. Noble metal NPs of diverse structures such as rods [9.155], wires [9.156], triangles [9.157], stars [9.158], flowers [9.159, 160], etc., can be synthesized using this method. Tuning of size is possible by varying the amount of seed NPs added to the growth solution. This strategy has been successfully used for the synthesis of GNRs. The presence of external agents such as molecules or ions can influence the growth direction and can result in the formation of a different morphology. For example, the presence of iodide ion in the growth solution during the synthesis of GNRs, results in the formation of triangular nanoprisms [9.161]. Iodide ions adsorbs on gold seeds to suppress the growth along the Au(111) direction, leading to the formation of Au(111)-faced triangular nanoprisms. Even the counter-ion present on the surfactant used can influence the morphology. When the counter-anions on cetyltrimethylammonium bromide (CTAB) were replaced with chloride ions (instead of the original bromide), a rice-shaped NP formed instead of rods. The concentration of surfactant molecules is another parameter that affects the shape, since the shape of the micelles formed by the surfactant during the growth changes with the concentration. A method developed by *Mirkin* et al. [9.48] is an excellent example for this concentration dependence; they synthesized nanoprisms by changing the parameters in seed mediated synthesis. This involves a three-step growth process where gold seed NPs of ≈ 5 nm were added into the growth solution containing the capping agent CTAB, gold ions, a reducing agent (ascorbic acid), and NaOH, resulting in the formation of gold nanoprisms in very good yield. Synthesis required a saturated CTAB solution for good yield with uniform morphology.

Seedless Synthesis: Modification of Seed-Mediated Synthesis

Seedless synthesis is a slight modification of the above-mentioned method. In the above method, the purity of the seeds determines the quality of the resulting structures. Hence, *Pradeep* et al. [9.162] and *Jana* [9.163] separately showed that gold nanostructures can also be formed without the presence of the seeds. Jana illustrated that, without the use of seeds, near-monodisperse gold and silver NRs, spheroids, NWs, platelets, or cubes of 4–50 nm dimension and controllable aspect ratio (AR), can be prepared by introducing a mixture of strong and weak reducing agents into the micellar solution of a metal salt. Here, the strong reducing agent initiates nucleation and the weak reducing agent induces the NP growth [9.163]. This strategy was found to be extendable to semiconductors as well. *Pradeep* et al. studied the role of sodium borohydride ($NaBH_4$) in the formation of GNRs [9.162]. They found that addition of a calculated amount of $NaBH_4$ directly into the growth solution leads to the formation of uniform GNRs. They also studied the formation of GNRs with various seeds of metals of widely differing crystal structures, and understood that there is no variation in the properties of the GNRs formed. The role of $NaBH_4$ in the growth of

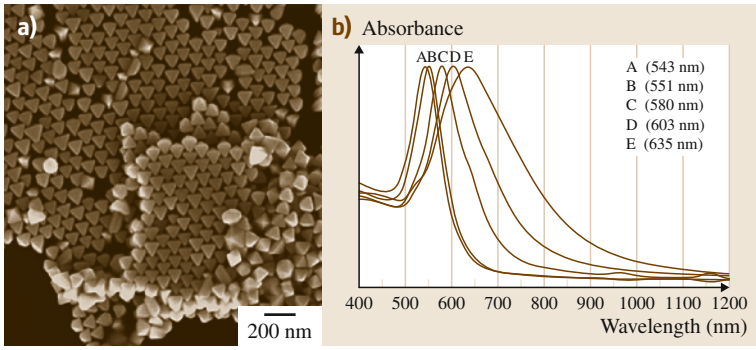

Fig. 9.5 **(a)** Scanning electron microscopy (SEM) image of octahedral gold nanocrystals. The imaged regions show extensive self-assembled structures. **(b)** UV/Vis absorption spectra of octahedral NPs of different sizes. Maximum absorbance of the spectra has been normalized (after [9.150])

GNRs, which was not well understood in earlier reports, was investigated in detail. They found that there is a relation between the longitudinal plasmon peak and the concentration of $NaBH_4$. To validate this further, the observed dependence was compared with the dependence of the residual concentration of $NaBH_4$ in the seed solution left over from the growth solution after the GNR growth. It was suggested that the addition of $NaBH_4$ leads to in situ formation of the seed particles, which enables the growth of GNRs.

Biological Synthesis

As an alternative to the use of chemicals, biological synthesis was advertised as a safe and ecofriendly approach for synthesis of GNPs. Here, the NPs are synthesized using organisms ranging from bacteria to fungi, various parts of plants, biological extracts, etc. One important advantage of this method is that it yields NPs capped with biological entities, which consequently have improved biocompatibility so that they can be used in many biomedical applications. Noble metal NPs of various shapes such as triangles, wires, spheres, plates, etc., have been synthesized via this method. A classical example is the high yield synthesis of thin, flat, single-crystalline gold nanotriangles (NTs) by the reduction of aqueous chloroaurate ions ($[AuCl_4]^-$) using an extract of the lemongrass plant (*Cymbopogon flexuosus*) [9.164]. The reducing agent in the reaction was found to be *aldoses* (reducing sugars) present in the lemongrass extract. Similar examples of Au NP preparation using extracts of tamarind leaf [9.165], *Cinnamomum zeylanicum* leaf [9.166], the unicellular green algae *Chlorella vulgaris* [9.167], *Rhodopseudomonas capsulata*, are available in the literature.

Hydro/Solvothermal Synthesis

This method involves the synthesis of NPs in a solvent at elevated temperatures under high pressure in an autoclave. The solvent (in most cases water) acts both as a catalyst and occasionally as a component of solid phases. Since several other solvents, including water, can be used for the synthesis this approach is generally termed solvothermal synthesis [9.168]. In hydrothermal processes, initial properties of water can be modified by introducing additives. This is a versatile strategy where various solvent systems such as polar solvents (e.g., aqueous solutions containing HF, or other acids or bases to modulate pH) or nonpolar solvents (e.g., pure, supercritical) are used for the dissolution–recrystallization process. Various nanostructures have been synthesized using this approach. The hydrothermal reaction of an aqueous solution of $HAuCl_4$, trisodium citrate and CTAB has been reported to produce octahedral gold nanocrystals (Fig. 9.5a) [9.150]. Gold octahedra with varying average sizes were synthesized by heating the different reactants at 110 °C for different time periods. Evidence of the formation of differently sized octahedra was seen in the absorption spectra where the surface plasmon resonance (SPR) band shifted from 543 to 635 nm (Fig. 9.5b). Structurally, the octahedra are bounded by specifically bound by (111) facets [9.150]. Technologically important nanostructures composed of Pd–Cd having high hydrogen storage capacity were also synthesized by this method. Here, various nanostructures with varying concentrations of Cd were grown directly on a solid substrate [9.169]. Because the method is low cost and environmentally friendly where substrates are at comparatively lower temperatures it is advantageous for the creation of diverse nanostructures on temperature-sensitive substrates.

Galvanic Replacement Reactions

This method (also called electroless plating) was introduced by *Brenner* and *Riddell* [9.170]. In this method the spontaneous reduction of metal ions to metallic particles and films occurs at equilibrium in the absence

of an external electric field. Due to its ease of operation, this method has attracted wide attention. It is highly versatile and can be used to make a wide range of metal/substrate combinations, including metal-on-metal, metal-on-semiconductor, and metal-on-insulator types. This is particularly important in the area of electronics with regard to metal deposition on a circuit board, for example. The process, *electroless deposition* includes three fundamentally different mechanisms such autocatalytic, substrate catalyzed, and galvanic displacement (immersion) processes in which the galvanic displacement reaction proceeds in an entirely different manner and the deposition is carried out in the absence of an external reducing agent.

Galvanic replacement reactions are single-step reactions that work depending on the differences in the standard electrode potentials of various elements, leading to deposition of the more noble element and dissolution of the less noble component. The electrons for the reduction are derived from the valance-band electrons of the substrate (Fig. 9.6a). Until the permeation of oxidized substrate ion into the solution though the metals film stops, the reaction will continue. The formation of a dielectric layer of oxidized substrate that hinders the electron transfer can also arrest the reaction. There are several advantages with this approach. For example, most synthetic processes use surfactants to obtain anisotropic nanostructures with smooth surfaces. However, attachment of surfactant molecules on the surface is not desirable for many applications. The presence of surfactants usually increases the electrical resistance, hence limits the use of these NPs as conductive components in electronics. Electroless deposition avoids the use of surfactant molecules whereby the NPs can be directly utilized without loss of electrical properties.

Preparation of pristine Ag nanoplates on semiconducting GaAs wafers (Fig. 9.6b) has been reported [9.171] through a galvanic reaction between an aqueous solution of $AgNO_3$ and GaAs (9.11). A droplet of aqueous solution of $AgNO_3$ was added on a GaAs wafer (treated with aqueous hydrofluoric acid solution) to grow silver micro/nanostructures via the galvanic reaction

$$12AgNO_3 + 2GaAs + 6H_2O \rightarrow 12Ag + Ga_2O_3 + As_2O_3 + 12HNO_3 . \quad (9.11)$$

Controlling the concentration of $AgNO_3$ resulted in the tuning of the morphological parameters of the Ag nanoplates. At high concentration of $AgNO_3$, thicker Ag nanoplates were obtained. Electrons for the reduction are provided by the germanium–germanium bonds leading to the formation of Ag(s) from Ag^+ and Ga(s) becomes oxidized during the process via a redox reaction.

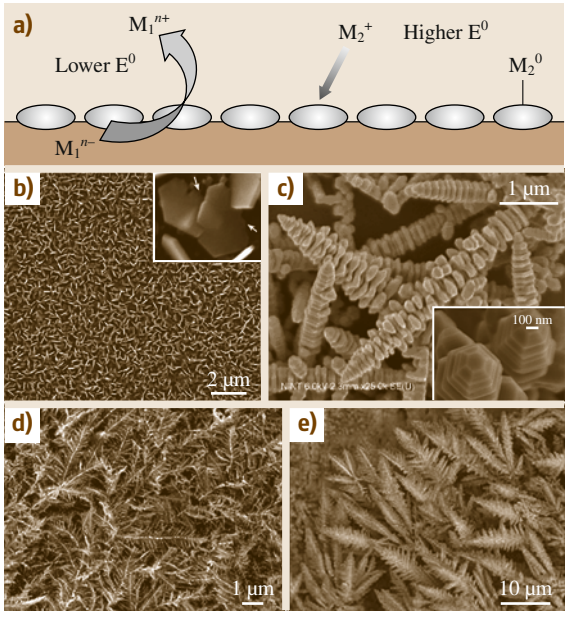

Fig. 9.6 **(a)** Schematic of galvanic displacement reaction. **(b)** SEM image of Ag nanoplates formed on the surface of n-type (110) GaAs wafer. **(c)** Silver nanoinukshuks prepared by immersing n-type Ge(100) in aqueous $AgNO_3$ solution. *Inset* shows a close-up view of facets on the tips of silver metallic nanoinukshuks. SEM images of silver **(d)** and gold **(e)** dendrites formed on zinc plates. (**(b,e)** after [9.171–174])

An unusual variety of Ag nanostructures called nanoinukshuks (Fig. 9.6c), was synthesized by immersing n-type Ge(100) in aqueous $AgNO_3$ solution [9.172]. When the Ag^+ ion concentration reached 1 mM, nanoinukshuks were obtained at room temperature on flat or rough, oxidized germanium surfaces. The nanoinukshuks were composed of 300 nm-diameter stacked hexagons, which can grow perpendicular to the (111) planes of the silver hexagons. Synthesis was carried out with different Ag salts, such as $AgClO_4$ and $Ag(CH_3CO_2)$. With $AgSO_4$, flat dendritic structures formed. A close-up view of the tip of the nanoinukshuks is given in Fig. 9.6c. Gold dendritic nanostructures can also be synthesized using $HAuCl_4$, H_2O, and zinc through this methodology. Dendritic structures formed by immersing a Zn plate in a container with $HAuCl_4$ solution at room temperature and ambient pressure (Fig. 9.6e) [9.173].

The same strategy can be employed for preparing Ag dendritic nanostructures as well (Fig. 9.6d) [9.174].

Hollow metal nanostructures can also be produced in this way. The structure can be made hollow or have porous walls. This change can be brought about by using a less active metal salt precursor. A wide variety of gold-based hollow nanostructures of different morphologies, including cubic nanoboxes, cubic nanocages, nanorings, nanoboxes, single-walled nanotubes, and multi-walled nanoshells or nanotubes [9.175–177] have been synthesized using this strategy. More details of these reactions is given in the discussion of the reactivity of these anisotropic systems in Sect. 9.5.1.

Photochemical Synthesis

As described in previously, the reduction of metal salt precursors can also be carried out by radiolytic and photochemical methods. Here, there is no eternal reducing agent involved and radiation becomes absorbed regardless of the light-absorbing solutes and products. Also, the number of reducing equivalents generated by radiation being known exactly, the rate of the reduction reaction can be accurately determined. This methodology does not require any specific and expensive instrument. All this makes this approach highly attractive for synthesis on metallic nanostructures.

Rod-shaped NPs were the first anisotropic NPs to be synthesized by reduction of metal salt by UV irradiation [9.178]. Here, a rod-like micelle formed by hexadecyltrimethylammonium chloride becomes embedded by $AuCl_4$, and the reduction of these ions to Au^0 is achieved through photochemical irradiation ($\lambda_{max} = 253.7\,nm$). However, synthesizing uniform, AR-controlled rods is difficult because an increase in length of NRs will always result in an increase in spherical NP impurities. *Yang* et al. [9.179] reported an improved methodology which produces NRs with well-controlled AR. This method was similar to the electrochemical method described earlier and the reaction mixture had the surfactant CTAB and tetradodecylammonium bromide and the precursor $HAuCl_4 \cdot 3H_2O$. The reduction was achieved by photoirradiation for 30 h ($\lambda_{max} = 254\,nm$, $I = 420\,\mu W/cm^2$). During the process, acetone and cyclohexane were used for loosening the micellar structure. However, additionally, silver nitrate was used in this process to control the AR of the NRs. Also, an increase in the silver ion concentration led to a decrease in the AR of the NRs and when the silver ion was absent a large number of spherical particles formed.

Photo-induced methods have found useful the preparation of large quantities of silver nanoprisms in high yield in the form of a colloidal suspension as well [9.180]. The as-synthesized colloids had distinctive optical properties that directly relate to the shape. The first step of the reaction includes the synthesis of spherical silver particles from an aqueous solution of $AgNO_3$ using $NaBH_4$ in the presence of trisodium citrate. A stabilizing agent, bis(*p*-sulfonatophenyl) phenylphosphine dihydrate dipotassium (BSPP) was introduced dropwise into the reaction mixture. The mixture was irradiated with a conventional fluorescent light. The edge length of the nanoprisms in this process was found to be tunable to 30–120 nm range [9.181]. Using dual beam illumination of the NPs, the growth can be controlled, and the process is believed to be driven by surface plasmon excitations. Depending on the wavelength of the illumination, the plasmon excitations lead to the fusion of nanoprisms. The bimodal growth process observed occurs through an edge-selective particle fusion mechanism, with four type 1 nanoprisms coming together in stepwise manner to form a type 2 nanoprism (Fig. 9.7). GNPs of various morphologies such as triangular or hexagonal shapes can be generated using the photoreduction method by mixing Au^{3+} with sodium oxalate and a reducing agent, in aqueous solution under illumination by a mercury lamp for more than 10 min. The size of the GNPs varies from 25 to 200 nm, mainly depending on the duration of light illumination and the concentration of sodium oxalate [9.182].

Electrochemical Synthesis

This is a modification of the process described above, developed to create anisotropy in the formed structures. The electrochemical method was first proposed by *Reetz* and *Helbig* in 1994 [9.108]. They demonstrated that by adjusting current density, highly size-selective NPs can be synthesized via an electrochemical reduction method. Diverse nanostructures such as cubes, rods, triangles, plates, etc., have been synthesized by this method [9.183]. It has many advantages over other methods since it has a lower processing temperature and low cost, requires modest equipment, and offers good control of size, shape, and morphology. The experimental setup (Fig. 9.8) for the electrolytic process includes a two-electrode setup for 50–250 ml electrolyte solutions in which the sacrificial anode consists of the bulk metal to be transformed into a metal colloid. In a two-electrode setup, GNRs were recently synthesized in high yield [9.184]. In this process, gold and platinum

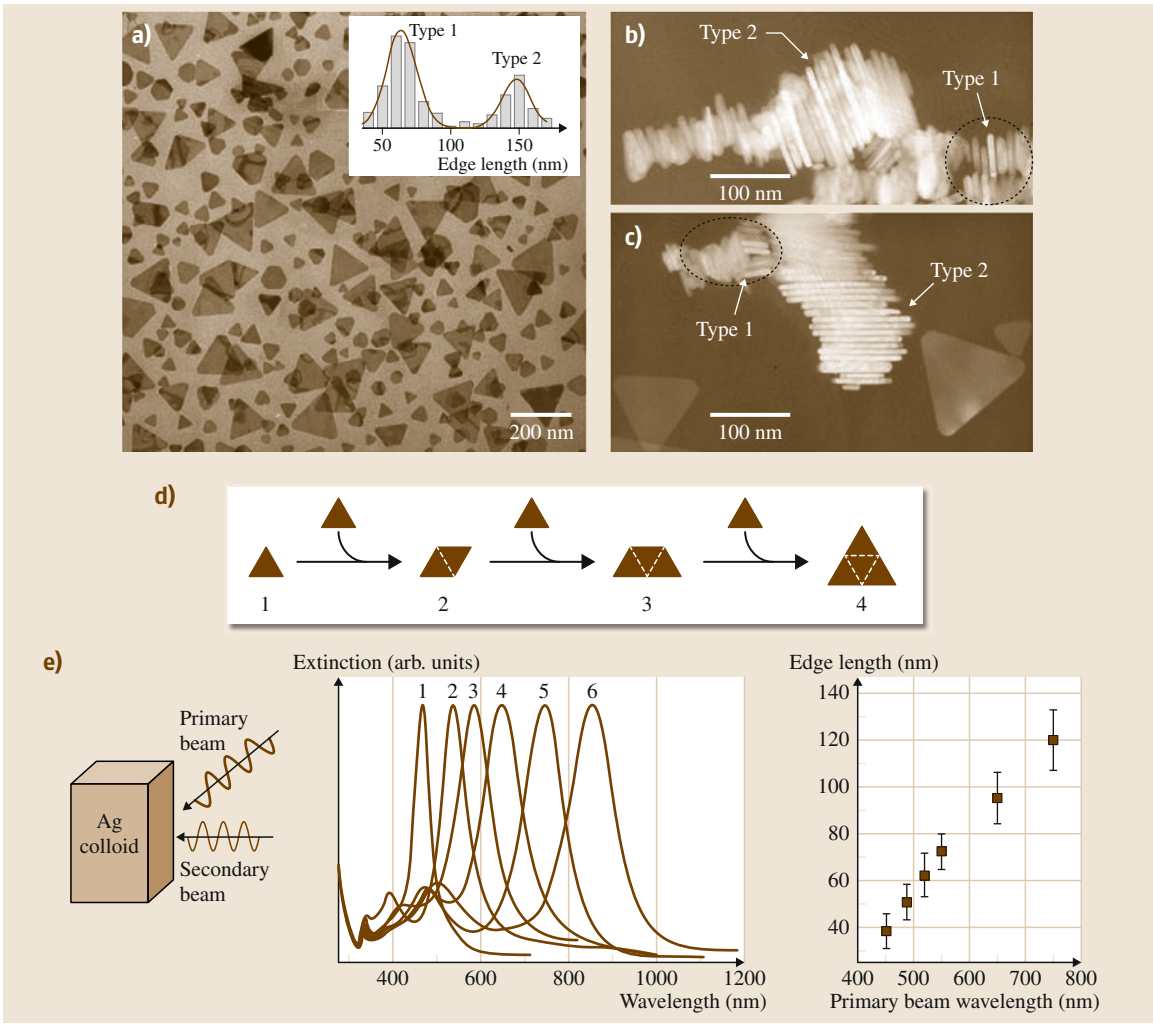

Fig. 9.7a–e Bimodal growth of Ag nanoprisms. **(a)** TEM image of a sample of Ag nanoprisms formed using single-beam excitation; *inset* histograms used to characterize the size distribution as bimodal. **(b,c)** SEM images of nanoprism stacks showing that nanoprisms have nearly identical thicknesses. **(d)** Schematic diagram of the proposed light-induced fusion growth of Ag nanoprisms. **(e)** *Left*: schematic diagram of dual-beam excitation. *Middle*: the optical spectra (normalized) for six different-size nanoprisms prepared by varying the primary excitation wavelength. *Right*: the edge lengths as a function of the primary excitation wavelength (after [9.181])

plates were used as the anode and cathode, respectively. The electrolytic solution had a mixture of a cationic surfactant or stabilizing agent and a cosurfactant, and the electrodes were immersed in it. During electrolysis, bulk gold metal is oxidized at the anode, and the metal cations at the interfacial region of the cathodic surface are reduced, and in the presence of the capping agent, form GNRs. GNRs with various ARs can be synthesized by this method.

Highly monodisperse gold nanocubes can be synthesized by an electrochemical method, using a surfactant solution and acetone [9.185]. Here also a two-electrode setup with gold and platinum plates as the anode and cathode is used. These electrodes are placed vertically face-to-face inside the cell, separated by Teflon spacers in an aqueous solution of CTAB and a much more hydrophobic cationic cosurfactant, tetradecyltrimethylammonium bromide. Acetone was

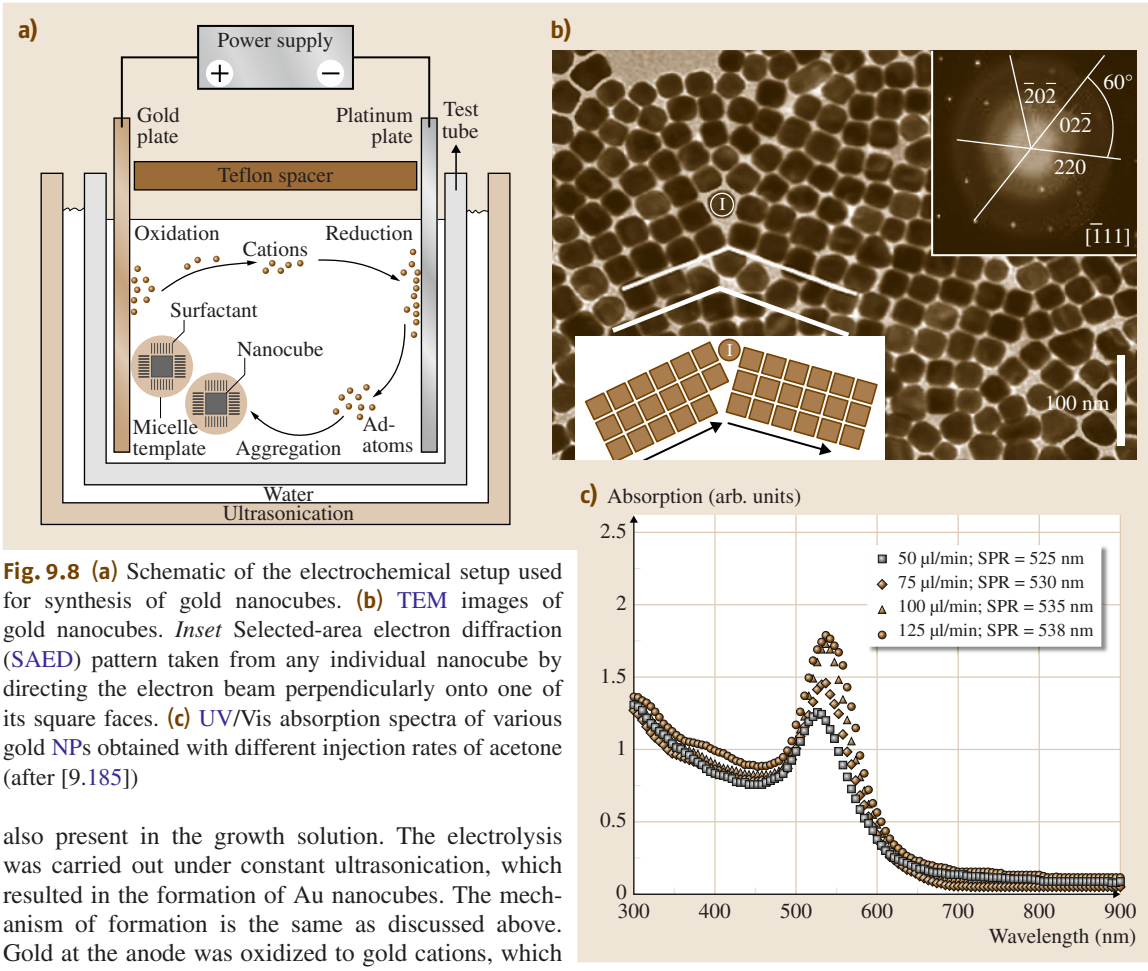

Fig. 9.8 **(a)** Schematic of the electrochemical setup used for synthesis of gold nanocubes. **(b)** TEM images of gold nanocubes. *Inset* Selected-area electron diffraction (SAED) pattern taken from any individual nanocube by directing the electron beam perpendicularly onto one of its square faces. **(c)** UV/Vis absorption spectra of various gold NPs obtained with different injection rates of acetone (after [9.185])

also present in the growth solution. The electrolysis was carried out under constant ultrasonication, which resulted in the formation of Au nanocubes. The mechanism of formation is the same as discussed above. Gold at the anode was oxidized to gold cations, which then migrated to the cathode, where reduction occurred with the formation of gold adatoms (Fig. 9.8a). These adatoms were trapped by the surfactant to form nanocubes (Fig. 9.8b). The surfactant, which doubles as the electrolyte and the stabilizer, also forms a micelle template to control the size and shape of the NPs. The rate of injection of acetone was found to influence the shape of the NP formed. Spherical NPs were formed at lower concentrations of acetone. As the amount of acetone increased a red-shift was observed in the UV/Vis absorption spectra (Fig. 9.8c) of gold nanostructures.

Synthesis of GNRs has also been carried out via an electrochemical method using a simple two-electrode cell [9.186]. In this process, a gold metal plate acts as the anode and a platinum plate as the cathode. A cationic surfactant, CTAB, and a rod-inducing cosurfactant were used as the electrolyte. Using a standard three-electrode cell with a potentiostat, a platinum foil counter electrode, and a saturated calomel electrode, platinum nanothorns were synthesized electrochemically at room temperature [9.187]. Here, platinum nanothorns (Fig. 9.9) were electrodeposited on glassy carbon substrate in 2 mM K_2PtCl_6 and 0.5 M H_2SO_4 solution by applying a square wave potential between −0.20 and 0.80 V at 10 Hz for 20 min.

Using a templateless, surfactantless, electrochemical method, single-crystalline Ag dendrites were fabricated on a Ni/Cu substrate by [9.188, 189]. The applied potential controlled the morphology and geometry of the Ag particles. The morphology changed from Ag polyhedrons to Ag dendrites, which preferentially grow along the directions in a fractal mode, upon decreasing the potential from −0.4 to −2.0 V [9.190].

Template Mediated Synthesis

Recently, the template-mediated synthesis of 1-D nanostructures with uniform size and controllable physical dimensions has attracted a great deal of interest. The advantages of this method over other methods are: ease of fabrication, adaptability to various compositions of materials, low cost, and high throughput [9.190, 192, 193].

Usually, nanoporous polycarbonate or alumina are used as the template. Metals from which NP is to be synthesized (Au, Ag etc.) are electrochemically deposited in the template structure. First, a small amount of Ag or Cu is sputtered on the template to make a conductive film for electrodeposition. Subsequently, metal is electrochemically deposited onto the conductive template. The template is removed by selective dissolution in the presence of a polymeric stabilizer (e.g., PVP), and the nanostructures are dispersed either in water or an organic medium by means of sonication. Template-mediated synthesis of GNRs is shown in Fig. 9.10. By controlling the pore size of the template, the diameters of synthesized structures can be controlled [9.194]. Similarly, by regulating the amount of metal deposited, the length of the structures can be controlled [9.191].

Other Methods

Gold and silver NPs can also be synthesized via top-down approaches. Nanosphere lithography [9.195] is a powerful tool to produce NP arrays with controlled shape, size, and interparticle spacing. This approach uses self-assembled polystyrene nanospheres as templates. Diverse nanostructures such as disks, chains, triangles, rings, etc., have been fabricated using this method [9.195]. The atomic force microscopy (AFM)-based soft lithographic technique called dip-pen nanolithography [9.196] can produce layers on Au and in combination with wet chemical etching is able to fabricate various nanostructures such as dots, lines, rings, triangles, etc., with nanoscale precision. GNPs have been generated using other top-down strategies such as photolithography, electron beam lithography, etc. [9.197]. However, these processes follow expensive synthetic pathways and are industrially nonscalable. Hence, bottom-up approaches are far more popular for synthesis of NPs.

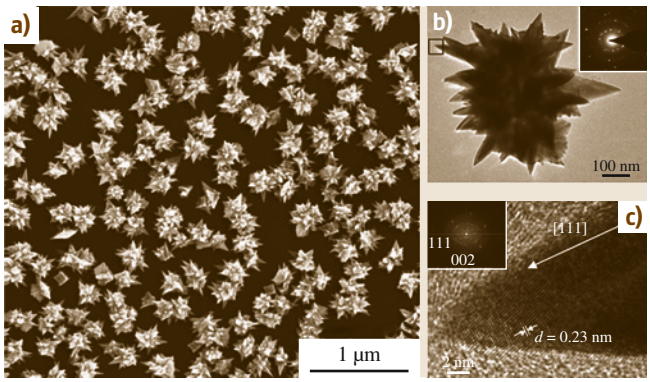

Fig. 9.9 (a) Large area SEM image of platinum nanothorns. TEM images of the platinum nanothorn (b,c) with the corresponding selected area diffraction (SAED) pattern and fast Fourier transform (FFT) in the *insets* (after [9.187])

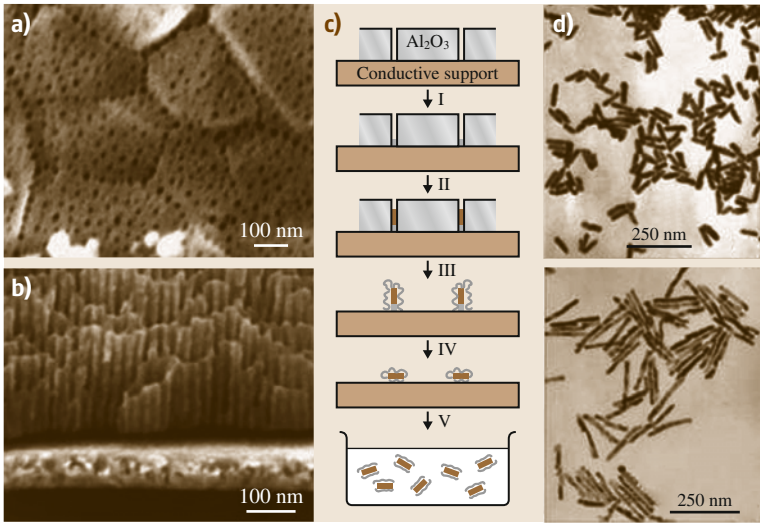

Fig. 9.10 (a,b) Field-emission SEM (FESEM) images of an alumina membrane. (c) Schematic representation of the successive stages during formation of GNRs via the template method. (d) TEM micrographs of GNRs obtained by the template method (after [9.191])

9.4 Properties of Noble Metal Nanoparticles

Noble metal NPs have received a great deal of attention for many applications due to their extraordinary properties. The spatial confinement of electrons controls the physical and chemical properties of NPs. GNPs are classic systems though which the properties of noble metal NPs can be understood. Properties of GNPs can be varied by altering the size, shape, degree of aggregation, and local environment. They exhibit characteristic colors and unusual optical properties that strongly depend on their size, shape, and the dielectric constant of the surrounding medium. The characteristic wine-red color of spherical GNPs stems from a phenomenon termed localized surface plasmon resonance (LSPR) [9.199, 200]. When electromagnetic radiation of an appropriate wavelength interacts with a metallic nanostructure, the conduction electrons near a metal–dielectric interface will be excited and undergo a collective oscillation relative to the lattice of positive nuclei with the frequency of the incoming light resulting in LSPR (Fig. 9.11). A momentary electric field is generated on the surface of the NP as a result of the oscillations. This can extend into the dielectric over nanometer length scale and hence can give rise to an enhancement of the incident field by several orders of magnitude, resulting in novel properties of NPs. One of the first investigations of the interaction between NPs and light was done by Faraday in the nineteenth century on his gold colloid.

A complete theory to understand plasmon resonance absorption and color of metal colloids in solution was developed by *Gustav Mie* in 1908 when he studied the theory behind the scattering and absorption of electromagnetic radiation by a sphere [9.201]. In its original form, Mie's theory was able to explain the spectral properties of spherical particles. The theory showed that the total extinction cross-section comprises contributions from the scattering and absorption cross-sections, i. e., the extinction cross-section, $\sigma_{\text{ext}} = \sigma_{\text{abs}} + \sigma_{\text{scat}}$ (absorption cross-section + scattering cross-section). When the size of the NP is smaller than the wavelength of light ($\lambda \gg 2r$, where r is the radius of the NPs), Mie's theory reduces to [9.202–204]

$$\sigma_{\text{ext}}(\omega) = 9\frac{\omega}{c}\varepsilon_{\text{m}}^{3/2} V \frac{\varepsilon_2(\omega)}{[\varepsilon_1(\omega)+2\varepsilon_{\text{m}}]^2+\varepsilon_2(\omega)^2}\,, \tag{9.12}$$

where V is the volume of the particle [$(4\pi/3)r^3$], ω is the angular frequency of the exciting light, c is the velocity of light, ε_{m} is the dielectric function of the surrounding medium of the NPs, and ε_1 and ε_2 are the real and imaginary parts of the dielectric function of the NPs, respectively, i. e., $\varepsilon(\omega) = \varepsilon_1(\omega) + \text{i}\varepsilon_2(\omega)$. The condition for resonance is $\varepsilon_1(\omega) = -2\varepsilon m$, if ε_2 is small and is a weak function of ω. For Au NPs in air, this can happen around $\lambda = 520$ nm [9.205].

In order to explain the properties of other shapes (oblate and prolate spheroidal particles), in 1912 *Gans* remodeled Mie's theory and predicted two well-defined, distinct surface plasmon modes for these metal NPs [9.206]. It is important to note that the details of the LSPR response of metal nanostructures depend on

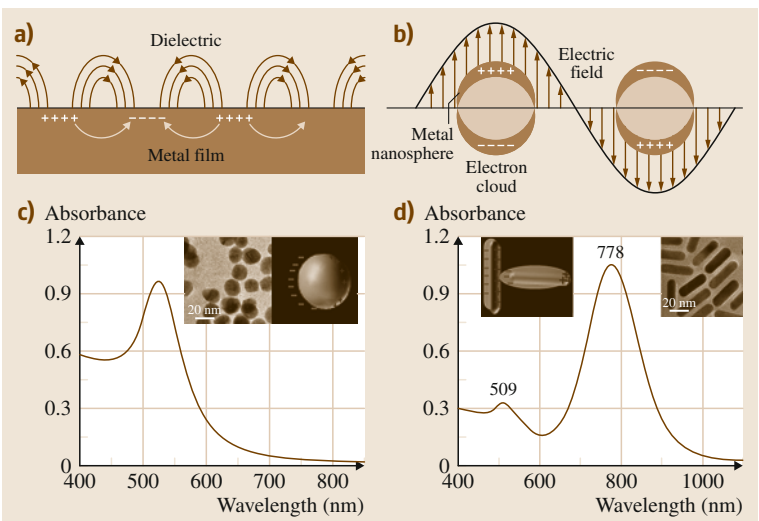

Fig. 9.11 **(a)** Propagation of surface plasmons on a metal surface. **(b)** Localized surface plasmons in metal nanospheres (after [9.198]). **(c,d)** Absorption spectra of gold nanospheres and NR, respectively. Corresponding TEM images of spherical and rod-shaped GNPs are shown in the *inset*

different variables such as size, shape, environment, dielectric function, effective mass, and electron density. GNRs are classical examples to demonstrate the shape-dependent LSPR properties. Unlike nanospheres (which have only one well-defined resonance peak), GNRs in their optical spectrum exhibit two bands in the visible/near-infrared (NIR) regions (Fig. 9.11). According to theoretical calculations, the first band near 530 nm (called transverse LSPR) is due to electron oscillation perpendicular to the long axis of the NR and the other one, appearing at a longer wavelength (called longitudinal LSPR mod) is assigned to an oscillation parallel to the long axis (Fig. 9.11). For anisotropic NPs like disks and triangular prisms, LSPRs are split into distinctive dipole and quadrupole plasmon modes [9.207].

The advent of new spectroscopic techniques has resulted in the capability to use surface plasmons for imaging single NPs. *Sonnichsen* et al. have developed a fast and flexible technique using total internal reflection spectroscopy to measure the optical scattering spectra of single metallic NPs [9.208]. By embedding noble metal NPs in an electrooptical material such as a liquid crystal, which induces a spectral shift of the particle's plasmon resonance by applying an electric field, the same group later showed that single NP scattering can be measured [9.209]. Using a similar method based on single-particle scattering, biomolecular recognition has also been proposed [9.210]. By this technique, GNRs were used as nonbleaching plasmon-based orientation sensors recently [9.211]. The polarized light scattering from individual GNRs was monitored in a dark-field microscope, and through observation of the rotational diffusion of gold rods attached to a glass surface, it was demonstrated that their orientation as a function of time can be determined [9.211]. This property was used for probing protein–membrane interaction as well [9.212]. Using plasmon spectroscopy, *Mulvaney* et al. recently showed that chemical reactions on single molecules can be probed [9.213]. They investigated the kinetics of atomic deposition onto a single gold nanocrystal. The electron injection and extraction during a redox reaction involving the oxidation of ascorbic acid on a gold nanocrystal surface was also monitored. Hence, for the first time it was established that direct measurement of the rates of redox catalysis on single nanocrystals is possible. It was established that 2-D array detectors would enable the acquisition of spectra from pixels along a line in the field of view and using push-broom scanning technology, 2-D hyperspectral images can be obtained [9.214]. *Becker* et al. selectively measured spectra of up to 20 plasmonic NPs per exposure using an electronically addressable mask [9.215]. However, a condition such that only a few NPs are present within the field of view was maintained throughout the measurements. Here for the first time they used single-particle spectroscopy to monitor the growth process of GNPs [9.215]. Using a grating monochromator to select a 2 nm spectral band for dark-field illumination, *Liu* et al. were able to achieve high-resolution imaging [9.216]. Au plasmonic NPs (PNPs) and NWs were imaged with relatively high spectral resolution and exposure time of 2 s per band. SPR plasmon resonance can result in a huge enhancement in the local electric field around the GNP surfaces [9.200, 217]. The local electric field around the NP surfaces can get a huge enhancement due to SPR [9.200, 217]. At the tip of a metal NP or a rough metallic surface, a highly localized and strong electric field can develop due to the interaction between the electromagnetic field and the free electrons. This results in the creation of a large electric field at the sharp tips or vertices of the NPs, leading to an enhancement in the Raman scattering cross-section by several orders of magnitude [9.218, 219]. This effect, known as surface-enhanced Raman scattering (SERS), was first observed by *Fleischman* et al. in 1974 [9.220]. This huge enhancement enables single-molecule spectroscopy, and the SERS activity depends on different parameters such as the size and shape of the NPs, the dielectric environment, the wavelength of the excitation light source, and the interparticle spacing between the NPs [9.221]. Shape dependence can be explained well by considering different GNPs. Gold mesoflowers [9.160] and triangles [9.157] were found to have higher SERS activity compared to their spherical analogs, owing to the higher electric field generated at the tips and edges of these NPs.

Chemical reactivity of NPs is also dependent on their surface area. These NPs are made-up of tens to several thousands of atoms. Each NP has a hybrid electronic structure having aspects of both discrete energy levels as in atoms or molecules and the band structure seen in metals. At considerably lower size regimes, i. e., below 2 nm, gold and silver NPs lose their metallic character substantially and start to exhibit molecular-like transitions under ambient conditions. Size ranges below 2 nm will not have the continuous band structure like bulk gold, and hence very small NPs (< 2 nm) do not possess continuous band structure like bulk gold and will start to demonstrate fascinating electronic properties. This aspect is briefly described in a later section (Sect. 9.8). Noble metals are considered to be the most

inert of all metallic elements. However, gold and silver NPs are known to show very good catalytic activity. In 1987, *Haruta* found that, when deposited on metal oxide supports, Au NPs smaller than 10 nm have high degree of catalytic activity [9.222]. They were found to be excellent in converting toxic carbon monoxide into carbon dioxide at room temperature. Moreover, due to their nontoxic nature and high surface-to-volume ratio, noble metal NPs were found to be excellent candidates as catalysts for a variety of chemical reactions including hydrogenation, CO oxidation, selective oxidation, and nucleophilic additions [9.223, 224].

9.5 Postsynthetic Tuning of Properties

Tuning the properties of nanosystems is usually done during synthesis. Postsynthetically, properties can be tuned via chemical interactions or through assembly. Nanosystems that interact with chemical entities can result in either reactions or organization. Before using any system in practical applications, the reactivity of the system must be studied thoroughly. Reactions can lead to size changes, shape or morphology changes, or composite formation. All this will result in changes in properties, and through precise control over the reaction conditions, we can tune the resultant properties. Small molecular interactions can sometimes result in self-organization as well. Self-organization can sometimes result in the creation of new superstructures with novel or enhanced properties. The resultant properties can be regulated by controlling self-organization. Considerable efforts have been dedicated to this, and some of these are reviewed below.

9.5.1 Tuning Properties Through Chemical Reactions

Postsynthetic chemical transformations of nanostructures through controlled reactions are attracting growing interest. Through this method we can greatly diversify the composition of the material, or sometimes it can result in the formation of novel structures consisting of multiple components, which may not be possible through direct synthetic processes [9.225–227]. The high mechanical stress generated during the transformations enables the creation of novel structures [9.228]. The main chemical transformation reactions frequently employed in nanosystems are redox reactions and ion-exchange reactions. Redox reactions, especially galvanic displacement reactions, are some of the most studied reactions for bringing about chemical transformation in metallic nanosystems [9.229]. The reactivity of spherical NPs has been extensively reviewed [9.1, 230–232]. Hence, this section mainly concentrates on nonspherical, anisotropic particles. Moreover, the inherent diversity in the surface structure of anisotropic NPs gives us an additional tool to regulate the reaction of these NPs and the resultant properties. Change in size or shape can greatly influence change in properties. A review of efforts that have been made to tune properties postsynthetically is presented below.

Reactions of Gold Nanorods

GNRs belong to the most studied class of 1-D nanosystems and can be taken as the best example to illustrate the reactivity of 1-D nanosystems. Optical properties of metallic NPs that originate from SPR have many application possibilities. The absorption cross-section of NPs, being orders of magnitude stronger than the strongest absorbing molecules, can impart intense color to the suspensions. In the case of isotropic spherical GNPs, a single, strong SPR absorption band in the visible region around 520 nm is observed. In contrast, anisotropic GNPs can have several plasmon resonance modes spreading from the visible to NIR region due to various excitation modes. The absorption in the NIR region has both therapeutic and imaging applications in tissues, because in this range of wavelengths, biomaterials do not have significant absorption. Hence anisotropic NPs have applications in biochemical sensors [9.233], biological imaging, and medical therapeutics [9.234]. The UV/Vis spectrum of GNRs has two characteristic maxima [9.235]. The first one, called the transverse surface plasmon resonance (TSP), is located around 520 nm and originates from the oscillation of electrons along the breadth of the NR. The second maximum is due to the longitudinal surface plasmon (LSP) resonance and is due to the oscillation of the electron cloud along the length of the NR, appearing at a longer wavelength. This band will shift to a higher wavelength region with an increase in AR (length/breadth). As mentioned earlier, the exceptional tunability of the photophysical properties of GNRs gives them an edge over their isotropic counterparts. This aspect is illustrated in Fig. 9.12. Doubling the diameter of a spherical NP only results in a minimal change in the spectral position. The sizes of GNRs are represented by a term called the AR

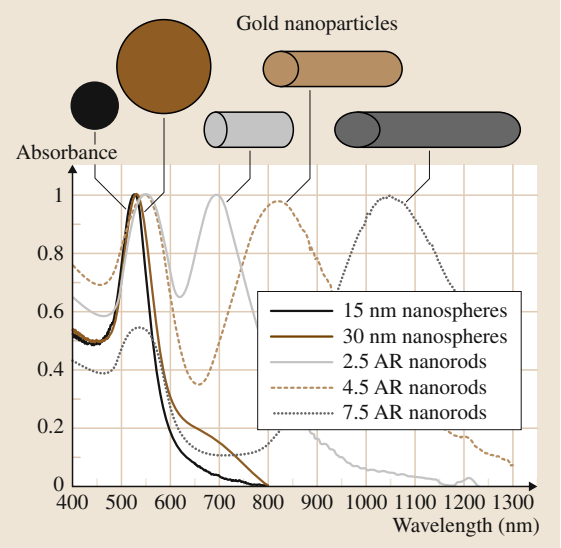

Fig. 9.12 UV/Vis spectra of spherical and rod-shaped GNPs indicating the tunability of anisotropic NRs (after [9.236])

which is the length divided by the breadth of the NR. A change in the AR of GNRs will change the spectrum considerably, and absorption can be tuned throughout the UV/Vis/NIR window [9.236].

The surface structures of isotropic and anisotropic GNPs differ drastically from each other. GNRs especially have an anisotropic crystal structure and have different fractions of atoms at edges, faces, and tips. Spherical GNPs are generally composed of either {111} or {100}. Usually {110} facets will be absent owing to their inherent instability compared with the other two low-index planes [9.237, 238]. However, in GNRs, the rod axis will be oriented along the {001} direction and the side faces are composed of {110} [9.239]. The tips will be mainly composed of {111} and {100} facets [9.239]. Recently, it was found that high-index planes such as {250} also can be present on GNRs [9.240].

CTAB, the surfactant used in synthesis of GNRs, has high affinity towards the {110} surface and will preferentially stabilize {110} planes, giving anisotropic surface structures for GNRs [9.239]. Due to the anisotropy of the surface crystal structure, the distribution of surfactant on the surface is also anisotropic. Due to the presence of {110} facets, the distribution of CTAB on the side faces is thicker compared with on the tips. This gives an additional tool to control the reactivity of GNRs. Incoming species attack the end faces first, and reaction starts from the tip of the NRs. *Jana* et al. studied the reactivity of gold spheroids and NRs prepared in the presence of silver nitrate ($AgNO_3$) with cyanide and persulfate [9.241]. They showed that, in the presence of cyanide, dissolution of GNRs (AR 2–5) occurs. They also found that the reaction starts at the tips and that throughout the reaction the width remains constant, leading to the formation of lower-aspect-ratio NRs. The reaction leads to the formation of spheres, which also ultimately dissolve. Time-dependent UV/Vis spectroscopy showed progressive dampening of LSP and a blue-shift indicating the decrease in the AR of NRs. After some time, only the TSP was seen, indicating the transformation of rod-shaped NPs into spheres. After the completion of the reaction, no feature pertaining to gold nanostructures remained, indicating complete dissolution of the GNRs. No clear mechanism of reaction was proposed. The reactivity of GNRs prepared in the absence of $AgNO_3$ was examined as well [9.242]. Here the reactivity was found to be different. Instead of decreasing the AR, dissolution occurred at various spots along the side edges. During the reaction, various pits were formed on the side faces but the length of the NRs remained the same. Here also, no mechanism was put forward for this anomalous behavior of long NRs prepared in the absence of $AgNO_3$.

Charge-induced instabilities of GNRs were also studied [9.243]. They found that shape changes can be introduced in metallic NRs through double-layer charging. They found that addition of electrons in the form of reducing agents such as sodium borohydride ($NaBH_4$) or ascorbic acid (AA) can induce size and shape changes in small metallic NRs. Introduction of small quantities of electron densities resulted in red-shift of the surface plasmon band, and the end caps of the rods underwent increased faceting. Charge-induced faceting results in the creation of the lower-energy {111} facets. They found that more sharp edges are formed during the process. This is explained as an unusual example of Le Chatelier's principle in action. At crystallographic discontinuities, the particle electric field will be the highest. These edges can provide hot spots for driving hydrogen evolution, which catalyzes the discharge of the GNR double layer. In the presence of higher electron densities, the Rayleigh threshold is crossed and the rods fragment into clouds of smaller spheres. By the formation of spherical NPs which have predominant {111} facets, the formation of the more stable crystal facets results in the surface stress being relieved in a favorable pathway.

Reshaping GNRs by thermal treatment is also reported in [9.244]. It was found that, with increase in

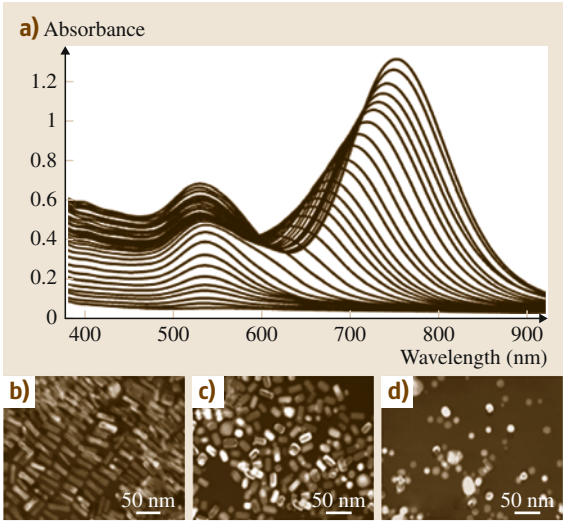

Fig. 9.13a–d Oxidation of GNRs. **(a)** UV/Vis spectra acquired every 1 min. TEM images of **(b)** initial GNRs, **(c)** shortened NRs, and **(d)** spherical particles formed due to oxidation (after [9.247])

temperature, the length of the NR decreases, resulting in decrease of the mean AR of the NRs in solution. Heating the dried NRs on the TEM grid itself did not produce a similar shape change. Hence, it was concluded that the relative instability is due to the instability of micelles capping the NRs. The calculated activation energy needed for the thermal decomposition of the micelles was found to be 21.0 ± 1.0 kcal/mol. A photon-induced shape transition process was reported by *Chang* et al. [9.245]. NRs were exposed to laser lines of two different frequencies, 532 and 1064 nm, and it was found that, due to photoannealing, rod-to-sphere conversion occurred. In the case of 1064 nm, new *ϕ-shaped* structures formed. A shape change of NRs induced by femtosecond and nanosecond laser pulses has been reported by *Link* and *El-Sayed* as well [9.246].

A mild oxidation method using O_2 which results in continuous selective shortening of GNRs was reported by *Tsung* et al. [9.247]. Figure 9.13a shows the UV/Vis spectral changes accompanying the oxidation. The LSP blue-shifts and decreases in intensity with oxidation, while the TSP remains at 520 nm and decreases in intensity, pointing to shortening of the GNRs. As further oxidation happens, the LSP disappears and only the TSP is seen, pointing to the formation of spherical NPs. Subsequently, oxidization also occurs, as demonstrated by the disappearance of the TSP. Similar observations were seen by TEM as well (Fig. 9.13b–d). The rate of oxidation can be controlled by manipulating the temperature and acid concentration. At the same time, a strategy to fine-tune the AR of GNRs using Cu^{2+} was devised by *Pradeep* et al. [9.248]. The advantage of the reaction was that it can be stopped at any point of time by simply removing the heating device, and the NR of desired AR can be obtained (Fig. 9.14). It was also found that the reaction can be controlled in such a way that it starts from either the tip or the rod body by adjusting the presence or absence of the surfactant [9.248].

Spatially directed oxidation of GNRs by the Au(III)–CTAB complex has also been reported [9.249] through a redox reaction between Au^0 and $[AuCl_4]^-$. Oxidation preferentially occurs at surface sites with higher curvature such as the tips of the NRs. This peculiar oxidation was attributed to the differences in the flux of micelles to highly curved and flat surfaces of GNRs. Morphological transformation of GNRs induced by iodide formed in situ by the reaction between potassium iodide and copper chloride was reported by *Wang* et al. [9.250]. It was found that the thus-formed iodide could fuse GNRs in the side-by-side mode, which in turn can result in morphological transformation of GNRs to spheres. Characteristic changes in the absorption spectra with the decrease of AR, such as blue-shift of the LSP band, red-shift of the TSP band, as well as a broadening of both of these bands, were seen. They proposed this methodology for quantification of iodide without the interference of elements such as F^-, Cl^-, and Br^-, etc.

Curvature-directed oxidation of GNRs and gold pyramids was investigated by *Kou* et al. [9.251]. Oxidation was found to happen selectively at surface sites with high curvature. By varying the amount of H_2O_2 and HCl, the oxidation rate can be controlled. The oxidation rate increased in the order: CTBAB-stabilized Au bipyramids, CTBAB-stabilized GNRs, CTAB-stabilized GNRs. Through this method, the LSP band can be precisely controlled from 650 to 1300 nm. Overgrowth of different metals on GNR was also investigated [9.252]. They found that, depending upon the metal used, either single-crystalline or polycrystalline shells will grow on GNRs. In the case of Au and Ag, single-crystalline thin shells were formed, and for Pd the shell was polycrystalline. This was attributed to the lattice mismatch between Au and Pd. Because of the anisotropic surface structure, the competition between the overgrowth on different surface facets resulted in highly anisotropic overgrowth. Due to the strong interaction between the {110} facet and CTAB, {110} was less accessible for overgrowth compared with the {111} and {100} facets. Hence, anisotropic overgrowth occurs,

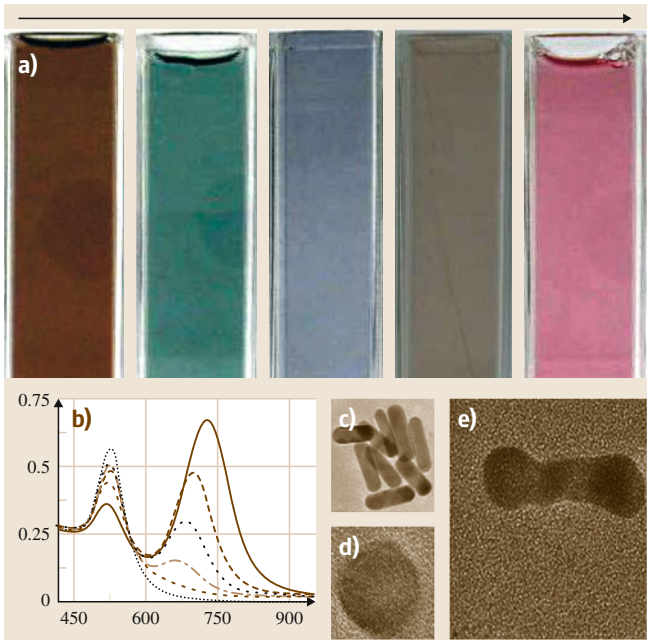

Fig. 9.14 **(a)** Reaction mixture at different time intervals of reaction, depiction of color changes. **(b)** Time-dependent UV/Vis spectra of reaction (*y*-axis: extinction (O.D.), *y*-axis: wavelength (nm)). **(c–e)** TEM images of the NR, nanosphere, and intermediate structure. Formation of GNRs with various aspect ratios is evident from **(b)** (after [9.248]) ▶

and this results in the formation of dumbbell-shaped NRs.

Transverse overgrowth of GNRs by the attachment of thiol-containing molecules such as glutathione and cysteine onto their ends was reported [9.254]. It was found that, as the concentration of the Au precursor increased, the shape underwent a gradual change from rods, peanuts, and truncated octahedra to faceted spheres. The attachment of glutathione and cysteine onto the end faces blocks longitudinal growth and allows growth on the side faces, resulting in an increase of diameter while retaining the length constant. This was also found to be excellent for tailoring the plasmonic characteristics of the GNRs. By combining the selective shortening and controlled transverse overgrowth, *Ni* et al. devised a strategy to tune the LSP band of GNRs [9.255]. GNRs were used as the seed for making silver nanostructures, utilizing the anisotropic surface structure [9.253]. Both homogeneous and anisotropic coatings of Ag were created. This resulted in the formation of an *orange slice-like* shape for the Au@Ag nanocrystal. Figure 9.15 shows the UV/Vis extinction spectra during the formation of the Ag shell. The inset image shows SEM images of the structures formed. The preferential growth of the {110} facets was found to be the primary reason for the formation of the structure. Two neighboring {110} facets among the four present on the side faces grow faster compared with the others. The strong stabilization of CTAB onto the {110} facets of Ag and the minimization of the overall surface energy were given as the reasons for this selective growth. *Carbó-Argibay* et al. reported a chemical method for sharpening the GNRs which results in the rod to octahedron shape transition [9.256]. Rods with sharp tips and strongly faceted lateral faces were formed first. Later, they transformed into octahedrons. The growth rates on different facets were found to be different, following the order: {111} < {110} < {100}. This is believed to be due to the preferential attachment of poly(vinyl pyrrolidone) (PVP) to different body-centered cubic (bcc) facets, which alters the surface energies.

Competing growth of the Pd shell between {110} and {100} facets on the side faces of GNRs, which resulted in the formation of rectangular Pd/Au bimetallic NRs, was reported by *Xiang* et al. [9.257]. The surface energy of the {110} facet is higher compared with that of {100}. Hence, a driving force to minimize

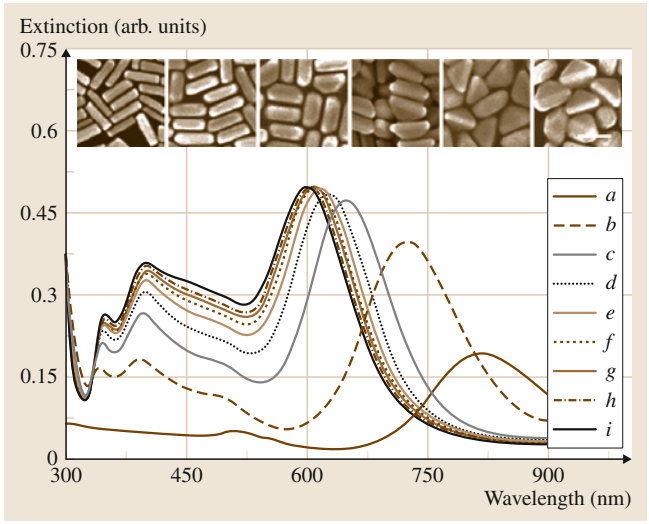

Fig. 9.15 UV/Vis extinction spectra during the formation of the Ag shell after seed addition at: (*a*) 0 min, (*b*) 2 min, (*c*) 4 min, (*d*) 6 min, (*e*) 8 min, (*f*) 10 min, (*g*) 12 min, (*h*) 14 min, and (*i*) 30 min. *Inserts*: SEM images showing intermediate shapes of the Au@Ag nanocrystals during the growth process (after [9.253])

the overall surface energy by changing the morphology exists. As a result, palladium grows faster along the {110} planes than along the {100} planes. This in turn produces an enlargement of the {100} surfaces by sacrificing {110}. After some time, {110} facets disappear and a rectangular Pd shell terminated with four {100} side surfaces is formed, as illustrated in Fig. 9.16. GNRs were used as a template for synthesis of other anisotropic structures as well. *Obare* et al. used polystyrene and silica-coated GNRs as templates for creating hollow nanotubes [9.258]. Silica-coated GNRs (AR 13) were coated with polystyrene. Dissolution of the GNR core by the use of KCN resulted in the formation of hollow nanotubes.

Other Common Reactions on Noble Metal Nanostructures: Examples

As was discussed earlier, there is keen interest in enhancing the properties of anisotropic nanosystems by carefully engineering their structure and composition. Of the many strategies employed, galvanic replacement reactions deserve special mention. The high tunability and versatility, and the possibility to study alloying and dealloying in metallic nanostructures give these reactions utmost importance in postsynthetic design of nanosystems. Galvanic reactions are spontaneous reactions occurring when the atoms of one metal react with ions of another metal having a different electrochemical potential, whereby the metal atoms having lesser reduction potential are oxidized and dissolved into the solution, while the metal ions are reduced. Through this methodology, versatile structures such as hollow NPs, alloyed nanostructures with controllable elemental composition, and nanosystems with tunable optical properties have been created [9.259, 260]. Figure 9.17 shows such a reaction done on truncated Ag nanocubes. Another advantage of the galvanic replacement reaction is the controllability of the final morphology, which closely resembles the starting template.

Galvanic replacement reactions of Ag nanocubes have been well studied. With $HAuCl_4$, Ag nanocubes are reported to show interesting galvanic reactions. The reaction can be divided into two half-reactions as follows: The half-reaction showing dissolution of metal at the anode is (standard hydrogen electrode (SHE)

$$Ag^{+}_{aq} + e^{-}_{aq} \rightarrow Ag_s (0.80\,V \text{ versus SHE}) . \qquad (9.13)$$

The half-reaction showing reduction/deposition of the metal ions at the cathode is

$$Au^{3+}_{aq} + 3e^{-}_{aq} \rightarrow Au_s (1.50\,V \text{ versus SHE}) . \qquad (9.14)$$

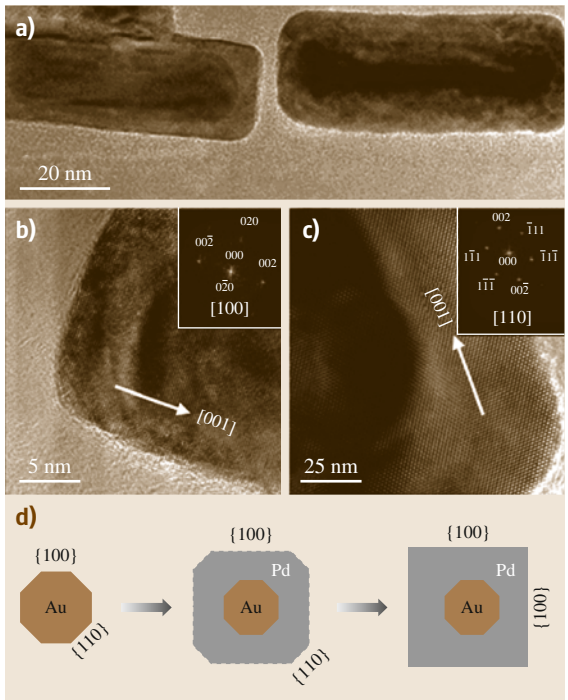

Fig. 9.16 **(a)** Low-resolution TEM image of single bimetallic NRs. High-resolution TEM images of bimetallic NRs when the electron beam is aligned in the [001] **(b)** and [011] **(c)** directions, showing the distribution of the atoms on the {001} and {111} faces, respectively. *Insets* show the corresponding FFT transform images. **(d)** Cross-section showing the morphology transition from pure GNRs to Pd/Au bimetallic NRs (after [9.257])

Hence, the total reaction is

$$Au^{3+}_{aq} + 3Ag^{0}_{aq} \rightarrow Au_s + 3Ag^{+}_{aq} . \qquad (9.15)$$

These equations are valid only at standard conditions (at 25 °C). A change in temperature to 100 °C, the presence of Cl^- ions, and other nonstandard conditions can affect the potentials [9.261, 262].

Starting with a variety of shape-controlled nanomaterials as templates, hollow nanostructures of a variety of materials with well-defined and controllable sizes and shapes have been reported through galvanic reactions. Reaction between Ag nanocubes and $HAuCl_4$ where hollow nanostructures are formed has been reported [9.175]. The reaction was done at 100 °C to avoid deposition of AgCl on the surface of the nanostructures formed. Time-dependent SEM analysis showed that small pits formed on the surface of the cubes, first mainly at defect sites. As the reaction continued, these

pits expanded into the interior of the nanocubes, resulting in hollow structures. It was also found that, by controlling the reaction parameters, different structures such as nanocages, nanoboxes, etc., could be generated using this methodology. The creation of nanocages with controllable pores was possible when different facets were present on the surface of the starting Ag nanocubes [9.263]. Galvanic reaction on 42 nm Ag nanocubes with truncated corners having six {100} facets and eight {111} facets, and some {110} facets at the truncated parts, resulted in the formation of final pores selectively on the {111} facets at the corners. After the replacement reaction, the pores found at all eight corners (consisting of {111} facets) were uniform in size and shape. The facet-selective reactivity observed is explained as being due to the preferential binding of PVP to {100} facets of Ag compared with {111} facets, thereby making the {111} surface more exposed for reactions.

Galvanic reactions normally preserve the morphology of the starting materials. However, when the facet-selective reaction was started with 24 nm spherical Ag particles, this morphology changed to octahedrons [9.266]. Starting Ag particles had {111} and {100} facets. As discussed above, the pitting reaction happened on the {111} facet and deposition of Au on the {100} facet. Due to the smaller size of the particles, this resulted in a change in morphology. A similar transition was seen in the case of 11 nm Ag spheres as well [9.267]. Similar reactions are also applicable for polycrystalline materials [9.268–270].

Hollow nanotubes can also be made using an analogous method. Ag NWs having five twin-planes along the length of the wire together with a pentagonal cross-section were treated with $HAuCl_4$ [9.271]. Multi-walled structures such as nanorattles, multi-walled nanoshells, and multi-walled nanotubes can be made using this reaction [9.77, 271]. By electroplating, a thin layer of pure Ag was coated on the surface of Au-Ag alloy particles, and the consequent reaction resulted in multi-walled structures. Using a comparable strategy, a single-step, large-scale methodology for the production of nanoframes of different morphologies was reported by *Sun* et al. [9.77].

The difference in surface energies between common facets of face-centered cubic (fcc) metals were used for fabricating hollow Au-Ag octahedrons containing GNRs [9.272]. The difference in surface energy resulted in an uneven growth rate and a complete change in the morphology. GNRs to begin with had {111}, {100}, and {110} facets. After deposition of Ag, all the rods

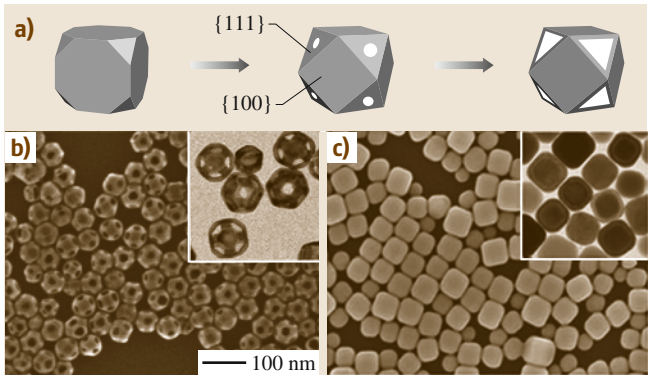

Fig. 9.17 **(a)** Schematic showing the morphological changes during the different stages of the galvanic replacement reaction with truncated Ag nanocubes. **(b)** SEM (with TEM *inset*) of truncated Ag nanocubes. **(c)** SEM (with TEM *inset*) of Au nanocubes with rounded edges (after [9.264])

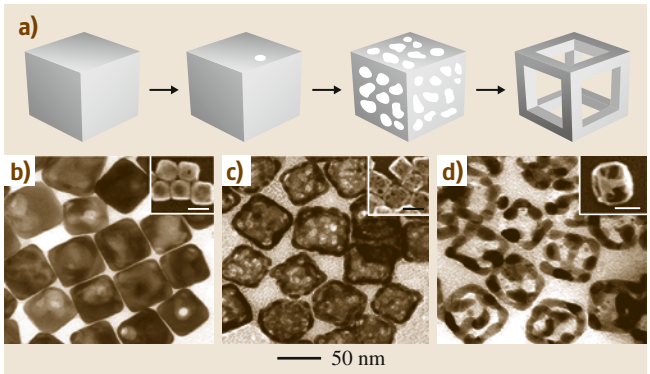

Fig. 9.18 **(a)** Schematic summarizing the formation of cubic Au nanoframes by treating Ag nanocubes with $HAuCl_4$ to form Au-Ag nanoboxes **(b)**, and then etching with ferric nitrate to form thin-walled nanoboxes, **(c)** and eventually cubic nanoframes **(d)**. *Inset scale bars* are 50 nm (after [9.265])

transformed into Au@Ag octahedrons capped by {111} facets. When the resultant particles were treated with excess $HAuCl_4$, hollow Au-Ag octahedra containing GNRs were formed. A similar reaction has been observed out in organic media as well.

Galvanic reactions of Pd NRs with $HAuCl_4$ did not produce hollow structures. Instead, solid tadpole-like structures having a Pd tail and an Au head were formed [9.273]. As the reaction proceeded, Au was deposited first at one end and then both ends. The selective deposition was attributed to electron–electron repulsion, which pushes the electrons generated during Pd oxidation to either ends of the rod, resulting in the

reduction of Au^{3+}. After some time, the Au head increased in size and eventually fell off the structures. A similar study of polycrystalline Pd rods resulted in a nonrandom alloy with an Au-rich core and a Pd-rich shell. A similar morphology was formed when Co NRs were treated with Au precursors as well [9.274].

Introduction of a wet etchant such as ferric nitrate ($Fe(NO_3)_3$) can influence the galvanic reaction between Au and Ag [9.276, 277]. This enables removal of Ag without deposition of Au, resulting in better control of wall thickness, composition, and resultant optical properties. Ag nanocubes were treated with $HAuCl_4$ first, which resulted in the formation of small pits. On treatment with $Fe(NO_3)_3$ solution, thin-walled nanoboxes were formed. As the concentration of $Fe(NO_3)_3$ added increased, the thin-walled nanoboxes were converted to nanoframes. This transition was attributed to the higher susceptibility of {100} facet towards etching (Fig. 9.18).

Due to their catalytic applications galvanic replacement of Ag nanocubes with Pt and Pd precursors have been well studied [9.278]. Reaction between 50 nm Ag cubes and Pt precursor resulted in hollow structures with rough exterior. This was attributed to the lack of miscibility between Pt and Ag at the reaction temperature (100 °C), but when the reaction was done with Pd, the surface of the structures formed was smooth. However, the reaction never went beyond the nanobox stage. When the galvanic reaction was done with two or more metal ions, the order of addition was found to influence the resultant morphology [9.78]. In the case of Au and Pd reaction with Ag nanostructures, addition of Pd before Au resulted in products with large pores. However, first reaction with Au and subsequent reaction with Pd resulted in solid walls. In the case of Au, there was a difference in reactivity between $[AuCl_4]^-$ and $[AuCl_2]^-$. The striking difference between Au(I) and Au(III) was the early disappearance of the pinhole in the case of Au(I), due to the larger amount of Au deposited for the same amount of Ag being dissolved. Structure-wise, in the case of Au(I), the walls of the nanocages were thicker compared with those formed for Au(III).

An epitaxial growth process by which Au nanooctahedra were changed to Pd and Ag nanocubes was reported by *Fan* et al. [9.279]. Au nanooctahedra were used as seeds, and through the use of a seed-mediated growth method, shape transition was realized. The formation of an asymmetric hollow structure from a heterometallic NR by partial galvanic reaction was demonstrated by *Seo* and *Song* [9.275]. They found that asymmetric single-hollow or symmetric double-hollow

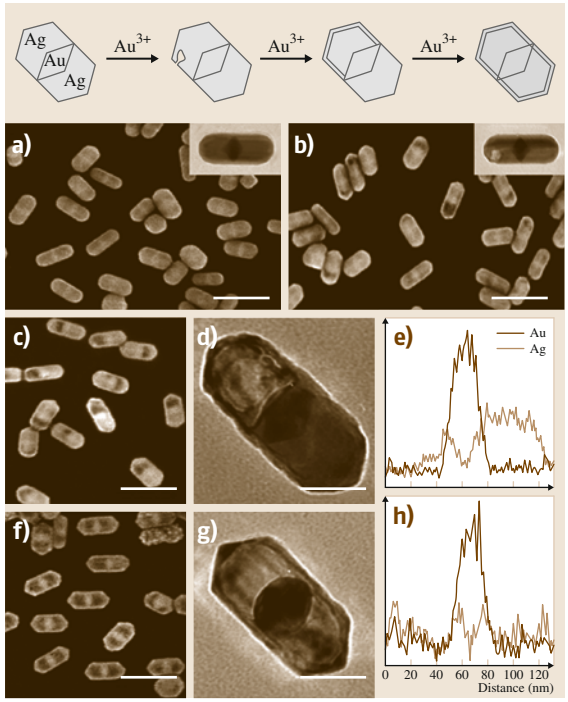

Fig. 9.19a–h Schematic representation of the galvanic replacement in Ag-Au-Ag heterometallic NR. SEM and TEM (*insets*) images of **(a)** original heterometallic NR and **(b–d)**, **(f)**, and **(g)** hollow structures at different concentrations of Au^{3+}. **(e,h)** Energy-dispersive x-ray spectroscopy (EDAX) line profiles along the long axes of the hollow structures (after [9.275])

NRs could be generated from Ag-Au-Ag heterometallic NRs. The breaking of symmetry was a result of random pit formation on the Ag end. The reaction scheme and the structures formed are shown in Fig. 9.19. Production of triangular gold nanorings by galvanic replacement reaction of ultrasonically synthesized Ag nanoplates was reported by *Jiang* et al. [9.280]. The nanoplates and nanorings were highly single crystalline and had (111) planes as the basal planes.

The diffusivity difference between metals can give rise to the formation of hollow structures by a phenomenon known as the Kirkendall effect (KE). If the inner material diffuses outwards faster than the rate at which the outer material diffuses inwards, voids will form. In nanosystems, such an effect can result in the formation of hollow structures. Several reports exist in this regard [9.267, 281–284]. Recent studies reveal that the formation of some of the hollow structures discussed above through galvanic replacement reactions can also

have a contribution from the KE [9.283]. Reaction between cobalt nanocrystals in solution with oxygen and either sulfur or selenium can result in the formation of hollow nanocrystals through the KE [9.281]. Recently, a size-dependent nanoscale KE observed during the oxidation of nickel NPs was reported by *Railsback* et al. [9.285]. Depending upon the size of the NP, either single-pored or multipored NiO nanostructures were formed. It was found that the fast self-diffusion of Ni compared with its rate of diffusion through the NiO shell resulted in the single-pore structure. When the diffusion was not fast enough, multiple pores resulted.

9.5.2 Modification of Properties – Formation of Superstructures

Tapping the incredible properties exhibited by NPs into useful applications is challenging when one is working with individual NPs. Assembling them into well-arranged superstructures is one of the ways to make use of these systems in modern day science and technology. Assemblies of NPs are important for many fruitful applications. Functionalization of noble metal NPs is comparatively easier and this makes them attractive candidates for making diverse superstructures. Creation of their one, two, or three-dimensional assembled structures can enhance the properties or can sometimes give rise to novel improved properties due to the effective coupling of different domains. Noble metals (mainly gold and silver) owing to their biocompatibility, tunable optical properties, and easy synthesis, have been extensively used to create superstructures that are useful in studying various properties including SERS, metal–insulator transitions, interplasmon coupling, etc.

Assembly can be brought about by using molecular linkers, templates, or spacers in well-organized periodic one, two- or three-dimensional superstructures. For spherical NPs solid superstructures called particle crystals or SLs [9.286–288] can be generated via bottom-up or top-down approaches. A high degree of monodispersity is the prerequisite for making such SLs over a long range. The changes in properties of individual NPs in the collection can be understood by studying these structures. For example, changes in optical properties such as interplasmon coupling and changes in transport properties including metal–insulator transitions, etc., can be understood in a better way by studying the properties of SLs [9.286]. Various strategies such as electrostatic self-assembly, solvent evaporation on a substrate, self-organization at interfaces, covalent and hydrogen bonding, biochemical interaction, van der

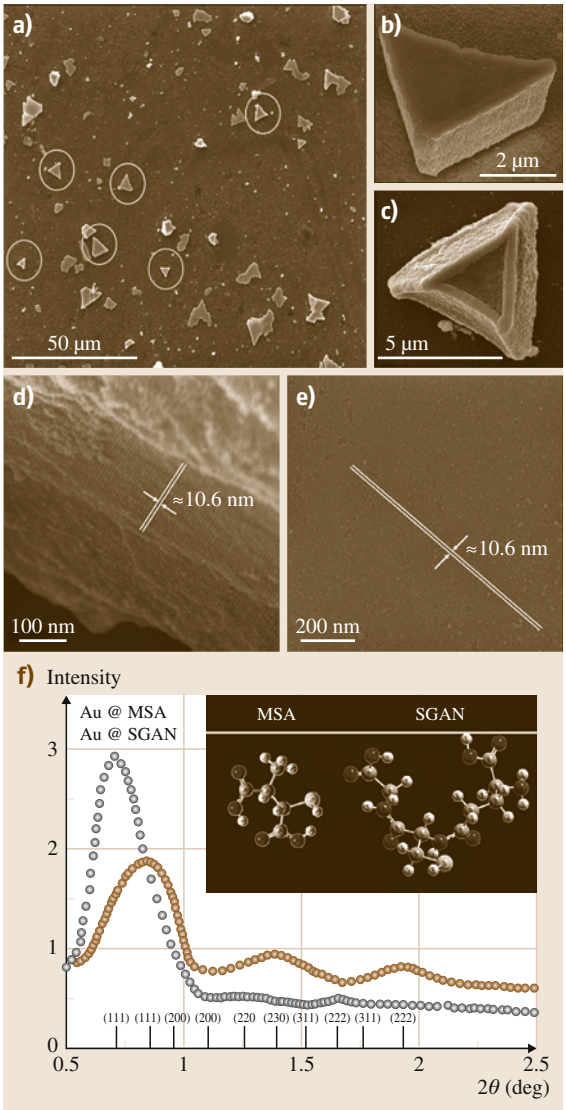

Fig. 9.20 **(a–e)** SEM images of superlattices made of GNPs at various magnifications. **(d,e)** Clear images of large area ordered arrays of NPs. **(f)** Small-angle x-ray scattering showing the regular array of atoms in SLs. From the authors' laboratory

Waals and dipole interactions, etc. [9.289], have been utilized to create SLs of GNPs. Several well-written reviews are available on this topic [9.289, 290].

Digestive ripening, the SMAD method, and hydrogen-bonding methods are used extensively to create SLs [9.289]. Thiol-protected GNPs synthesized by the SMAD process upon digestive ripening will

spontaneously form 2-D and 3-D SL crystals via self-organization. Changing the pH of the solution by the addition of acid (pH ≈ 2) resulted in the organization of MSA acid-protected GNPs into beautiful 3-D structures [9.287, 291]. The formation of hydrogen bonding between the dicarboxylic acid moieties present on the adjacent NPs drive the assembly formation. Formation of a brown mirror-like appearance on the air/water interface after a few days indicates SL formation [9.292]. Diverse morphologies such as triangles, hexagons, etc., were adopted during the crystal formation. Some representative SLs formed by these interactions are shown in Fig. 9.20.

Spherical particles that are isotropic will experience the same interactions in all directions in a 3-D assembly and the resultant effect as well as collective properties will be the same. Only the extent of interaction and hence the change in properties will vary depending upon the dimensionality of the assembly. Unlike isotropic NPs, the inherent anisotropy of anisotropic NPs adds a directional dependence on the assembly and the consequent interactions between NPs. A variety of factors plays seminal roles in assembling NPs in an ordered manner, without the formation of complex 3-D aggregates. The following section reviews different assemblies of various nanostructures and various forces inducing such assemblies.

Assembly of Gold Nanorods

The crystal structure and crystallographic planes present on the NP surface plays important part in regulating their assembly. Unlike spherical NPs, which have an isotropic crystal structure entirely composed of either ⟨111⟩ or ⟨100⟩ planes, the surface structure of anisotropic NPs are different. GNRds are classical examples of this anisotropic surface crystal structure. The GNR surface is highly anisotropic consisting of different facets (Fig. 9.21a,b) [9.239]. The edges (side faces) of GNRs are constructed by ⟨110⟩, and their tips consists of either ⟨111⟩ or ⟨100⟩ facets [9.239]. Due to this anisotropic crystal structure, the distribution of surfactant molecules (the CTAB bilayer coverage) on the surface of GNRs will also be anisotropic, and the bilayer will be thicker on the side faces due to the higher affinity of CTAB towards ⟨110⟩ facets. A lattice-resolved image of a GNR showing the specific planes is given in Fig. 9.21b.

Anisotropy in the crystal structure and in surface reactivity can be used as tools for selective functionalization of GNRs to bring about specific interactions between GNRs leading to different types of assembled structures. Because the tips of GNRs are less populated with CTAB they are more susceptible to functionalization strategies and can thus can trigger end-to-end interactions to form linear chains where GNRs are connected in an end-to-end fashion. The shape anisotropy of GNRs opens up another type of linear assembly where the sides of the NRs interact with each other (termed as side-to-side assembly). The free energy of bilayer stabilization between CTAB molecules is 6 kJ/mol per two methylene groups and hence the removal of CTAB from the side faces is rather difficult [9.293]. Hence, to bring about the functionalization of this face, rigorous procedures must be followed. The possible interactions and different kinds of resultant assemblies are pictorially depicted in Fig. 9.21c. Theoretical studies have established that side-by-side assembly leads to a blue-shift in the UV/Vis spectrum, whereas end-to-end assembly imparts a red-shift [9.294]. The extent of the shift in the spectra depends on the extent of assembly. For example, in a 2-D or 3-D assembly where multiple interactions are present, the resultant shift can be a combination of all of these interactions.

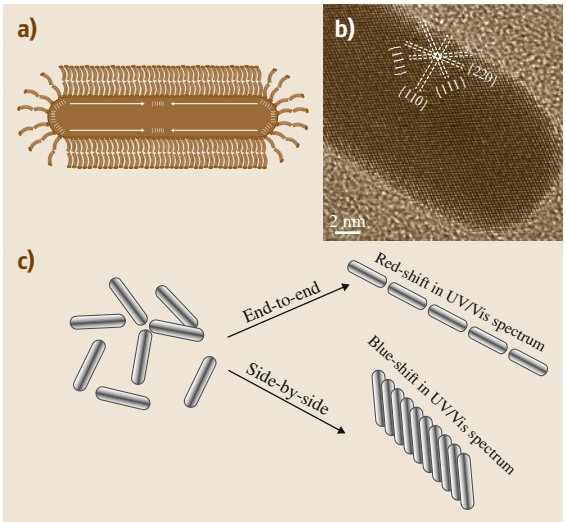

Fig. 9.21 **(a)** Schematic of a single GNR. **(b)** High-resolution TEM (HRTEM) image showing the different crystal planes and lattice structure. **(c)** Schematic showing the different ways of arranging the NRs

Spontaneous assembly without any external aid is often called self-assembly. GNRs are known to self-assemble under optimum conditions such as concentration, pH, ionic strength, etc. Controlling the interactions between the constituents can lead to mod-

ification of self-assembly. Generally, environmental conditions such as pH and ionic strength are modulated for this purpose. Then the process will be termed *programmed self-assembly*. The assembly process can be controlled by chemical modifications or functionalizations as well. Surface functionalization of GNRs with specific molecular groups can result in precisely programmed self-assembled structures. Due to its simplicity, versatility, and low cost, programmed self-assembly with functionalized NRs is used extensively for nanofabrication purposes. One of the disadvantages of this strategy is that it normally produces ordered structures with small area and does not allow control over the design or interparticle distance in the NR architecture. Also, once triggered, further manipulation of the assembly is rather difficult. However, a better understanding of the system and the advent of new techniques are helping us to overcome these limitations. Programmed assembly can be brought about using a wide variety of operating forces, by changing the functionalizing molecules. The operating forces involved in the assembly can be covalent, hydrogen bonding, electrostatic, biochemical interaction, van der Waals, dipole interactions, etc.

The following section illustrates a brief review about the different kinds of assemblies and the operating forces leading to the assembly, taking GNRs as the example.

Self-Assembly of Gold Nanorods upon Solvent Evaporation

GNR suspensions are stabilized due to the electrostatic repulsion between the head groups of CTAB (the stabilizing bilayer) on adjacent rods avoiding aggregation. Removing excess surfactant by centrifugation and at optimum concentration, pH and ionic strength, the hydrophobic–hydrophobic interaction between the CTAB tails can compensate the electrostatic repulsion facilitating the assembly of NRs where the distance between the NRs depends on the compensation of the above-mentioned interactions. Therefore, NRs form assembled structures with an optimum separation between NRs upon solvent evaporation, with all forces being compensated. In 2000 *Nikoobakht* et al. made one of the first attempts to study the self-assembly of GNRs [9.295]. GNRs prepared by electrochemical methods (AR $\approx$ 4.6) were centrifuged at 14 000 rpm and were resuspended in water. The sample was diluted to an optical density of 1.5–1.7. A 1 : 1 solution of the above suspension and 0.1 M NaCl solution was made and was dropcasted onto a TEM grid as shown in the inset of Fig. 9.22. Long-range (over micrometer areas) 1-D, 2-D, and 3-D assemblies of GNRs were formed on the grid upon solvent evaporation. Here the electrolyte (NaCl) was used to form the assembly. Later it was found that even without the use of electrolyte, removal of excess CTAB can result in self-assembly at appropriate NR concentrations [9.293]. It is also reported that liquid-crystalline assemblies of large-aspect-ratio GNRs will form when the as-prepared rods are centrifuged to remove associated spherical particles and are redispersed in an optimum concentration of CTAB (1–100 mM). The assembly was studied in detail using UV/Vis and small-angle x-ray scattering (SAXS) measurements.

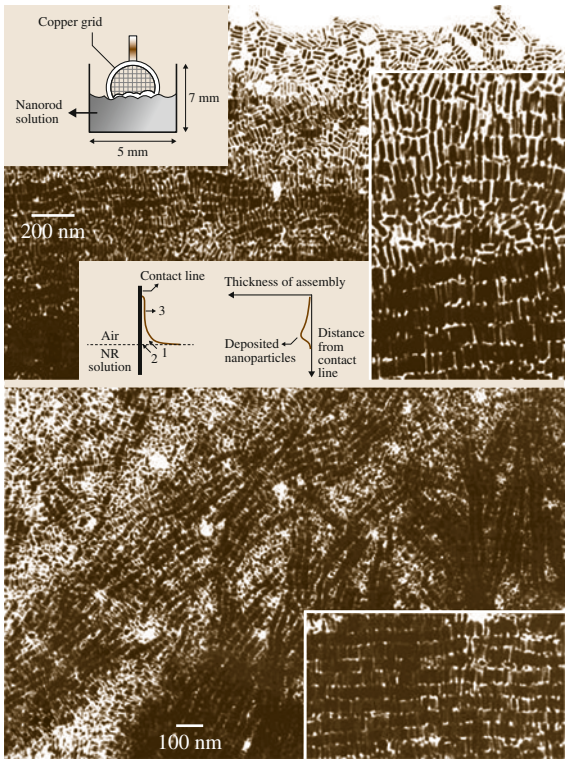

Fig. 9.22 Electron micrograph showing border of the self-assemblies. The thickness increases from *top* to *bottom*. The *insets* show magnified parts of the assembly. *Inset top left*: scheme of the deposition method (after [9.295])

Assembly Involving Biological Interaction and Bio-Recognition

Functional entities in biology are almost entirely assembled structures and the operating forces involved are very specific. GNRs have been assembled using such

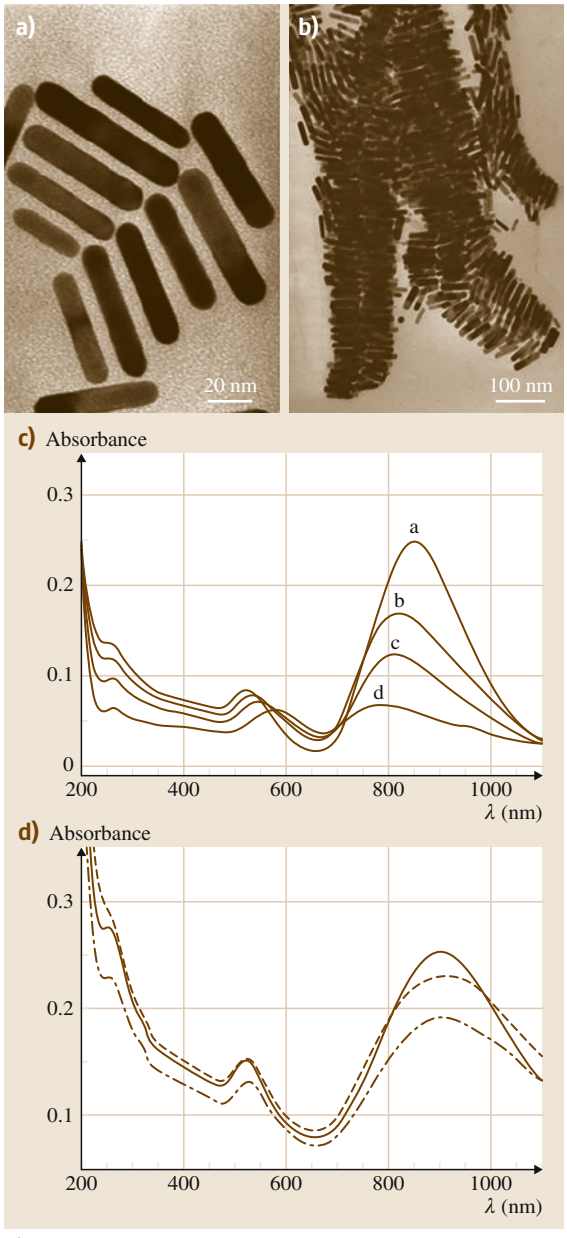

Fig. 9.23a–d TEM images of bundles of DNA-linked GNRs. The three-strand **(a)** and two-strand **(b)** DNA linking systems. UV/Vis spectra of **(c)** a suspension of non-complementary DNA functionalized NRs and **(d)** the two-strand NR system before (*solid line*) and after (*dash-dotted line*) duplexation at 25 °C. The *dashed curve* represents the spectrum after melting the DNA above 60 °C (after [9.296])

interactions as well. The first effort in this direction was made by *Dujardin* et al. [9.296]. In this work, NRs were functionalized with thiolated DNAs. Assembled structures were formed upon addition of duplex DNA into the above mixture. Figure 9.23a,b shows TEM images of the assembled structures and the associated UV/Vis spectral changes during the assembly (Fig. 9.23c,d).

End-to-end assembly of GNRs, surface-functionalized with mercaptoalkyloligonucleotide, was brought about by the addition of a target oligonucleotide [9.297]. Here, the thiol groups in the mercaptoalkyloligonucleotide binds to the ends of the NRs, which further assemble in end-to-end fashion through hybridization with the target oligonucleotide. *Chang* et al. utilized the specific binding of an antibody to an antigen to form an oriented assembly of GNRs in solution through a biomolecular recognition system [9.298]. In this work, thioctic acid (TA), used as a binding agent, was made to specifically self-assemble onto GNR tips. The conjugation of TA with various immunoglobulins (Ig) or other biomolecules resulted in the GNR to assemble. *Wang* et al. utilized a similar strategy to detect proteins such as IgG [9.299]. Compared to the spherical counterparts (detection limit 0.1 μg/ml), an enhanced detection limit of 60 ng/ml was shown by the NR assembly.

The biotin–streptavidin interaction is one of the most specific and strongest noncovalent interactions known in biology. Utilizing this interaction, a preferential end-to-end assembly of GNRs was fabricated. First, GNRs were surface-functionalized with biotin disulfide and the subsequent addition of the streptavidin linker gave GNRs assembled preferentially in end-to-end fashion [9.300]. A simple and versatile approach for end-to-end assembly of GNRs was reported by *Huang* et al. This strategy involved the specific molecular recognition between thymine-rich (T-rich) oligonucleotides and mercury(II). The high specificity of the oligonucleotide improved the selectivity of the process [9.301].

Assembly Involving Covalent Bonding

Longitudinal assemblies of GNRs were fabricated by the interaction of GNRs and α,ω-alkanedithiols of varying chain lengths, and the mechanism, structure, as well as changes in properties were investigated using absorption spectroscopy and TEM by *Thomas* et al. [9.302]. A decrease in the longitudinal plasmon absorption was observed upon addition of dithiols. The simultaneous appearance of a new red-shifted band above a critical dithiol concentration resulting from the interplasmon

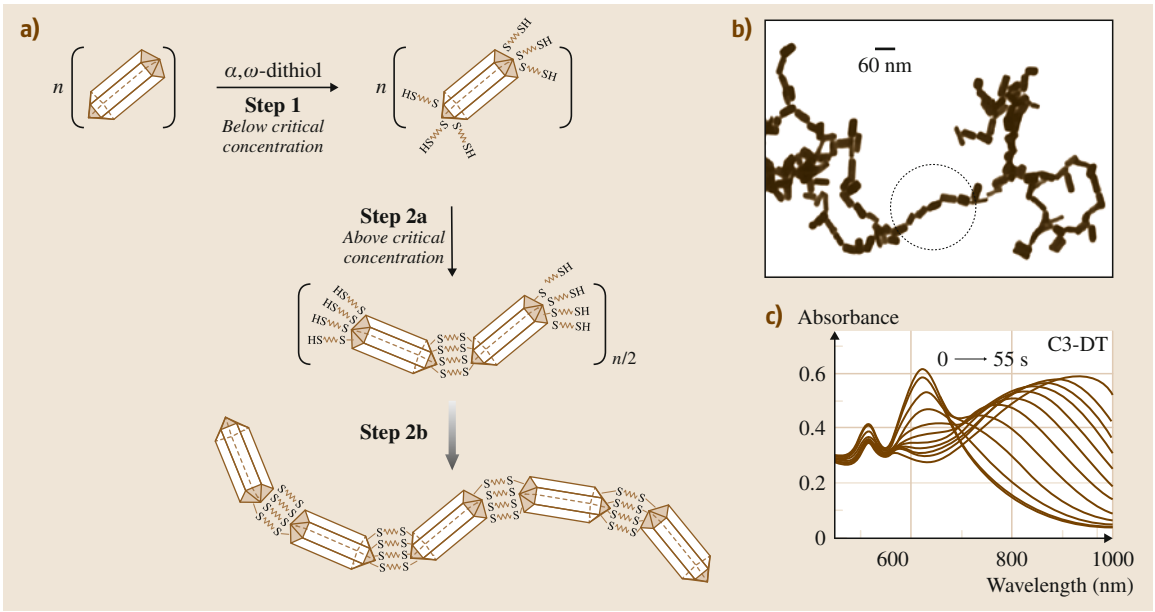

Fig. 9.24 **(a)** Schematic of the general mechanism of GNR nanochain formation due to electrostatic interaction of cysteine and glutathione. **(b)** Transmission electron micrograph of nanochains. **(c)** 1,3-Propanedithiol (C3-DT) (0.83 μM) to Au NR of AR 2.2 at a time interval of 5 s (after [9.302])

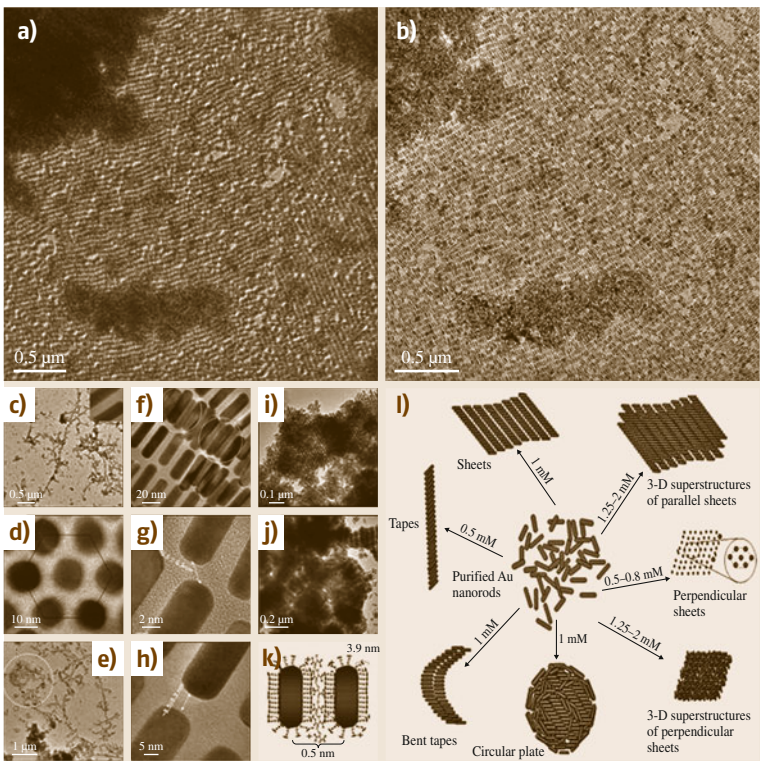

Fig. 9.25a–l TEM images taken in the **(a)** low MAG and **(b)** MAG I modes of the same area, showing self-assembly of NRs, induced by DMSA. Different self-assembled structures obtained at different concentrations of DMSA; **(c)** a parallel assembly of NRs leading to a tape-like structure, **(d)** high-magnification image of perpendicularly oriented assembly showing the hexagonal nature of the rods, **(e)** circular structures and bent tapes, and **(f)** magnified portion of the same assembly showing the staggered configuration of NRs in the same plane. The NRs in the top layer (*circled*) are located in the grooves of the bottom layer. **(g,h)** High magnification images showing the spacing between the NR in a monolayer. TEM images of 3-D superstructures formed by **(i)** perpendicular orientation and **(j)** parallel orientation with respect to substrate. **(k)** Schematic showing the mechanism of the self-assembly. **(l)** Cartoon representation of various superstructures formed from Au NRs in the presence of different concentrations of DMSA. From the authors' laboratory (after [9.303])

coupling in the assembled NRs was also observed. The presence of clear isosbestic points in the time-dependent absorption spectrum, and TEM investigations proved the formation of dimers, indicating the existence of a dimerization step in the chain-up process. It was also understood that the process is not diffusion controlled but activation controlled with large activation energy [9.302].

Assembly Through Hydrogen Bonding

The cooperative intermolecular hydrogen bond formed between two thioacids anchored onto the end faces of GNRs was utilized to precisely control the longitudinal assembly and modulate the plasmon coupling. Adjusting the concentration of thioacids added into the mixture resulted in the modulation of plasmon band positions. An increase in concentration of thioacids produced a plasmon shift to a higher wavelength. Precise tuning of the optoelectronic properties is possible through this method [9.304]. Recently, hydrogen-bonding-directed assembly of GNRs in aqueous solution was investigated by *Ni* et al. [9.305]. Theoretical as well as experimental investigations of the mechanism behind the formation of end-to-end assemblies of GNRs modified with bifunctional linking molecule were made in this study.

Assembly Through Electrostatic Forces

Electrostatic interactions are one of the most common forces encountered in the living world and in assemblies. Electrostatic forces between amino acids anchored onto GNR surfaces were utilized to assemble NRs [9.306]. Two thiol containing amino acids, namely cysteine and glutathione were added to the GNR solution. Due to the thiol-gold affinity, they became anchored onto the GNR end faces and the electrostatic interaction between adjacent amino acids on separate GNRs resulted in the preferential longitudinal assembly (Fig. 9.24). This was manifested by a red-shift of the LSP. This change in the plasmonic characteristics was used for specific detection of cysteine and glutathione at micromolar concentrations. Gold bipyramids and rods were assembled into different types of nanonecklaces using a similar methodology by *Zhang* et al. [9.307].

The time-dependent shift in LSP at a specific concentration of assembly-inducing agents was always constant and it was not precisely controllable in any of the above methods. *Kawamura* et al. reported a more controllable fabrication method for GNRs assembly, in which the shift of the LSP can be stopped at a desired point to obtain a stable suspension with a desired absorption range [9.308]. A gradual red-shift of the LSP was observed upon addition of sodium citrate to GNRs, which can be stopped at any point simply by the addition of CTAB to the reaction mixture. The preferential adsorption of citrate anions onto the end faces of the GNRs, which results the neutralizations of the surface charge of the GNR ends, triggers the end-to-end assembly of the GNRs. High AR GNRs (AR of 16) assembled in an end-to-end fashion upon decreasing the CTAB concentration and the assembled GNRs became welded at their connecting points upon a further decrease of the CTAB concentration [9.308]. A pH-dependent self-assembly of GNRs into ordered structures using adipic acid was reported by *Orendorff* et al. [9.309]. Here, the electrostatic interactions between the cationic surfactant bilayer around the NRs and the negatively charged deprotonated adipic acid result in pH-dependent self-assembly of the NRs into 2-D ordered structures. A similar but more refined strategy to assemble GNRs into 1-D, 2-D, and 3-D superstructures was reported by the authors of this chapter (Fig. 9.25). The addition of dimercaptosuccinic acid (DMSA) to the NR solution-induced self-assembly of the latter into 1-D *tape-like*, 2-D *sheet-like*, and 3-D *SL-like* structures depending on the DMSA concentration. A smectic structure where the NR long axes are parallel to each other was found to be followed throughout the assembly process. Different parameters that determine the quality of the assembly including DMSA concentration, pH, and monodispersity of the sample were studied. Immediately after the addition of DMSA to the NR solution, UV/Vis spectral changes were observed. The peak position was found to be stable (after the initial shift) even after 24 h of incubation. A gradual shift was observed for the LSP, while the TSP remained unchanged. An increase in concentration of DMSA resulted in an increased red-shift. There was a marginal increase in width of the LSP as well. At lower concentrations, a longitudinal assembly formed was transformed into a lateral assembly upon increase of the DMSA concentration. As the concentration was increased, the assembly changed from 1-D *tape-like* to 2-D *sheet-like*, and finally to 3-D *SL-like* structures. Perpendicular arrangement of NRs (NR long axis perpendicular to the TEM grid) was also seen at places. At lower pH (below the pK_a of DMSA) where DMSA molecules are not ionized no assembly was produced. Detailed investigation indicated that charge neutralization of the NRs by the carboxylic group of DMSA was found to be the principal reason for such an assembly, while the mercapto groups render additional stability to

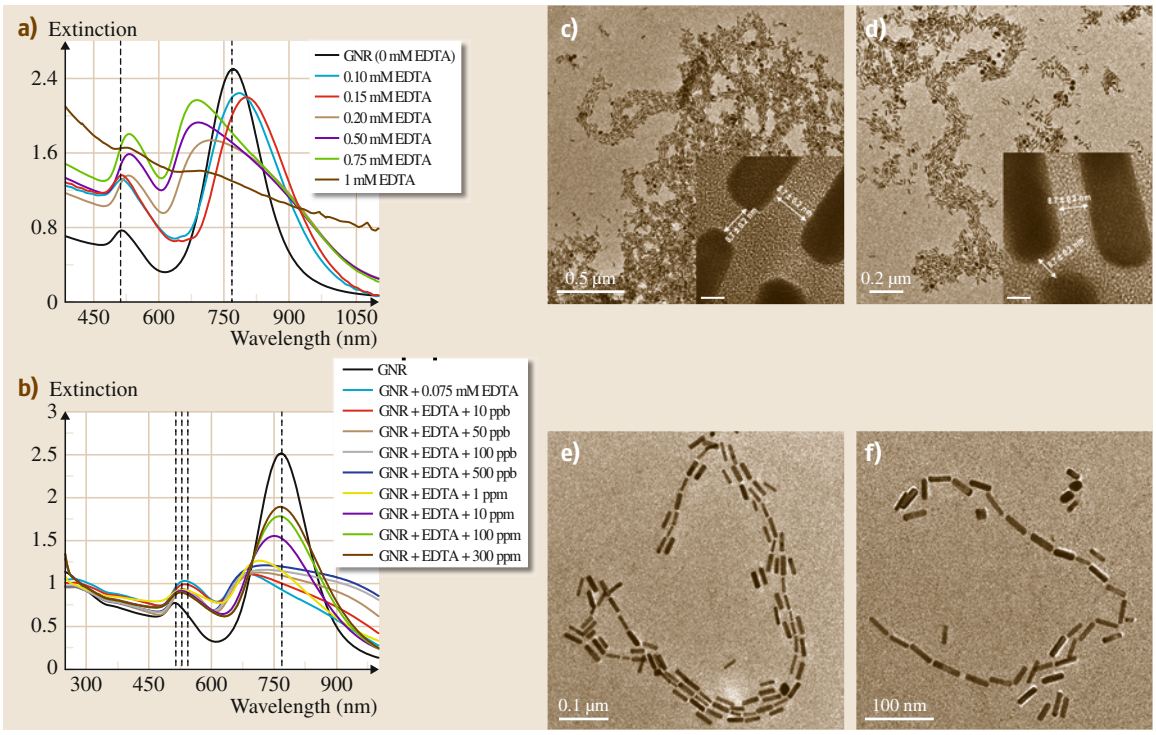

Fig. 9.26a–f UV/Vis spectral changes of the assembly **(a)** and disassembly **(b)** processes. TEM images of assembly and disassembly by EDTA–Pb^{2+} interaction **(c–f)**. From the authors' laboratory (after [9.303])

the superstructure. A mechanistic model of the assembly has also been proposed [9.310].

Electrostatic assemblies are difficult to manipulate once they have been formed. However, recently a strategy for the reversible assembly and disassembly of GNRs was also devised [9.303] A labile ligand ethylenediaminetetraacetic acid (EDTA) was used. The disassembly followed a peculiar pattern by forming bundled chains and then single chains before forming discrete NRs. It was also observed that the assembled structures are highly SERS in nature and through use of the disassembly method SERS activity can be tuned. Figure 9.26 illustrates the UV/Vis spectral changes of the assembly (Fig. 9.26a) and disassembly (Fig. 9.26b) process. The TEM images of the disassembly also can be seen (Fig. 9.26c–f) [9.303].

Gold Nanorod Assembly Involving van der Waals and Dipole Interaction

Changing the hydrophilic nature of the GNR surface (due to the presence by of CTAB) to hydrophobic by treating with mercaptopropyltrimethoxysilane (MPS) and subsequently octadecyltrimethoxysilane (ODS) can induce formation of assembled structures. Well-ordered 2-D or 3-D superstructures of hydrophobic NRs on a substrate by solvent evaporation technique was reported by *Mitamura* et al. [9.311]. The concentration of the NRs controlled the 2-D assemblies and at lower concentration, the NRs assembled parallel to the substrate. Upon increasing the concentration, NRs started to stand on the substrate to form perpendicular assemblies forming hexagonal arrays. 3-D assemblies with a hexagonal close-packed structure due to their side-by-side interaction leading to lamellar structure (over small range) were observed when the NR sample was converted into a solid state.

Nakashima et al. devised a strategy to prepare surface-directed, lateral or perpendicular GNR assemblies [9.312]. This was achieved by anchoring a homemade peptide, 1,2-dipalmitoyl-*sn*-glycero-3-phosphothioethanol (DPPTE) onto the GNR surface. The drying method and the hydrophilic or hydrophobic nature of the Si surface influenced the form of self-assembled superstructures (Fig. 9.27). Driven by intermolecular interactions of surface-anchored lipids, the GNR–DPPTE hybrid formed characteristic 1-D and 2-D self-assemblies

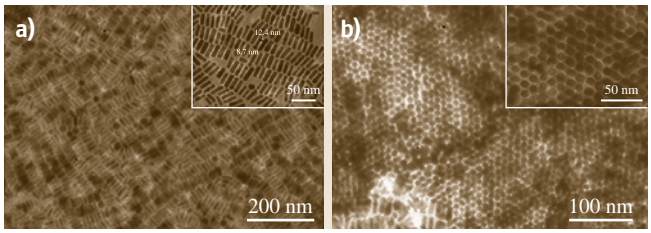

Fig. 9.27a,b TEM images of assemblies of hydrophobic GNRs arranged **(a)** parallel and **(b)** perpendicular to the substrate. *Insets* are the corresponding high magnification images (after [9.311])

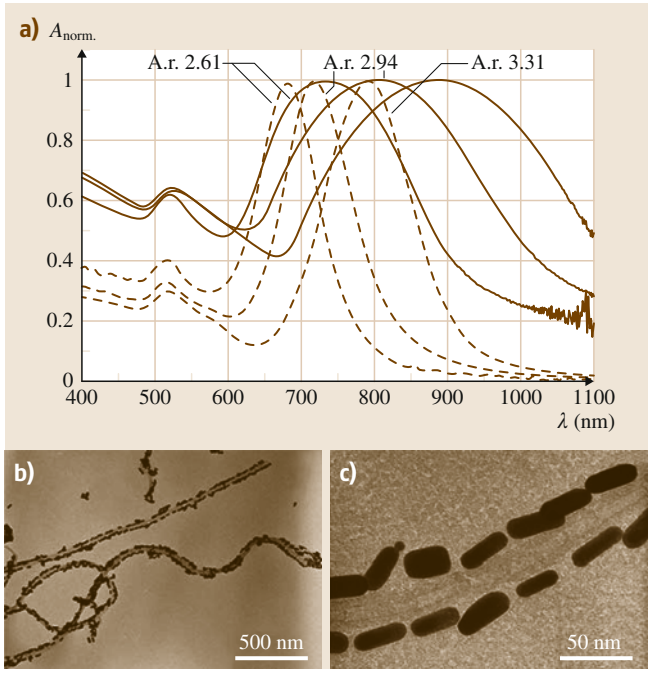

Fig. 9.28 **(a)** UV/Vis spectral changes and TEM images of GNRs (average AR 2.94) assembled on MWNTs (average diameter 30 nm) at different magnifications **(b,c)**

upon controlled drying process. Solvent evaporation from the sample drop in combination with interfacial hydrophilicity or hydrophobicity induced a variety of self-assembled structures. *Walker* and *Gupta* reported a reversible, pH-dependent strategy to form end-to-end assembly of GNRs functionalized with disulfide-modified poly(L-glutamic acid) [9.313].

Changes in pH of the medium-induced corresponding changes in the secondary conformation.

Recently, GNRs were assembled, disassembled, and reassembled by *Chan* et al. who used a bis(terpyridine)–metal connectivity [9.314]. A special molecular moiety (disulfide-modified terpyridine)2–M(II) (M = Fe or Cd) was used as interconnectors to form end-to-end linear and branched assembly of GNRs into multicomponent structures. Basic conditions destabilized the prepared (terpyridine)2–M(II) complexes and the addition of NaOH resulted in disassembly. When Cd was used to induce the assembly, the complexes formed were labile and the resultant assembly was also found to be labile. At low concentrations of Cd, assemblies were formed and in the presence of excess Cd(II) ions, they disassembled. Upon addition of Fe(II) to this disassembled system, they again reassembled into end-to-end chains. This also could also again be disassembled by a mere change in the pH as mentioned above [9.314].

Assembly on Templates

Assembly of NPs on templates is a widely utilized strategy. *Correa-Duarte* et al. was the first group to form GNR superstructures via this approach [9.315]. Multi-walled carbon nanotubes (MWNT) were used as the templates in this work. First the CTAB covering on the GNRs was interchanged with PVP. Then, MWNTs were coated with a polyelectrolyte, mainly polystyrene sulfonate (PSS), followed by poly(diallyldimethyl)ammonium chloride (PDDA). This wrapping resulted in the production of adsorption sites on the carbon nanotubes (CNTs) where GNRs could be deposited electrostatically. A preferential end-to-end assembly of GNRs, forming a string-like alignment (Fig. 9.28) resulted through this method. A broadened absorption feature exhibited by the superstructures indicated the formation of end-to-end assembly and the resultant plasmon coupling between neighboring NRs. It was also noted that these NRs can serve as a label to monitor the alignment of CNTs within polymer films [9.315, 316]. Using drying droplets as the templates, rings of NRs were fabricated by *Zubarev* and *Khanal* [9.317]. A simple and quantitative model for the formation of GNR rings was also described. Here, condensed water droplets from humid air on the surface of nonpolar solvents acted as templates for the spontaneous assembly of hybrid gold–polymer core–shell NRs.

Pradeep et al. reported the use of microgels as a template for a solution-phase method for assembling NRs into a hexagonal pattern [9.318]. First, poly(*N*-isopropyl acrylamide) (PNIPAm) microgels coated with GNRs were synthesized. For this purpose, microgels loaded with CTAB-coated GNPs of 4–5 nm size (used as seed particles) were added to the growth solution used for the seed-mediated growth method for GNRs. This helped in achieving the required population of

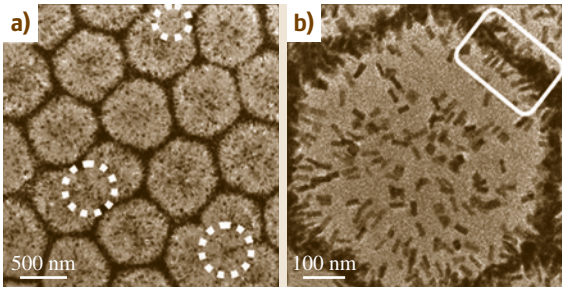

Fig. 9.29a,b TEM images of the GNR-PNIPAm composite. **(a)** Large-area image of the hexagonal pattern with defect sites marked with *dashed circles*. **(b)** Higher magnification image of a single cell of the hexagonal pattern confirming that the anisotropic structures sitting on the microgels are GNRs. From the authors' laboratory (after [9.318])

NRs on the microgels (Fig. 9.29a,b). These NR-loaded microgels were allowed to self-assemble to obtain a hexagonal pattern (Fig. 9.29c,d). Similar experiments performed with NP-coated or prefabricated NR-coated microgels did not give such hexagonal patterns because of the reduced number density of NPs. The interpenetration and interlocking of the NR structures were thought to be the reason for the formation of these patterns [9.318]. *Fava* et al. made use of the affinity of NRs for PNIPAm-based microgels for their sequestering by cationic, anionic, and close-to-neutral-state microgels [9.319]. Cationic, anionic, or near neutral microgels were fabricated by adjusting the pH of the solution. Sequestration of GNRs occurred independently of the charge of the microgels when added to the above solutions. This indicates that electrostatic interactions alone do not govern the loading of microgels with NRs. Electrostatic interactions and subsequent coating of silica with controllable thickness was used to assemble GNRs by *Wang* et al. [9.320].

Assembly on Substrates

Assembly of nanostructures on suitable substrates has the extra edge that it can be directly used for applications. *Mieszawska* et al. reported a methodology for directly growing highly aligned GNRs on a NH_2-functionalized Si(100) substrate with a remarkable degree of parallel alignment over large areas [9.321]. When a similar reaction was carried out on amorphous glass no assembled structure was observed, which pointed towards the importance of having a crystalline structure. However, throughout the sample, the alignment direction varied and no direct correlation between the arrangement of Si atoms and GNR assembly was seen. Hence it was concluded that the crystallinity of the substrate will not affect the direction of assembly. The exact mechanism of the assembly is still not well understood. Control experiments with mercaptopropyltrimethoxysilane (MPTMS) – and (aminopropyl) triethoxysilane (APTES) functionalized, or bare Si(100) did not produce any assembled structures, which indicates the importance of surface chemistry. However, the exact role of the amidation reaction in the alignment is not yet clear. *Mieszawska* et al. observed alignment on acetic and succinic acid surfaces implying the minimal role played by surface hydrophobicity [9.321]. End-to-end alignment of phosphatidylcholine-passivated GNRs adsorbed on polyanion-modified glass substrates were demonstrated by *Yamada* et al. [9.322]. *Zhang* and *Imae* successfully used a patterned silicon substrate with hydrophobic stripes for growing gold NR SLs [9.323]. Perpendicular SLs were also fabricated by this method. The most important factor governing the assembly was the substrate surface. GNRs should be either positively attracted or at least not repelled by hydrophobic surfaces in order to obtain a well-defined assembly. GNRs stayed in solution when the silicon substrate was hydrophilic. Another important criterion was the monodispersity of the sample devoid of particles without shape difference. *Zareie* et al. reported a protocol to directly grow end-to-end assembled long chains on a substrate embedded with a mixed self-assembled monolayer (SAM) that had been functionalized with streptavidin [9.324]. Assemblies extending over a micrometer in length with 5 nm inter-rod separation were obtained by this process.

Assembling by Polymer Tethering

A novel strategy where self-organization of GNRs into a predefined pattern by attaching multiple polymer arms termed *pom-poms* was reported by *Kumacheva* et al. [9.319, 325, 326]. NRs that are end-terminated with polystyrene (PS) when dispersed in dimethylformamide (DMF)/water mixtures tend to self-assemble into higher-order structures. The length and distribution of the PS molecules between the ends and the longitudinal facets of the NRs controls the ordering. Changing the structure of the polymer pom-poms also can modulate the assembly. Depending upon the variation in the molecular weight of the polymers and their relative location on the long side of the NRs, various kinds of NR assemblies namely bundles, bundled chains, and chains involving side-by-side and end-to-end assembly were generated. By changing the concentration of

water in the system, one form of assembly can be changed to another one. It was also understood that the evolution of the self-assembled structures of GNRs end-terminated with PS occurs through competition between side-to-side and end-to-end assemblies. This competition is due to the difference in solubilities of the PS and CTAB-coated metal blocks in the solvent mixture. The tendency to side-to-side aggregation was found to be dominant over most of the compositional range. The above tendency was reduced at high DMF or water content and at very low THF/DMF weight ratios [9.319, 325, 326].

Layer-by-Layer Assembly of Gold Nanorods into Gold Nanorod Films

Yun et al. recently developed a protocol for assembling GNRs into 2-D arrays at a water/hexane interface without the aid of any linker molecule [9.327]. In this method, aggregates of GNRs with a relatively clean surface and controlled NR density were obtained and the film thickness can also be controlled systematically. Because GNRs are hydrophilic, they have a contact angle of $< 90°$ at a water/hexane interface and they will always remain in the aqueous phase. However, when their contact angle is approximately equal to 90°, these particles start to adsorb to the water/hexane interface. A medium with high dielectric constant can separate the charged particles from each other. However, the introduction of a miscible solvent with lower dielectric constant will result in a decrease in the dielectric constant of the medium. Consequently, the surface charge of the particles will also be decreased as a function of the amount of miscible solvent added. When ethanol (with a lower dielectric constant) is added to the water/hexane interface, the surface charge density of the NRs decreases and the NRs are brought to the interface. The reduction in the interfacial energy at the water/oil interface upon the reduction of the dielectric constant of water is the driving force for this entrapment of the NRs. The thickness-dependent SERS activity of the resultant films (when molecules adsorbed on these NR films) has been investigated, and it was found that NR films have an order of magnitude stronger SERS enhancement compared to nanosphere films under similar experimental conditions [9.327].

Gold Nanorod Assembly by Surface Anchored Crown Ethers

Surface anchored crown ethers (end-functionalized) on GNRs were used to induce assembly of GNRs where the addition of specific metal ions resulted in the assembly formation. The approach was reported by *Nakashima* et al. [9.328]. They synthesized two thiol-modified crown ethers, 2-((6-mercaptohexyl)oxy)methyl-15-crown-5 (15-crown-5-SH) and 2-((6-mercaptohexyl)oxy)methyl-12-crown-4 (12-crown-4-SH) and the synthesized crown ethers were added to purified NR dispersions. Covalent attachment of these crown ethers onto the end faces of the NRs through the thiol moieties is possible. In the presence of metal ions corresponding to the anchored crown ethers, assembly of the GNRs resulted. The concentrations of crown ethers and cations added controlled the structure of the GNR aggregates assembled (side-to-side and end-to-end fashion). UV/Vis spectra demonstrated the corresponding changes and the intensity of the longitudinal absorption of the NRs gradually decreased, and the peak was initially red-shifted and then blue-shifted. Potassium ions (K^+) can form a 2 : 1 sandwich complex between the 15-crown-5 moiety, leading to assembly formation and resultant coupling of the plasmon absorbance, in turn leading to changes in the spectral features. This was used for specific detection of metal ions.

Gold Nanorod Assembly Induced by a Magnetic Field

Magnetic field-induced assembly of GNRs is possible by imparting magnetic characteristics to GNRs. For this, Pt-doped GNRs (Fig. 9.30a) were homogeneously coated with metallic Ni through hydrazine reduction in aqueous solutions. This resulted in a quasi-epitaxial growth of an Ni shell on the GNRs (Fig. 9.30b) [9.329]. Since Pt has a much higher redox potential, it will become reduced first compared to nickel. Upon reduction Pt forms small nuclei which act as a *nucleation agent*, on which Ni can be catalytically reduced. When the Ni-coated GNRs (Au@Ni NR) were allowed to dry on a TEM grid under the influence of an external magnetic field (0.2 T), the NRs became aligned in a chain-like structure in the direction of the applied field (Fig. 9.30c). However, the orientation of individual rods within the chains was not found to be the same and coexistence of both *side-to-side* and *end-to-end* assemblies was observed, pointing towards the complex magnetic response of the system [9.329].

Assembly of Various Anisotropic Nanostructures of Silver

Compared to gold, anisotropic silver NPs are more diverse. The main limitation in the case of Ag anisotropic particles is the difficulty to synthesize of them in

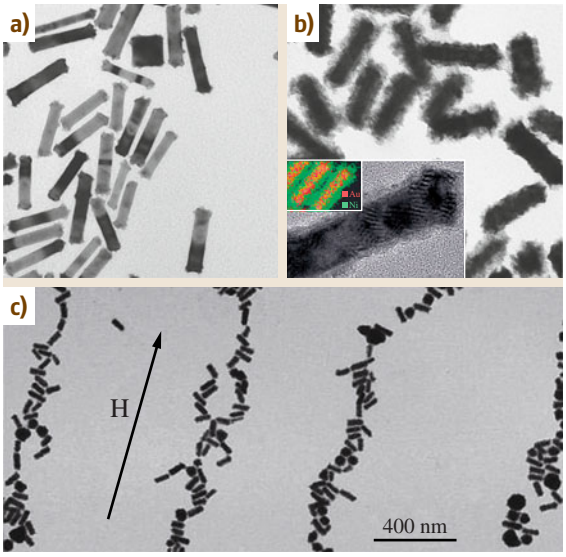

Fig. 9.30a–c Large area TEM of **(a)** GNRs after tip-coating with platinum and **(b)** nickel coated GNRS in the absence of magnetic field. *Inset* shows a high magnification image of a single Au@Ni NR and STEM-EDAX (STEM: scanning TEM) analysis of Au@Ni NRs, showing the relative distribution of the elements (Au = *red*; Ni = *green*). **(c)** Au@Ni NRs, dried on the TEM grid under an external magnetic field (0.2 T) (after [9.329])

a monodisperse fashion. The presence of a surfactant that caps the nanostructures formed and avoids their aggregation is common in all synthetic methodologies, and hence surfactant-induced assembly of these structures upon solvent evaporation is highly feasible. *Jana* et al. devised a seed-mediated growth approach for preparation of silver NRs with varied ARs [9.330]. The approach was very similar to that used for making GNRs. A spontaneous self-assembly process assisted by solvent evaporation was observed upon shape separation of these NRs, resulting in a 2-D smectic liquid-crystal-like superstructure (Fig. 9.31a,b). Recently, a new method to produce monodisperse size-controlled faceted pentagonal silver NRs by thermal regrowth of decahedral silver NPs using citrate as the reducing agent was reported by *Pietrobon* et al. [9.43]. The resultant structures were highly monodisperse and showed a great tendency to self-assemble into smectic mesophases such as densely packed rafts and 3-D arrays when the dispersions dried (Fig. 9.31c–h). It was also noted that the fivefold symmetry of the constituent NRs is always overridden by the long-range hexagonal order within the layers [9.43].

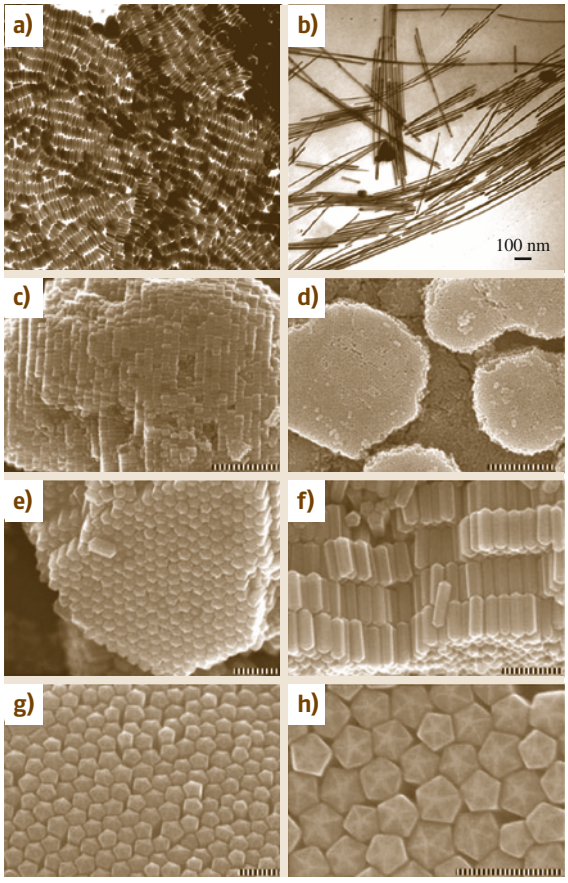

Fig. 9.31a–h TEM image of shape-separated **(a)** silver NRs self-assembled on TEM grids and **(b)** silver NWs. **(c–f)** SEM images of self-assembled packing of monodisperse faceted pentagonal rod AgNRs with different aspect ratio forming 3-D superlattices. **(g,h)** show the top view of the assembly (**(a,b)** after *Jana* et al. [9.330] and **(c–f)** after [9.43])

The Langmuir–Blodgett (LB) technique is one of the most widely used methods to assemble a large area monolayer of nanosystems. Nanowires (NWs) with ≈ 50 nm diameter and 2–3 μm length were assembled into a large area of about 20 cm^2 by *Tao* et al. using this approach (Fig. 9.32) [9.331]. First, the PVP capping of the as-prepared NWs was replaced with 1-hexadecanethiol ligands to make them hydrophobic.

These NWs were then redispersed in chloroform, followed by transferal onto a water surface of the LB trough and were then assembled by the LB method. Large area, side-by-side aligned NWs resembling the nematic 2-D ordering of a liquid crystal were obtained.

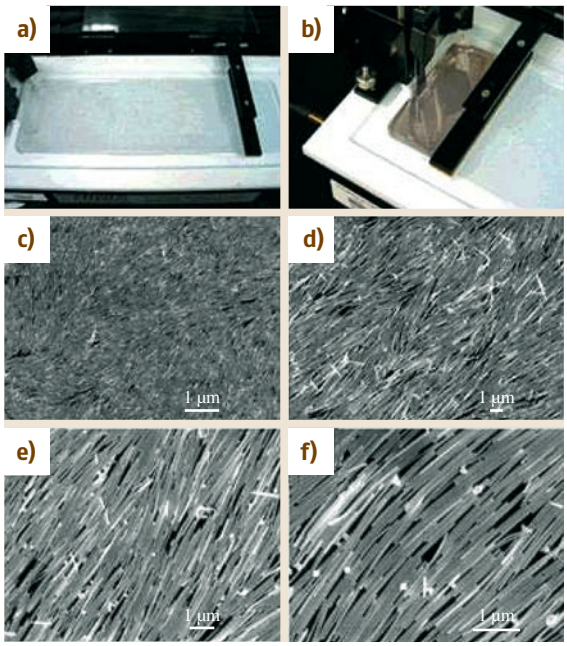

Fig. 9.32 (a,b) Photographs of LB NW assembly process at different compression stages. (c–f) SEM images (at different magnifications) of the silver NW monolayer deposited on a silicon wafer (after [9.333])

An alternating extinction pattern was exhibited by these aligned NW areas when the sample was rotated every 45° [9.331]. The same group, following a similar methodology, was able to create novel SL architectures composed of different polyhedral building blocks, including truncated cubes, cuboctahedra, and octahedra of Ag nanocrystals [9.332]. In the superstructures formed, the packing and the dimensions were determined by the choice of the nanocrystal building block. For example, truncated cubes formed a square lattice by assembling in a face-to-face manner. However, cuboctahedra (which are comparatively more truncated polyhedral particles) assembled to make a rhombohedral unit cell, formed by shearing of the square lattice [9.332].

Bae et al. recently reported the assembly of Ag nanoprisms (Fig. 9.33a,b) [9.334]. They were able to assemble the prisms with anisotropic orientation and studied the orientation-dependent properties of these assemblies [9.334]. *Rycenga* et al. reported an interesting strategy to assemble Ag nanocubes by selective functionalization of each face [9.332]. They prepared five distinct SAM-modified Ag nanocubes from the possible combinations of hydrophobic and hydrophilic faces and these were assembled into four different nanostructures and one microstructure (Fig. 9.33c–f). The mechanism of the assembly was explained on the basis of hydrophobic interaction and solvation-free energy. Figure 9.33c depicts the methodology adopted for selective functionalization of the Ag cube faces. The selective functionalization was carried out by protecting the Ag nanocube, faces which are in direct contact with

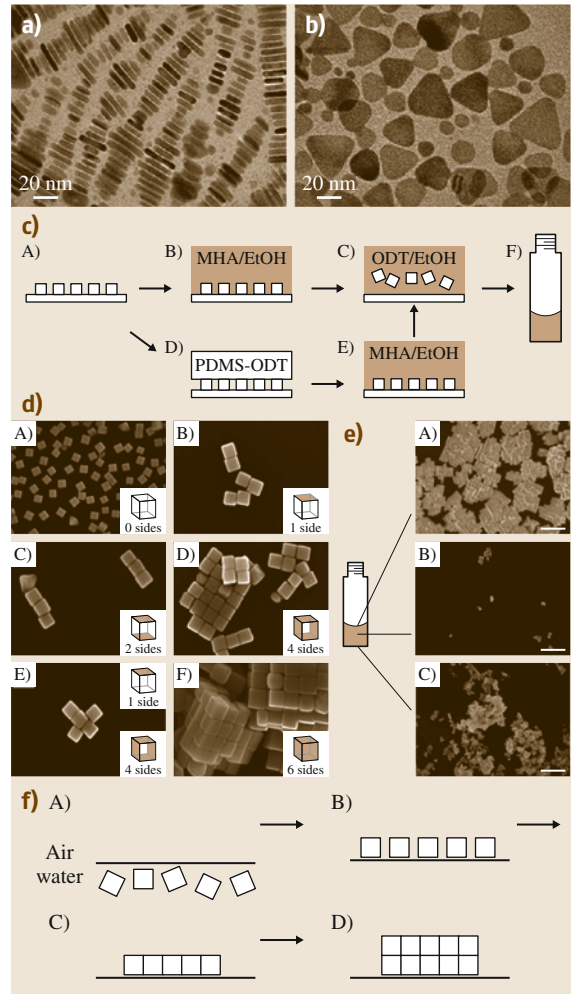

Fig. 9.33a–f TEM images of assembly A (a) and B (b) (after *Bae* et al. [9.332]). (c) A schematic representation of specific functionalization of Ag nanocube faces. (d) SEM images of Ag nanocubes and the assemblies depending upon the functionalization. (e) SEM images of ODT-functionalized Ag nanocubes sampled at different parts in a reaction vessel. (f) Schematics depicting the mechanism of formation of self-assembly at the air–water interfaces (after [9.332])

a clean Si substrate, and the free faces were functionalized sequentially with solutions of alkanethiols, and polydimethylsiloxane (PDMS) inked with alkanethiols. Nanocubes that were not functionalized did not show any tendency to assemble. Single face functionalization of the nanocube with hydrophobic octadecanethiol (ODT), resulted in the formation of dimers, joined at the hydrophobic faces in order to try and move this face away from water. Nanocubes with two opposing faces functionalized with ODT formed linear chains.

When four faces of the nanocubes were functionalized with ODT, a sheet-like superstructure was obtained. Upon mixing Ag nanocubes with four hydrophobic faces and one hydrophobic face (1 : 4 ratio), star-shaped structures were obtained. When all six faces were functionalized, they formed 3-D SLs. Figure 9.33f schematically illustrates the self-assembly process of Ag nanocubes, completely functionalized with a hydrophobic SAM, at the air–water interface [9.332].

9.6 Functionalized Metal NPs

The adding of more functional capabilities and preparing functionalized nanomaterials has received considerable attention in the recent past. The main strategies for functionalization are ligand exchange reaction, using modified thiol as the capping agent in the Brust method or adding more components to the system such as making core–shell structures. In this section, various methods employed for the functionalization of monolayer-protected NPs and various approaches for the synthesis of functional core–shell particles are discussed. The presence of thiol end groups on the ligand have been utilized to anchor various photoactive molecules such as derivatives of porphyrenes [9.336], fullerenes [9.337], pyrenes [9.338], stilbenes [9.339], fluorenes [9.340], resorcinarenes [9.341], azobenzenes [9.342], etc., on the surface of GNPs.

GNPs having a double shell structure with the inner shell made of spiropyran have been used to control the photo-controlled binding and release of the outer shell of amino acids [9.343]. In the absence of light, spiropyran moieties exist as closed-rings (a nonpolar colorless form). Upon irradiation of light, spiropyran changes to the highly polar, colored merocyanine form. This merocyanine (the open ring form) can complex with amino acids to form the second layer (Fig. 9.34). Thus, this system can be used for the light-mediated binding and release of amino acid derivatives.

In specific cases, the attachment of a fluorescent moiety onto the surface of NPs was found to alter the fluorescence intensity. For example, attachment of pyrenemethylamine on GNPs found to increase in the fluorescence of pyrene [9.343]. Generally, metals quench the fluorescence and the observed trend was different. This difference was explained as follows. The binding of nitrogen onto gold suppresses the electron transfer between the nitrogen and the pyrene ring (Fig. 9.35), which results in enhanced fluorescence.

9.6.1 Core–Shell Nanoparticles

Particles with a well-defined core and a shell (both in the nanometer regime) are called core–shell NPs. They have found applicability in diverse fields such as pharmaceuticals, chemical engineering, biology, optics, drug delivery, and many other related areas in addition to chemistry. Recent years have seen large efforts

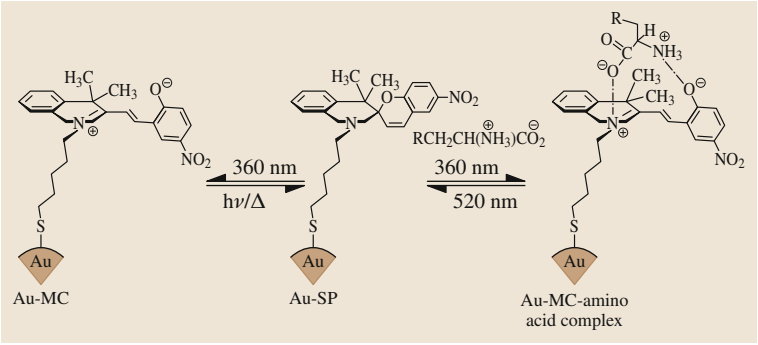

Fig. 9.34 Reversible binding of amino acids with spiropyran-capped GNPs (MC: metal cluster) (after [9.335])

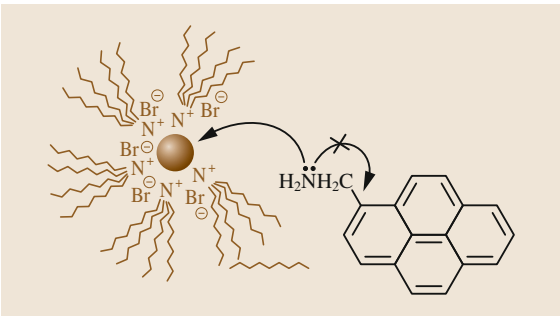

Fig. 9.35 Gold NP-assisted enhancement of fluorescence in pyrenemethylamine. Due to the attachment of nitrogen onto the NPs, conjugation between the lone pair on nitrogen and the pyrene ring is blocked. This is indicated by an *arrow with a cross mark* (after [9.343])

to develop core–shell colloidal NPs with tailored structural, optical, surface, and other properties [9.344, 345]. The formation of a protecting shell to the core imparts several functional attributes to these hybrid structures. They are:

1. Solubility and stability
2. Monodispersity in size
3. Ease of self-assembly
4. Core and shell processability
5. Applications in catalytic, magnetic, chemical, and biological fields, as well as in nanoscale electronics and optics.

A brief description of the diversity of core–shell systems involving noble metals is presented below.

Metal–Metal Oxide Core–Shell NPs

The scientific community has shown tremendous interest in this category of NPs, and these are among the most widely studied core–shell nanosystems. As discussed in an earlier section, the intense color exhibited by metallic NPs can be varied by controlling the size of these NPs. However, the chance of aggregation is a major problem associated with their handling. Making core–shell structures is one of most efficient ways to overcome this difficulty. Various strategies such as coating with silica [9.346], titania [9.347], zirconia [9.348], and maghemite [9.349] have been reported in this direction. A procedure to prepare silica-coated nanosized metal NPs was reported by *Liz-Marzán* et al.. This procedure is applicable for various metals such as Au, Ag, and CdS [9.350]. The approach involves the use of 3-aminopropyltrimethoxysilane (APS), the silane coupling agent, which can bind to the NP surface. This also

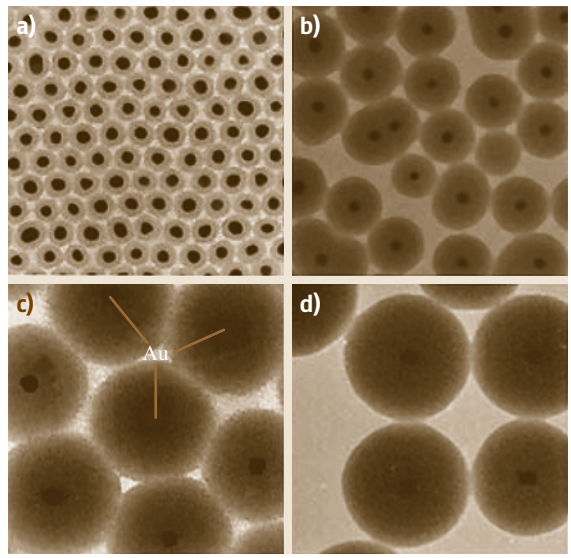

Fig. 9.36a–d TEM images of silica-coated GNPs. The shell thicknesses are **(a)** 10 nm, **(b)** 23 nm, **(c)** 58 nm, and **(d)** 83 nm (after [9.344])

acts as an anchor point for chemical deposition of silica (SiO_3^{2-}).

In this method, the shell thickness of the silica can be controlled (from 10–83 nm) and according to the thickness, the absorption characteristics are also tunable [9.344]. TEM images of Au@SiO_2 NPs with different shell thicknesses synthesized using the above method are shown in Fig. 9.36. Methodologies for the creation of various other inorganic coatings such as zirconia, yttrium basic carbonate, titania, titanium nitride, and Fe_2O_3 are available in the literature. Factors such as the size and shape of the core particles and the relative ratios of the reactants can control the thickness of the shell. *Liz-Marzán* et al. prepared TiO_2-coated Ag NPs by simultaneous reduction of Ag^+ and condensation of titanium butoxide [9.347]. As an extension to this methodology, ZrO_2- and TiO_2-coated Au and Ag NPs were prepared later [9.348].

A single-pot method for the synthesis of Pt–maghemite (Fe_2O_3) core–shell NPs where the reduction of platinum acetylacetonate in octyl ether produces Pt NPs and subsequent thermal decomposition of iron pentacarbonyl creates layers of iron oxide on the surface was reported recently [9.349]. The complexation of a negatively charged titanium(IV) bis(ammonium lactate) dihydroxide with poly(dimethyldiallylammonium hydroxide) was used for coating Au NPs with titania by *Mayya* et al. [9.351].

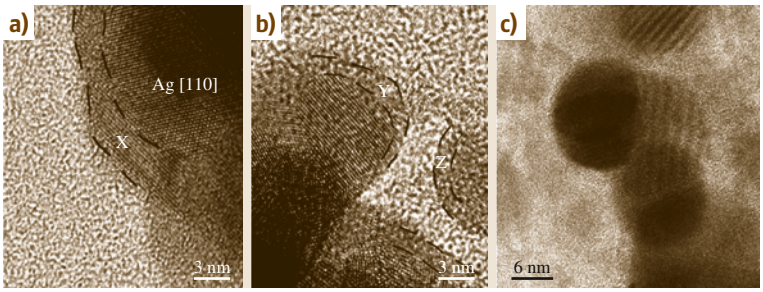

Fig. 9.37 HRTEM images of $Ag@ZrO_2$ core–shell NPs functionalized with a stearate monolayer (after [9.352])

Reverse micelle and sol–gel techniques are also employed for synthesis of metal–metal oxide core–shell NPs. The inorganic coatings around the NPs modify the optical properties of the systems in addition to stabilizing them against coalescence. The core–shell geometry also allows shell functionalization using appropriate organic monolayers [9.352] for better redispersibility and ease of handling. High-resolution TEM images of a stearate-functionalized $Ag@ZrO_2$ core–shell NP are shown in Fig. 9.37. Although the organic monolayer build-up around the ZrO_2 shell is not clearly seen, the distinct core–shell geometry is visible from the image.

A special approach to synthesize $Au@SiO_2$ core–shell NPs by incorporating a mercaptosilane at the core–shell interface was devised by *Chen* and *Katz*, who exploited the strong interaction between thiols and gold [9.353]. They achieved the highest degree of functional group organization at the core–shell interface. Recently, Wang et al. synthesized Au–SiO_2 inverse opals by colloidal crystal templating.

Bimetallic Core–Shell NPs

Due to the high demand for catalysis, a large number of bimetallic core–shell NPs has been synthesized lately. Some important examples are the synthesis of Au-Pt core–shell alloys by the simultaneous reduction of chloroauric acid and chloroplatinic acid by *Henglein* [9.117], a single-step procedure for the synthesis of Au-Pt core–shell NPS by *Yonezawa* and *Toshima* [9.354], the synthesis of Au core–Pt shell NPs by simultaneous reduction of $PtCl_6^{2-}$ in aqueous gold sol by *Schmid* et al. [9.355], etc. The synthesis of a variety of bimetallic systems including Ag/Cd, Ag/Pb, and Ag/In by a γ-irradiation-based approach was reported as early as 1980 by *Henglein* [9.117]. Synthesis of Ag-Au core–shell NPs by *Mulvaney* et al. [9.356] and *Link* et al. (NPs of 17–25nm size) are also available in the literature [9.357]. *Kim* et al. synthesized Au-Ag core–shell NPs and studied their optical characteristics such as linear extinction and resonant hyper-Rayleigh scattering [9.358].

The optical behavior and stability of Ag core–Co shell NPs was studied by *Sobal* et al. They showed that the core–shell particles exhibit an optical behavior distinct from the individual components, and the presence of a noble metal also protects the Co shell against oxidation [9.359]. *Cai* et al. developed a low-temperature synthetic protocol for Cu@Au core–shell NPs [9.360]. The formation of core–shell alloy NPs resulted in a good voltammetric response of Cu, which was utilized for electrochemical DNA hybridization detection assays. The oxidative peak current of the Cu colloid is much higher than that of Au of the same size and quantity. The coating of a layer of Au on the Cu core helped to protect the Cu from oxidative degradation and can also provide an active surface for immobilization of oligonucleotides. The synthesis of dumbbell-shaped Au-Ag core–shell NRs by seed-mediated growth under alkaline conditions was reported by *Huang* and *Matijevic* [9.361]. This method uses GNRs as seeds in the presence of Ag and ascorbate ions. Ag ions that are reduced by ascorbate are deposited on the surface of the Au NRs to form dumbbell-shaped Au-Ag core–shell NRs. Recently, the synthesis of Au-Ag core–shell NPs using tyrosine as a pH-dependent reducing agent was reported by *Sastry* et al. [9.362].

Semiconductor Core–Shell NPs

Similarly to metallic NPs, semiconductor nanocrystals also exhibit interesting size-dependent optical properties (fluorescence) due to the confinement of electronic wave functions. However, in order to obtain highly luminescent nanocrystals, their surface must be precisely controlled. The presence of a large number of surface defects (e.g., nonstoichiometry, unsaturated bonds, etc.) can have a large impact on their luminescence. Core–shell-type semiconductor NPs or quantum dots demonstrate novel properties that make them attractive for various applications. The photoluminescence quantum

yield can be increased by covering the nanocrystallites with higher-band-gap inorganic material, which passivates the surface nonradiative recombination sites. Moreover, compared to their organic analogs, NPs covered with inorganic composite materials are much sturdier and more stable. *Yang* et al. reported the off-resonance optical nonlinearities of Au@CdS core–shell NPs, embedded in $BaTiO_3$ thin films [9.363]. Due to their large third-order nonlinearities and ultrafast nonlinear optical response, semiconductor NPs are attracting a great deal of attention.

Polymer-Coated Core–Shell NPs

Polymer-coated core–shell NPs have found application possibilities in diverse fields ranging from catalysis to industry where these NPs are used in making additives, paints, and pigments, etc. There are mainly two classes of synthetic methodologies for polymer capping of NPs, namely: (a) polymerization at the NP surface, and (b) adsorption of preformed polymer onto the NP cores. The most common methods used for the preparation of polymer core–shell structures are:

1. Monomer adsorption onto NPs followed by polymerization [9.360, 365–367]
2. Heterocoagulation polymerization [9.364]
3. Emulsion polymerization [9.368, 369].

The colloidal particles themselves or an external initiator added to the reaction mixture can catalyze the polymerization. Using a pretreatment method, *Huang* and *Matijevic* [9.361] reported the synthesis of polydivinylbenzene coated silica particles. Following a similar strategy, polydivinylbenzene–poly(vinylbenzyl chloride) copolymers, poly(vinylbenzyl chloride), and double shells of polydivinylbenzene and poly(vinylbenzyl chloride) were also synthesized. In specific cases, where cores consist of dyes, polymer coating of the particles allowed the dyes to be retained inside the nanocores because the polymer shells are permeable only to small inorganic ions and not to big dye molecules. As was mentioned before, polymerization can also take place in the presence of catalytically active cores.

Several factors affect the thickness of the polymer coating: the contact time with the core, the type of core employed, and the nature of the polymer [9.360]. *Feldheim* et al. reported an excellent strategy for the synthesis of polymer-coated NPs [9.364] where the particles in the pores of a membrane were trapped and aligned by vacuum filtration. Then, inside the pore, the monomers were polymerized. Through this method, polypyrrole coated Au NPs can be prepared; corresponding TEM images are shown in Fig. 9.38. Figure 9.38b illustrates the increased shell thickness as a result of the change in the monomer for the polymer shell. Hence, this methodology allows control of the thickness and composition of the polymer coating. Generally for most of these polymerization reactions, the thickness of the coating depends on the polymerization time. Heterocoagulation of small particles with larger ones assisted with heating is another widely used method for preparing polymer coating. Through this method, polystyrene cores coated with a uniform layer of polybutylmethacrylate have been prepared.

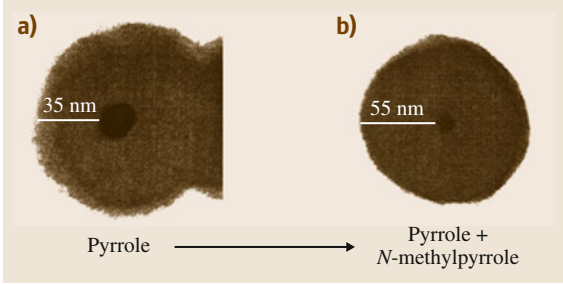

Fig. 9.38a,b TEM of polypyrrole-capped Au NPs **(a)** and with further increase in shell thickness by polymerization with poly(*N*-methylpyrrole) **(b)** (after [9.364])

The third technique, emulsion polymerization, has been widely employed for the synthesis of polymer-capped core–shell NPs. The important feature of this approach is that NPs of different size regime (from sub-nanometer to micrometer-sized organic and inorganic particles) can be coated with polymer. Polymerization of styrene and/or methacrylic acid in emulsions of oleic acid resulted in the formation of a uniform polymer layer around the metal core. Compared to uncoated particles, the polymer-coated particles are highly etch-resistant and can be easily centrifuged and redispersed. These NPs can be made in the form of thin films through the use of self-assembly techniques. The layer-by-layer (LbL) templating strategy is commonly used for this. Here, a polymer solution (having an opposite charge to that on the particles) in excess of that required for saturation adsorption is added to the colloidal dispersion. The polymer adsorbs onto the NPs through electrostatic interactions.

9.7 Applications of Gold and Silver Nanoparticles

The unique properties exhibited by gold and silver NPs such as SPR, SERS, nonlinear optical properties, quantized charging effect, etc., have been utilized for a variety of applications in the areas of biolabeling, bioimaging, sensors, catalysis, nanodevices, nanoelectronics, etc. [9.1, 154, 370, 371]. Although noble metal NPs have a long history as materials for many therapeutic applications, the advancements in the area of nanochemistry have broadened their potential in various biomedical applications. Apart from their biocompatibility, unique properties, and ease of functionalization with various biological molecules, noble metal NPs have been used for targeting and delivery of therapeutic doses of drugs to cancer cells. The large extinction cross-sections and tunable optical absorption of NPs such as NRs, NTs, nanocages, etc., in the NIR region (a wavelength region where blood and tissues are relatively transparent to radiation) make them good candidates for diagnosis and many other medical applications. The strong SPR of metal NPs enables imaging of individual particle locations with the use of various optical microscopic techniques such as dark-field optical and two-photon luminescence (TPL) microscopy [9.372]. GNRs and nanocages are ideal candidates for cancer cell imaging due to their tunable SPR peaks and scattering in the near infrared. The usefulness of gold nanocages as optical contrast agents has been demonstrated by optical coherence tomography (OCT) imaging [9.144]. They are the perfect raw material for robust and rapid diagnostic testing for many diseases. Living cells are highly sensitive to temperature, and increases of a few degrees can lead to cell death. NIR absorption and related photothermal effect are other important features of anisotropic GNPs [9.144, 370]. Compared with other nonmetallic photothermal absorbers, GNPs enable dual imaging/therapy functions. It has been demonstrated that several anisotropic nanomaterials such as NRs, NTs, nanocages, nanoshells, nanostars, etc., can be used for photothermal therapy [9.144, 370].

Gold and silver NPs have been found to be useful for optical limiting applications as well. Optical limiters have found applicability in fields including sensor and eye protection, optical communications, and optical information processing. Optical bistable materials are useful for functions such as logic gating and pattern recognition in optical computers. The applicability of Au, Ag, and Au-Ag alloy nanosystems for optical limiting applications was investigated in 2000 [9.373]. Initially, octanethiol and octadecanethiol-protected Au, Ag, and Au-Ag alloy NPs were synthesized, and optical nonlinearity was induced by 35 ps pulses at 532 nm. The samples were investigated using the Z-scan technique. It was found that they behaved either as saturable absorbers or reverse saturable absorbers, depending on the intensity of excitation. It was also found that Au and Ag NPs show nearly the same efficiency for optical limiting; however, the alloy clusters were found to be less efficient in limiting and were less photostable. An explanation based on the electron dynamics of the excited-state species was given for the behavior observed [9.373].

Gold and silver NPs have attracted considerable attention due to their high SERS [9.217, 374] activity, thus possessing strong advantages for the detection of molecules. They have been found to be useful for many applications in trace analysis of pesticides, biomolecules, bacteria, viruses, specific antigens, glucose, DNA, explosive materials, etc. [9.375]. Recently, it has been found that silica-coated GNPs can enhance the sensitivity of this method, and even detection of adsorbed hydrogen is possible with such materials [9.376]. Single-molecule detection is possible using SERS, and several protein and nucleic acid biosensors have been designed using this property of GNPs [9.375].

The properties of GNPs such as intense SPR and scattering of visible light have also been used for sensing applications. A variety of schemes based on the LSPR of GNPs have been developed for sensing organic vapors [9.377]. A composite material made of GNPs with pH-sensitive polymers has been used in a variety of pH-sensing schemes. GNP-based technologies are showing great promise in providing solutions to a number of environmentally important issues. They are highly promising for sensing and removal of heavy metal ions from water [9.378]. GNP-based colorimetric sensors have been widely used in this direction, overcoming some of the limitations of conventional methods because these assays do not use organic solvents, light-sensitive dye molecules, or sophisticated instrumentation. GNRs are capable of quick and selective sensing of mercury in tap water samples at the ppt level [9.379]. The selectivity and sensitivity towards mercury are due to the amalgamation of mercury and gold. Complete removal of mercury from water can be done by using GNPs supported on alumina [9.380].

Catalysis by active oxide-supported gold, silver, platinum, and palladium NPs is an ever-expanding area,

and a large number of new catalytic systems for various reactions have been widely exploited for many applications. GNPs can oxidize highly toxic CO to far less toxic carbon dioxide [9.222, 380]. More recent investigations have shown that GNPs adsorbed and dispersed on an oxide support can be used as an efficient catalyst for hydrogenation of unsaturated substrates [9.1]. Thus, shape and crystal structure differences can lead to different catalytic rates [9.381]. In homogeneous catalysis, *Narayanan* and *El-Sayed* demonstrated that shapes with more corners and edge atoms have higher reactivity than similar NPs with fewer corner and edge atoms [9.382]. Catalytically active bimetallic gold–palladium NPs proved to degrade organic pesticides effectively [9.383]. GNPs are also used in solar cells to improve the efficiency, as the GNPs enhance the optical absorption in the range of visible light [9.1]. It has been recognized that NIR absorbing films made from GNPs can be used as an alternative to reflective coatings for blocking infrared (IR) radiation. NP-based approaches are highly desirable, being more economically viable than other methods. Certain nanomaterials have been used for the development of IR filters. Using a prototypical device, *Pradeep* and *Sajanlal* have demonstrated that the NIR-IR absorption exhibited by gold MFs can absorb a significant amount of heat, thereby reducing the temperature rise in an enclosure exposed to daylight [9.160]. A few of these application possibilities are described in detail in the following section.

9.7.1 Water Purification

Among all these application possibilities, water purification remains one of the most important fields of application for any material. Noble metal NPs have also found tremendous possibilities in this arena as well. A specific review on this topic was discussed by the author in recent work, where a description about the important events during last 200 years in the area of drinking water purification was presented [9.23]. This section gives an overview about the use of noble metal NPs for the removal and detection of severely toxic contaminants including pesticides, halogenated organics, heavy metals, and microorganisms found in drinking water.

Degradation and/or Removal of Pesticides with Noble Metal NPs

The chemistry of noble metals (even in bulk form) for catalytic synthesis of organic compounds is well documented. However, their reactivity with halogenated hydrocarbons was not explored until recently. The first example for a metal (here, a transition metal) interacting with halogenated organics was initiated following the discovery that zero-valent iron catalyzed degradation of halogenated aliphatics [9.384]. Similarly, there were attempts to study the degradation of halocarbons [9.385] by using other reactive metals such as magnesium, tin, and zinc. However, until 1998, noble metals were never thought to be attacked by halocarbons. Noble metals had very low reactivity. However, later investigations revealed that in colloidal state noble metals are reactive. It was postulated in early 1998, based on absorption studies of silver colloid with oxygen and carbon tetrachloride, that carbon tetrachloride induces oxidation of silver colloid in a manner similar to oxygen [9.386]. Another study concluded that the degradation of noble metal clusters can be done by chlorine radicals produced by UV irradiation of halogenated organics [9.387]. It was also suggested that many organosulfur compounds adsorb on noble metal NP surfaces [9.388] and carbon disulfide undergoes dissociation on silver surfaces.

In early 2003, the first detailed report, from the authors' group, appeared on the interaction of noble metal NPs with halocarbons [9.389]. In a manner strikingly similar to the reaction of other metals with halocarbons, nanoscale noble metals also react with halocarbons. Through reductive dehalogenation, the reaction leads to the formation of metal halide. An important thing to be noted is the formation of amorphous carbon in this process [9.389], and harmful that the reaction proceeds efficiently at room temperature [9.389]. The reaction of noble metal NPs with halocarbons could be considered as a classic example of the particle size-based reactivity of metals [9.389] as noble metals in bulk form are not attacked by halocarbons.

Using a number of spectroscopic techniques, this reaction was studied to understand the reaction mechanism [9.389]. It was observed that plasmon intensity in the absorption spectrum gradually decreases without any shift in the plasmon peak position. When the reaction product obtained at the end of the reaction was analyzed using x-ray diffraction (XRD), features were similar to AgCl. Thus the conversion of metal to metal halide was confirmed. In the Raman spectra, broad G and D-band signatures of the amorphous carbon centered at 1550 and 1288 cm^{-1} was seen, pointing towards the formation of amorphous carbon.

Gas chromatographic and IR spectroscopic measurements also confirmed the complete mineralization of the halocarbon, as there were no reaction prod-

ucts. A reaction mechanism was suggested that depends on the spectroscopic observations [9.389]. We can represent the reductive dehalogenation of carbon tetrachloride as

$$4\mathrm{Ag} + \mathrm{CCl_4} \rightarrow 4\mathrm{AgCl} + \mathrm{C} \quad \Delta H = 1.2\,\mathrm{kJ/mol}\,.$$

We can also consider the reaction from an electrochemical standpoint as

$$\begin{aligned} \mathrm{Ag} &\rightarrow \mathrm{Ag^+} + \mathrm{e} \\ &\Delta E_{\mathrm{OXDN}} = -0.80\,\mathrm{V} \\ \mathrm{CCl_4} + \mathrm{H^+} + 2\mathrm{e} &\rightarrow \mathrm{CHCl_3} + \mathrm{Cl^-} \\ &\Delta E_{\mathrm{RDCN}} = +0.67\,\mathrm{V} \\ \mathrm{CHCl_3} + \mathrm{H^+} + 2\mathrm{e} &\rightarrow \mathrm{CH_2Cl_2} + \mathrm{Cl^-} \\ &\Delta E_{\mathrm{RDCN}} = +0.56\,\mathrm{V}\,. \end{aligned}$$

The excess surface energy of the NPs is the reason behind the reaction proceeding at the nanodimension. This is very helpful in overcoming the thermochemical barrier and the reductive dehalogenation reaction is exothermic [9.389]. After understanding the mineralization of halocarbons, the research was extended to the field of pesticides. They are another important family of halogenated organics. Pesticides such as endosulfan [9.390] and chlorpyrifos [9.391,392] belong to halogenated organic family, and malathion [9.391, 392] is an organophosphate type pesticide.

When the pesticides interacted with gold and silver NPs, their spectroscopic behaviors were different. A decrease in plasmonic absorption intensity was observed when endosulfan reacted on gold. There was the emergence of an additional peak at higher wavelengths as well [9.393]. This was due to adsorbate binding onto the NP surface, thereby leading to particle aggregation. IR measurement on the residue obtained after the adsorption process showed a substantially broadened signature of the pesticide. There were significant changes in the feature at 1192 $\mathrm{cm^{-1}}$ (Si=O bond) and negligible changes in the feature at 750 $\mathrm{cm^{-1}}$. This indicated that the interaction largely occurs through the sulfur. The reverse was the case with endosulfan and silver. The plasmon absorption did not change significantly in the case of endosulfan on silver surfaces. The IR spectrum of the residue obtained after the reaction was analyzed and the adsorption of endosulfan onto silver surface was confirmed.

The heterogeneous adsorption of pesticides onto NP surfaces was one of the major aspects of the reaction chemistry [9.391]. For removal of pesticides from solution, noble metal NPs supported on alumina were found to be very effective. When the input concentration was 50 ppb, using alumina-supported noble metal NPs, pesticides could be completely removed from the aqueous phase. The complete removal was confirmed using gas chromatography, which did not show any significant signature of pesticides [9.391]. It is very clear that the chemistry of supported noble metal NPs can comfortably be utilized for the complete removal of most of the pesticides from drinking water whether they are organochlorine (e.g., simazine, lindane, atrazine, etc.) or organosulfur pesticides (e.g., triazophos, quinalphos, etc.), or contain nitrogen-based functional groups (e.g., carbaryl, carbofuran, monocrotophos, etc.). This versatility of noble metal NPs in removing a wide variety of pesticides makes them an attractive candidate for drinking water purification. The strong attachment of NPs on substrates such as alumina can ensure the stability of the supported hybrid structures and can ensure that the NPs will not be released into water under the conditions used in water purifiers.

Detection of Pesticides in Drinking Water with Noble Metal NPs

Ultralow concentration sensing of pesticides in drinking water is as important as it is to remove these toxic pesticides. A large number of water resources across the world are becoming severely polluted by the widespread, large-scale use of different pesticides. Hence, it is imperative to develop rapid, sensitive, and selective detection protocols for detecting such molecules [9.394,395]. Several protocols have been put forward for ultralow-concentration detection of pesticides during the past 25 years [9.396]. Methods such as chromatography, mass spectrometry, and biosensors are some of most practiced methods for this and they offer high sensitivity and selectivity. However, the high sophistication, amount of time required to evaluate the data are the main limitations when considered for common use.

Nanomaterials are expected to contribute in this area as well by developing rapid and facile measurement methods based on nanomaterial chemistry [9.397]. Oligonucleotide-modified GNPs are being used for the biomolecular colorimetric detection of polynucleotides at ultralow concentrations [9.306]. Unlike materials chosen as adsorbents where a higher surface area is a prerequisite, the substrate used for contaminant detection should produce a large change in the surface with adsorbate interaction and a consequent manifestation in reliable spectroscopic signatures. Another important aspect about contaminant detection is the se-

lectivity. This can be ensured by choosing appropriate nanomaterials and functionalizing them with suitable ligands. A good example regarding selective detection of cysteine and glutathione at micromolar concentrations using GNR is described in more detail in another section (Sect. 9.5.2) [9.306].

Two general strategies have been employed for the ultralow-concentration detection of pesticides using GNPs:

1. Variation in the principal properties of a functional group attached to the noble metal NP surface in the presence of organic molecules. This approach has not yet been utilized for the detection of pesticides in drinking water. However, the nature of the molecules detected being similar, this technique can be modified for detection of pesticides as well. Europium ions (Eu^{3+}) when anchored on the surface of a GNP are known to show enhanced fluorescence intensity [9.398, 399]. The interaction of organophosphorus molecules with this will result in the fluorescence being quenched. Organophosphorus molecules tend to bind with GNPs, resulting in the release of Eu^{3+} ions. In another study, a zirconium–phosphate-terminated surface was fabricated by treating GNPs supported on silica gel with zirconium (Zr^{4+}) and $POCl_3$ [9.400, 401]. This surface demonstrated a strong affinity towards organophosphorus compounds. The resultant interaction induced visible changes in the optical properties of the GNPs. In another approach, paraoxon was detected using GNPs functionalized with an antibody specific to paraoxon [9.402]. The electrochemical properties of the system were modified upon interaction with paraoxon. Low concentrations (at ppb level) were detected in this method. Using a metalloenzyme, organophosphorus hydrolase (OPH), which can hydrolyze a large variety of organophosphate pesticides and neurotoxins, an ultralow-concentration detection strategy was devised recently [9.403]. GNPs were functionalized with OPH enzyme. Later fluorophore molecules were positioned at the OPH active sites. These fluorophore molecules were released upon addition of organophosphorus compounds, resulting in changes in the fluorescence intensity. Enzyme-mediated hydrolysis of acetylthiocholine can generate species with reducing capabilities, and Au NPs can be synthesized using this [9.404]. The presence of toxic organic molecules can hinder the catalytic activity of the enzyme, acetylcholine esterase (AChE). This inhibition of the enzyme can result in quenching Au NP production due to the unavailability of the reducing agent. This quenching can even be effected by nanomolar concentrations of toxic organic molecules. The resultant changes are manifested in the optical properties of the GNPs. A similar reaction will result in changes in electrochemical currents as well. Au NPs functionalized with AChE were used to hydrolysis acetylthiocholine, and the reaction was utilized as a pesticide sensor through measurement of the electrochemical current, which depends on the extent of formation of thiocholine in the presence of pesticides [9.405]. A summary of efforts related to the use of biomolecular immobilized Au NPs for electrochemical sensing can be found in a recent review article [9.406]. The enzyme is known to catalyze conversion of acetylcholine chloride in the following way [9.407]:

$$\text{Acetylcholine} + H_2O \xrightarrow{\text{AChE}} \text{acetic acid} + \text{chloine}\,.$$

As discussed above, the presence of organophosphorus pesticide molecules inhibit the activity of AChE to hydrolyze Ach. An attenuation of light when AChE is covalently bound onto GNP surfaces which can be correlated with the pesticide concentration manifests this inhibition [9.408]. The dephosphorylation by 2-pyridine-aldoxime methiodide (2-PAM) can reactivate AChE. Thus the sensor can be reused for many operations. Detection of pesticides in the ppb limit is possible by this method. A correlation between the shift in plasmon wavelength of Ag NPs and the pesticide concentration was also used to detect pesticides [9.409]. Indoxyl, a product of the reaction of certain organophosphorus compounds and indole is fluorescent in nature. Indole anchored on the Au NP surface was reacted with organophosphorus pesticides and the fluorescence (resulting from the indoxyl formation) was utilized for the pesticide detection [9.410]. A ppt level detection was reported by this method.

2. Interaction with pesticides results in changes in the optical properties of noble metal NPs. Chemistry at the nanolevel is extremely sensitive. Hence, even at ultralow concentrations, the interaction between pesticides and NPs brings about considerable changes in properties. The interaction of an endosulfan–noble metal NP system can be followed spectroscopically by using different techniques such as the UV/Vis absorption spectrum, the Fourier

transform IR (FTIR) spectrum, etc., which use the changes in the signatures of the NPs to detect the presence of pesticide on NP surfaces. One of the easiest ways is to observe sensitive color changes of the solution [9.393]. Colorimetric methods are simple, user-friendly, and comparatively less sophisticated. Moreover, the intensity of the color change is nearly quantitative. Reports suggest that the colorimetric detection of pesticides at a concentration level of 1 ppm (this is more than 100 times the permissible levels) is possible. To take nanochemistry-based methods to the levels relevant to drinking water, different strategies have been employed. One of the most established approaches is salt-induced aggregation of noble metal NPs in the presence of pesticide [9.411, 412]. Studies showed exceptional colorimetric changes due to pesticides at low concentrations in a salt-induced aggregation method, which can be easily followed by absorption measurements. A recent study indicated that chlorpyrifos induces severe aggregation to GNP-Na_2SO_4 solution, and this results in the change in the solution color and thus absorption characteristics [9.411]. Figure 9.39a shows the UV/Vis spectral changes and the corresponding color changes. The fast response time and simplicity of the method points to the on-field adaptability of the process [9.411]. A change in the SPR band position and the intensity of humic acid-protected silver NPs were utilized for detection of herbicides. However, these changes were observed only at high concentrations of herbicides [9.413].

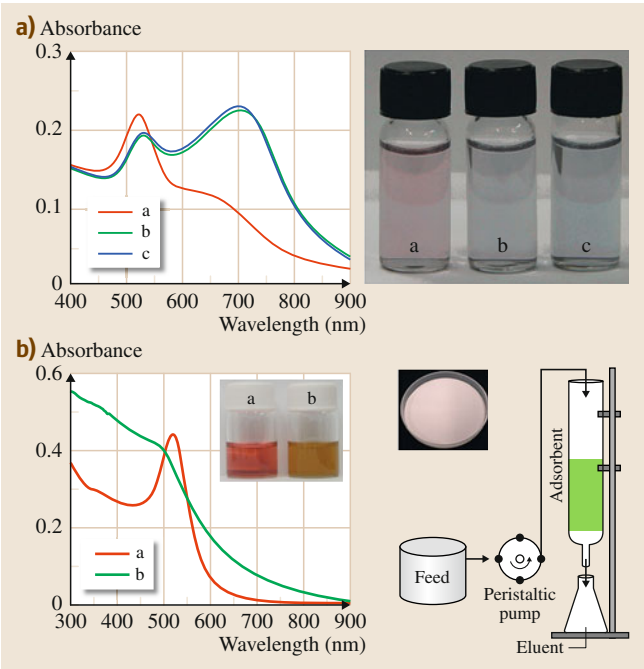

Fig. 9.39 (a) UV/Vis spectra of Au@citrate/Na_2SO_4 mixture before and after the addition of chlorpyrifos-spiked water. (a) Au@citrate/Na_2SO_4 mixture, (b) 20 ppb and (c) 25 ppb chlorpyrifos in Au@citrate/Na_2SO_4 mixture. The corresponding photographs are also shown. From the authors' laboratory. **(b)** UV/Vis spectra of GNPs (a) before and (b) after mercury treatment. *Inset*: Photograph of gold nanoparticles and mercury treated GNPs. Schematic of the down-flow column apparatus used is also shown. From the authors' laboratory (after [9.381, 414])

In addition to the above-mentioned two general approaches, the enhancement of Raman signals in the presence of noble metal NPs has been extensively utilized for detection of organic molecules. A dye molecule, rhodamine 6G, where very low concentration (equal to single rhodamine 6G molecule) detection through an SERS-based method is the most studied example [9.414–417]. Recent investigations indicated higher Raman signal enhancements in the presence of anisotropic gold and silver nanostructures, which can lead to the detection of ultralow concentrations of organic molecules [9.418, 419]. Using the Langmuir–Blodgett assembly of anisotropic nanostructures, the detection limit can be further improved [9.331]. This is discussed in more detail in another section (Sect. 9.7.6). Molecular level details about the interaction between proteins and DNA interactions were studied using this method recently [9.420]. Another study revealed the feasibility of using humic acid-protected GNPs for the detection of organic contaminants [9.421]. The high affinity of humic acid (HA) towards a variety of organic molecules and the low background SERS spectrum of HA (the spectrum is relatively weak in absolute intensity) also helps in the detection process.

Chemistry of Heavy Metal Ions with Noble Metal NPs

Sequestration of heavy metals is considered to be one of the most interesting application areas of noble metal NPs in drinking water purification. The pioneering studies regarding the interaction of metal ions with noble metal NPs were carried out in the early 1990s [9.386] and indicated that many of the previously known properties of metals do not hold true as the size goes down to the nanometer regime.

As the size of the particle increases, the redox potential of a microelectrode becomes more positive

$$Ag_n \rightarrow Ag_n^+ + e^- .$$

For a free silver atom ($n = 1$), the reduction potential is -1.8 V. However when $n \rightarrow \infty$ (for conventional silver electrodes) the potential reaches a value of 0.799 V [9.422]. Such drastic size-dependent changes in electrochemical properties will have high impact in the interaction of these NPs with pesticides and heavy metals in water. The conversion of Ag clusters into colloidal metal particles catalyzed by Cu^{2+} illustrates this effect. The reaction follows the following scheme [9.423]

$$Ag_n + Cu^{2+} \rightarrow Ag_{n-1} + Ag^+ + Cu ,$$

followed by similar reaction of Ag_{n-1},

$$Cu^+ + Ag_{n+m} \rightarrow Cu^{2+} + Ag_{n+m}^- Ag^+ + Ag_{n+m}^- \rightarrow Ag_{n+m+1} .$$

Here, the cluster containing n atoms is depicted as Ag_n, and Ag_{n+m} correspond to a colloidal particle composed of $n + m$ atoms. Aggregation of unstable clusters results in the formation of colloidal particles. The reaction becomes feasible due to the rather negative potential of silver clusters. The reaction can be followed by the disappearance of the absorption feature of clusters and an increase in the intensity of the 380 nm band of metallic silver. A similar study on the interaction of Cd^{2+} with 4 nm colloidal silver particles is also available [9.424]. In this reaction, 1-hydroxyethylmethyl radicals generated radiolytically in a mixed solvent system (acetone + 2-propanol) results in the production of colloidal cadmium via electron transfer. An absorption feature corresponding to colloidal cadmium starts to appear around 250–280 nm, confirming this reduction. A concurrent red-shift was observed for the silver plasmon band (375–383 nm). Another study about the interaction between Ag NPs (0.25 mM in water) with Cd^{2+} solution (0.02 mM) reported the appearance of a separate absorption feature around the 550–600 nm region [9.425]. It is worth noting that in both studies, the size of the silver NPs remained constant. However, different spectral observations were made in the two methods. One method did not show any change after the addition of metal ions, while the other showed an instantaneous appearance of a new feature. Similar observations were seen in the case of other metal ions as well.

Several adsorbent systems including activated carbon [9.426], polyethyleneimine-modified cellulose [9.427], functionalized membranes [9.428], silica [9.429], and graphene [9.430] have been employed for the removal of mercury from drinking water. All good adsorbents should have an extremely high metal adsorption capacity, minimum contamination of the water (e.g., minimum ion exchange), zero desorption under environmental conditions, and economic adaptability.

During the sequestration of heavy metals from drinking water by NPs, the adsorption chemistry plays an important role. Depending on the phase stability two metals can exist as an alloy with varying compositions. For example, gold and mercury can exist as Au_3Hg, AuHg, and $AuHg_3$. Therefore, for 1 g of Au, a maximum adsorption of 3.05 g of Hg is possible. Hence, utilizing the alloy formation, a high efficiency adsorption process can be devised. Zero-valent iron was the first system where metal alloying induced sequestration of heavy metals was reported [9.431]. However, surface corrosion can reduce the capacity of iron to alloy with heavy metals. The use of noble metal NPs for this concept pointed towards the large possibility of these NPs in water purification [9.380]. An increased adsorption capacity of 4.065 g/g of gold is reported when mercury was reduced to the zero-valent state followed by alloying with GNPs. The mechanism of the reaction was studied using various techniques. Microscopic images demonstrated an increase in the size of the NPs upon addition of Hg. An amorphous layer of mercury was also observed around the NPs. In the absorption spectrum, a shift in the plasmon position along with a significant modification in the peak shape was observed (Fig. 9.38b). An X-ray diffractogram confirmed the formation of an alloy Au_3Hg phase. Quantitatively 738 mg gold can be used to decontaminate 3500 l of 1 ppm mercury [9.380].

Silver NPs have enhanced ability to function as a reducing agent for mercury and can exist with mercury in different phases as an alloy as well. Surface plasmon of Ag NPs experiences a blue-shift along with a decrease in intensity immediately upon introduction of Hg^{2+} ions. The partial oxidation of Ag NPs to silver ions results in the decrease in plasmon intensity whereas the shift can be due to the incorporation of mercury into the silver NPs [9.432, 433]. Aqueous mercury NP solutions are reported to exhibit a plasmon absorption band below 300 nm [9.434]. Hg-Ag alloy NPs synthesized via simultaneous reduction with sodium borohydride showed a plasmon in the region of 300–400 nm [9.435].

Silver NPs (average size 60–80 nm) prepared by the Turkevich method (discussed earlier) are known to show a tremendous growth in size up to over 600 nm upon mercury incorporation. This was attributed to the

nucleation of reduced mercury on the silver surface. Energy-dispersive x-ray analysis confirmed the homogeneous distribution of mercury on the silver NPs. The edges of the particles had a slightly higher concentration of Hg compared to the center. The surface adsorbed mercury atoms might diffuse rapidly into the silver core, resulting in a very fast disappearance of the silver plasmon band. In order to understand this, the reaction needs to be analyzed thermodynamically. The reduction reaction is

$$\begin{aligned} \mathrm{Ag} &\rightarrow \mathrm{Ag}^{+} + \mathrm{e}^{-} & E^{\circ}_{\mathrm{OXDN}} &= -0.8\,\mathrm{V} \\ \mathrm{Hg}^{2+} + 2\mathrm{e}^{-} &\rightarrow \mathrm{Hg} & E^{\circ}_{\mathrm{RDN}} &= 0.85\,\mathrm{V} \\ 2\mathrm{Ag} + \mathrm{Hg}^{2+} &\rightarrow \mathrm{Hg} + 2\mathrm{Ag}^{+} & E^{\circ} &= 0.05\,\mathrm{V}\,. \end{aligned}$$

According to the potential in bulk scale, this reaction is thermodynamically feasible. However, as discussed earlier, the conditions are different in the nanoregime. At atomic scale, the $\mathrm{Ag}^{+}|\mathrm{Ag}$ (atom) cell has a reduction potential of $-1.80\,\mathrm{V}$. Hence it is reasonable to think that the reduction potential of the silver NP is likely to be much less than 0.8 V, which creates a strong driving force for the galvanic reaction to occur. The difference in the reduction potential of silver NPs and in the bulk state can be understood from the Ag-HCl system [9.436]. Silver in bulk form will not react with HCl. However, silver NPs prepared by the sodium borohydride reduction method demonstrate an unusually high reactivity with HCl. The plasmon band of silver NPs vanishes after the addition of HCl, confirming the dissolution. A white residue obtained after the reaction of silver NPs with HCl (AgCl) confirmed this.

This result can also be understood from the reaction

$$\begin{aligned} &\mathrm{Ag(s)} + \mathrm{H}^{+} + \mathrm{Cl}^{-} \rightarrow \mathrm{AgCl(s)} + \tfrac{1}{2}\mathrm{H}_2 \\ &E^{\circ} = -0.22\,\mathrm{V}\,. \end{aligned}$$

Hence, with bulk silver, there is no driving force for the reaction. However, at the nanoscale, the feasibility of the reaction points to the continuous increase of the reducing nature of the silver as the size reaches the nanoregime. Utilizing the ability of silver NPs to reduce a number of heavy metals, a variety of alloy NPs (e.g., Ag-Hg bimetallic NPs) have been prepared. Similarly Pd-Ag and Pt-Ag NPs [9.437] have also been synthesized using galvanic etching.

Recently, the authors' group has carried out extensive studies on the mechanism of Hg removal by silver NPs. A detailed study of the chemical interaction of heavy metal ions such as Hg(II), Hg(I), Pb(II), and Cd(II) with naked and protected silver NPs was carried out [9.438]. Silver NPs protected by citrate (Ag@citrate, 30 nm average diameter) and MSA (Ag@MSA, 8 nm) were taken as the model nanosystems. With the help of various spectroscopic and microscopic techniques, it was concluded that the metal ions interact with both the core of the NPs and the functional groups of the capping agents, especially carboxylic acid functionalities (Fig. 9.40). It was also observed that both NPs studied were able reduce Hg(II) and Hg(I) ions to metallic mercury, because of the feasibility of the redox reaction, and that no reduction occurred for Cd(II) and Pb(II). It was concluded that the reduction of Hg(I) and Hg(II) ions was by electrons supplied by the core silver atoms of the NPs at lower metal ion concentrations. At higher concentrations, the metal ions were chemically bonded to the carboxylate groups of the citrate and MSA, in turn, forming sulfides.

Using this same basic chemistry, a practical silver NP-based adsorbent for removal of Hg(II) from water was developed by the authors of this chapter [9.439]. The NPs were supported on alumina and its efficiency in removing Hg(II) from water was demonstrated. The study was also extended to novel noble metal nanosystems known as quantum clusters (discussed later in Sect. 9.8). The interaction of novel unsupported and supported MSA-protected clusters such as Ag_7 and Ag_8 with Hg(II), Cd(II), and Pb(II) in water at different concentrations was investigated [9.440]. It was understood that the interaction with these clusters is similar to that for corresponding larger NPs. It was concluded that Hg(II) was reduced to metallic mercury by both supported and unsupported clusters, due to the feasibility of the redox reaction discussed above, whereas no reduction happened for Cd(II) and Pb(II). This interaction resulted in the disappearance of the luminescence of the cluster, which may aid in sensing Hg(II). The metal ions were chemically bonded to the carboxylate groups of MSA at lower concentration, and due to this chemical affinity of the ligands and the lower silver content per cluster compared with the number of carboxylate groups, Hg(II) was not reduced at these lower concentrations.

Detection of Heavy Metals in Drinking Water with Noble Metal NPs

The maximum contamination limit (MCL) for various contaminants in drinking water was reviewed recently and MCLs for various contaminants were reduced. For example, the MCL for lead has been changed from 15 to 10 ppb and the MCL for arsenic has been revised from 50 to 10 ppb. Various methodologies for the detection

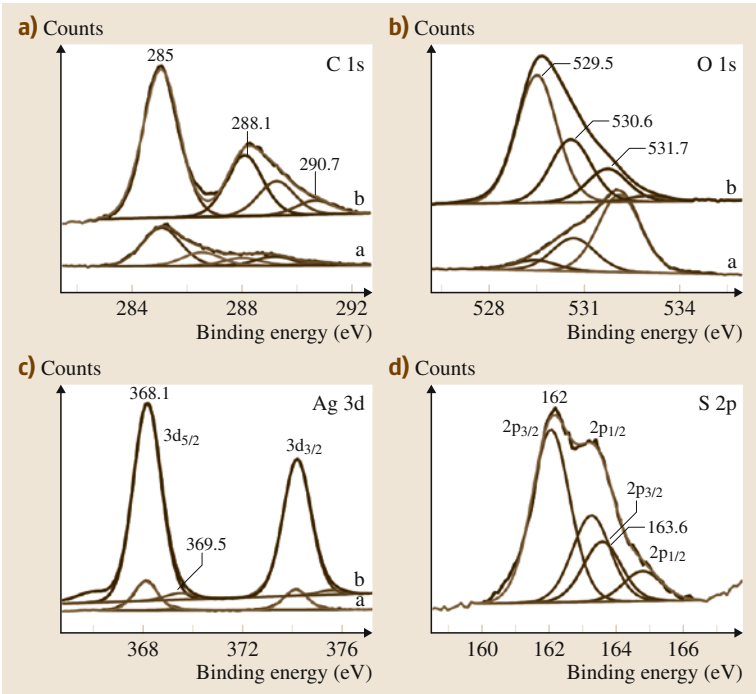

Fig. 9.40a–d X-ray photoelectron spectroscopy (XPS) spectra in the **(a)** C 1s, **(b)** O 1s, and **(c)** Ag 3d of Ag@citrate and Ag@MSA and **(d)** S 2p region of Ag@MSA. Traces (a) and (b) in **(a–c)** are due to Ag@citrate and Ag@MSA, respectively. From the authors' laboratory (after [9.439])

of mercury [9.441], arsenic [9.442], lead [9.443], and anions [9.444] are available. Similar to the methodology adopted for the detection of pesticides, there are two possible ways to detect metal ions by noble metal NPs.

Colorimetric Detection. Noble metal NPs can anchor various types of ligands on the surface and can intercede in several ligand-mediated reactions. Moreover, this anchoring or functionalization of metal surfaces generally results in sensitive changes in their optical properties [9.445]. Heavy metals can be detected using surface functionalized NPs [9.446]. Biomolecule-functionalized GNPs were used for this application recently. The interaction between metal ion and nucleotide, for example the Hg^{2+}-promoted formation of thymine–thymine base pairs [9.447, 448], was used for detection. Based on this interaction a scanometric device involving the use of an oligonucleotide chip array for the low concentration detection of metal ions was reported [9.449]. The aggregation of Au NPs functionalized with a DNA strand due to the hybridization action of enzymes in the presence of a substrate is another example of a similar approach [9.450–453]. The presence of specific metal ions can hinder the hybridization by catalytic cleavage of the substrate. Hence upon addition of metal ions, the aggregates of GNPs become disengaged. This method has a detection limit of 100 ppb. Peptide-functionalized Au NPs were also utilized for colorimetric detection of Hg^{2+} and Pb^{2+} at the ppb level (distinct color changes for the two ions), via a similar methodology [9.454]. The peptide (Flg-A3 peptide with specific sequence, -Asp-Tyr-Lys-Asp-Asp-Asp-Asp-Lys-Pro-Ala-Tyr-Ser-Ser-Gly-Pro-Ala-Pro-Pro-Met-Pro-Pro-Phe-) was anchored on NP surfaces which also acted as the stabilizing agent due to its negative charge. The aromatic, charged, and hydroxyl groups in the peptide sequence distinguish heavy metal ions leading to plasmon shifts in the absorption spectrum-based nanomolar detection. Metal ion-induced assembly of GNPs in the presence of carboxylated peptide (tyrosine containing peptide NH_2-Leu-Aib-Tyr-OMe) was also used for the ppm level detection of various metal ions [9.455]. Simple colorimetric approaches based on the specific action of DNA enzymes towards metal ions (e.g., Cu^{2+} and Zn^{2+}) have also been also utilized for the targeted detection of metal ions [9.456, 457].

The mechanism of colorimetric detection usually depends on the complexation of ligands functionalized onto noble metal NP surfaces with specific metal ions. This results in observable optical changes at concentra-

tions in the ppm level. Various ligands such as gallic acid (Pb^{2+}), cysteine (Hg^{2+}, Cu^{2+}) [9.458], and mercaptoundecanoic acid (Pb^{2+}, Cd^{2+}, Hg^{2+}) [9.459] have been employed for this purpose.

The chemistry of metal NPs can also be utilized for the removal of heavy metals. The alloy formation between the metals gives rise to notable changes in the optical properties of noble metal NPs (as was discussed earlier) [9.379, 380]. Aggregation of Au NP surfaces modified by carboxylate groups can be induced by Hg^{2+} and pyridinedicarboxylic acid, leading to a colorimetric response [9.460, 461], fluorescence quenching [9.462], and enhancement of hyper-Rayleigh scattering intensity [9.463]. The selectivity of metal ions depends on the choice of carboxylate group. Generally, 3-mercaptopropionic acid [9.460, 461, 463], adenosine monophosphate [9.460], and mercaptoundecanoic acid [9.462] are used.

SERS-Based Detection. Utilizing the SERS activity of noble metal NPs, trace quantities of contaminants in drinking water can be detected. As was explained earlier (Sect. 9.4), the large electric field generation near the metal surface due to the collective oscillations of conduction electrons with the incident light leads to signal amplification. Charge transfer between the chemisorbed species and the metal surface leads to electronic transitions from the highest occupied molecular orbital (HOMO) the to lowest unoccupied molecular orbital (LUMO). Excellent reviews on SERS can be found in the literature [9.464]. Various attributes of SERS such as size-dependent SERS activity [9.415], single-molecule detection [9.416], and enhanced activity from assembled nanostructures [9.465] can be utilized for detection of contaminant molecules in drinking water. A recent study demonstrated the shape dependency of SERS-based concentration detection of arsenic in drinking water [9.466]. A detailed description of this is given in a later section (Sect. 9.7.6). Alterations in the conformation of DNA can inhibit their binding capacity to NP surface. This difference in binding capacity induced by Hg^{2+} on thymine-rich single-strand DNA tagged with a fluorescent dye was used for the detection of Hg^{2+}. NPs aggregated upon addition salt when DNA (which can prevent this aggregation) was not anchored on the surface leading to the detection [9.467]. It was also understood that Hg^{2+} can catalyze the formation of stable duplex DNA from single-strand DNA-functionalized GNPs through thymine–Hg^{2+}–thymine linkage [9.468]. This temperature-dependent process can be modulated by controlling the extent of thymine–thymine mismatch. Surface modification of Au NPs with suitable molecules can result in enhanced metal ion capacity [9.469]. Raman vibrational modes are extremely sensitive towards the heavy metal coordination, which will become enhanced upon coupling with noble metal NPs.

Ultralow quantities of anions can be detected using SERS-based protocols. Perchlorate, thiocyanate, and cyanide ions have been detected using positively charged silver NPs protected by amino and amide groups which are immobilized on the silica surface [9.470].

Chemistry of Microorganisms with Noble Metal NPs

Silver, in zero-valent and ionic form, is known to possess antimicrobial effects [9.471–475]. As is illustrated in the historical perspective as well, it has been widely used as a common disinfectant for surgical masks [9.476], textile fibers [9.477], wound dressing [9.478], etc. Several scientific studies have been undertaken to understand the mechanism of this effect, and there exist a number of reviews regarding this [9.479–484]. Here, some important aspects of NP chemistry with microorganisms, that are relevant to drinking water purification are summarized.

Toxic effects of Ag NPs on a broad spectrum of microorganisms, including *Escherichia coli* [9.471, 474, 475, 484–486], *Pseudomonas aeruginosa* [9.484], *Vibrio cholera* [9.484], *Bacillus subtilis*, and the human immunodeficiency virus (HIV)-1 [9.487] are well documented. Before going into the mode of action of Ag NPs, it is important to understand the biocidal activity of silver ions. The precise mechanism behind the effect is not fully understood. However, protein inactivation and loss of replication ability of DNA are suggested as the route cause for this effect based on certain key observations:

1. When cells are subjected to external stimuli like heat, they will try to protect the DNA by forming a defense around the nucleus [9.488]. However, this defense mechanism cannot withstand certain external stimuli, which will result in denaturation of the DNA (loss of replication ability). When Ag ions were injected to *E. coli* and *Staphylococcus aureus,* a similar observation was made[9.489]. DNA condensation resulting from the formation of protective layers around the DNA was observed in this investigation [9.489]. A large-scale movement in the cellular components when encountering Ag ions

points to the capability of the cell to protect itself against external stimuli.
2. Studies indicated that the interaction of silver ions with the sulfur present in many proteins leads to protein inactivation [9.490]. It was also observed that external addition of sulfur-containing compounds led to neutralization of the antibacterial activity of silver. This confirmed the interaction between sulfur and silver.

The effectiveness of Ag ions is closely related to the nature of the charges on the cell surface (due to the presence of various functional groups) and the antibacterial composition. For example, if the antibacterial composition and charge on the cell surface are negative, the contact between these two entities will be minimal due to repulsion [9.491]. Silver can absorb oxygen in atomic form and this has been widely utilized for many organic reactions such as conversion of methanol to formaldehyde [9.492]. Also, bulk silver in water enriched with oxygen is known to oxidatively destroy microorganisms [9.493]. Cell viability is maintained by cellular membranes and in the case of gram-negative bacteria such as *E. coli*, the cellular permeability is controlled by a lipopolysaccharide (LPS) layer on the outer surface of the cellular membrane. The saturated fatty acids on LPS bind to the negative ions present on the membrane backbone. This renders LSPs to have high affinity towards cations. This allows the permeation of polycationic antibiotics into the cytoplasm. Also, cations such as Mg^{2+} and Ca^{2+} can act as electrostatic linkers to bind adjacent LPS chains [9.494]. However, this also makes LSPs to be highly susceptible towards cations and it has been reported that even simple cations can bind to LSP and can induce weakness in the membrane's backbone, leading to disintegration of the membrane and can lead to loss of cellular viability [9.494]. Now the effect of Ag NPs on microorganisms can be looked at.

The severe and irreparable damage caused by silver NPs to the cellular membrane [9.474, 485, 495] leading to the accumulation of NPs in the cytoplasm [9.474] has been investigated in detail. The damage these Ag NPs bring to cells stems from this and is not due to their toxicity [9.485]. This can be easily understood by the significant amount of pits formed after treatment. Another requirement of Ag NPs to have good biocidal activity is that they should be supported to have a considerable amount of antibacterial effects. Generally, cellular proteins, which help cells to guard against metal toxicity, bind to the NP surface, leading to the aggregation of NPs. In this aggregated state the NPs become immobile [9.474]. The size of the NP particle plays an important role in the permeation of NPs into the cell, and small NPs are expected to penetrate across the cell membrane easily [9.484, 485]. Consequently, the biocidal activity of Ag NPs is also dependent on their size and shape. For example, compared to NRs and spherical particles, triangular nanoplates were found to have more activity. The crystal structure of the surface of the NPs can also influence the activity. It is understood that bacteria will interact more with high atom density (111) crystal planes [9.484]. Hence, a crystal with a larger number of (111) planes will demonstrate higher antibacterial activity [9.485].

The formation of superoxide (detected by the dismutation activity of superoxide dismutase) has been also proposed to be a reason for the antibacterial activity. It was also found that the addition of dismutase resulted in a reduction in antibacterial activity [9.496].

Another opinion suggests that the chemistry of silver ions is important in the antibacterial effect of silver NPs. Study showed that oxidized silver NPs are nontoxic towards *E. coli* strains, pointing towards the importance of chemisorbed Ag^{+} ions in determining silver NP toxicity [9.486].

Studies showed that Ag NPs interact with the glycoproteins of HIV-1 and particles greater than 10 nm attach to the viral envelope. HIV cell infection also occurs due to the binding of glycoproteins with receptor sites on host cells. The sulfur-bearing residues on the protein surface actively participate in the binding process with Ag NPs and make the glycoprotiens incapable of binding with host cells, deactivating the HIV virus [9.487].

The stabilization of Ag NPs in organic media such as plastics, oils, etc., is also important to attain optimum antibacterial action. There are two major approaches for this:

1. Synthesis of organic-soluble Ag NPs via different methods, for example, polymerization of benzylthiocyanate on silver NPs [9.497].
2. Preparing Ag NPs directly in vegetable oil by reduction of the metal salt by oxidative drying process in oils [9.498].

Ag NPs and their antibacterial properties have also been utilized for making bacteriostatic separation membranes [9.499–501]. Biofouling and inability to remove viruses are recurring problems in many membrane-based technologies. Thus, Ag NPs can contribute greatly to this area and incorporation of Ag NPs

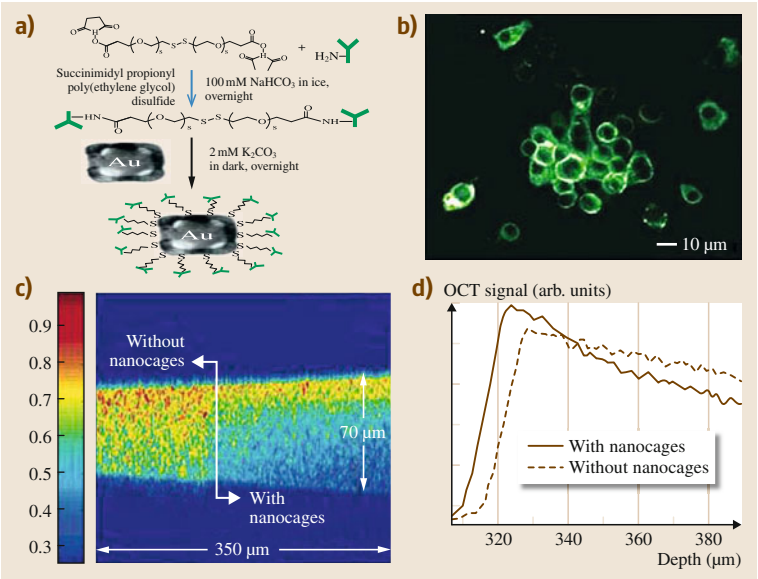

Fig. 9.41 **(a)** Schematic illustration of the protocol used to conjugate antibodies to the surface of Au nanocages. **(b)** Fluorescence image of SK-BR-3 cells whose surfaces were treated with anti-HER_2 antibodies, followed by incubation with fluorescence-labeled IgG. **(c)** OCT image of a gelatin phantom embedded with TiO_2; the concentration of TiO_2 was controlled at 1 mg/mL to mimic the background scattering of soft tissues. **(d)** OCT signals on log scale as a function of depth (after [9.503])

onto the membrane solves both problems. The loading can be done via two processes namely, addition of silver in zero-valent form or reduction of silver ions in the membrane casting solution. Addition of Ag NPs improved the bioresistance as well as the permeability [9.500]. Investigations pointed out that the biocidal properties of silver NP loaded membranes are due to the leaching of Ag^+ ions from the NPs [9.502].

Size and shape-dependent physical and chemical properties of anisotropic nanomaterials make them attractive candidates for various applications. The higher efficiency of these particles over spherical NPs has been demonstrated in various applications. Hence, a few of the important applications of different kinds of anisotropic nanostructures are mentioned below. This section does not provide a comprehensive review of the literature.

9.7.2 Bioconjugation and Labeling

Functionalization of NPs with biological entities can increase their biocompatibility and thus improve their utility for targeting cancer cells. *Hafner* et al. stabilized, conjugated to antibodies, and characterized GNRs for biological applications. To this end, the stabilizing surfactant bilayer surrounding GNRs was replaced with thiol-terminated methoxypoly(ethylene glycol). Bioconjugation of GNRs was carried out using a heterobifunctional crosslinker and the antibody activity was confirmed by a strip plate assay. Antibody-functionalized NRs were conjugated to murine macrophage cells by *Cortie* et al. [9.504] to study their photothermal properties. Bioconjugation of GNRs with phosphatidylcholine for controlled release of plasmid DNA by NIR radiation was reported by *Takahasi* et al. [9.505]. Nanocages made of gold were also bioconjugated with entities including antibodies, nucleic acids, and small-molecule inhibitors. These were used to target cancer cells for early-stage diagnostics and thermal therapy of tumors [9.506]. Figure 9.41a shows a schematic illustration of the procedure used to conjugate antibodies onto the surface of Au nanocages. The molecular specific binding of these cages were tested on breast cancer cell line SK-BR-3, which overexpresses epidermal growth factor receptor 2 (EGFR2 or HER2) [9.506]. The monoclonal anti-HER2 antibody from a mouse was anchored onto cancer cells by incubating the cells and the antibody. Secondary antibodies (anti-mouse immunoglobulin G, IgG) were immobilized on gold nanocages in a buffer solution (Fig. 9.41). When the two solutions came into contact, SK-BR-3 cells conjugated with anti-HER2 antibodies became anchored on the cages. A uniform green color, indicating homogeneous distribution of the primary anti-HER2 antibody on the cell surface, was seen in the fluorescence image (Fig. 9.41b).

9.7.3 Optical Contrast Agents

Anisotropic noble metal NPs are ideal candidates as contrast agents for NIR imaging applications due to

their strong SPR, biocompatibility, ease of bioconjugation, and large scattering cross-section [9.506, 507]. The strong, tunable SPR features in the NIR region and smaller size of Au nanocages make them attractive contrast agents [9.506]. Gold nanocages were used as optical contrast agents in the OCT imaging on phantom samples. OCT imaging (Fig. 9.41c) was conducted using a 7 fs Ti:sapphire laser with a wavelength of 825 nm and a bandwidth of 155 nm. The presence of Au nanocages significantly improved the spectroscopic imaging contrast for tissues. The high absorption cross-section (2.9×10^{-20} m^2 at 800 nm) exhibited by the Au nanocages was about five orders of magnitude stronger than the conventional dye indocyanine green. This emphasizes the usefulness of these structures for OCT imaging. Figure 9.41d shows the log of the OCT signal as a function of depth.

9.7.4 Photothermal Therapy

Living cells being extremely temperature sensitive can be adversely affected by an increase of a few degrees and can even lead to cell death. Anisotropic NPs with NIR absorption can be used for photothermal therapy where heat is generated by plasmonic absorption [9.509, 510]. Moreover, these particles can function as dual imaging/therapy capable entities. Several anisotropic NPs including NRs, nanocages, nanoshells, and nanostars have demonstrated a good NIR absorbing capacity which can be used for photothermal therapy [9.259, 504, 506, 508, 511–516]. Selective bioconjugation of Au nanocages can cause targeted delivery of these systems into cancer cells where they can produce a local temperature rise that can provide a therapeutic effect on cancer cells [9.260, 503, 506, 508, 511, 512, 514]. As mentioned in Sect. 9.7.2, the large absorption cross-sections of Au nanocages can aid these structures to covert absorbed photons into phonons. This results in an increase in the temperature of the system. Using an ultrafast laser-induced heating process, Ag nanocages can create extremely high lattice temperatures [9.514]. Such therapy is less invasive than chemotherapy or surgery and holds strong promise as a novel form of cancer treatment. *Xia* et al. demonstrated the photothermal destruction of breast cancer cells in vitro using immunotargeted Au nanocages [9.259]. Gold nanocages (with an average edge length of 65 ± 7 nm and an absorption peak at 800 nm) were conjugated with anti-HER2, which enabled the specific targeting of breast cancer cells (SK-BR-3) [9.508, 513, 514]. When the targeted cells were irradiated with a pulsed NIR laser, photothermal heating resulted in cell death. Treatment conditions such as the power density, the duration of laser exposure, and the response time after irradiation can be varied to achieve effective destruction of cancer cells. Cells targeted with Au nanocages responded immediately to laser irradiation, and irreversible cellular damage occurred at power densities greater than 1.6 W/cm^2 (Fig. 9.42). As the time of exposure increased, more and more cell death was observed.

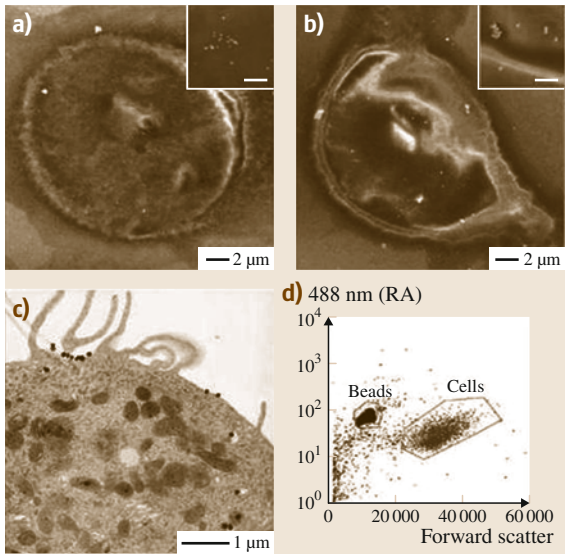

Fig. 9.42a–d SEM images of SK-BR-3 cells targeted with immuno-Au nanospheres **(a)** and nanocages **(b)**. SEM images at higher magnification (*insets*) reveal that the *bright spots* in the SEM images are indeed nanospheres and nanocages, respectively. The *scale bar* in the *insets* represents 500 nm. **(c)** TEM image of a microtomed SK-BR-3 cell conjugated with immuno Au nanocages. **(d)** Typical flow cytometry graph indicating how the forward scatter (*x*-axis) and right angle (RA) scatter (*y*-axis) can be used to differentiate the size difference between beads and cells (after [9.508])

Salem et al. demonstrated a novel nonviral gene therapy approach using multisegmented metal NRs [9.517, 518]. Cancer treatment can make use of NTs as well. Hyperthermic treatments can be carried out using NTs, which also possess large NIR absorption. Because the surface of NTs is flat, it facilitates high contact between the NTs and cancer cells, which in turn helps to reduce the required exposure time. Hence even at low dosage NTs can be effectively delivered into cancer cells, and the low dosage reduces the metal toxicity as well.

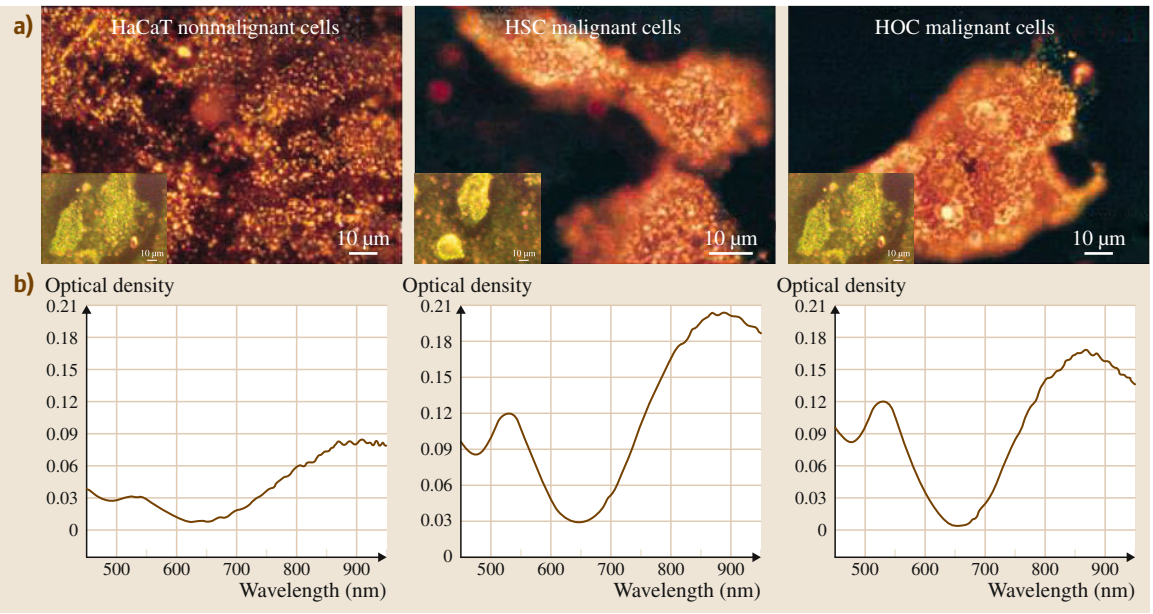

Fig. 9.43 **(a)** Light scattering images of anti-EGFR conjugated Au NRs after incubation with cells for 30 min at room temperature. **(b)** Average extinction spectra of anti-EGFR conjugated Au NRs from 20 different single cells for each kind. *Insets* show the corresponding light scattering images of anti-EGFR-Au nanospheres after incubation with cells for 30 min at room temperature (after [9.519])

9.7.5 Cancer Cell Imaging

Using dark-field optical microscopy and TPL microscopy, individual anisotropic NPs can be imaged due to the strong SPR exhibited by them. They are ideal candidates for biomedical imaging because of the large scattering cross-section [9.510]. GNRs in particular, are well suited for cancer cell imaging due to their strong absorption and scattering in the NIR region (650–900 nm) [9.509, 510, 517–523]. *Huang* et al. used GNRs functionalized with negatively charged PSS for cancer cell imaging [9.519]. The PSS coated GNRs on mixing with an antibody solution in 4-(2-hydroxyethyl)-1-piperazineethanesulfonic acid (HEPES) buffer, conjugated with anti-epidermal growth factor receptor (anti-EGFR) monoclonal antibodies. Two malignant cells, namely HOC 313 clone 8 and HSC 3, and one nonmalignant Ha-Cat cell were used in the experiment. The anti-EGFR antibody-conjugated NRs showed higher affinity to malignant cells due to the over-expressed EGFR on the cytoplasmic membrane and bound specifically to the surface of the malignant-type cells. The light scattering images of anti-EGFR-conjugated GNRs after binding to malignant and nonmalignant cells are shown in Fig. 9.43. The dominant orange color in the image corresponds to the surface plasmonic enhancement of the longitudinal oscillation in the NIR of GNR. After antibody conjugation, GNRs only interact with the malignant cells. The nature of the interaction is distinguished by light scattering imaging; Fig. 9.43 shows the quantity of NRs bound to the cell. From the extinction spectra, it is clear that the cancerous cells with nanocages have twice the intensity compared to noncancerous cells. The difference in interaction of anti-EGFR-conjugated GNRs with malignant (target specific) and nonmalignant (nonspecific random) cells gives rise to this difference in intensity. *Wang* et al. showed that GNRs, when excited at appropriate wavelengths (corresponding to LSPR peak position) using a two-photon scheme, can produce a luminescence signal 58 times stronger than the fluorescence signal from a rhodamine molecule [9.524]. *Durr* et al. used GNRs as contrast agents for imaging of cancer cells and the huge TPL of GNRs was found to be excellent for this application [9.525]. Gold nanocages are also known to exhibit a broad two-photon photoluminescence band (from 450 to 650 nm) when excited by a 800 nm Ti:sapphire laser. Use of Au nanocages as optical imaging agents for two-photon microscopy has recently been demonstrated by *Xia* et al., who

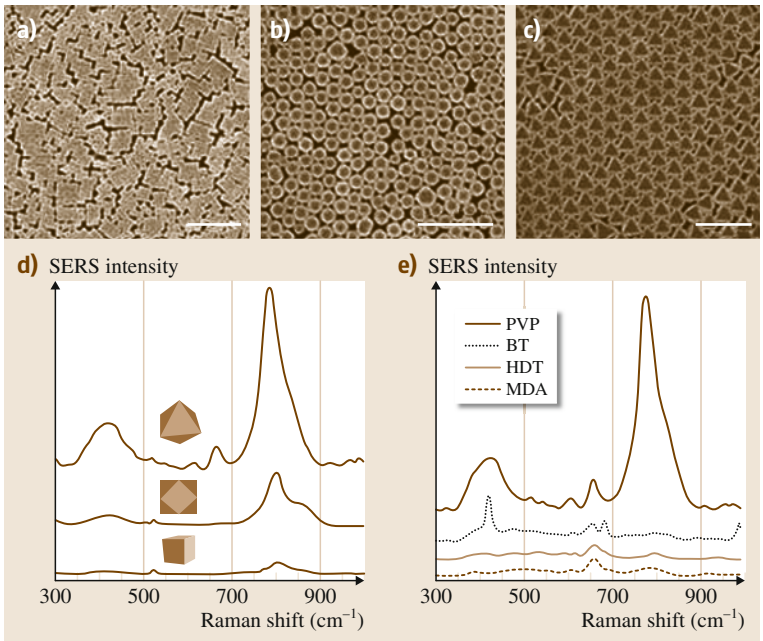

Fig. 9.44a–e SEM images showing closely packed films of the three nanocrystal shapes: **(a)** cubes, **(b)** cuboctahedra, and **(c)** octahedra; *scale bars* are 1 μm. **(d)** SERS spectra collected on LB films of each of the nanocrystal shapes of 10^{-6} M arsenate solution. Peaks at 800 and 425 cm^{-1} can be assigned to Na_2HAsO_4. **(e)** SERS response of octahedra LB arrays coated with various organic species: benzenethiol (BT), hexadecanethiol (HDT), mercaptodecanoic acid (MDA), and PVP (after [9.466])

directly examined the uptake of antibody-conjugated and PEGylated Au nanocages by U87MGwtEGFR cells [9.512].

9.7.6 Surface-Enhanced Raman Scattering Substrates

Ultrahigh sensitivity and specificity are the marked features of SERS. So it is a well-established technique and an attractive tool for trace level chemical detection. An excellent number of fine reviews are available on this topic in the literature [9.414, 417, 464, 526–534]. The SERS signal sensitivity strongly depends on the shape of the NPs [9.526, 527] This technique can be used for the detection of arsenate and arsenite in aqueous solutions with a detection limit of 1 ppb (Fig. 9.44d), an order of magnitude below the standard set by the World Health Organization (WHO) [9.466, 535]. Yang et al. successfully demonstrated this by using LB assemblies of various polyhedral Ag nanocrystals (Fig. 9.44a–c), made by a polyol process. Octahedra LB arrays coated with various organic species such as benzenethiol, hexadecanethiol, and mercaptodecanoic acid have very good SERS response, as is shown in Fig. 9.44e. We know that contaminated ground water becomes a curse to public health in most developing nations. So there is a need for a reliable and simple device to detect arsenic in ground water. This SERS substrate has proven to be a good solution for the above crisis. It is reliable, reproducible, highly portable, and could be easily implemented for field detection. Another SERS substrate NP that exhibits strong SERS activity is AuNF. By packaging RhB@AuNF particles with denatured BSACE94 molecules the AuNF particles could be developed into Raman-active tags, whose application in living cells was demonstrated by using the RAW264.7 macrophage cell line [9.536, 537].

Real-time detection of biomolecules using SERS has also been reported [9.528–530]. It is known that SERS activity varies depending on several factors. For example, *Nogami* et al. reported that triangular plates having sharper corners and edges have higher SERS activity [9.531]. Similarly, silver nanoplates in aggregated form have higher SERS activity than single-form ones due to strong electromagnetic coupling between neighboring nanoplates [9.51, 538]. When we consider anisotropic metal NPs, it is clear that their unusual LSPR properties and sharp corners on the surface are the factors contributing to higher SERS activity. These sharp corners can create a more localized electric field in comparison with spherical particles [9.535, 537].

9.7.7 Superhydrophobic Surfaces

The wettability of a surface depends on the chemical composition and morphology of that surface.

Some surfaces have a very high water repellency. The creation of a local geometry with a large geometric area relative to the projected area or the use of roughness combined with hydrophobic coatings can result in increased surface hydrophobicity. Such superhydrophobic surfaces have many advantages. Water droplets that are in contact with such surfaces (contact angle $> 150°$) form nearly spherical beads. They are self-cleaning surfaces in which contaminants of any type, whether inorganic or organic, adhere to water droplets and will be removed when the water droplets roll off. Superhydrophobic surfaces can be made by using anisotropic nanomaterials. A single-crystalline Ag dendritic film (thickness $\approx 10\,\mu m$) when functionalized with a SAM of n-dodecanethiol can form a superhydrophobic surface with a contact angle of $154.5 \pm 1.0°$ and a tilt angle lower than 2° [9.188]. From contact angle measurements, we can infer that the presence of Ag crystallites on the substrate increases hydrophobicity compared with substrates without Ag crystallites (Fig. 9.45). We can grow Ag nanoplates on GaAs substrates by direct reaction between aqueous solutions of $AgNO_3$ and the GaAs surface, and it then shows the Lotus effect [9.189]. These Ag nanoplates can be coated with 1-hexadecanethiol molecules to decrease the surface energy of Ag plates. One of the major advantages of this methodology is that we can change the wettability of such a surface. This is done by controlling the dimensions and nanoscale surface roughness of individual nanoplates using appropriate variation of the reaction conditions.

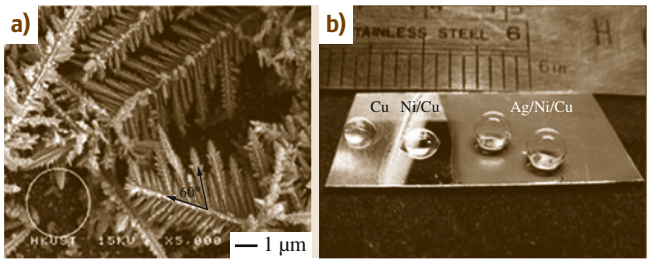

Fig. 9.45 **(a)** SEM image of Ag crystallites. **(b)** Photograph of water droplets on the Ag dendritic film surface, Ni surface, and Cu surface. All surfaces were modified with *n*-dodecanethiol (after [9.188])

9.7.8 Mercury Sensor

Mercury, a highly toxic pollutant which is harmful to the environment, is released from various sources such as power plants, burning fossil fuels, etc. Exposure to high Hg can harm our organs and affect the immune system. So it is important to monitor Hg levels in aquatic ecosystems. Owing to the amalgamation of gold and mercury, GNRs can selectively detect the presence of mercury in tap water samples at the ppt level [9.379]. The main highlight of this method is that it is very fast and the entire sensing process takes place in less than 10 min, with no sample separation and even ultralow levels of Hg can be detected very easily. The amalgamation process of Hg with GNRs is schematically represented in Fig. 9.46. Mercury was added into the growth solution during the synthesis of GNRs and it was found that the AR of the GNRs is inversely propor-

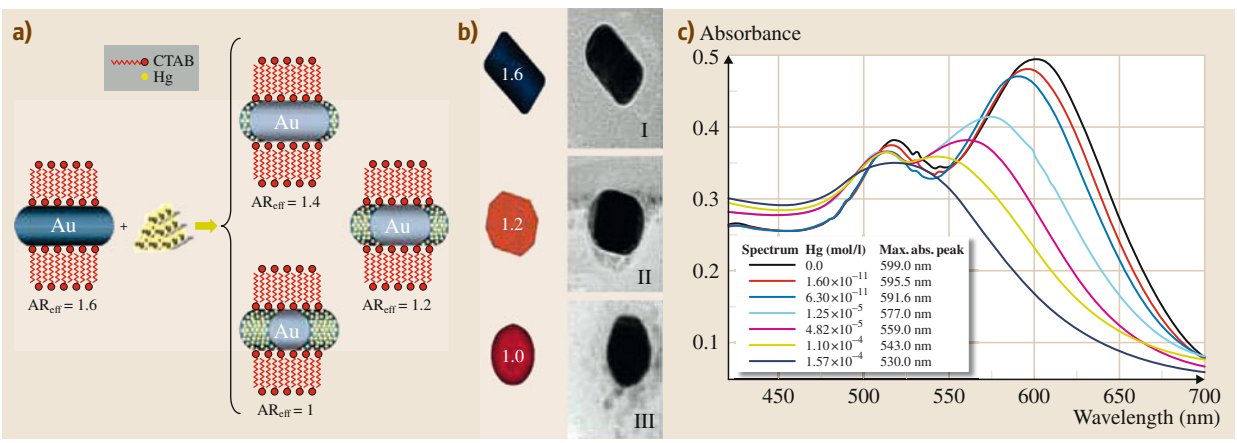

Fig. 9.46 **(a)** Schematic representation of the amalgamation of Hg with GNRs. **(b)** TEM images of GNRs in the absence and the presence of Hg. (I) no Hg, (II) 1.25×10^{-5} M, and (III) $1.57-4$ M of Hg^{2+}. **(c)** UV/Vis absorption shift in the concentration range between 1.6×10^{-11} and 6.3×10^{-11} M of Hg(II) (after [9.379])

tional to the concentration of Hg^{2+} at constant $NaBH_4$ concentration. A quantitative analysis can be made by connecting the wavelength shift and the mercury concentration (Fig. 9.46). The detection limit of Hg in tap water for this method was 6.6×10^{-13} g/l.

9.7.9 Infrared Absorbing Material

NIR absorbing films based on gold can be effectively used for blocking IR radiation. NP-based methods have a high efficiency and are economically more viable compared to other methods. Thus they can be used as an alternative way of blocking IR rays instead of reflective coatings. We can develop IR filters using nanomaterials with NIR-IR absorption capacity. Using a prototypical device, it was demonstrated that gold mesoflowers (MFs) can be successfully used to reduce the temperature rise in an enclosure exposed to daylight [9.539]. They were able to absorb a significant portion of heat. Along with a blank glass substrate as the control, a monolayer and a bilayer of MF-coated glass slides were used to take the heat absorption measurements. Results showed that the MF-coated glass (monolayer) gave an average temperature inside the cardboard box which was lower by 2 °C, whereas the bilayer coated substrate showed a reduction of 4.3 °C compared to the blank glass substrate. In future this can lead to the application of such NIR absorbing materials to make heat absorbing optical coating of windows [9.419, 539].

9.7.10 Plasmonic Waveguides

Another application of nanomaterials is in the area of photonic devices. They can have the role of waveguides if we carefully fabricate them to guide electromagnetic energy. This can be realized with lateral mode confinement below the diffraction limit of light, which is not possible through conventional waveguides or photonic crystals. Chains of closely spaced metal NPs that convert the optical mode into nonradiating surface plasmons can be prepared through electron beam lithography or self-assembly techniques. *Maier* et al. experimentally demonstrated that closely spaced silver NRs can guide electromagnetic energy from a localized subwavelength source to a localized detector over a distance of about 0.5 μm [9.540]. The waveguide structures have individual AgNRs (90 nm – long and 30 nm × 30 nm width/thickness) with spacing of 50 nm between adjacent particles. An increase in near-field coupling between the particles was created due to the perpendicular orientation of the NRs (long axis) with respect to waveguide chain axis. The waveguides used the tip of a scanning near-field optical microscope. For this, a dye laser (wavelength of 570 nm) corresponding to the single-particle resonance was used. The energy transfer through the waveguide was probed using fluorescent nanospheres made up of carboxyl-coated polystyrene. Fluorescent nanospheres placed on top of a waveguide at a distance from the excitation source became excited (illustrated by the dye emission from the fluorescent particle) by the local excitation given to the NR, which proves the propagation of these excitons along the NR array. The study demonstrated that energy attenuation lengths of several hundred nanometers is possible through nanostructure arrays pointing towards the utility of these plasmon waveguides as functional end-structures in integrated optical devices [9.540].

9.7.11 Biosensors

Anisotropic NPs with strong SPR features, which are greatly influenced by the changes in local environment, can be used for sensing [9.541]. GNRs with high-value shape factor (surface curvature), are ideal candidates for plasmon sensing. A multiplex biosensor assay for different targets was constructed using GNRs by *Yu* and *Irudayaraj* [9.542]. GNRs of different ARs were conjugated with the IgG of humans, rabbits, and mice using the 11-mercaptoundecanoic acid linker. The shifts in SPR wavelengths of these NRs were used to probe their coupling with respective complements (anti-IgGs). Detection of multiplex surface markers of breast cancer cells by the use of antibody-conjugated GNR molecular probes also employs a similar strategy [9.543]. A glucose sensor based on the layered superstructure of gold nanooctahedra was demonstrated by *Choi* et al. [9.544]. The superstructure was fabricated via a molecularly mediated assembly approach. Compared to spherical particles/glucose oxidase (GOx) system, the single-layered Au nanooctahedra/GOx system exhibited a greater voltammetric response under same conditions pointing towards the dependence of the sensor activity on the shape of the Au particles used. The Au nanooctahedra-based glucose biosensor demonstrated a high level of sensitivity in the range of 0.349 μA/mM and fast response (within few seconds) with a wide response range (between 0.125–12 mM) [9.544].

9.7.12 Photovoltaic Devices

Photovoltaic devices consisting of nanocrystals rely on the electron acceptor capability of constituent NPs from

conjugated polymers. However, the limitation of electron extraction through the nanocrystal is a big problem of photovoltaic devices made with spherical nanocrystals [9.39, 40]. The use of anisotropic structures (e.g. NRs) instead of spherical nanocrystals can give significantly higher efficiencies because of the smaller number of interparticle hops necessary for electrons to leave the device [9.545]. Generally, either TiO_2 [9.546] or ZnO [9.547] NPs are used for this application. Recent studies indicate that noble metal nanosystems can be also used for this application. Incorporation of noble metal NPs are reported to increase the efficiency of solar cells containing ZnO [9.548] and TiO_2 [9.549, 550] nanomaterials. The overall transport properties of the system will become modified by the incorporation this nanophase into the composite. Moreover, this will also permit optical tunability by adjusting the size of the metal NPs present. The overall absorption of light is also believed to be enhanced by the presence of noble metals.

Hasobe et al. pioneered works in this direction in 2003 [9.551]. Organic solar cells containing self-organized porphyrin (donor), fullerene (acceptor), and SnO_2 electrodes containing Au NPs were prepared. A large enhancement in the photoelectrochemical performance and a broader photoresponse in the visible and IR ranges were demonstrated by the Au NP containing cells. A self-assembled composite of Au NP and porphyrin was used for photovoltaic applications by *Yamada* et al. [9.552]. *Kim* and *Carroll* did a detailed study regarding the enhancement of poly(3-octylthiophene)/fullerene bulk heterojunction photovoltaic devices by gold and silver NPs [9.553]. *Derkacs* et al. reported an increase in the efficiency of amorphous-silicon solar cells by metallic NPs [9.554]. Others have reported similar enhancement in the case of polymer-based voltaic cells [9.555,556]. Dye-sensitized solar cells (both iodide/triiodide electrolyte-based and solid-state) made up of core–shell $Au-SiO_2$ NPs, which help in plasmon-enhanced light absorption leading to enhanced photocurrent and efficiency have been demonstrated by *Brown* et al. [9.557]. *Yildiz* et al. reported a solar cell consisting of oligoaniline crosslinked Au/CdS NP arrays on electrodes with enhanced photocurrent efficiency [9.558]. *Isikawa* et al. investigated the effect of the SPR of Ag NPs on dye-sensitized solar cells [9.559]. An increased photovoltaic efficiency for tandem ultrathin-film organic photovoltaic cells was found by the incorporation of Ag NPs [9.560].

9.8 New Gold and Silver Materials – Quantum Clusters

The dimensions of noble metal NPs are decreasing. In the very recent past, subnanometer particles and their associated properties have attracted intense interest. Quantum clusters (QCs) are a new class of materials made up of a few to tens of atoms, giving core sizes below 1 nm, which exhibit unusual physical and chemical properties due to their molecule-like nature [9.561,562]. QCs act as a bridge between molecular and NP behaviors, and they possess properties that are entirely different from both of these size regimes. They possess an intermediate chemical composition between the bulk and molecular regimes, with an electronic band structure modified into discrete electronic states as a result of quantum confinement. Just as in the nanometer regime, the subnanometer regime is also dominated by optical properties. While it was absorption for the former, it is luminescence for the latter. QCs exhibit strong and core size-dependent, tunable photoluminescence properties. They show characteristic absorption features and are also photostable. The quantum yield of gold QCs is several orders of magnitude higher than that of bulk gold. The photoluminescence, photostability, and biocompatibility exhibited by gold QCs make them potential materials for use in many biorelated applications such as labeling, cell imaging, drug delivery, detection, etc. [9.562]. Coupled with the possibility of chemical functionalization and due to the absence of cytotoxicity, these materials are beginning to enter biomaterials; the possibility that such clusters can directly nucleate in proteins expands the scope of this application. The clusters that have been investigated using the tools of gas-phase spectroscopy are now being made in the condensed phase. Adaptation of the properties of gas-phase clusters to their condensed-phase analogs will enrich this area in the years to come. Newer spectroscopy and mass spectrometry tools would enable the exploration of these novel properties. Several of the phenomena exhibited by such materials cannot be fully studied without comprehensive theoretical calculations. Newer insights are expected on the structure, properties, and dynamics of these systems from such studies. Although several types of cluster have been synthesized,

very few have been fully characterized by crystallography (Au_{25}, Au_{40}, Au_{102}).

Monolayer-protected gold QCs can be synthesized by various methods [9.561, 563]. They can be directly synthesized from precursor ions (Au^{3+}), which are reduced by a reducing agent (e.g., $NaBH_4$) in the presence of stabilizing ligands such as thiols, amino acids, proteins, dendrimers, etc. [9.562, 564]. A series of glutathione-capped gold QCs have been synthesized by reducing gold ions in the presence of glutathione, followed by their separation using the polyacrylamide gel electrophoresis method. A new QC can be made from another QC by treating it with the appropriate ligands. QCs are also synthesized by core etching processes [9.563]. In this process, core etching of NPs using appropriate ligands such as dendrimers, thiols, Au^{3+} ions, etc., results in the formation of QCs. Gold clusters are also highly stable at ambient conditions.

Recently our group devised a strategy for synthesis of Au QCs with the aid of cyclodextrin (Fig. 9.47b) [9.564]. They showed interesting solvent-dependent luminescence, indicating a large number of applications in sensing and security. In the case of gold QCs, the electronic bands resolve into discrete energy levels which resemble those of molecules; hence, they can be treated as molecular entities. For example, Au_{25} shows multiple molecular-like transitions in its optical spectrum [9.565]. The luminescence quantum yield of synthesized gold QCs ranges from 0.1 to 25%. Although the mechanism of luminescence in QCs is not fully known, it is believed that the emission originates from radiative intraband transitions within the sp bands, across the HOMO–LUMO gap. As the size of the cluster decreases, the spacing between the discrete states increases, which leads to a blue-shift in the emission of smaller QCs as compared with their larger analogs. Since QCs are biocompatible and luminescent, they are promising candidates for biorelated applications such as targeted imaging of cancer cells, biolabeling, drug delivery, etc. [9.561, 566]. Recently, the cluster formation process inside a protein was studied using various spectroscopic techniques [9.567]. These clusters can easily be conjugated with biological molecules, further enhancing their application potential. Most of the metal quantum clusters emit in the NIR region and hence they can be used for two-photon imaging with IR excitation [9.563]. Two-photon emission of Au_{25} observed at 830 nm with excitation at 1290 nm can be useful for two-photon imaging [9.561]. QCs also exhibit electroluminescence at room temperature and hence provide facile routes to produce strong single-photon emitters [9.561]. The luminescence of gold QCs is exploited for metal ion sensing [9.568]. Fluorescent gold QCs can be used to sense mercury(II) based on fluorescence quenching through Hg(II)-induced aggregations [9.569]. Quantum clusters are very good catalysts [9.561]. As the crystal structures of QCs are known, it is possible to correlate the particle structure with catalytic properties. It was found that metal oxide (e.g., Fe_2O_3, TiO_2)-supported gold QCs show higher catalytic activity and yield compared with unsupported QCs [9.561].

Silver analogs of these fascinating materials, however, are more reactive compared to their gold counterparts. Hence, comparatively fewer reports exist. Nevertheless, diverse methods have been reported for the preparation of Ag clusters [9.570] and most of them are highly luminescent in both solution and the solid state. The pioneering effort in this direction was done via gas-phase and low-temperature matrix-isolation methods [9.571, 572]. The formation of excited Ag_2 and Ag_3 clusters and the resulting chemiluminescence during Ag condensation with Ar has also been reported [9.573]. Nonluminescent silver clusters have been synthesized in frozen solutions and zeolites [9.574]. Diverse methods such as radiolytic reduction [9.575, 576], sonochemical synthesis [9.577, 578], chemical reduction [9.579–583], photoreduction [9.584], etc. have also been employed for synthesis of Ag clusters. A solid-state route for synthesis of Ag_9 clusters was recently reported by *Pradeep* et al. (Fig. 9.47a) [9.579]. The same group also made silver clusters by following an interfacial method (Fig. 9.47c) [9.585, 586].

Due to the higher reactivity of silver clusters, they are prone to aggregation and the resultant growth to form larger clusters/NPs. Usually this problem is avoided by using some preformed templates or capping agents to synthesize stable entities [9.587]. Both organic and inorganic scaffolds are being used for this purpose. Organic scaffolds for fluorescent silver QCs were first employed by the group of *Dickson* in 2002, who employed dendrimers as scaffolds [9.588]. Since then, several organic scaffolds such as dendrimers, polymers, short molecules containing both carboxylic groups and thiols groups, DNA, proteins, and peptides have all been employed for this purpose. *Kumacheva* et al. employed poly(*N*-isopropylacrylamide-acrylic acid-2-hydroxyethyl acrylate) microgel particles as a scaffold for preparing luminescent silver QCs [9.584]. The use of acrylates for synthesis of small silver QCs, which do not exhibit fluorescence, by applying γ radiation was reported earlier by *Ershov* and *Henglein* [9.589]. It has also been reported that, as compared with small poly-

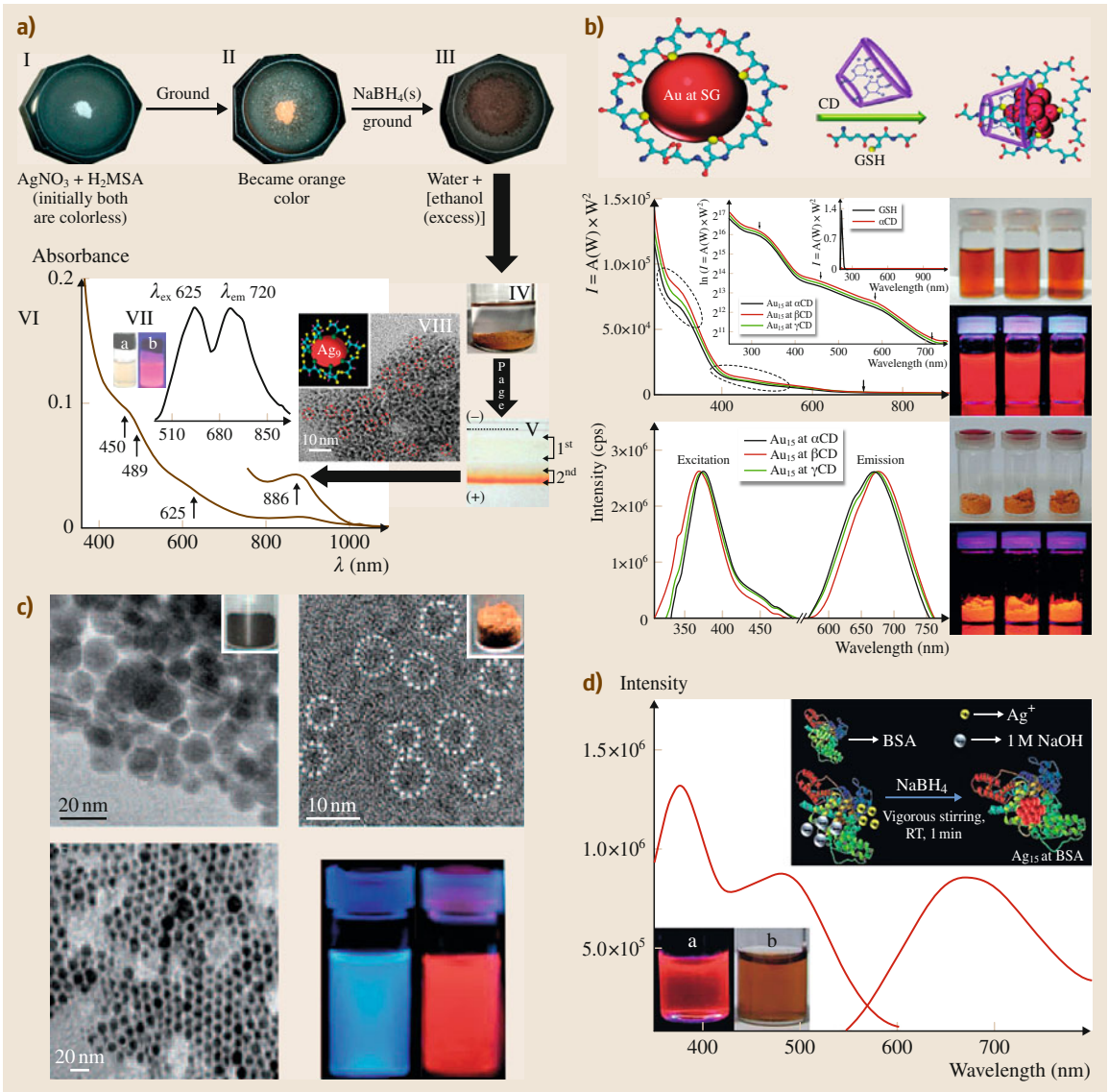

Fig. 9.47 **(a)** Scheme of preparation of Ag clusters synthesized through solid-state route and their characterization. **(b)** Au clusters synthesized using cyclodextrin, UV/Vis spectrum, and luminescence (CD: cyclodextrin; GSH: glutathione). **(c)** TEM image of Ag clusters synthesized by interfacial etching method and photograph showing the luminescence. **(d)** Scheme for the preparation of BSA-protected silver clusters and their luminescence characterization. From the authors' laboratory

mers, a high density of COOH-groups is better for the formation of fluorescent silver QCs [9.590]. Recently, small molecules having carboxylic or thiol functionalities were also used for synthesis of small clusters. Molecules such as captopril and glutathione [9.591], and dihydrolipoic acid [9.592] are reported to produce silver clusters with weak fluorescence. *Pradeep* and *Bhaskara Rao* used MSA as a scaffold for the preparation of Ag_7 and Ag_8 QCs via interfacial etching of large NPs in several aqueous/organic biphasic systems [9.586]. Ag_9 clusters have been synthesized using a solid-state route as well [9.579].

The use of biomolecules as scaffolds is a step towards developing green chemistry protocols for making quantum clusters, and it also enables the clusters to permeate into cells. Due to their luminescence property, molecular events such as replication of DNA and other genomic events happening inside cells can be visualized, measured, and tracked. Linear oligonucleotides having 12 bases were reported to be excellent scaffolds for preparation of Ag clusters [9.593–596]. It was also reported that, of these bases, Ag has more affinity towards cytosine [9.597] and guanine [9.598] residues. Efforts to use proteins as scaffolds for silver clusters due to the high affinity of silver to proteins have also been reported. Enzymes such as bovine pancreatic a-chymotrypsin (CHT) were used as templates for preparation of fluorescent silver clusters [9.599]. Cluster preparation by photoreduction in the presence of thioflavin T (ThT) has also been reported [9.600]. Synthetic oligopeptides also are being used for the preparation of silver clusters [9.601, 602]. A supramolecular hydrogel made up of dipeptides was also employed for synthesis of Ag clusters [9.603]. Proteins are also very actively used as scaffolds. Similar to dendrimers, the cage effect of the protein stabilizes the clusters and enhances their optical properties. Recently, *Liu* et al. synthesized BSA-protected Au and Au@Ag clusters using a sonochemical approach [9.578]. A protocol using BSA as the template for synthesis of Ag clusters was developed by our group recently (Fig. 9.47d) [9.604]. The conversion of Ag@citrate NPs to luminescent quantum clusters was also reported by our group [9.605]. The chemical synthesis of these systems has advanced tremendously. It is possible to create precisely controlled alloy clusters (Ag_7Au_6) through chemical means, as illustrated by our group very recently [9.606].

Inorganic templates such as glasses have also been used for preparing quantum clusters. This involves several steps. The first step involves doping of the glass with Ag^+, followed by activation by external means in the second step. The activation can be done through laser irradiation [9.607, 608], synchrotron irradiation [9.609], thermal annealing, or controlled quenching of the melt [9.571]. Zeolites have also been employed for synthesis of clusters [9.610, 611]. Here also, activation can be done by various means including heat treatment [9.612], UV light excitation [9.611], and two-photon excitation [9.613].

The application possibilities of these new nanosystems are enormous, and their exploration is in its infancy. One of the most obvious applications of these systems is in biology, especially in bioimaging [9.563, 568, 614, 615]. They have shown tremendous promise in catalysis as well [9.616–618]. These materials have been investigated for use in water purification as well. Their reactivity with heavy metals was recently explored by our group, and it was proved that the chemistry is essentially similar to that of corresponding larger NPs [9.440]. It has been demonstrated that such clusters are useful for detecting heavy metals in water as well [9.619]. The feasibility of using these materials in composites for novel applications such as antibacterial scaffolds has also been explored [9.620]. However, the authors feel that these materials are going to make a large impact in many fields, including water purification, ultrasmall sensors, diagnosis, and therapy.

9.9 Conclusions

Nanomaterials in general and noble metal NPs in particular are interesting materials for a large number of applications. This chapter illustrates the potential of noble metal NPs in various fields. The diversity and tunable properties of noble metal NPs make them superior over other categories of NPs for several key applications. In comparison with other nanoscale systems, noble metal NPs are much more stable and exhibit much less cytotoxicity. Hence, the applicability of these NPs is far greater than that of other nanosystems, especially in biology. However, most properties of many of these nanosystems, especially the anisotropic analogs, have been studied only to a limited extent, and more work is needed to understand them better. There are many promising avenues in terms of their medical and material science applications, and consistent efforts are needed to bring these to reality. The properties of gold and silver NPs and clusters are extremely sensitive to their size and shape. Detailed understanding is possible only through precise computational analyses. Rapid and sensitive responses of these NPs would be useful for developing new sensing devices. Recent research and understanding of the use of various gold and silver NPs in cancer diagnostics and therapy have already provided a platform for the development of clinical applications in the near future. A better understanding of the kinetics and dynamics of the evolution of a single NP and the development

of a more precise kinetic theory to provide an insight into the influence of various parameters on the growth of NPs under a range of conditions are also desirable. Before using these nanosystems for various applications, especially in biology and for clinical purposes, a thorough evaluation of the cytotoxicity of NPs as a function of their size, shape, and surface coating is needed.

References

9.1 M.-C. Daniel, D. Astruc: Gold nanoparticles: Assembly, supramolecular chemistry, quantum-size-related properties, and applications toward biology, catalysis, and nanotechnology, Chem. Rev. **104**(1), 293–346 (2003)

9.2 A. Moores, F. Goettmann: The plasmon band in noble metal nanoparticles: An introduction to theory and applications, New J. Chem. **30**(8), 1121–1132 (2006)

9.3 Faraday 2, http://faradayclubaward.org/wp-content/uploads/2012/08/Michael_Faraday.jpg

9.4 The Royal Institution of Great Britain, http://www.rigb.org/rimain/heritage/faradaypage.jsp

9.5 Lycurgus cup, British Museum http://www.britishmuseum.org/explore/highlights/highlight_objects/pe_mla/t/the_lycurgus_cup.aspx

9.6 M. Faraday: The Bakerian lecture: Experimental relations of gold (and other metals) to light, Philos. Trans. R. Soc. **147**, 145–181 (1857)

9.7 T. Graham: Liquid diffusion applied to analysis, Philos. Trans. R. Soc. **151**, 183–224 (1861)

9.8 Salt Lake Metals: *Antibacterial effects of silver* (Salt Lake Metals, Salt Lake City 2011), available online at http://www.saltlakemetals.com/Silver_Antibacterial.htm

9.9 Herodotus: *The History of Herodotus, translated by George Rawlinson* (Mille Tre, Vienna 2010), 1858, e-book

9.10 A.B.G. Lansdown: Silver I: Its antibacterial properties and mechanism of action, J. Wound Care **11**(4), 125–130 (2002)

9.11 A.B. Searle: *The Use of Colloids in Health and Disease* (Constable, London 1920)

9.12 E.J. Laubusch: *Water Quality and Treatment*, 3rd edn. (McGraw-Hill, New York 1971)

9.13 A.B.G. Lansdown: Silver in health care: Antimicrobial effects and safety in use, Curr. Probl. Dermatol. **33**, 17–34 (2006)

9.14 P.C. Grammaticos, A. Diamantis: Useful known and unknown views of the father of modern medicine, Hippocrates and his teacher Democritus, Hell. J. Nucl. Med. **11**(1), 2–4 (2008)

9.15 A.D. Russell, W.B. Hugo, G.P. Ellis, D.K. Luscombe: Antimicrobial activity and action of silver, Prog. Med. Chem. **31**, 351–370 (1994)

9.16 A.L. Roe: Collosol argentum and its ophthalmic uses, Br. Med. J. **1**(2820), 104 (1915)

9.17 C.E.A. Macleod: Electric metallic colloids and their therapeutical applications, Lancet **179**(4614), 322–323 (1912)

9.18 W.A. Hollis: Eighty-first Annual Meeting of the British Medical Association President's address, Br. Med. J. **2**(2759), 1282–1302 (1913)

9.19 M.C. Fung, D.L. Bowen: Silver products for medical indications: Risk-benefit assessment, Clin. Toxicol. **34**(1), 119–126 (1996)

9.20 I.M. Rutkow: *The History of Surgery in the United States* (Jeremy Norman, New York 1988)

9.21 G. Cresci, J. Mellinger: The history of nonsurgical enteral tube feeding access, Nutr. Clin. Pract. **21**(5), 522–528 (2006)

9.22 S. Simeon: On the prevention of blindness by the ophthalmia of the new-born, Lancet **132**(3392), 412–413 (1888)

9.23 T. Pradeep, Anshup: Noble metal nanoparticles for water purification: A critical review, Thin Solid Films **517**(24), 6441–6478 (2009)

9.24 A. Searle: *The Use of Metal Colloids in Health and Disease* (Sutton, New York 1919)

9.25 H. Bechhold: *Colloids in Biology and Medicine, translated by J.G.M. Bullow* (Van Nostrand, New York 1919)

9.26 O. Michael: P. William Stewart Halsted: His life and contributions to surgery, Lancet Oncol. **8**(3), 256–265 (2007)

9.27 Physician's Desk Reference: About herbs: Colloidal silver (Memorial Sloan-Kettering Cancer Center, New York 2012), available online at http://www.mskcc.org/cancer-care/herb/colloidal-silver

9.28 P.L. Drake, E. Pribitkin, W. Weber: *Colloidal Silver Products* (National Center for Complementary and Alternative Medicine, Bethesda 2006), available online at http://nccam.nih.gov/health/silver/

9.29 G. Frens, J.T.G. Overbeek: Carey Lea's colloidal silver, Colloid Polym. Sci. **233**(1), 922–929 (1969)

9.30 M.C. Lea: Allotropic forms of silver, Am. J. Sci. **37**, 476 (1889)

9.31 M. Peter-Varbanets, C. Zurbrügg, C. Swartz, W. Pronk: Decentralized systems for potable water and the potential of membrane technology, Water Res. **43**(2), 245–265 (2009)

9.32 V. Goetsch: *Free Online Colloidal Silver Ebook* (Synergenesis, Coker Creek 2010), available at http://wishgranted.com/colloidal_silver_pages_breif_history.htm

9.33 G.A. Krause: Patent 2046467 (7 July 1936) available online at http://books.google.co.in/patents/US2046467

9.34 C.E. Renn: Method of disinfecting potable water, Patent 3268444 (1966)

9.35 O. Blank: German Patent No. DRP 228697 (1910)
9.36 T.E. Lefort: French Patent No. 729952 (27 March 1931)
9.37 H. Wang, D.W. Brandl, P. Nordlander, N.J. Halas: Plasmonic nanostructures: Artificial molecules, Acc. Chem. Res. **40**(1), 53–62 (2006)
9.38 M.A. El-Sayed: Small is different: Shape-, size-, and composition-dependent properties of some colloidal semiconductor nanocrystals, Acc. Chem. Res. **37**(5), 326–333 (2004)
9.39 A.R. Tao, S. Habas, P. Yang: Shape control of colloidal metal nanocrystals, Small **4**(3), 310–325 (2008)
9.40 M.P. Pileni: Control of the size and shape of inorganic nanocrystals at various scales from nano to macrodomains, J. Phys. Chem. C **111**(26), 9019–9038 (2007)
9.41 J. Perez-Juste, I. Pastoriza-Santos, L.M. Liz-Marzán, P. Mulvaney: Gold nanorods: Synthesis, characterization and applications, Coord. Chem. Rev. **249**(17/18), 1870–1901 (2005)
9.42 S. Guo, S. Dong, E. Wang: Rectangular silver nanorods: Controlled preparation, liquid liquid interface assembly, and application in surface-enhanced Raman scattering, Cryst. Growth Des. **9**(1), 372–377 (2008)
9.43 B. Pietrobon, M. McEachran, V. Kitaev: Synthesis of size-controlled faceted pentagonal silver nanorods with tunable plasmonic properties and self-assembly of these nanorods, Am. Chem. Soc. Nano **3**(1), 21–26 (2008)
9.44 H.M. Chen, R.-S. Liu, K. Asakura, L.-Y. Jang, J.-F. Lee: Controlling length of gold nanowires with large-scale: X-ray absorption spectroscopy approaches to the growth process, J. Phys. Chem. C **111**(50), 18550–18557 (2007)
9.45 S.E. Hunyadi, C.J. Murphy: Bimetallic silver-gold nanowires: Fabrication and use in surface-enhanced Raman scattering, J. Mater. Chem. **16**(40), 3929–3935 (2006)
9.46 D. Zhang, L. Qi, J. Yang, J. Ma, H. Cheng, L. Huang: Wet chemical synthesis of silver nanowire thin films at ambient temperature, Chem. Mater. **16**(5), 872–876 (2004)
9.47 J. Hu, T.W. Odom, C.M. Lieber: Chemistry and physics in one dimension: Synthesis and properties of nanowires and nanotubes, Acc. Chem. Res. **32**(5), 435–445 (1999)
9.48 J.E. Millstone, S. Park, K.L. Shuford, L. Qin, G.C. Schatz, C.A. Mirkin: Observation of a quadrupole plasmon mode for a colloidal solution of gold nanoprisms, J. Am. Chem. Soc. **127**(15), 5312–5313 (2005)
9.49 Y. He, G. Shi: Surface plasmon resonances of silver triangle nanoplates: Graphic assignments of resonance modes and linear fittings of resonance peaks, J. Phys. Chem. B **109**(37), 17503–17511 (2005)
9.50 C. Kan, X. Zhu, G. Wang: Single-crystalline gold microplates: Synthesis, characterization, and thermal stability, J. Phys. Chem. B **110**(10), 4651–4656 (2006)
9.51 X. Zou, S. Dong: Surface-enhanced Raman scattering studies on aggregated silver nanoplates in aqueous solution, J. Phys. Chem. B **110**(43), 21545–21550 (2006)
9.52 A. Swami, A. Kumar, P.R. Selvakannan, S. Mandal, R. Pasricha, M. Sastry: Highly oriented gold nanoribbons by the reduction of aqueous chloroaurate ions by hexadecylaniline langmuir monolayers, Chem. Mater. **15**(1), 17–19 (2002)
9.53 C. Zhan, J. Wang, J. Yuan, H. Gong, Y. Liu, M. Liu: Synthesis of right- and left-handed silver nanohelices with a racemic gelator, Langmuir **19**(22), 9440–9445 (2003)
9.54 Y. Chen, S. Milenkovic, A.W. Hassel: Arrays of isooriented gold nanobelts, Nano Lett. **8**(2), 737–742 (2008)
9.55 Y. Sun, B. Mayers, Y. Xia: Transformation of silver nanospheres into nanobelts and triangular nanoplates through a thermal process, Nano Lett. **3**(5), 675–679 (2003)
9.56 N. Zhao, Y. Wei, N. Sun, Q. Chen, J. Bai, L. Zhou, Y. Qin, M. Li, L. Qi: Controlled synthesis of gold nanobelts and nanocombs in aqueous mixed surfactant solutions, Langmuir **24**(3), 991–998 (2008)
9.57 Y. Khalavka, J. Becker, C. Sönnichsen: Synthesis of rod-shaped gold nanorattles with improved plasmon sensitivity and catalytic activity, J. Am. Chem. Soc. **131**(5), 1871–1875 (2009)
9.58 J. Burgin, M. Liu, P. Guyot-Sionnest: Dielectric sensing with deposited gold bipyramids, J. Phys. Chem. C **112**(49), 19279–19282 (2008)
9.59 J. Henzie, E.-S. Kwak, T.W. Odom: Mesoscale metallic pyramids with nanoscale tips, Nano Lett. **5**(7), 1199–1202 (2005)
9.60 C.L. Nehl, H. Liao, J.H. Hafner: Optical properties of star-shaped gold nanoparticles, Nano Lett. **6**(4), 683–688 (2006)
9.61 J.L. Burt, J.L. Elechiguerra, J. Reyes-Gasga, J.M. Montejano-Carrizales, M. Jose-Yacaman: Beyond Archimedean solids: Star polyhedral gold nanocrystals, J. Cryst. Growth **285**(4), 681–691 (2005)
9.62 P.R. Sajanlal, T.S. Sreeprasad, A.S. Nair, T. Pradeep: Wires, plates, flowers, needles, and core shells: Diverse nanostructures of gold using polyaniline templates, Langmuir **24**(9), 4607–4614 (2008)
9.63 B.K. Jena, C.R. Raj: Seedless, surfactantless room temperature synthesis of single crystalline fluorescent gold nanoflowers with pronounced SERS and electrocatalytic activity, Chem. Mater. **20**(11), 3546–3548 (2008)
9.64 B.K. Jena, C.R. Raj: Synthesis of flower-like gold nanoparticles and their electrocatalytic activity towards the oxidation of methanol and the reduction of oxygen, Langmuir **23**(7), 4064–4070 (2007)
9.65 M.S. Bakshi, F. Possmayer, N.O. Petersen: Role of different phospholipids in the synthesis of pearl-necklace-type gold silver bimetallic nanoparticles

as bioconjugate materials, J. Phys. Chem. C **111**(38), 14113–14124 (2007)
9.66 E. Hao, R.C. Bailey, G.C. Schatz, J.T. Hupp, S. Li: Synthesis and optical properties of "branched" gold nanocrystals, Nano Lett. **4**(2), 327–330 (2004)
9.67 H.M. Chen, C.F. Hsin, R.-S. Liu, J.-F. Lee, L.-Y. Jang: Synthesis and characterization of multi-pod-shaped gold/silver nanostructures, J. Phys. Chem. C **111**(16), 5909–5914 (2007)
9.68 O.M. Bakr, B.H. Wunsch, F. Stellacci: High-yield synthesis of multi-branched urchin-like gold nanoparticles, Chem. Mater. **18**(14), 3297–3301 (2006)
9.69 S. D'Agostino, F. Della Sala: Silver nanourchins in plasmonics: Theoretical investigation on the optical properties of the branches, J. Phys. Chem. C **115**(24), 11934–11940 (2011)
9.70 J. Hu, Y. Zhang, B. Liu, J. Liu, H. Zhou, Y. Xu, Y. Jiang, Z. Yang, Z.-Q. Tian: Synthesis and properties of tadpole-shaped gold nanoparticles, J. Am. Chem. Soc. **126**(31), 9470–9471 (2004)
9.71 L. Tian, M.T. Ng, N. Venkatram, W. Ji, J.J. Vittal: Tadpole-shaped $AgInSe_2$ nanocrystals from a single molecular precursor and its nonlinear optical properties, Cryst. Growth Des. **10**(3), 1237–1242 (2010)
9.72 S.E. Skrabalak, L. Au, X. Li, Y. Xia: Facile synthesis of Ag nanocubes and Au nanocages, Nat. Protoc. **2**(9), 2182–2190 (2007)
9.73 M. Hu, J. Chen, M. Marquez, Y. Xia, G.V. Hartland: Correlated rayleigh scattering spectroscopy and scanning electron microscopy studies of Au Ag bimetallic nanoboxes and nanocages, J. Phys. Chem. C **111**(34), 12558–12565 (2007)
9.74 C.E. Talley, J.B. Jackson, C. Oubre, N.K. Grady, C.W. Hollars, S.M. Lane, T.R. Huser, P. Nordlander, N.J. Halas: Surface-enhanced Raman scattering from individual Au nanoparticles and nanoparticle dimer substrates, Nano Lett. **5**(8), 1569–1574 (2005)
9.75 H. Wang, D.W. Brandl, F. Le, P. Nordlander, N.J. Halas: Nanorice: A hybrid plasmonic nanostructure, Nano Lett. **6**(4), 827–832 (2006)
9.76 T. Teranishi, Y. Inoue, M. Nakaya, Y. Oumi, T. Sano: Nanoacorns: Anisotropically phase-segregated copd sulfide nanoparticles, J. Am. Chem. Soc. **126**(32), 9914–9915 (2004)
9.77 Y. Sun, B.T. Mayers, Y. Xia: Template-engaged replacement reaction: A one-step approach to the large-scale synthesis of metal nanostructures with hollow interiors, Nano Lett. **2**(5), 481–485 (2002)
9.78 C.M. Cobley, D.J. Campbell, Y. Xia: Tailoring the optical and catalytic properties of gold-silver nanoboxes and nanocages by introducing palladium, Adv. Mater. **20**(4), 748–752 (2008)
9.79 R. Gunawidjaja, S. Peleshanko, H. Ko, V.V. Tsukruk: Bimetallic nanocobs: Decorating silver nanowires with gold nanoparticles, Adv. Mater. **20**(8), 1544–1549 (2008)
9.80 G.S. Metraux, Y.C. Cao, R. Jin, C.A. Mirkin: Triangular nanoframes made of gold and silver, Nano Lett. **3**(4), 519–522 (2003)
9.81 C.-C. Huang, Z. Yang, H.-T. Chang: Synthesis of dumbbell-shaped Au Ag core shell nanorods by seed-mediated growth under alkaline conditions, Langmuir **20**(15), 6089–6092 (2004)
9.82 J.D. Swalen, D.L. Allara, J.D. Andrade, E.A. Chandross, S. Garoff, J. Israelachvili, T.J. McCarthy, R. Murray, R.F. Pease, J.F. Raboldt, K.J. Wynne: Molecular monolayers and films. A panel report for the materials sciences division of the department of energy, Langmuir **3**(6), 932–950 (1987)
9.83 K.S. Morley, P.C. Marr, P.B. Webb, A.R. Berry, F.J. Allison, G. Moldovan, P.D. Brown, S.M. Howdle: Clean preparation of nanoparticulate metals in porous supports: A supercritical route, J. Mater. Chem. **12**(6), 1898–1905 (2002)
9.84 Y. Xuan, Q. Li: Heat transfer enhancement of nanofluids, Int. J. Heat Fluid Flow **21**(1), 58–64 (2000)
9.85 X. Wang, X. Xu, S.U.S. Choi: Thermal conductivity of nanoparticle-fluid mixture, J. Thermophys. Heat Transf. **13**(4), 474–480 (1999)
9.86 M.G. DaGue, J.S. Landers, H.L. Lewis, J.L. Dye: Alkali metal anions and trapped electrons formed by evaporating metal ammonia solutions which contain cryptands, Chem. Phys. Lett. **66**(1), 169–182 (1979)
9.87 J.L. Dye, K.-L. Tsai: Small alloy particles formed by co-reduction of soluble precursors with alkalides or electrides in aprotic solvents, Faraday Discuss. **92**, 45–55 (1991)
9.88 B.A. Korgel, S. Fullam, S. Connolly, D. Fitzmaurice: Assembly and self-organization of silver nanocrystal superlattices: Ordered soft spheres, J. Phys. Chem. B **102**(43), 8379–8388 (1998)
9.89 G.B. Birrell, K.K. Hedberg, O.H. Griffith: Pitfalls of immunogold labeling: Analysis by light microscopy, transmission electron microscopy, and photoelectron microscopy, J. Histochem. Cytochem. **35**(8), 843–853 (1987)
9.90 A. Frattini, N. Pellegri, D. Nicastro, O. de Sanctis: Effect of amine groups in the synthesis of Ag nanoparticles using aminosilanes, Mater. Chem. Phys. **94**(1), 148–152 (2005)
9.91 F. Bonet, S. Grugeon, R. Herrera Urbina, K. Tekaia-Elhsissen, J.M. Tarascon: In situ deposition of silver and palladium nanoparticles prepared by the polyol process, and their performance as catalytic converters of automobile exhaust gases, Solid State Sci. **4**(5), 665–670 (2002)
9.92 P.V. Kamat, M. Flumiani, G.V. Hartland: Picosecond dynamics of silver nanoclusters. Photoejection of electrons and fragmentation, J. Phys. Chem. B **102**(17), 3123–3128 (1998)
9.93 T. Teranishi, M. Miyake: Size control of palladium nanoparticles and their crystal structures, Chem. Mater. **10**(2), 594–600 (1998)

9.94 H. Bönnemann, R.A. Brand, W. Brijoux, H.W. Hofstadt, M. Frerichs, V. Kempter, W. Maus-Friedrichs, N. Matoussevitch, K.S. Nagabhushana, F. Voigts, V. Caps: Air stable Fe and Fe–Co magnetic fluids – synthesis and characterization, Appl. Organomet. Chem. **19**(6), 790–796 (2005)

9.95 J. Turkevich, P.C. Stevenson, J. Hillier: A study of the nucleation and growth processes in the synthesis of colloidal gold, Discuss. Faraday Soc. **11**, 55–75 (1951)

9.96 G. Frens: Controlled nucleation for the regulation of the particle size in monodisperse gold suspensions, Nat. Phys. Sci. **241**(105), 20–22 (1973)

9.97 B.V. Enüstün, J. Turkevich: Coagulation of colloidal gold, J. Am. Chem. Soc. **85**(21), 3317–3328 (1963)

9.98 M. Brust, M. Walker, D. Bethell, D.J. Schiffrin, R. Whyman: Synthesis of thiol-derivatized gold nanoparticles in a two-phase liquid-liquid system, J. Chem. Soc. Chem. Commun. **7**, 801–802 (1994)

9.99 A.C. Templeton, W.P. Wuelfing, R.W. Murray: Monolayer-protected cluster molecules, Acc. Chem. Res. **33**(1), 27–36 (1999)

9.100 N. Sandhyarani, T. Pradeep: Current understanding of the structure, phase transitions and dynamics of self-assembled monolayers on two- and three-dimensional surfaces, Int. Rev. Phys. Chem. **22**(2), 221–262 (2003)

9.101 K. Vijaya Sarathy, G.U. Kulkarni, C.N.R. Rao: A novel method of preparing thiol-derivatised nanoparticles of gold, platinum and silver forming superstructures, Chem. Commun. **6**, 537–538 (1997)

9.102 B.L.V. Prasad, S.I. Stoeva, C.M. Sorensen, K.J. Klabunde: Digestive-ripening agents for gold nanoparticles: Alternatives to thiols, Chem. Mater. **15**(4), 935–942 (2003)

9.103 A. Taleb, C. Petit, M.P. Pileni: Optical properties of self-assembled 2-D and 3-D superlattices of silver nanoparticles, J. Phys. Chem. B **102**(12), 2214–2220 (1998)

9.104 T.G. Schaaff, G. Knight, M.N. Shafigullin, R.F. Borkman, R.L. Whetten: Isolation and selected properties of a 10.4 kDa gold: Glutathione cluster compound, J. Phys. Chem. B **102**(52), 10643–10646 (1998)

9.105 S. Chen, K. Kimura: Synthesis and characterization of carboxylate-modified gold nanoparticle powders dispersible in water, Langmuir **15**(4), 1075–1082 (1999)

9.106 K. Kimura, S. Sato, H. Yao: Particle crystals of surface modified gold nanoparticles grown from water, Chem. Lett. **30**(4), 372–373 (2001)

9.107 Y. Negishi, K. Nobusada, T. Tsukuda: Glutathione-protected gold clusters revisited: Bridging the gap between gold(i) thiolate complexes and thiolate-protected gold nanocrystals, J. Am. Chem. Soc. **127**(14), 5261–5270 (2005)

9.108 M.T. Reetz, W. Helbig: Size-selective synthesis of nanostructured transition metal clusters, J. Am. Chem. Soc. **116**(16), 7401–7402 (1994)

9.109 L. Rodriguez-Sanchez, M.C. Blanco, M.A. López-Quintela: Electrochemical synthesis of silver nanoparticles, J. Phys. Chem. B **104**(41), 9683–9688 (2000)

9.110 M.B. Mohamed, Z.L. Wang, M.A. El-Sayed: Temperature-dependent size-controlled nucleation and growth of gold nanoclusters, J. Phys. Chem. A **103**(49), 10255–10259 (1999)

9.111 I.G. Draganic, Z.D. Draganic: *The Radiolysis of Water* (Academic, New York 1971)

9.112 A. Henglein: Radiolytic preparation of ultrafine colloidal gold particles in aqueous solution: Optical spectrum, controlled growth, and some chemical reactions, Langmuir **15**(20), 6738–6744 (1999)

9.113 S. Wang, H. Xin: Fractal and dendritic growth of metallic Ag aggregated from different kinds of gamma-irradiated solutions, J. Phys. Chem. B **104**(24), 5681–5685 (2000)

9.114 A. Henglein: Formation and absorption spectrum of copper nanoparticles from the radiolytic reduction of $Cu(CN)_2$, J. Phys. Chem. B **104**(6), 1206–1211 (2000)

9.115 B.G. Ershov, N.L. Sukhov, E. Janata: Formation, absorption spectrum, and chemical reactions of nanosized colloidal cobalt in aqueous solution, J. Phys. Chem. B **104**(26), 6138–6142 (2000)

9.116 J.H. Hodak, A. Henglein, G.V. Hartland: Photophysics of nanometer sized metal particles: Electron-phonon coupling and coherent excitation of breathing vibrational modes, J. Phys. Chem. B **104**(43), 9954–9965 (2000)

9.117 A. Henglein: Preparation and optical aborption spectra of Au core Pt shell and Pt core Au shell colloidal nanoparticles in aqueous solution, J. Phys. Chem. B **104**(10), 2201–2203 (2000)

9.118 P. Mulvaney, M. Giersig, A. Henglein: Surface chemistry of colloidal gold: Deposition of lead and accompanying optical effects, J. Phys. Chem. **96**(25), 10419–10424 (1992)

9.119 A. Henglein, D. Meisel: Radiolytic control of the size of colloidal gold nanoparticles, Langmuir **14**(26), 7392–7396 (1998)

9.120 Y. Kato, S. Sugimoto, K. Shinohara, N. Tezuka, T. Kagotani, K. Inomata: Magnetic properties and microwave absorption properties of polymer-protected cobalt nanoparticles, Mater. Trans. Jpn. Inst. Met. **43**(3), 406–409 (2002)

9.121 T.W. Smith, D. Wychick: Colloidal iron dispersions prepared via the polymer-catalyzed decomposition of iron pentacarbonyl, J. Phys. Chem. **84**(12), 1621–1629 (1980)

9.122 J. Van Wonterghem, S. Mørup, S. Charles, S. Wells, J.R. Villadsen: Formation and chemical stability of metallic glass particles prepared by thermolysis of $Fe(CO)_5$, Hyperfine Interact. **27**(1), 333–336 (1986)

9.123 J. van Wonterghem, S. Mørup, S.W. Charles, S. Wells, J.R. Villadsen: Formation of a metallic glass by thermal decomposition of Fe $(CO)_5$, Phys. Rev. Lett. **55**(4), 410 (1985)

9.124 D.P. Dinega, M.G. Bawendi: A solution-phase chemical approach to a new crystal structure of cobalt, Angew. Chem. Int. Ed. **38**(12), 1788–1791 (1999)

9.125 V.F. Puntes, K.M. Krishnan, A.P. Alivisatos: Colloidal nanocrystal shape and size control: The case of cobalt, Science **291**(5511), 2115–2117 (2001)

9.126 V.F. Puntes, D. Zanchet, C.K. Erdonmez, A.P. Alivisatos: Synthesis of hcp-co nanodisks, J. Am. Chem. Soc. **124**(43), 12874–12880 (2002)

9.127 S. Sun, C.B. Murray, D. Weller, L. Folks, A. Moser: Monodisperse FePt nanoparticles and ferromagnetic FePt nanocrystal superlattices, Science **287**(5460), 1989–1992 (2000)

9.128 J.-I. Park, J. Cheon: Synthesis of solid solutio- and core–shell-type cobaltplatinum magnetic nanoparticles via transmetalation reactions, J. Am. Chem. Soc. **123**(24), 5743–5746 (2001)

9.129 C. Amiens, D. de Caro, B. Chaudret, J.S. Bradley, R. Mazel, C. Roucau: Selective synthesis, characterization, and spectroscopic studies on a novel class of reduced platinum and palladium particles stabilized by carbonyl and phosphine ligands, J. Am. Chem. Soc. **115**(24), 11638–11639 (1993)

9.130 F. Dumestre, B. Chaudret, C. Amiens, M.-C. Fromen, M.-J. Casanove, P. Renaud, P. Zurcher: Shape control of thermodynamically stable cobalt nanorods through organometallic chemistry, Angew. Chem. Int. Ed. **41**(22), 4286–4289 (2002)

9.131 K.J. Rao, B. Vaidhyanathan, M. Ganguli, P.A. Ramakrishnan: Synthesis of inorganic solids using microwaves, Chem. Mater. **11**(4), 882–895 (1999)

9.132 I. Pastoriza-Santos, L.M. Liz-Marzán: Formation of PVP-protected metal nanoparticles in DMF, Langmuir **18**(7), 2888–2894 (2002)

9.133 F. Fievet, J.P. Lagier, M. Figlarz: Preparing monodisperse metal powders in micrometer and submicrometer sizes by the polyol process, MRS Bulletin **24**, 29 (1989)

9.134 W. Yu, W. Tu, H. Liu: Synthesis of nanoscale platinum colloids by microwave dielectric heating, Langmuir **15**(1), 6–9 (1998)

9.135 M. Tsuji, M. Hashimoto, T. Tsuji: Fast preparation of nano-sized nickel particles under microwave irradiation without using catalyst for nucleation, Chem. Lett. **31**(12), 1232–1233 (2002)

9.136 W. Tu, H. Liu: Continuous synthesis of colloidal metal nanoclusters by microwave irradiation, Chem. Mater. **12**(2), 564–567 (2000)

9.137 B.L. Cushing, V.L. Kolesnichenko, C.J. O'Connor: Recent advances in the liquid-phase syntheses of inorganic nanoparticles, Chem. Rev. **104**(9), 3893–3946 (2004)

9.138 K.S. Suslick, S.-B. Choe, A.A. Cichowlas, M.W. Grinstaff: Sonochemical synthesis of amorphous iron, Nature **353**(6343), 414–416 (1991)

9.139 G. Aharon: Using sonochemistry for the fabrication of nanomaterials, Ultrason. Sonochem. **11**(2), 47–55 (2004)

9.140 K. Dick, T. Dhanasekaran, Z. Zhang, D. Meisel: Size-dependent melting of silica-encapsulated gold nanoparticles, J. Am. Chem. Soc. **124**(10), 2312–2317 (2002)

9.141 S. Eustis, H.-Y. Hsu, M.A. El-Sayed: Gold nanoparticle formation from photochemical reduction of Au^{3+} by continuous excitation in colloidal solutions. A proposed molecular mechanism, J. Phys. Chem. B **109**(11), 4811–4815 (2005)

9.142 F. Kim, J.H. Song, P. Yang: Photochemical synthesis of gold nanorods, J. Am. Chem. Soc. **124**(48), 14316–14317 (2002)

9.143 M.R. Jones, K.D. Osberg, R.J. Macfarlane, M.R. Langille, C.A. Mirkin: Templated techniques for the synthesis and assembly of plasmonic nanostructures, Chem. Rev. **111**(6), 3736–3827 (2011)

9.144 S.E. Skrabalak, J. Chen, Y. Sun, X. Lu, L. Au, C.M. Cobley, Y. Xia: Gold nanocages: Synthesis, properties, and applications, Acc. Chem. Res. **41**(12), 1587–1595 (2008)

9.145 B. Wiley, Y. Sun, J. Chen, H. Cang, Z.-Y. Li, X. Li, Y. Xia: Shape-controlled synthesis of silver and gold nanostructures, MRS Bulletin **30**(5), 356–361 (2005)

9.146 K. An, T. Hyeon: Synthesis and biomedical applications of hollow nanostructures, Nano Today **4**(4), 359–373 (2009)

9.147 C.-H. Su, P.-L. Wu, C.-S. Yeh: Sonochemical synthesis of well-dispersed gold nanoparticles at the ice temperature, J. Phys. Chem. B **107**(51), 14240–14243 (2003)

9.148 Y.-J. Zhu, X.-L. Hu: Microwave-polyol preparation of single-crystalline gold nanorods and nanowires, Chem. Lett. **32**(12), 1140–1141 (2003)

9.149 S. Horikoshi, H. Abe, T. Sumi, K. Torigoe, H. Sakai, N. Serpone, M. Abe: Microwave frequency effect in the formation of Au nanocolloids in polar and nonpolar solvents, Nanoscale **3**(4), 1697–1702 (2011)

9.150 C.-C. Chang, H.-L. Wu, C.-H. Kuo, M.H. Huang: Hydrothermal synthesis of monodispersed octahedral gold nanocrystals with five different size ranges and their self-assembled structures, Chem. Mater. **20**(24), 7570–7574 (2008)

9.151 R. Gans: Form of ultramicroscopic particles of silver, Ann. Phys. **47**, 270–284 (1915)

9.152 K.R. Brown, M.J. Natan: Hydroxylamine seeding of colloidal Au nanoparticles in solution and on surfaces, Langmuir **14**(4), 726–728 (1998)

9.153 N.R. Jana, L. Gearheart, C.J. Murphy: Seed-mediated growth approach for shape-controlled synthesis of spheroidal and rod-like gold nanoparticles using a surfactant template, Adv. Mater. **13**(18), 1389–1393 (2001)

9.154 C.J. Murphy, A.M. Gole, J.W. Stone, P.N. Sisco, A.M. Alkilany, E.C. Goldsmith, S.C. Baxter: Gold nanoparticles in biology: Beyond toxicity to cellular imaging, Acc. Chem. Res. **41**(12), 1721–1730 (2008)

9.155 B. Nikoobakht, M.A. El-Sayed: Preparation and growth mechanism of gold nanorods (NRs) us-

ing seed-mediated growth method, Chem. Mater. **15**(10), 1957–1962 (2003)
9.156 X. Lu, M.S. Yavuz, H.-Y. Tuan, B.A. Korgel, Y. Xia: Ultrathin gold nanowires can be obtained by reducing polymeric strands of oleylamine-AuCl complexes formed via aurophilic interaction, J. Am. Chem. Soc. **130**(28), 8900–8901 (2008)
9.157 P.R. Sajanlal, T. Pradeep: Electric-field-assisted growth of highly uniform and oriented gold nanotriangles on conducting glass substrates, Adv. Mater. **20**(5), 980–983 (2008)
9.158 F. Hao, C.L. Nehl, J.H. Hafner, P. Nordlander: Plasmon resonances of a gold nanostar, Nano Lett. **7**(3), 729–732 (2007)
9.159 Z. Wang, J. Zhang, J.M. Ekman, P.J.A. Kenis, Y. Lu: DNA-mediated control of metal nanoparticle shape: One-pot synthesis and cellular uptake of highly stable and functional gold nanoflowers, Nano Lett. **10**(5), 1886–1891 (2010)
9.160 P.R. Sajanlal, T. Pradeep: Mesoflowers: A new class of highly efficient surface-enhanced Raman active and infrared-absorbing materials, Nano Res. **2**(4), 306–320 (2009)
9.161 T.H. Ha, H.-J. Koo, B.H. Chung: Shape-controlled syntheses of gold nanoprisms and nanorods influenced by specific adsorption of halide ions, J. Phys. Chem. C **111**(3), 1123–1130 (2006)
9.162 A. Samal, T.S. Sreeprasad, T. Pradeep: Investigation of the role of $NaBH_4$ in the chemical synthesis of gold nanorods, J. Nanopart. Res. **12**(5), 1777–1786 (2010)
9.163 N.R. Jana: Gram-scale synthesis of soluble, near-monodisperse gold nanorods and other anisotropic nanoparticles, Small **1**(8/9), 875–882 (2005)
9.164 S.S. Shankar, A. Rai, B. Ankamwar, A. Singh, A. Ahmad, M. Sastry: Biological synthesis of triangular gold nanoprisms, Nat. Mater. **3**(7), 482–488 (2004)
9.165 B. Ankamwar, M. Chaudhary, M. Sastry: Gold nanotriangles biologically synthesized using tamarind leaf extract and potential application in vapor sensing, Synth. React. Inorg. Met.-Org. Nano-Met. Chem. **35**(1), 19–26 (2005)
9.166 S.L. Smitha, D. Philip, K.G. Gopchandran: Green synthesis of gold nanoparticles using *Cinnamomum zeylanicum* leaf broth, Spectrochim. Acta A **74**(3), 735–739 (2009)
9.167 M. Hosea, B. Greene, R. McPherson, M. Henzl, M.D. Alexander, D.W. Darnall: Accumulation of elemental gold on the alga *Chlorella vulgaris*, Inorg. Chim. Acta **123**(3), 161–165 (1986)
9.168 C. Lu, L. Qi, J. Yang, L. Tang, D. Zhang, J. Ma: Hydrothermal growth of large-scale micropatterned arrays of ultralong zno nanowires and nanobelts on zinc substrate, Chem. Commun. **33**, 3551–3553 (2006)
9.169 B.D. Adams, G. Wu, S. Nigro, A. Chen: Facile synthesis of Pd-Cd nanostructures with high capacity for hydrogen storage, J. Am. Chem. Soc. **131**(20), 6930–6931 (2009)
9.170 A.R. Brenner, G.E. Riddell: Nickel plating on steel by chemical reduction, J. Res. Natl. Bur. Standard **37**, 31–34 (1946)
9.171 Y. Sun: Direct growth of dense, pristine metal nanoplates with well-controlled dimensions on semiconductor substrates, Chem. Mater. **19**(24), 5845–5847 (2007)
9.172 M. Aizawa, A.M. Cooper, M. Malac, J.M. Buriak: Silver nano-inukshuks on germanium, Nano Lett. **5**(5), 815–819 (2005)
9.173 J. Fang, H. You, P. Kong, Y. Yi, X. Song, B. Ding: Dendritic silver nanostructure growth and evolution in replacement reaction, Cryst. Growth Des. **7**(5), 864–867 (2007)
9.174 J.X. Fang, X.N. Ma, H.H. Cai, X.P. Song, B.J. Ding: Nanoparticle-aggregated 3-D monocrystalline gold dendritic nanostructures, Nanotechnology **17**(23), 5841 (2006)
9.175 Y. Sun, Y. Xia: Mechanistic study on the replacement reaction between silver nanostructures and chloroauric acid in aqueous medium, J. Am. Chem. Soc. **126**(12), 3892–3901 (2004)
9.176 L. Au, Y. Chen, F. Zhou, P. Camargo, B. Lim, Z.-Y. Li, D. Ginger, Y. Xia: Synthesis and optical properties of cubic gold nanoframes, Nano Res. **1**(6), 441–449 (2008)
9.177 Y. Sun, Y. Xia: Multiple-walled nanotubes made of metals, Adv. Mater. **16**(3), 264–268 (2004)
9.178 K. Esumi, K. Matsuhisa, K. Torigoe: Preparation of rodlike gold particles by UV irradiation using cationic micelles as a template, Langmuir **11**(9), 3285–3287 (1995)
9.179 F. Kim, J.H. Song, P. Yang: Photochemical synthesis of gold nanorods, J. Am. Chem. Soc. **124**(48), 14316–14317 (2002)
9.180 R. Jin, Y. Cao, C.A. Mirkin, K.L. Kelly, G.C. Schatz, J.G. Zheng: Photoinduced conversion of silver nanospheres to nanoprisms, Science **294**(5548), 1901–1903 (2001)
9.181 R. Jin, Y. Charles Cao, E. Hao, G.S. Metraux, G.C. Schatz, C.A. Mirkin: Controlling anisotropic nanoparticle growth through plasmon excitation, Nature **425**(6957), 487–490 (2003)
9.182 W.-C. Huang, Y.-C. Chen: Photochemical synthesis of polygonal gold nanoparticles, J. Nanopart. Res. **10**(4), 697–702 (2008)
9.183 P.R. Sajanlal, T.S. Sreeprasad, A.K. Samal, T. Pradeep: Anisotropic nanomaterials: Structure, growth, assembly, and functions, Nano Rev. **2**, 5883 (2011)
9.184 Y.-Y. Yu, S.-S. Chang, C.-L. Lee, C.R.C. Wang: Gold nanorods: Electrochemical synthesis and optical properties, J. Phys. Chem. B **101**(34), 6661–6664 (1997)
9.185 C.-J. Huang, P.-H. Chiu, Y.-H. Wang, W.R. Chen, T.H. Meen: Synthesis of the gold nanocubes by elec-

trochemical technique, J. Electrochem. Soc. **153**(8), D129–D133 (2006)
9.186 S.-S. Yu, C.-L. Chang Lee, C.R.C. Wang: Gold nanorods: Electrochemical synthesis and optical properties, J. Phys. Chem. B **101**(34), 6661–6664 (1997)
9.187 N. Tian, Z.-Y. Zhou, S.-G. Sun, L. Cui, B. Ren, Z.-Q. Tian: Electrochemical preparation of platinum nanothorn assemblies with high surface enhanced Raman scattering activity, Chem. Commun. **39**, 4090–4092 (2006)
9.188 C. Gu, T.-Y. Zhang: Electrochemical synthesis of silver polyhedrons and dendritic films with superhydrophobic surfaces, Langmuir **24**(20), 12010–12016 (2008)
9.189 Y. Sun, R. Qiao: Facile tuning of superhydrophobic states with Ag nanoplates, Nano Res. **1**(4), 292–302 (2008)
9.190 C.R. Martin: Nanomaterials: A membrane-based synthetic approach, Science **266**(5193), 1961–1966 (1994)
9.191 B.M.I. van der Zande, M.R. Böhmer, L.G.J. Fokkink, C. Schönenberger: Colloidal dispersions of gold rods: Synthesis and optical properties, Langmuir **16**(2), 451–458 (1999)
9.192 H.-W. Liang, S. Liu, S.-H. Yu: Controlled synthesis of one-dimensional inorganic nanostructures using pre-existing one-dimensional nanostructures as templates, Adv. Mater. **22**(35), 3925–3937 (2010)
9.193 G. Meng, F. Han, X. Zhao, B. Chen, D. Yang, J. Liu, Q. Xu, M. Kong, X. Zhu, Y.J. Jung, Y. Yang, Z. Chu, M. Ye, S. Kar, R. Vajtai, P.M. Ajayan: A general synthetic approach to interconnected nanowire/nanotube and nanotube/nanowire/nanotube heterojunctions with branched topology, Angew. Chem. Int. Ed. **48**(39), 7166–7170 (2009)
9.194 J.C. Hulteen, C.R. Martin: A general template-based method for the preparation of nanomaterials, J. Mater. Chem. **7**(7), 1075–1087 (1997)
9.195 J.P. Camden, J.A. Dieringer, J. Zhao, R.P. Van Duyne: Controlled plasmonic nanostructures for surface-enhanced spectroscopy and sensing, Acc. Chem. Res. **41**(12), 1653–1661 (2008)
9.196 K. Salaita, Y. Wang, C.A. Mirkin: Applications of dip-pen nanolithography, Nat. Nano **2**(3), 145–155 (2007)
9.197 G.M. Wallraff, W.D. Hinsberg: Lithographic imaging techniques for the formation of nanoscopic features, Chem. Rev. **99**(7), 1801–1822 (1999)
9.198 X. Lu, M. Rycenga, S.E. Skrabalak, B. Wiley, Y. Xia: Chemical synthesis of novel plasmonic nanoparticles, Annu. Rev. Phys. Chem. **60**(1), 167–192 (2009)
9.199 P.K. Jain, X. Huang, I.H. El-Sayed, M.A. El-Sayed: Noble metals on the nanoscale: Optical and photothermal properties and some applications in imaging, sensing, biology, and medicine, Acc. Chem. Res. **41**(12), 1578–1586 (2008)
9.200 K.A. Willets, D.R.P. Van: Localized surface plasmon resonance spectroscopy and sensing, Annu. Rev. Phys. Chem. **58**, 267–297 (2007)
9.201 G. Mie: Beiträge zur Optik trüber Medien speziell kolloidaler Metallösungen, Ann. Phys. **25**, 377–445 (1908)
9.202 E. Hutter, J.H. Fendler: Exploitation of localized surface plasmon resonance, Adv. Mater. **16**(19), 1685–1706 (2004)
9.203 U. Kreibig, M. Vollmer: *Optical Properties of Metal Clusters* (Springer, Berlin, Heidelberg 1995)
9.204 S. Link, M.A. El-Sayed: Shape and size dependence of radiative, non-radiative and photothermal properties of gold nanocrystals, Int. Rev. Phys. Chem. **19**(3), 409–453 (2000)
9.205 S. Link, M.A. El-Sayed: Size and temperature dependence of the plasmon absorption of colloidal gold nanoparticles, J. Phys. Chem. B **103**(21), 4212–4217 (1999)
9.206 R. Gans: Über die Form ultramikroskopischer Goldteilchen, Ann. Phys. **342**, 881 (1912)
9.207 J. Nelayah, M. Kociak, O. Stephan, F.J. Garcia de Abajo, M. Tence, L. Henrard, D. Taverna, I. Pastoriza-Santos, L.M. Liz-Marzán, C. Colliex: Mapping surface plasmons on a single metallic nanoparticle, Nat. Phys. **3**(5), 348–353 (2007)
9.208 C. Sönnichsen, S. Geier, N.E. Hecker, G. von Plessen, J. Feldmann, H. Ditlbacher, B. Lamprecht, J.R. Krenn, F.R. Aussenegg, V.Z.H. Chan, J.P. Spatz, M. Möller: Spectroscopy of single metallic nanoparticles using total internal reflection microscopy, Appl. Phys. Lett. **77**(19), 2949–2951 (2000)
9.209 J. Müller, C. Sönnichsen, H. von Poschinger, G. von Plessen, T.A. Klar, J. Feldmann: Electrically controlled light scattering with single metal nanoparticles, Appl. Phys. Lett. **81**(1), 171–173 (2002)
9.210 G. Raschke, S. Kowarik, T. Franzl, C. Sönnichsen, T.A. Klar, J. Feldmann, A. Nichtl, K. Kärzinger: Biomolecular recognition based on single gold nanoparticle light scattering, Nano Lett. **3**(7), 935–938 (2003)
9.211 C. Sönnichsen, A.P. Alivisatos: Gold nanorods as novel nonbleaching plasmon-based orientation sensors for polarized single-particle microscopy, Nano Lett. **5**(2), 301–304 (2004)
9.212 C.L. Baciu, J. Becker, A. Janshoff, C. Sönnichsen: Protein membrane interaction probed by single plasmonic nanoparticles, Nano Lett. **8**(6), 1724–1728 (2008)
9.213 C. Novo, A.M. Funston, P. Mulvaney: Direct observation of chemical reactions on single gold nanocrystals using surface plasmon spectroscopy, Nat. Nano **3**(10), 598–602 (2008)
9.214 M.J. Crow, G. Grant, J.M. Provenzale, A. Wax: Molecular imaging and quantitative measurement of epidermal growth factor receptor expression in live cancer cells using immunolabeled gold nanoparticles, Am. J. Roentgenol. **192**(4), 1021–1028 (2009)

9.215 J. Becker, O. Schubert, C. Sönnichsen: Gold nanoparticle growth monitored in situ using a novel fast optical single-particle spectroscopy method, Nano Lett. **7**(6), 1664–1669 (2007)

9.216 G. Liu, J. Doll, L. Lee: High-speed multispectral imaging of nanoplasmonic array, Opt. Express **13**(21), 8520–8525 (2005)

9.217 G.C. Schatz: Theoretical studies of surface enhanced Raman scattering, Acc. Chem. Res. **17**(10), 370–376 (1984)

9.218 P.R. Sajanlal, C. SubRamaniam, P. Sasanpour, B. Rashidian, T. Pradeep: Electric field enhancement and concomitant Raman spectral effects at the edges of a nanometre-thin gold mesotriangle, J. Mater. Chem. **20**(11), 2108–2113 (2010)

9.219 J. Zhao, A.O. Pinchuk, J.M. McMahon, S. Li, L.K. Ausman, A.L. Atkinson, G.C. Schatz: Methods for describing the electromagnetic properties of silver and gold nanoparticles, Acc. Chem. Res. **41**(12), 1710–1720 (2008)

9.220 M. Fleischmann, P.J. Hendra, A.J. McQuillan: Raman spectra of pyridine adsorbed at a silver electrode, Chem. Phys. Lett. **26**(2), 163–166 (1974)

9.221 M.D. Porter, R.J. Lipert, L.M. Siperko, G. Wang, R. Narayanan: SERS as a bioassay platform: Fundamentals, design, and applications, Chem. Soc. Rev. **37**(5), 1001–1011 (2008)

9.222 M. Haruta, T. Kobayashi, H. Sano, N. Yamada: Novel gold catalysts for the oxidation of carbon monoxide at a temperature far below 0 °C, Chem. Lett. **2**, 405–408 (1987)

9.223 J. Xiao, L. Qi: Surfactant-assisted, shape-controlled synthesis of gold nanocrystals, Nanoscale **3**(4), 1383–1396 (2011)

9.224 O. Vaughan: A golden opportunity, Nat. Nanotechnol. **5**(1), 5–7 (2010)

9.225 G.D. Moon, S. Ko, Y. Xia, U. Jeong: Chemical transformations in ultrathin chalcogenide nanowires, Am. Chem. Soc. Nano **4**(4), 2307–2319 (2010)

9.226 R.D. Robinson, B. Sadtler, D.O. Demchenko, C.K. Erdonmez, L.-W. Wang, A.P. Alivisatos: Spontaneous superlattice formation in nanorods through partial cation exchange, Science **317**(5836), 355–358 (2007)

9.227 L. Dloczik, R. Könenkamp: Nanostructure transfer in semiconductors by ion exchange, Nano Lett. **3**(5), 651–653 (2003)

9.228 A.E. Henkes, R.E. Schaak: Trioctylphosphine: A general phosphorus source for the low-temperature conversion of metals into metal phosphides, Chem. Mater. **19**(17), 4234–4242 (2007)

9.229 C.M. Cobley, Y. Xia: Engineering the properties of metal nanostructures via galvanic replacement reactions, Mater. Sci. Eng. Rep. **70**, 44–62 (2011)

9.230 M. Chen, D.W. Goodman: Catalytically active gold: From nanoparticles to ultrathin films, Acc. Chem. Res. **39**(10), 739–746 (2006)

9.231 M.A. El-Sayed: Some interesting properties of metals confined in time and nanometer space of different shapes, Acc. Chem. Res. **34**(4), 257–264 (2001)

9.232 P.K. Jain, X. Huang, I.H. El-Sayed, M.A. El-Sayed: Noble metals on the nanoscale: Optical and photothermal properties and some applications in imaging, sensing, biology, and medicine, Acc. Chem. Res. **41**(12), 1578–1586 (2008)

9.233 C.A. Mirkin, R.L. Letsinger, R.C. Mucic, J.J. Storhoff: A DNA-based method for rationally assembling nanoparticles into macroscopic materials, Nature **382**(6592), 607–609 (1996)

9.234 L.R. Hirsch, R.J. Stafford, J.A. Bankson, S.R. Sershen, B. Rivera, R.E. Price, J.D. Hazle, N.J. Halas, J.L. West: Nanoshell-mediated near-infrared thermal therapy of tumors under magnetic resonance guidance, Proc. Natl. Acad. Sci. USA **100**(23), 13549–13554 (2003)

9.235 Y.Y. Yu, S.-S. Chang, C.-L. Lee, C.R.C. Wang: Gold nanorods: Electrochemical synthesis and optical properties, J. Phys. Chem. B **101**(34), 6661–6664 (1997)

9.236 S. Eustis, M.A. El-Sayed: Why gold nanoparticles are more precious than pretty gold: Noble metal surface plasmon resonance and its enhancement of the radiative and nonradiative properties of nanocrystals of different shapes, Chem. Soc. Rev. **35**(3), 209–217 (2006)

9.237 B.D. Todd, R.M. Lynden-Bell: Surface and bulk properties of metals modelled with Sutton–Chen potentials, Surf. Sci. **281**(1/2), 191–206 (1993)

9.238 J. Uppenbrink, R.L. Johnston, J.N. Murrell: Modeling transition metal surfaces with empirical potentials, Surf. Sci. **304**(1/2), 223–236 (1994)

9.239 Z.L. Wang, R.P. Gao, B. Nikoobakht, M.A. El-Sayed: Surface reconstruction of the unstable {110} surface in gold nanorods, J. Phys. Chem. B **104**(23), 5417–5420 (2000)

9.240 E. Carbó-Argibay, B. Rodríguez-González, S. Gómez-Graña, A. Guerrero-Martínez, I. Pastoriza-Santos, J. Pérez-Juste, L.M. Liz-Marzán: The crystalline structure of gold nanorods revisited: Evidence for higher-index lateral facets, Angew. Chem. Int. Ed. **49**(49), 9397–9400 (2010)

9.241 N.R. Jana, L. Gearheart, S.O. Obare, C.J. Murphy: Anisotropic chemical reactivity of gold spheroids and nanorods, Langmuir **18**(3), 922–927 (2002)

9.242 N.R. Jana, L. Gearheart, C.J. Murphy: Wet chemical synthesis of high aspect ratio cylindrical gold nanorods, J. Phys. Chem. B **105**(19), 4065–4067 (2001)

9.243 C. Novo, P. Mulvaney: Charge-induced Rayleigh instabilities in small gold rods, Nano Lett. **7**(2), 520–524 (2007)

9.244 M.B. Mohamed, K.Z. Ismail, S. Link, M.A. El-Sayed: Thermal reshaping of gold nanorods in micelles, J. Phys. Chem. B **102**(47), 9370–9374 (1998)

9.245 S.-S. Chang, C.-W. Shih, C.-D. Chen, W.-C. Lai, C.R.C. Wang: The shape transition of gold nanorods, Langmuir **15**(3), 701–709 (1999)

9.246 S. Link, M.A. El-Sayed: Shape and size dependence of radiative, non-radiative and photothermal properties of gold nanocrystals, Int. Rev. Phys. Chem. **19**(3), 409–453 (2000)

9.247 C.-K. Tsung, X. Kou, Q. Shi, J. Zhang, M.H. Yeung, J. Wang, G.D. Stucky: Selective shortening of single-crystalline gold nanorods by mild oxidation, J. Am. Chem. Soc. **128**(16), 5352–5353 (2006)

9.248 T.S. Sreeprasad, A.K. Samal, T. Pradeep: Body- or tip-controlled reactivity of gold nanorods and their conversion to particles through other anisotropic structures, Langmuir **23**(18), 9463–9471 (2007)

9.249 J. Rodriguez-Fernandez, J. Perez-Juste, P. Mulvaney, L.M. Liz-Marzán: Spatially-directed oxidation of gold nanoparticles by Au(III)-CTAB complexes, J. Phys. Chem. B **109**(30), 14257–14261 (2005)

9.250 J. Wang, Y.F. Li, C.Z. Huang: Identification of iodine-induced morphological transformation of gold nanorods, J. Phys. Chem. C **112**(31), 11691–11695 (2008)

9.251 X. Kou, W. Ni, C.-K. Tsung, K. Chan, H.-Q. Lin, G.D. Stucky, J. Wang: Growth of gold bipyramids with improved yield and their curvature-directed oxidation, Small **3**(12), 2103–2113 (2007)

9.252 J.H. Song, F. Kim, D. Kim, P. Yang: Crystal overgrowth on gold nanorods: Tuning the shape, facet, aspect ratio, and composition of the nanorods, Chemistry **11**(3), 910–916 (2005)

9.253 Y. Xiang, X. Wu, D. Liu, Z. Li, W. Chu, L. Feng, K. Zhang, W. Zhou, S. Xie: Gold nanorod-seeded growth of silver nanostructures: From homogeneous coating to anisotropic coating, Langmuir **24**(7), 3465–3470 (2008)

9.254 X. Kou, S. Zhang, Z. Yang, C.-K. Tsung, G.D. Stucky, L. Sun, J. Wang, C. Yan: Glutathione- and cysteine-induced transverse overgrowth on gold nanorods, J. Am. Chem. Soc. **129**(20), 6402–6404 (2007)

9.255 W. Ni, X. Kou, Z. Yang, J. Wang: Tailoring longitudinal surface plasmon wavelengths, scattering and absorption cross sections of gold nanorods, Am. Chem. Soc. Nano **2**(4), 677–686 (2008)

9.256 E. Carbó-Argibay, B. Rodríguez-González, J. Pacifico, I. Pastoriza-Santos, J. Pérez-Juste, L.M. Liz-Marzán: Chemical sharpening of gold nanorods: The rod-to-octahedron transition, Angew. Chem. Int. Ed. **46**(47), 8983–8987 (2007)

9.257 Y. Xiang, X. Wu, D. Liu, X. Jiang, W. Chu, Z. Li, Y. Ma, W. Zhou, S. Xie: Formation of rectangularly shaped Pd/Au bimetallic nanorods: Evidence for competing growth of the Pd shell between the {110} and {100} side facets of Au nanorods, Nano Lett. **6**(10), 2290–2294 (2006)

9.258 S.O. Obare, N.R. Jana, C.J. Murphy: Preparation of polystyrene- and silica-coated gold nanorods and their use as templates for the synthesis of hollow nanotubes, Nano Lett. **1**(11), 601–603 (2001)

9.259 S.E. Skrabalak, J. Chen, L. Au, X. Lu, X. Li, Y. Xia: Gold nanocages for biomedical applications, Adv. Mater. **19**(20), 3177–3184 (2007)

9.260 E. Prodan, C. Radloff, N.J. Halas, P. Nordlander: A hybridization model for the plasmon response of complex nanostructures, Science **302**(5644), 419–422 (2003)

9.261 A. Dursun, D.V. Pugh, S.G. Corcoran: Dealloying of Ag-Au alloys in halide-containing electrolytes, J. Electrochem. Soc. **150**(7), B355–B360 (2003)

9.262 J. Greeley, J.K. Nørskov: Electrochemical dissolution of surface alloys in acids: Thermodynamic trends from first-principles calculations, Electrochim. Acta **52**(19), 5829–5836 (2007)

9.263 J. Chen, J.M. McLellan, A. Siekkinen, Y. Xiong, Z.-Y. Li, Y. Xia: Facile synthesis of goldsilver nanocages with controllable pores on the surface, J. Am. Chem. Soc. **128**(46), 14776–14777 (2006)

9.264 S.E. Skrabalak, J. Chen, Y. Sun, X. Lu, L. Au, C.M. Cobley, Y. Xia: Gold nanocages: Synthesis, properties, and applications, Acc. Chem. Res. **41**(12), 1587–1595 (2008)

9.265 C.M. Cobley, Y. Xia: Engineering the properties of metal nanostructures via galvanic replacement reactions, Mater. Sci. Eng. Rep. **70**(3/6), 44–62 (2010)

9.266 M.H. Kim, X. Lu, B. Wiley, E.P. Lee, Y. Xia: Morphological evolution of single-crystal Ag nanospheres during the galvanic replacement reaction with HAuCl(4), J. Phys. Chem. C **112**(21), 7872–7876 (2008)

9.267 Y. Yin, C. Erdonmez, S. Aloni, A.P. Alivisatos: Faceting of nanocrystals during chemical transformation: From solid silver spheres to hollow gold octahedra, J. Am. Chem. Soc. **128**(39), 12671–12673 (2006)

9.268 Y. Yin, Z.-Y. Li, Z. Zhong, B. Gates, Y. Xia, S. Venkateswaran: Synthesis and characterization of stable aqueous dispersions of silver nanoparticles through the tollens process, J. Mater. Chem. **12**(3), 522–527 (2002)

9.269 A. Pyatenko, M. Yamaguchi, M. Suzuki: Synthesis of spherical silver nanoparticles with controllable sizes in aqueous solutions, J. Phys. Chem. C **111**(22), 7910–7917 (2007)

9.270 Y. Sun, Y. Xia: Alloying and dealloying processes involved in the preparation of metal nanoshells through a galvanic replacement reaction, Nano Lett. **3**(11), 1569–1572 (2003)

9.271 Y. Sun, B. Wiley, Z.-Y. Li, Y. Xia: Synthesis and optical properties of nanorattles and multiple-walled nanoshells/nanotubes made of metal alloys, J. Am. Chem. Soc. **126**(30), 9399–9406 (2004)

9.272 E.C. Cho, P.H.C. Camargo, Y. Xia: Synthesis and characterization of noble-metal nanostructures containing gold nanorods in the center, Adv. Mater. **22**(6), 744–748 (2010)

9.273 P.H.C. Camargo, Y. Xiong, L. Ji, J.M. Zuo, Y. Xia: Facile synthesis of tadpole-like nanostructures consisting of Au heads and Pd tails, J. Am. Chem. Soc. **129**(50), 15452–15453 (2007)

9.274 F. Wetz, K. Soulantica, A. Falqui, M. Respaud, E. Snoeck, B. Chaudret: Hybrid Co–Au nanorods:

Controlling Au nucleation and location, Angew. Chem. **119**(37), 7209–7211 (2007)
9.275 D. Seo, H. Song: Asymmetric hollow nanorod formation through a partial galvanic replacement reaction, J. Am. Chem. Soc. **131**(51), 18210–18211 (2009)
9.276 X. Lu, L. Au, J. McLellan, Z.-Y. Li, M. Marquez, Y. Xia: Fabrication of cubic nanocages and nanoframes by dealloying Au/Ag alloy nanoboxes with an aqueous etchant based on $Fe(NO_3)_3$ or NH_4OH, Nano Lett. **7**(6), 1764–1769 (2007)
9.277 R.C. Newman, K. Sieradzki: Metallic corrosion, Science **263**(5154), 1708–1709 (1994)
9.278 J. Chen, B. Wiley, J. McLellan, Y. Xiong, Z.-Y. Li, Y. Xia: Optical properties of PdAg and PtAg nanoboxes synthesized via galvanic replacement reactions, Nano Lett. **5**(10), 2058–2062 (2005)
9.279 F.-R. Fan, D.-Y. Liu, Y.-F. Wu, S. Duan, Z.-X. Xie, Z.-Y. Jiang, Z.-Q. Tian: Epitaxial growth of heterogeneous metal nanocrystals: From gold nanooctahedra to palladium and silver nanocubes, J. Am. Chem. Soc. **130**(22), 6949–6951 (2008)
9.280 L.-P. Jiang, S. Xu, J.-M. Zhu, J.-R. Zhang, J.-J. Zhu, H.-Y. Chen: Ultrasonic-assisted synthesis of monodisperse single-crystalline silver nanoplates and gold nanorings, Inorg. Chem. **43**(19), 5877–5883 (2004)
9.281 Y. Yin, R.M. Rioux, C.K. Erdonmez, S. Hughes, G.A. Somorjai, A.P. Alivisatos: Formation of hollow nanocrystals through the nanoscale Kirkendall effect, Science **304**(5671), 711–714 (2004)
9.282 H.J. Fan, M. Knez, R. Scholz, K. Nielsch, E. Pippel, D. Hesse, M. Zacharias, U. Gösele: Monocrystalline spinel nanotube fabrication based on the Kirkendall effect, Nat. Mater. **5**(8), 627–631 (2006)
9.283 H.J. Fan, U. Gösele, M. Zacharias: Formation of nanotubes and hollow nanoparticles based on Kirkendall and diffusion processes: A review, Small **3**(10), 1660–1671 (2007)
9.284 A. Cabot, R.K. Smith, Y. Yin, H. Zheng, B.R.M. Reinhard, H. Liu, A.P. Alivisatos: Sulfidation of cadmium at the nanoscale, Am. Chem. Soc. Nano **2**(7), 1452–1458 (2008)
9.285 J.G. Railsback, A.C. Johnston-Peck, J. Wang, J.B. Tracy: Size-dependent nanoscale Kirkendall effect during the oxidation of nickel nanoparticles, Am. Chem. Soc. Nano **4**(4), 1913–1920 (2010)
9.286 C.B. Murray, C.R. Kagan, M.G. Bawendi: Synthesis and characterization of monodisperse nanocrystals and close-packed nanocrystal assemblies, Annu. Rev. Mater. Sci. **30**, 545–610 (2000)
9.287 N. Nishida, E.S. Shibu, H. Yao, T. Oonishi, K. Kimura, T. Pradeep: Fluorescent gold nanoparticle superlattices, Adv. Mater. **20**(24), 4719–4723 (2008)
9.288 E.S. Shibu, K. Kimura, T. Pradeep: Gold nanoparticle superlattices: Novel surface enhanced Raman scattering active substrates, Chem. Mater. **21**(16), 3773–3781 (2009)
9.289 B.L.V. Prasad, C.M. Sorensen, K.J. Klabunde: Gold nanoparticle superlattices, Chem. Soc. Rev. **37**(9), 1871–1883 (2008)
9.290 K. Kimura, T. Pradeep: Functional noble metal nanoparticle superlattices grown at interfaces, Phys. Chem. Chem. Phys. **13**(43), 19214–19225 (2011)
9.291 E.S. Shibu, J. Cyriac, T. Pradeep, J. Chakrabarti: Gold nanoparticle superlattices as functional solids for concomitant conductivity and SERS tuning, Nanoscale **3**(3), 1066–1072 (2011)
9.292 E.S. Shibu, M.A.H. Muhammed, K. Kimura, T. Pradeep: Fluorescent superlattices of gold nanoparticles: A new class of functional materials, Nano Res. **2**(3), 220–234 (2009)
9.293 C.J. Murphy, T.K. Sau, A.M. Gole, C.J. Orendorff, J. Gao, L. Gou, S.E. Hunyadi, T. Li: Anisotropic metal nanoparticles: Synthesis, assembly, and optical applications, J. Phys. Chem. B **109**(29), 13857–13870 (2005)
9.294 P.K. Jain, S. Eustis, M.A. El-Sayed: Plasmon coupling in nanorod assemblies: Optical absorption, discrete dipole approximation simulation, and exciton-coupling model, J. Phys. Chem. B **110**(37), 18243–18253 (2006)
9.295 B. Nikoobakht, Z.L. Wang, M.A. El-Sayed: Self-assembly of gold nanorods, J. Phys. Chem. B **104**(36), 8635–8640 (2000)
9.296 E. Dujardin, S. Mann, L.-B. Hsin, C.R.C. Wang: DNA-driven self-assembly of gold nanorods, Chem. Commun. **14**, 1264–1265 (2001)
9.297 B. Pan, L. Ao, F. Gao, H. Tian, R. He, D. Cui: End-to-end self-assembly and colorimetric characterization of gold nanorods and nanospheres via oligonucleotide hybridization, Nanotechnology **9**, 1776 (2005)
9.298 J.-Y. Chang, H. Wu, H. Chen, Y.-C. Ling, W. Tan: Oriented assembly of Au nanorods using biorecognition system, Chem. Commun. **8**, 1092–1094 (2005)
9.299 C. Wang, Y. Chen, T. Wang, Z. Ma, Z. Su: Biorecognition-driven self-assembly of gold nanorods: A rapid and sensitive approach toward antibody sensing, Chem. Mater. **19**(24), 5809–5811 (2007)
9.300 K.K. Caswell, J.N. Wilson, U.H.F. Bunz, C.J. Murphy: Preferential end-to-end assembly of gold nanorods by biotin-streptavidin connectors, J. Am. Chem. Soc. **125**(46), 13914–13915 (2003)
9.301 Y. Wang, Y.F. Li, J. Wang, Y. Sang, C.Z. Huang: End-to-end assembly of gold nanorods by means of oligonucleotide-mercury(II) molecular recognition, Chem. Commun. **46**(8), 1332–1334 (2010)
9.302 S.T.S. Joseph, B.I. Ipe, P. Pramod, K.G. Thomas: Gold nanorods to nanochains: Mechanistic investigations on their longitudinal assembly using α,ω-alkanedithiols and interplasmon coupling, J. Phys. Chem. B **110**(1), 150–157 (2005)
9.303 T.S. Sreeprasad, T. Pradeep: Reversible assembly and disassembly of gold nanorods induced by EDTA and

its application in SERS tuning, Langmuir **27**(7), 3381–3390 (2011)
9.304 K.G. Thomas, S. Barazzouk, B.I. Ipe, S.T.S. Joseph, P.V. Kamat: Uniaxial plasmon coupling through longitudinal self-assembly of gold nanorods, J. Phys. Chem. B **108**(35), 13066–13068 (2004)
9.305 W. Ni, R.A. Mosquera, J. Pérez-Juste, L.M. Liz-Marzán: Evidence for hydrogen-bonding-directed assembly of gold nanorods in aqueous solution, J. Phys. Chem. Lett. **1**(8), 1181–1185 (2010)
9.306 P.K. Sudeep, S.T.S. Joseph, K.G. Thomas: Selective detection of cysteine and glutathione using gold nanorods, J. Am. Chem. Soc. **127**(18), 6516–6517 (2005)
9.307 S. Zhang, X. Kou, Z. Yang, Q. Shi, G.D. Stucky, L. Sun, J. Wang, C. Yan: Nanonecklaces assembled from gold rods, spheres, and bipyramids, Chem. Commun. **18**, 1816–1818 (2007)
9.308 G. Kawamura, Y. Yang, M. Nogami: End-to-end assembly of CTAB-stabilized gold nanorods by citrate anions, J. Phys. Chem. C **112**(29), 10632–10636 (2008)
9.309 C.J. Orendorff, P.L. Hankins, C.J. Murphy: pH-triggered assembly of gold nanorods, Langmuir **21**(5), 2022–2026 (2005)
9.310 T.S. Sreeprasad, A.K. Samal, T. Pradeep: One-, two-, and three-dimensional superstructures of gold nanorods induced by dimercaptosuccinic acid, Langmuir **24**(9), 4589–4599 (2008)
9.311 K. Mitamura, T. Imae, N. Saito, O. Takai: Fabrication and self-assembly of hydrophobic gold nanorods, J. Phys. Chem. B **111**(30), 8891–8898 (2007)
9.312 H. Nakashima, K. Furukawa, Y. Kashimura, K. Torimitsu: Self-assembly of gold nanorods induced by intermolecular interactions of surface-anchored lipids, Langmuir **24**(11), 5654–5658 (2008)
9.313 D.A. Walker, V.K. Gupta: Reversible end-to-end assembly of gold nanorods using a disulfide-modified polypeptide, Nanotechnology **43**, 435603 (2008)
9.314 Y.-T. Chan, S. Li, C.N. Moorefield, P. Wang, C.D. Shreiner, G.R. Newkome: Self-assembly, disassembly, and reassembly of gold nanorods mediated by bis(terpyridine)–metal connectivity, Chemistry **16**(14), 4164–4168 (2010)
9.315 M.A. Correa-Duarte, J. Pérez-Juste, A. Sánchez-Iglesias, M. Giersig, L.M. Liz-Marzán: Aligning Au nanorods by using carbon nanotubes as templates, Angew. Chem. Int. Ed. **44**(28), 4375–4378 (2005)
9.316 M.A. Correa-Duarte, L.M. Liz-Marzán: Carbon nanotubes as templates for one-dimensional nanoparticle assemblies, J. Mater. Chem. **16**(1), 22–25 (2006)
9.317 B.P. Khanal, E.R. Zubarev: Rings of nanorods, Angew. Chem. Int. Ed. **46**(13), 2195–2198 (2007)
9.318 V.R.R. Kumar, A.K. Samal, T.S. Sreeprasad, T. Pradeep: Gold nanorods grown on microgels leading to hexagonal nanostructures, Langmuir **23**(17), 8667–8669 (2007)
9.319 D. Fava, Z. Nie, M.A. Winnik, E. Kumacheva: Evolution of self-assembled structures of polymer-terminated gold nanorods in selective solvents, Adv. Mater. **20**(22), 4318–4322 (2008)
9.320 C. Wang, Y. Chen, T. Wang, Z. Ma, Z. Su: Monodispersed gold nanorod-embedded silica particles as novel Raman labels for biosensing, Adv. Funct. Mater. **18**(2), 355–361 (2008)
9.321 A.J. Mieszawska, G.W. Slawinski, F.P. Zamborini: Directing the growth of highly aligned gold nanorods through a surface chemical amidation reaction, J. Am. Chem. Soc. **128**(17), 5622–5623 (2006)
9.322 K. Honda, Y. Niidome, N. Nakashima, H. Kawazumi, S. Yamada: End-to-end assemblies of gold nanorods adsorbed on a glass substrate modified with polyanion polymers, Chem. Lett. **35**(8), 854–855 (2006)
9.323 X. Zhang, T. Imae: Perpendicular superlattice growth of hydrophobic gold nanorods on patterned silicon substrates via evaporation-induced self-assembling, J. Phys. Chem. C **113**(15), 5947–5951 (2009)
9.324 M.H. Zareie, X. Xu, M.B. Cortie: In situ organization of gold nanorods on mixed self-assembled-monolayer substrates, Small **3**(1), 139–145 (2007)
9.325 Z. Nie, D. Fava, M. Rubinstein, E. Kumacheva: Supramolecular assembly of gold nanorods end-terminated with polymerpom-poms: Effect of pom-pom structure on the association modes, J. Am. Chem. Soc. **130**(11), 3683–3689 (2008)
9.326 Z. Nie, D. Fava, E. Kumacheva, S. Zou, G.C. Walker, M. Rubinstein: Self-assembly of metal-polymer analogues of amphiphilic triblock copolymers, Nat. Mater. **6**(8), 609–614 (2007)
9.327 S. Yun, Y.-K. Park, S.K. Kim, S. Park: Linker-molecule-free gold nanorod layer-by-layer films for surface-enhanced Raman scattering, Anal. Chem. **79**(22), 8584–8589 (2007)
9.328 H. Nakashima, K. Furukawa, Y. Kashimura, K. Torimitsu: Anisotropic assembly of gold nanorods assisted by selective ion recognition of surface-anchored crown ether derivatives, Chem. Commun. **10**, 1080–1082 (2007)
9.329 M. Grzelczak, B. Rodríguez-González, J. Pérez-Juste, L.M. Liz-Marzán: Quasi-epitaxial growth of Ni nanoshells on Au nanorods, Adv. Mater. **19**(17), 2262–2266 (2007)
9.330 N.R. Jana, L. Gearheart, C.J. Murphy: Wet chemical synthesis of silver nanorods and nanowires of controllable aspect ratio, Chem. Commun. **7**, 617–618 (2001)
9.331 A. Tao, F. Kim, C. Hess, J. Goldberger, R. He, Y. Sun, Y. Xia, P. Yang: Langmuir–Blodgett silver nanowire monolayers for molecular sensing using surface-enhanced Raman spectroscopy, Nano Lett. **3**(9), 1229–1233 (2003)
9.332 M. Rycenga, J. McLellan, Y. Xia: Controlling the assembly of silver nanocubes through selective functionalization of their faces, Adv. Mater. **20**(12), 2416–2420 (2008)

9.333 A. Tao, P. Sinsermsuksakul, P. Yang: Tunable plasmonic lattices of silver nanocrystals, Nat. Nano **2**(7), 435–440 (2007)

9.334 Y. Bae, N.H. Kim, M. Kim, K.Y. Lee, S.W. Han: Anisotropic assembly of Ag nanoprisms, J. Am. Chem. Soc. **130**(16), 5432–5433 (2008)

9.335 B.I. Ipe, S. Mahima, K.G. Thomas: Light-induced modulation of self-assembly on spiropyran-capped gold nanoparticles: A potential system for the controlled release of amino acid derivatives, J. Am. Chem. Soc. **125**(24), 7174–7175 (2003)

9.336 H. Imahori, M. Arimura, T. Hanada, Y. Nishimura, I. Yamazaki, Y. Sakata, S. Fukuzumi: Photoactive three-dimensional monolayers: Porphyrin-alkanethiolate-stabilized gold clusters, J. Am. Chem. Soc. **123**(2), 335–336 (2000)

9.337 H. Fujihara, H. Nakai: Fullerenethiolate-functionalized gold nanoparticles: A new class of surface-confined metal-C_{60} nanocomposites, Langmuir **17**(21), 6393–6395 (2001)

9.338 T. Wang, D. Zhang, W. Xu, J. Yang, R. Han, D. Zhu: Preparation, characterization, and photophysical properties of alkanethiols with pyrene units-capped gold nanoparticles: Unusual fluorescence enhancement for the aged solutions of these gold nanoparticles, Langmuir **18**(5), 1840–1848 (2002)

9.339 J. Zhang, J.K. Whitesell, M.A. Fox: Photoreactivity of self-assembled monolayers of azobenzene or stilbene derivatives capped on colloidal gold clusters, Chem. Mater. **13**(7), 2323–2331 (2001)

9.340 T. Gu, T. Ye, J.D. Simon, J.K. Whitesell, M.A. Fox: Subpicosecond transient dynamics in gold nanoparticles encapsulated by a fluorophore-terminated monolayer, J. Phys. Chem. B **107**(8), 1765–1771 (2003)

9.341 R. BalasubRamanian, B. Kim, S.L. Tripp, X. Wang, M. Lieberman, A. Wei: Dispersion and stability studies of resorcinarene-encapsulated gold nanoparticles, Langmuir **18**(9), 3676–3681 (2002)

9.342 A. Manna, P.-L. Chen, H. Akiyama, T.-X. Wei, K. Tamada, W. Knoll: Optimized photoisomerization on gold nanoparticles capped by unsymmetrical azobenzene disulfides, Chem. Mater. **15**(1), 20–28 (2002)

9.343 K.G. Thomas, P.V. Kamat: Making gold nanoparticles glow: Enhanced emission from a surface-bound fluoroprobe, J. Am. Chem. Soc. **122**(11), 2655–2656 (2000)

9.344 L.M. Liz-Marzán, M. Giersig, P. Mulvaney: Synthesis of nanosized gold-silica core-shell particles, Langmuir **12**(18), 4329–4335 (1996)

9.345 R. Davies, G.A. Schurr, P. Meenan, R.D. Nelson, H.E. Bergna, C.A.S. Brevett, R.H. Goldbaum: Engineered particle surfaces, Adv. Mater. **10**(15), 1264–1270 (1998)

9.346 L.M. Liz-Marzán, M. Giersig, P. Mulvaney: Homogeneous silica coating of vitreophobic colloids, Chem. Commun. **6**, 731–732 (1996)

9.347 I. Pastoriza-Santos, D.S. Koktysh, A.A. Mamedov, M. Giersig, N.A. Kotov, L.M. Liz-Marzán: One-pot synthesis of Ag@TiO_2 core-shell nanoparticles and their layer-by-layer assembly, Langmuir **16**(6), 2731–2735 (2000)

9.348 R.T. Tom, A.S. Nair, N. Singh, M. Aslam, C.L. Nagendra, R. Philip, K. Vijayamohanan, T. Pradeep: Freely dispersible Au@TiO_2, Au@ZrO_2, Ag@TiO_2, and Ag@ZrO_2 core-shell nanoparticles: One-step synthesis, characterization, spectroscopy, and optical limiting properties, Langmuir **19**(8), 3439–3445 (2003)

9.349 X. Teng, D. Black, N.J. Watkins, Y. Gao, H. Yang: Platinum-maghemite core-shell nanoparticles using a sequential synthesis, Nano Lett. **3**(2), 261–264 (2003)

9.350 P. Mulvaney, L.M. Liz-Marzán, M. Giersig, T. Ung: Silica encapsulation of quantum dots and metal clusters, J. Mater. Chem. **10**(6), 1259–1270 (2000)

9.351 K.S. Mayya, D.I. Gittins, F. Caruso: Gold-titania core-shell nanoparticles by polyelectrolyte complexation with a titania precursor, Chem. Mater. **13**(11), 3833–3836 (2001)

9.352 A.S. Nair, T. Pradeep, I. MacLaren: An investigation of the structure of stearate monolayers on Au@ZrO_2 and Ag@ZrO_2 core-shell nanoparticles, J. Mater. Chem. **14**(5), 857–862 (2004)

9.353 M.M.Y. Chen, A. Katz: Synthesis and characterization of gold-silica nanoparticles incorporating a mercaptosilane core-shell interface, Langmuir **18**(22), 8566–8572 (2002)

9.354 T. Yonezawa, N. Toshima: Polymer- and micelle-protected gold/platinum bimetallic systems. Preparation, application to catalysis for visible-light-induced hydrogen evolution, and analysis of formation process with optical methods, J. Mol. Catal. **83**(1-2), 167–181 (1993)

9.355 G. Schmid, A. Lehnert, J.-O. Malm, J.-O. Bovin: Ligand-stabilized bimetallic colloids identified by HRTEM and EDX, Angew. Chem. Int. Ed. **30**(7), 874–876 (1991)

9.356 P. Mulvaney, M. Giersig, A. Henglein: Electrochemistry of multilayer colloids: Preparation and absorption spectrum of gold-coated silver particles, J. Phys. Chem. **97**(27), 7061–7064 (1993)

9.357 S. Link, C. Burda, Z. Wang, M. El-Sayed: Electron dynamics in gold and gold-silver alloy nanoparticles: The influence of a nonequilibrium electron distribution and the size dependence of the electron? Phonon relaxation, J. Chem. Phys. **111**(3), 1255 (1999)

9.358 Y. Kim, R.C. Johnson, J. Li, J.T. Hupp, G.C. Schatz: Synthesis, linear extinction, and preliminary resonant hyper-Rayleigh scattering studies of gold-core/silver-shell nanoparticles: Comparisons of theory and experiment, Chem. Phys. Lett. **352**(5/6), 421–428 (2002)

9.359 N.S. Sobal, M. Hilgendorff, H. Möhwald, M. Giersig, M. Spasova, T. Radetic, M. Farle: Synthesis and

structure of colloidal bimetallic nanocrystals: The non-alloying system Ag/Co, Nano Lett. **2**(6), 621–624 (2002)
9.360 H. Cai, N. Zhu, Y. Jiang, P. He, Y. Fang: Cu@Au alloy nanoparticle as oligonucleotides labels for electrochemical stripping detection of DNA hybridization, Biosens. Bioelectron. **18**(11), 1311–1319 (2003)
9.361 C.-L. Huang, E. Matijevic: Coating of uniform inorganic particles with polymers: III. Polypyrrole on different metal oxides, J. Mater. Res. **10**(05), 1327–1336 (1995)
9.362 M. Sastry, A. Swami, S. Mandal, P.R. Selvakannan: New approaches to the synthesis of anisotropic, core-shell and hollow metal nanostructures, J. Mater. Chem. **15**(31), 3161–3174 (2005)
9.363 Y. Yang, J. Shi, H. Chen, S. Dai, Y. Liu: Enhanced off-resonance optical nonlinearities of Au@CdS core-shell nanoparticles embedded in $BaTiO_3$ thin films, Chem. Phys. Lett. **370**(1-2), 1–6 (2003)
9.364 S.M. Marinakos, J.P. Novak, L.C. Brousseau, A.B. House, E.M. Edeki, J.C. Feldhaus, D.L. Feldheim: Gold particles as templates for the synthesis of hollow polymer capsules. Control of capsule dimensions and guest encapsulation, J. Am. Chem. Soc. **121**(37), 8518–8522 (1999)
9.365 I. Mekis, D.V. Talapin, A. Kornowski, M. Haase, H. Weller: One-pot synthesis of highly luminescent CdSe/CdS core-shell nanocrystals via organometallic and "greener" chemical approaches, J. Phys. Chem. B **107**(30), 7454–7462 (2003)
9.366 S.M. Marinakos, L.C. Brousseau, A. Jones, D.L. Feldheim: Template synthesis of one-dimensional Au, Au-poly(pyrrole), and poly(pyrrole) nanoparticle arrays, Chem. Mater. **10**(5), 1214–1219 (1998)
9.367 S.M. Marinakos, D.A. Shultz, D.L. Feldheim: Gold nanoparticles as templates for the synthesis of hollow nanometer-sized conductive polymer capsules, Adv. Mater. **11**(1), 34–37 (1999)
9.368 R. Ottewill, A. Schofield, J. Waters, N. Williams: Preparation of core-shell polymer colloid particles by encapsulation, Colloid Polym. Sci. **275**(3), 274–283 (1997)
9.369 L. Quaroni, G. Chumanov: Preparation of polymer-coated functionalized silver nanoparticles, J. Am. Chem. Soc. **121**(45), 10642–10643 (1999)
9.370 P.K. Jain, X. Huang, I.H. El-Sayed, M.A. El-Sayed: Noble metals on the nanoscale: Optical and photothermal properties and some applications in imaging, sensing, biology, and medicine, Acc. Chem. Res. **41**(12), 1578–1586 (2008)
9.371 R.A. Sperling, G.P. Rivera, F. Zhang, M. Zanella, W.J. Parak: Biological applications of gold nanoparticles, Chem. Soc. Rev. **37**(9), 1896–1908 (2008)
9.372 H. Wang, T.B. Huff, D.A. Zweifel, W. He, P.S. Low, A. Wei, J.-X. Cheng: In vitro and in vivo two-photon luminescence imaging of single gold nanorods, Proc. Natl. Acad. Sci. USA **102**(44), 15752–15756 (2005)
9.373 R. Philip, G.R. Kumar, N. Sandhyarani, T. Pradeep: Picosecond optical nonlinearity in monolayer-protected gold, silver, and gold-silver alloy nanoclusters, Phys. Rev. B **62**(19), 13160–13166 (2000)
9.374 A. Campion, P. Kambhampati: Surface-enhanced Raman scattering, Chem. Soc. Rev. **27**(4), 241–250 (1998)
9.375 M.J. Banholzer, J.E. Millstone, L. Qin, C.A. Mirkin: Rationally designed nanostructures for surface-enhanced Raman spectroscopy, Chem. Soc. Rev. **37**(5), 885–897 (2008)
9.376 J.F. Li, Y.F. Huang, Y. Ding, Z.L. Yang, S.B. Li, X.S. Zhou, F.R. Fan, W. Zhang, Z.Y. Zhou, D.Y. Wu, B. Ren, Z.L. Wang, Z.Q. Tian: Shell-isolated nanoparticle-enhanced Raman spectroscopy, Nature **464**(7287), 392–395 (2010)
9.377 K.M. Mayer, J.H. Hafner: Localized surface plasmon resonance sensors, Chem. Rev. **111**(6), 3828–3857 (2011)
9.378 G. Aragay, J. Pons, A. Merkoçi: Recent trends in macro-, micro-, and nanomaterial-based tools and strategies for heavy-metal detection, Chem. Rev. **111**(5), 3433–3458 (2011)
9.379 M. Rex, F.E. Hernandez, A.D. Campiglia: Pushing the limits of mercury sensors with gold nanorods, Anal. Chem. **78**(2), 445–451 (2005)
9.380 K.P. Lisha, Anshup, T. Pradeep: Towards a practical solution for removing inorganic mercury from drinking water using gold nanoparticles, Gold Bull. **42**(2), 144–152 (2009)
9.381 S. Eustis, M.A. El-Sayed: Why gold nanoparticles are more precious than pretty gold: Noble metal surface plasmon resonance and its enhancement of the radiative and nonradiative properties of nanocrystals of different shapes, Chem. Soc. Rev. **35**(3), 209–217 (2006)
9.382 R. Narayanan, M.A. El-Sayed: Catalysis with transition metal nanoparticles in colloidal solution: Nanoparticle shape dependence and stability, J. Phys. Chem. B **109**(26), 12663–12676 (2005)
9.383 H. Yu, X. Wang, H. Sun, M. Huo: Photocatalytic degradation of malathion in aqueous solution using an Au-Pd-TiO_2 nanotube film, J. Hazard. Mater. **184**(1-3), 753–758 (2010)
9.384 F.H. Rhodes, J.T. Carty: The corrosion of certain metals by carbon tetrachloride, Ind. Eng. Chem. **17**(9), 909–911 (1925)
9.385 T. Boronina, K.J. Klabunde, G. Sergeev: Destruction of organohalides in water using metal particles: Carbon tetrachloride/water reactions with magnesium, tin, and zinc, Environ. Sci. Technol. **29**(6), 1511–1517 (1995)
9.386 A. Henglein: Colloidal silver nanoparticles: Photochemical preparation and interaction with O_2, CCl_4, and some metal ions, Chem. Mater. **10**(1), 444–450 (1998)

9.387 N. Sandhyarani, T. Pradeep: Oxidation of alkanethiol monolayers on gold cluster surfaces, Chem. Phys. Lett. **338**(1), 33–36 (2001)

9.388 A. Henglein, D. Meisel: Spectrophotometric observations of the adsorption of organosulfur compounds on colloidal silver nanoparticles, J. Phys. Chem. B **102**(43), 8364–8366 (1998)

9.389 A.S. Nair, T. Pradeep: Halocarbon mineralization and catalytic destruction by metal nanoparticles, Curr. Sci. **84**, 1560–1564 (2003)

9.390 A. Sreekumaran Nair, R.T. Tom, T. Pradeep: Detection and extraction of endosulfan by metal nanoparticles, J. Environ. Mon. **5**(2), 363–365 (2003)

9.391 A.S. Nair, T. Pradeep: Extraction of chlorpyrifos and malathion from water by metal nanoparticles, J. Nanosci. Nanotechnol. **7**(6), 1871–1877 (2007)

9.392 T. Pradeep, A.S. Nair: A method of preparing purified water from water containing pesticides (chlorpyrifos and malatheon) and purified water prepared by the said method, Indian Patent Ser., Vol. 200767 (2006)

9.393 A.S. Nair, R.T. Tom, T. Pradeep: Detection and extraction of endosulfan by metal nanoparticles, J. Environ. Mon. **5**(2), 363–365 (2003)

9.394 D.L. Illman: Water analysis in the developing world, Anal. Chem. **78**(15), 5266–5272 (2006)

9.395 S.D. Richardson: Water analysis: Emerging contaminants and current issues, Anal. Chem. **79**(12), 4295–4324 (2007)

9.396 S. Andreescu, J.-L. Marty: Twenty years research in cholinesterase biosensors: From basic research to practical applications, Biomol. Eng. **23**(1), 1–15 (2006)

9.397 X.J. Huang, Y.K. Choi: Chemical sensors based on nanostructured materials, Sens. Actuators B **122**(2), 659–671 (2007)

9.398 D.J. Lewis, T.M. Day, J.V. MacPherson, Z. Pikramenou: Luminescent nanobeads: Attachment of surface reactive Eu(III) complexes to gold nanoparticles, Chem. Commun. **13**, 1433–1435 (2006)

9.399 S.S.R. Dasary, U.S. Rai, H. Yu, Y. Anjaneyulu, M. Dubey, P.C. Ray: Gold nanoparticle based surface enhanced fluorescence for detection of organophosphorus agents, Chem. Phys. Lett. **460**(1-3), 187–190 (2008)

9.400 J.D.S. Newman, J.M. Roberts, G.J. Blanchard: Optical organophosphate sensor based upon gold nanoparticle functionalized fumed silica gel, Anal. Chem. **79**(9), 3448–3454 (2007)

9.401 J.D.S. Newman, J.M. Roberts, G.J. Blanchard: Optical organophosphate/phosphonate sensor based upon gold nanoparticle functionalized quartz, Anal. Chim. Acta **602**(1), 101–107 (2007)

9.402 S.-Q. Hu, J.-W. Xie, Q.-H. Xu, K.-T. Rong, G.-L. Shen, R.-Q. Yu: A label-free electrochemical immunosensor based on gold nanoparticles for detection of paraoxon, Talanta **61**(6), 769–777 (2003)

9.403 D.P. Dumas, H.D. Durst, W.G. Landis, F.M. Raushel, J.R. Wild: Inactivation of organophosphorus nerve agents by the phosphotriesterase from pseudomonas diminuta, Arch. Biochem. Biophys. **277**(1), 155–159 (1990)

9.404 V. Pavlov, Y. Xiao, I. Willner: Inhibition of the acetycholine esterase-stimulated growth of Au nanoparticles: Nanotechnology-based sensing of nerve gases, Nano Lett. **5**(4), 649–653 (2005)

9.405 D. Du, J. Ding, Y. Tao, X. Chen: Application of chemisorption/desorption process of thiocholine for pesticide detection based on acetylcholinesterase biosensor, Sens. Actuators B **134**(2), 908–912 (2008)

9.406 J.M. Pingarrón, P. Yáñez-Sedeño, A. González-Cortés: Gold nanoparticle-based electrochemical biosensors, Electrochim. Acta **53**(19), 5848–5866 (2008)

9.407 K.A. Hassal: *The Biochemistry and Use of Pesticides* (Wiley, New York 1990)

9.408 T.J. Lin, K.T. Huang, C.Y. Liu: Determination of organophosphorous pesticides by a novel biosensor based on localized surface plasmon resonance, Biosens. Bioelectron. **22**(4), 513–518 (2006)

9.409 Rajan, S. Chand, B.D. Gupta: Surface plasmon resonance based fiber-optic sensor for the detection of pesticide, Sens. Actuators B **123**(2), 661–666 (2007)

9.410 X. Sun, K. Xia, B. Liu: Design of fluorescent self-assembled multilayers and interfacial sensing for organophosphorus pesticides, Talanta **76**(4), 747–751 (2008)

9.411 K.P. Lisha, Anshup, T. Pradeep: Enhanced visual detection of pesticides using gold nanoparticles, J. Environ. Sci. Health B **44**(7), 697–705 (2009)

9.412 C. Burns, W.U. Spendel, S. Puckett, G.E. Pacey: Solution ionic strength effect on gold nanoparticle solution color transition, Talanta **69**(4), 873–876 (2006)

9.413 S.T. Dubas, V. Pimpan: Humic acid assisted synthesis of silver nanoparticles and its application to herbicide detection, Mater. Lett. **62**(17/18), 2661–2663 (2008)

9.414 K. Kneipp, H. Kneipp, I. Itzkan, R.R. Dasari, M.S. Feld: Ultrasensitive chemical analysis by Raman spectroscopy, Chem. Rev. **99**(10), 2957–2976 (1999)

9.415 M. Moskovits: Surface-enhanced spectroscopy, Rev. Mod. Phys. **57**(3), 783–826 (1985)

9.416 K. Kneipp, Y. Wang, H. Kneipp, L.T. Perelman, I. Itzkan, R.R. Dasari, M.S. Feld: Single molecule detection using surface-enhanced Raman scattering (SERS), Phys. Rev. Lett. **78**(9), 1667–1670 (1997)

9.417 S. Nie, S.R. Emory: Probing single molecules and single nanoparticles by surface-enhanced Raman scattering, Science **275**(5303), 1102–1106 (1997)

9.418 V.S. Tiwari, T. Oleg, G.K. Darbha, W. Hardy, J.P. Singh, P.C. Ray: Non-resonance SERS effects of silver colloids with different shapes, Chem. Phys. Lett. **446**(1–3), 77–82 (2007)

9.419 P.R. Sajanlal, T. Pradeep: Electric-field-assisted growth of highly uniform and oriented gold nanotriangles on conducting glass substrates, Adv. Mater. **20**(5), 980–983 (2008)

9.420 A.J. Bonham, G. Braun, I. Pavel, M. Moskovits, N.O. Reich: Detection of sequence-specific protein-DNA interactions via surface enhanced resonance Raman scattering, J. Am. Chem. Soc. **129**(47), 14572–14573 (2007)

9.421 R.A. Alvarez-Puebla, J.D.S. dos Santos, R.F. Aroca: Sers detection of environmental pollutants in humic acid-gold nanoparticle composite materials, Analyst **132**(12), 1210–1214 (2007)

9.422 A. Henglein: Physicochemical properties of small metal particles in solution: "Microelectrode" Reactions, chemisorption, composite metal particles, and the atom-to-metal transition, J. Phys. Chem. **97**(21), 5457–5471 (1993)

9.423 A. Henglein: Non-metallic silver clusters in aqueous solution: Stabilization and chemical reactions, Chem. Phys. Lett. **154**(5), 473–476 (1989)

9.424 A. Henglein, P. Mulvaney, T. Linnert, A. Holzwarth: Surface chemistry of colloidal silver: Reduction of adsorbed cadmium(2+) ions and accompanying optical effects, J. Phys. Chem. **96**(6), 2411–2414 (1992)

9.425 Y. Liu, C.Y. Liu, L.B. Chen, Z.Y. Zhang: Adsorption of cations onto the surfaces of silver nanoparticles, J. Colloid Interface Sci. **257**(2), 188–194 (2003)

9.426 C. Namasivayam, K. Periasamy: Bicarbonate-treated peanut hull carbon for mercury(II) removal from aqueous solution, Water Res. **27**(11), 1663–1668 (1993)

9.427 R.R. Navarro, K. Sumi, N. Fujii, M. Matsumura: Mercury removal from wastewater using porous cellulose carrier modified with polyethyleneimine, Water Res. **30**(10), 2488–2494 (1996)

9.428 V. Smuleac, D.A. Butterfield, S.K. Sikdar, R.S. Varma, D. Bhattacharyya: Polythiol-functionalized alumina membranes for mercury capture, J. Membr. Sci. **251**(1/2), 169–178 (2005)

9.429 S.M. Evangelista, E. DeOliveira, G.R. Castro, L.F. Zara, A.G.S. Prado: Hexagonal mesoporous silica modified with 2-mercaptothiazoline for removing mercury from water solution, Surf. Sci. **601**(10), 2194–2202 (2007)

9.430 T.S. Sreeprasad, S.M. Maliyekkal, K.P. Lisha, T. Pradeep: Reduced graphene oxide"metal/metal oxide composites: Facile synthesis and application in water purification, J. Hazard. Mater. **186**(1), 921–931 (2011)

9.431 X.-Q. Li, W.-X. Zhang: Iron nanoparticles: The core-shell structure and unique properties for Ni(II) sequestration, Langmuir **22**(10), 4638–4642 (2006)

9.432 T. Morris, H. Copeland, E. McLinden, S. Wilson, G. Szulczewski: The effects of mercury adsorption on the optical response of size-selected gold and silver nanoparticles, Langmuir **18**(20), 7261–7264 (2002)

9.433 L. Katsikas, M. Gutiérrez, A. Henglein: Bimetallic colloids: Silver and mercury, J. Phys. Chem. **100**(27), 11203–11206 (1996)

9.434 J.A. Creighton, D.G. Eadon: Ultraviolet-visible absorption spectra of the colloidal metallic elements, J. Chem. Soc. Faraday Trans. **87**(24), 3881–3891 (1991)

9.435 A. Henglein, C. Brancewicz: Absorption spectra and reactions of colloidal bimetallic nanoparticles containing mercury, Chem. Mater. **9**(10), 2164–2167 (1997)

9.436 L. Li, Y.J. Zhu: High chemical reactivity of silver nanoparticles toward hydrochloric acid, J. Colloid Interface Sci. **303**(2), 415–418 (2006)

9.437 J. Chen, B. Wiley, J. McLellan, Y. Xiong, Z.Y. Li, Y. Xia: Optical properties of Pd-Ag and Pt-Ag nanoboxes synthesized via galvanic replacement reactions, Nano Lett. **5**(10), 2058–2062 (2005)

9.438 M.S. Bootharaju, T. Pradeep: Uptake of toxic metal ions from water by naked and monolayer protected silver nanoparticles: An x-ray photoelectron spectroscopic investigation, J. Phys. Chem. C **114**(18), 8328–8336 (2010)

9.439 E. Sumesh, M.S. Bootharaju, Anshup, T. Pradeep: A practical silver nanoparticle-based adsorbent for the removal of Hg^{2+} from water, J. Hazard. Mater. **189**(1/2), 450–457 (2011)

9.440 M.S. Bootharaju, T. Pradeep: Investigation into the reactivity of unsupported and supported Ag_7 and Ag_8 clusters with toxic metal ions, Langmuir **27**(13), 8134–8143 (2011)

9.441 E.M. Nolan, S.J. Lippard: Tools and tactics for the optical detection of mercuric ion, Chem. Rev. **108**(9), 3443–3480 (2008)

9.442 D. Melamed: Monitoring arsenic in the environment: A review of science and technologies with the potential for field measurements, Anal. Chim. Acta **532**(1), 1–13 (2005)

9.443 M.d.G.A. Korn, J.B. de Andrade, D.S. de Jesus, V.A. Lemos, M.L.S.F. Bandeira, W.N.L. dos Santos, M.A. Bezerra, F.A.C. Amorim, A.S. Souza, S.L.C. Ferreira: Separation and preconcentration procedures for the determination of lead using spectrometric techniques: A review, Talanta **69**(1), 16–24 (2006)

9.444 P.A. Mosier-Boss, S.H. Lieberman: Detection of anions by normal Raman spectroscopy and surface-enhanced Raman spectroscopy of cationic-coated substrates, Appl. Spectrosc. **57**(9), 1129–1137 (2003)

9.445 J.J. Storhoff, A.A. Lazarides, R.C. Mucic, C.A. Mirkin, R.L. Letsinger, G.C. Schatz: What controls the optical properties of DNA-linked gold nanoparticle assemblies?, J. Am. Chem. Soc. **122**(19), 4640–4650 (2000)

9.446 Y. Lu, J. Liu: Smart nanomaterials inspired by biology: Dynamic assembly of error-free nanomaterials in response to multiple chemical and biological stimuli, Acc. Chem. Res. **40**(5), 315–323 (2007)

9.447 A. Ono, H. Togashi: Highly selective oligonucleotide-based sensor for mercury(II) in aqueous solutions, Angew. Chem. Int. Ed. **43**(33), 4300–4302 (2004)

9.448 J.-S. Lee, M.S. Han, C.A. Mirkin: Colorimetric detection of mercuric ion (Hg^{2+}) in aqueous media using DNA-functionalized gold nanoparticles, Angew. Chem. Int. Ed. **46**(22), 4093–4096 (2007)

9.449 J.-S. Lee, C.A. Mirkin: Chip-based scanometric detection of mercuric ion using DNA-functionalized gold nanoparticles, Anal. Chem. **80**(17), 6805–6808 (2008)

9.450 J. Liu, Y. Lu: A colorimetric lead biosensor using DNAzyme-directed assembly of gold nanoparticles, J. Am. Chem. Soc. **125**(22), 6642–6643 (2003)

9.451 J. Liu, Y. Lu: Accelerated color change of gold nanoparticles assembled by DNAzymes for simple and fast colorimetric Pb^{2+} detection, J. Am. Chem. Soc. **126**(39), 12298–12305 (2004)

9.452 J. Liu, Y. Lu: Stimuli-responsive disassembly of nanoparticle aggregates for light-up colorimetric sensing, J. Am. Chem. Soc. **127**(36), 12677–12683 (2005)

9.453 Z. Wang, J.H. Lee, Y. Lu: Label-free colorimetric detection of lead ions with a nanomolar detection limit and tunable dynamic range by using gold nanoparticles and DNAzyme, Adv. Mater. **20**(17), 3263–3267 (2008)

9.454 J.M. Slocik, J.S. Zabinski, D.M. Phillips, R.R. Naik: Colorimetric response of peptide-functionalized gold nanoparticles to metal ions, Small **4**(5), 548–551 (2008)

9.455 S. Si, M. Raula, T.K. Paira, T.K. Mandal: Reversible self-assembly of carboxylated peptide-functionalized gold nanoparticles driven by metal-ion coordination, ChemPhysChem **9**(11), 1578–1584 (2008)

9.456 B. Cuenoud, J.W. Szostak: A DNA metalloenzyme with DNA ligase activity, Nature **375**(6532), 611–614 (1995)

9.457 S.W. Santoro, G.F. Joyce, K. Sakthivel, S. Gramatikova, C.F. Barbas: RNA cleavage by a DNA enzyme with extended chemical functionality, J. Am. Chem. Soc. **122**(11), 2433–2439 (2000)

9.458 S.-Y. Lin, S.-H. Wu, C.-H. Chen: A simple strategy for prompt visual sensing by gold nanoparticles: General applications of interparticle hydrogen bonds, Angew. Chem. Int. Ed. **45**(30), 4948–4951 (2006)

9.459 Y. Kim, R.C. Johnson, J.T. Hupp: Gold nanoparticle-based sensing of spectroscopically silent heavy metal ions, Nano Lett. **1**(4), 165–167 (2001)

9.460 C.-J. Yu, W.-L. Tseng: Colorimetric detection of mercury(II) in a high-salinity solution using gold nanoparticles capped with 3-mercaptopropionate acid and adenosine monophosphate, Langmuir **24**(21), 12717–12722 (2008)

9.461 C.-C. Huang, H.-T. Chang: Parameters for selective colorimetric sensing of mercury(II) in aqueous solutions using mercaptopropionic acid-modified gold nanoparticles, Chem. Commun. **12**, 1215–1217 (2007)

9.462 C.-C. Huang, Z. Yang, K.-H. Lee, H.-T. Chang: Synthesis of highly fluorescent gold nanoparticles for sensing mercury(II), Angew. Chem. Int. Ed. **46**(36), 6824–6828 (2007)

9.463 G.K. Darbha, A.K. Singh, U.S. Rai, E. Yu, H. Yu, P. Chandra Ray: Selective detection of mercury (II) ion using nonlinear optical properties of gold nanoparticles, J. Am. Chem. Soc. **130**(25), 8038–8043 (2008)

9.464 A. Campion, P. Kambhampati: Surface-enhanced Raman scattering, Chem. Soc. Rev. **27**(4), 241–250 (1998)

9.465 A.M. Michaels, J. Jiang, L. Brus: Ag nanocrystal junctions as the site for surface-enhanced Raman scattering of single rhodamine 6G molecules, J. Phys. Chem. B **104**(50), 11965–11971 (2000)

9.466 M. Mulvihill, A. Tao, K. Benjauthrit, J. Arnold, P. Yang: Surface-enhanced Raman spectroscopy for trace arsenic detection in contaminated water, Angew. Chem. Int. Ed. **47**(34), 6456–6460 (2008)

9.467 H. Li, L. Rothberg: Colorimetric detection of DNA sequences based on electrostatic interactions with unmodified gold nanoparticles, Proc. Natl. Acad. Sci. USA **101**(39), 14036–14039 (2004)

9.468 X. Xue, F. Wang, X. Liu: One-step, room temperature, colorimetric detection of mercury (Hg^{2+}) using DNA/nanoparticle conjugates, J. Am. Chem. Soc. **130**(11), 3244–3245 (2008)

9.469 V.M. Zamarion, R.A. Timm, K. Araki, H.E. Toma: Ultrasensitive SERS nanoprobes for hazardous metal ions based on trimercaptotriazine-modified gold nanoparticles, Inorg. Chem. **47**(8), 2934–2936 (2008)

9.470 S. Tan, M. Erol, S. Sukhishvili, H. Du: Substrates with discretely immobilized silver nanoparticles for ultrasensitive detection of anions in water using surface-enhanced Raman scattering, Langmuir **24**(9), 4765–4771 (2008)

9.471 P. Jain, T. Pradeep: Potential of silver nanoparticle-coated polyurethane foam as an antibacterial water filter, Biotechnol. Bioeng. **90**(1), 59–63 (2005)

9.472 T.J. Berger, J.A. Spadaro, S.E. Chapin, R.O. Becker: Electrically generated silver ions: Quantitative effects on bacterial and mammalian cells, Antimicrob. Agents Chemother. **9**(2), 357–358 (1976)

9.473 C. Aymonier, U. Schlotterbeck, L. Antonietti, P. Zacharias, R. Thomann, J.C. Tiller, S. Mecking: Hybrids of silver nanoparticles with amphiphilic hyperbranched macromolecules exhibiting antimicrobial properties, Chem. Commun. **24**, 3018–3019 (2002)

9.474 I. Sondi, B. Salopek-Sondi: Silver nanoparticles as antimicrobial agent: A case study on e. Coli as a model for gram-negative bacteria, J. Colloid Interface Sci. **275**(1), 177–182 (2004)

9.475 V. Sambhy, M.M. MacBride, B.R. Peterson, A. Sen: Silver bromide nanoparticle/polymer composites: Dual action tunable antimicrobial materials, J. Am. Chem. Soc. **128**(30), 9798–9808 (2006)

9.476 Y. Li, P. Leung, L. Yao, Q.W. Song, E. Newton: Antimicrobial effect of surgical masks coated with nanoparticles, J. Hosp. Infect. **62**(1), 58–63 (2006)

9.477 S.T. Dubas, P. Kumlangdudsana, P. Potiyaraj: Layer-by-layer deposition of antimicrobial silver nanoparticles on textile fibers, Colloid. Surf. A **289**(1–3), 105–109 (2006)

9.478 T. Maneerung, S. Tokura, R. Rujiravanit: Impregnation of silver nanoparticles into bacterial cellulose for antimicrobial wound dressing, Carbohydr. Polym. **72**(1), 43–51 (2008)

9.479 S. Silver: Bacterial silver resistance: Molecular biology and uses and misuses of silver compounds, FEMS Microbiol. Rev. **27**(2/3), 341–353 (2003)

9.480 S. Silver, L. Phung, G. Silver: Silver as biocides in burn and wound dressings and bacterial resistance to silver compounds, J. Ind. Microbiol. Biotechnol. **33**(7), 627–634 (2006)

9.481 A. Neal: What can be inferred from bacterium-nanoparticle interactions about the potential consequences of environmental exposure to nanoparticles?, Ecotoxicology **17**(5), 362–371 (2008)

9.482 M. Rai, A. Yadav, A. Gade: Silver nanoparticles as a new generation of antimicrobials, Biotechnol. Adv. **27**(1), 76–83 (2009)

9.483 V.K. Sharma, R.A. Yngard, Y. Lin: Silver nanoparticles: Green synthesis and their antimicrobial activities, Adv. Colloid Interf. Sci. **145**(1/2), 83–96 (2009)

9.484 J.R. Morones, J.L. Elechiguerra, A. Camacho, K. Holt, J.B. Kouri, J.T Ramírez, M.J. Yacaman: The bactericidal effect of silver nanoparticles, Nanotechnology **16**(10), 2346 (2005)

9.485 S. Pal, Y.K. Tak, J.M. Song: Does the antibacterial activity of silver nanoparticles depend on the shape of the nanoparticle? A study of the gram-negative bacterium *Escherichia coli*, Appl. Environ. Microbiol. **73**(6), 1712–1720 (2007)

9.486 C.-N. Lok, C.-M. Ho, R. Chen, Q.-Y. He, W.-Y. Yu, H. Sun, P. Tam, J.-F. Chiu, C.-M. Che: Silver nanoparticles: Partial oxidation and antibacterial activities, J. Biol. Inorg. Chem. **12**(4), 527–534 (2007)

9.487 J. Elechiguerra, J. Burt, J. Morones, A. Camacho-Bragado, X. Gao, H. Lara, M. Yacaman: Interaction of silver nanoparticles with HIV-1, J. Nanobiotechnol. **3**(1), 6 (2005)

9.488 L. Nover, K.D. Scharf, D. Neumann: Formation of cytoplasmic heat shock granules in tomato cell cultures and leaves, Mol. Cell. Biol. **3**(9), 1648–1655 (1983)

9.489 Q.L. Feng, J. Wu, G.Q. Chen, F.Z. Cui, T.N. Kim, J.O. Kim: A mechanistic study of the antibacterial effect of silver ions on *Escherichia coli* and *Staphylococcus aureus*, J. Biomed. Mater. Res. **52**(4), 662–668 (2000)

9.490 S.Y. Liau, D.C. Read, W.J. Pugh, J.R. Furr, A.D. Russell: Interaction of silver nitrate with readily identifiable groups: Relationship to the antibacterial action of silver ions, Lett. Appl. Microbiol. **25**(4), 279–283 (1997)

9.491 T. Hamouda, J.R. Baker: Antimicrobial mechanism of action of surfactant lipid preparations in enteric gram-negative bacilli, J. Appl. Microbiol. **89**(3), 397–403 (2000)

9.492 I.E. Wachs, R.J. Madix: The oxidation of methanol on a silver (110) catalyst, Surf. Sci. **76**(2), 531–558 (1978)

9.493 R.L. Davies, S.F. Etris: The development and functions of silver in water purification and disease control, Catal. Today **36**(1), 107–114 (1997)

9.494 M. Vaara: Agents that increase the permeability of the outer membrane, Microbiol. Rev. **56**(3), 395–411 (1992)

9.495 S.K. Gogoi, P. Gopinath, A. Paul, A. Ramesh, S.S. Ghosh, A. Chattopadhyay: Green fluorescent protein-expressing *Escherichia coli* as a model system for investigating the antimicrobial activities of silver nanoparticles, Langmuir **22**(22), 9322–9328 (2006)

9.496 Q. Chang, L. Yan, M. Chen, H. He, J. Qu: Bactericidal mechanism of Ag/Al_2O_3 against *Escherichia coli*, Langmuir **23**(22), 11197–11199 (2007)

9.497 V.R.R. Kumar, T. Pradeep: Polymerization of benzylthiocyanate on silver nanoparticles and the formation of polymer coated nanoparticles, J. Mater. Chem. **16**(9), 837–841 (2006)

9.498 A. Kumar, P.K. Vemula, P.M. Ajayan, G. John: Silver-nanoparticle-embedded antimicrobial paints based on vegetable oil, Nat. Mater. **7**(3), 236–241 (2008)

9.499 L. Zhenyu, H. Huimin, S. Tiecun, Y. Fan, Z. Wei, W. Ce, K.M. Sanjeev: Facile synthesis of single-crystal and controllable sized silver nanoparticles on the surfaces of polyacrylonitrile nanofibres, Nanotechnology **17**(3), 917 (2006)

9.500 W.L. Chou, D.G. Yu, M.C. Yang: The preparation and characterization of silver-loading cellulose acetate hollow fiber membrane for water treatment, Polym. Adv. Technol. **16**(8), 600–607 (2005)

9.501 W.K. Son, J.H. Youk, T.S. Lee, W.H. Park: Preparation of antimicrobial ultrafine cellulose acetate fibers with silver nanoparticles, Macromol. Rapid Commun. **25**(18), 1632–1637 (2004)

9.502 K. Zodrow, L. Brunet, S. Mahendra, D. Li, A. Zhang, Q. Li, P.J.J. Alvarez: Polysulfone ultrafiltration membranes impregnated with silver nanoparticles show improved biofouling resistance and virus removal, Water Res. **43**(3), 715–723 (2009)

9.503 J. Chen, F. Saeki, B.J. Wiley, H. Cang, M.J. Cobb, Z.-Y. Li, L. Au, H. Zhang, M.B. Kimmey, X. Li, Y. Xia: Gold nanocages: Bioconjugation and their potential use as optical imaging contrast agents, Nano Lett. **5**(3), 473–477 (2005)

9.504 D. Pissuwan, S. Valenzuela, M. Killingsworth, X. Xu, M. Cortie: Targeted destruction of murine macrophage cells with bioconjugated gold nanorods, J. Nanopart. Res. **9**(6), 1109–1124 (2007)

9.505 H. Takahashi, Y. Niidome, S. Yamada: Controlled release of plasmid DNA from gold nanorods induced by pulsed near-infrared light, Chem. Commun. **17**, 2247–2249 (2005)

9.506 J. Chen, M. Yang, Q. Zhang, E.C. Cho, C.M. Cobley, C. Kim, C. Glaus, L.V. Wang, M.J. Welch, Y. Xia: Gold nanocages: A novel class of multifunctional nanomaterials for theranostic applications, Adv. Funct. Mater. **20**(21), 3684–3694 (2010)

9.507 X. Huang, S. Neretina, M.A. El-Sayed: Gold nanorods: From synthesis and properties to biological and biomedical applications, Adv. Mater. **21**(48), 4880–4910 (2009)

9.508 L. Au, D. Zheng, F. Zhou, Z.-Y. Li, X. Li, Y. Xia: A quantitative study on the photothermal effect of immuno gold nanocages targeted to breast cancer cells, Am. Chem. Soc. Nano **2**(8), 1645–1652 (2008)

9.509 M. Hu, J. Chen, Z.-Y. Li, L. Au, G.V. Hartland, X. Li, M. Marquez, Y. Xia: Gold nanostructures: Engineering their plasmonic properties for biomedical applications, Chem. Soc. Rev. **35**(11), 1084–1094 (2006)

9.510 P.K. Jain, K.S. Lee, I.H. El-Sayed, M.A. El-Sayed: Calculated absorption and scattering properties of gold nanoparticles of different size, shape, and composition: Applications in biological imaging and biomedicine, J. Phys. Chem. B **110**(14), 7238–7248 (2006)

9.511 H. Liao, J.H. Hafner: Gold nanorod bioconjugates, Chem. Mater. **17**(18), 4636–4641 (2005)

9.512 L. Au, Q. Zhang, C.M. Cobley, M. Gidding, A.G. Schwartz, J. Chen, Y. Xia: Quantifying the cellular uptake of antibody-conjugated Au nanocages by two-photon microscopy and inductively coupled plasma mass spectrometry, Am. Chem. Soc. Nano **4**(1), 35–42 (2009)

9.513 C. Hrelescu, T.K. Sau, A.L. Rogach, F. Jäckel, J. Feldmann: Single gold nanostars enhance Raman scattering, Appl. Phys. Lett. **94**, 153113 (2009)

9.514 M. Hu, H. Petrova, J. Chen, J.M. McLellan, A.R. Siekkinen, M. Marquez, X. Li, Y. Xia, G.V. Hartland: Ultrafast laser studies of the photothermal properties of gold nanocages, J. Phys. Chem. B **110**(4), 1520–1524 (2006)

9.515 H. Liao, C.L. Nehl, J.H. Hafner: Biomedical applications of plasmon resonant metal nanoparticles, Nanomedicine **1**(2), 201–208 (2006)

9.516 C.M. Cobley, L. Au, J. Chen, Y. Xia: Targeting gold nanocages to cancer cells for photothermal destruction and drug delivery, Exp. Opin. Drug Deliv. **7**(5), 577–587 (2010)

9.517 A.K. Salem, P.C. Searson, K.W. Leong: Multifunctional nanorods for gene delivery, Nat. Mater. **2**(10), 668–671 (2003)

9.518 A.K. Salem, C.F. Hung, T.W. Kim, T.C. Wu, P.C. Searson, K.W. Leong: Multi-component nanorods for vaccination applications, Nanotechnology **16**(4), 484 (2005)

9.519 X. Huang, I.H. El-Sayed, W. Qian, M.A. El-Sayed: Cancer cell imaging and photothermal therapy in the near-infrared region by using gold nanorods, J. Am. Chem. Soc. **128**(6), 2115–2120 (2006)

9.520 S. Link, M.A. El-Sayed: Optical properties and ultrafast dynamics of metallic nanocrystals, Annu. Rev. Phys. Chem. **54**(1), 331–366 (2003)

9.521 A.R. Lowery, A.M. Gobin, E.S. Day, N.J. Halas: Immunonanoshells for targeted photothermal ablation of tumor cells, Int. J. Nanomed. **1**(2), 1–6 (2006)

9.522 M.B. Mohamed, T.S. Ahmadi, S. Link, M. Braun, M.A. El-Sayed: Hot electron and phonon dynamics of gold nanoparticles embedded in a gel matrix, Chem. Phys. Lett. **343**(1/2), 55–63 (2001)

9.523 C.J. Murphy, A.M. Gole, J.W. Stone, P.N. Sisco, A.M. Alkilany, E.C. Goldsmith, S.C. Baxter: Gold nanoparticles in biology: Beyond toxicity to cellular imaging, Acc. Chem. Res. **41**(12), 1721–1730 (2008)

9.524 H. Wang, T.B. Huff, D.A. Zweifel, W. He, P.S. Low, A. Wei, J.-X. Cheng: In vitro and in vivo two-photon luminescence imaging of single gold nanorods, Proc. Natl. Acad. Sci. USA **102**(44), 15752–15756 (2005)

9.525 N.J. Durr, T. Larson, D.K. Smith, B.A. Korgel, K. Sokolov, A. Ben-Yakar: Two-photon luminescence imaging of cancer cells using molecularly targeted gold nanorods, Nano Lett. **7**(4), 941–945 (2007)

9.526 C.J. Orendorff, A. Gole, T.K. Sau, C.J. Murphy: Surface-enhanced Raman spectroscopy of self-assembled monolayers: Sandwich architecture and nanoparticle shape dependence, Anal. Chem. **77**(10), 3261–3266 (2005)

9.527 J.Q. Hu, Q. Chen, Z.X. Xie, G.B. Han, R.H. Wang, B. Ren, Y. Zhang, Z.L. Yang, Z.Q. Tian: A simple and effective route for the synthesis of crystalline silver nanorods and nanowires, Adv. Funct. Mater. **14**(2), 183–189 (2004)

9.528 H. Wang, C.S. Levin, N.J. Halas: Nanosphere arrays with controlled sub-10-nm gaps as surface-enhanced Raman spectroscopy substrates, J. Am. Chem. Soc. **127**(43), 14992–14993 (2005)

9.529 P.D. O'Neal, G.L. Coté, M. Motamedi, J. Chen, W.-C. Lin: Feasibility study using surface-enhanced Raman spectroscopy for the quantitative detection of excitatory amino acids, SPIE Proc. **8**, 33–39 (2003)

9.530 R. Sulk, C. Chan, J. Guicheteau, C. Gomez, J.B.B. Heyns, R. Corcoran, K. Carron: Surface-enhanced Raman assays (SERA): Measurement of bilirubin and salicylate, J. Raman Spectrosc. **30**(9), 853–859 (1999)

9.531 Y. Yang, S. Matsubara, L. Xiong, T. Hayakawa, M. Nogami: Solvothermal synthesis of multiple shapes of silver nanoparticles and their SERS properties, J. Phys. Chem. C **111**(26), 9095–9104 (2007)

9.532 L. Rocks, K. Faulds, D. Graham: Rationally designed SERS active silica coated silver nanoparticles, Chem. Commun. **47**(15), 4415–4417 (2011)

9.533 M.J. Banholzer, J.E. Millstone, L. Qin, C.A. Mirkin: Rationally designed nanostructures for surface-enhanced Raman spectroscopy, Chem. Soc. Rev. **37**(5), 885–897 (2008)

9.534 K.A. Willets, R.P. Van Duyne: Localized surface plasmon resonance spectroscopy and sensing, Annu. Rev. Phys. Chem. **58**(1), 267–297 (2007)

9.535 J.J. Mock, M. Barbic, D.R. Smith, D.A. Schultz, S. Schultz: Shape effects in plasmon resonance of individual colloidal silver nanoparticles, J. Chem. Phys. **116**(15), 6755–6759 (2002)

9.536 J. Xie, Q. Zhang, J.Y. Lee, D.I.C. Wang: The synthesis of SERS-active gold nanoflower tags for in vivo applications, Am. Chem. Soc. Nano **2**(12), 2473–2480 (2008)

9.537 E. Hao: Electromagnetic fields around silver nanoparticles and dimers, J. Chem. Phys. **120**(1), 357 (2004)

9.538 Y. Wang, X. Zou, W. Ren, W. Wang, E. Wang: Effect of silver nanoplates on Raman spectra of p-aminothiophenol assembled on smooth macroscopic gold and silver surface, J. Phys. Chem. C **111**(8), 3259–3265 (2007)

9.539 P. Sajanlal, T. Pradeep: Mesoflowers: A new class of highly efficient surface-enhanced Raman active and infrared-absorbing materials, Nano Res. **2**(4), 306–320 (2009)

9.540 S.A. Maier, P.G. Kik, H.A. Atwater, S. Meltzer, E. Harel, B.E. Koel, A.A.G. Requicha: Local detection of electromagnetic energy transport below the diffraction limit in metal nanoparticle plasmon waveguides, Nat. Mater. **2**(4), 229–232 (2003)

9.541 K. Aslan, J.R. Lakowicz, C.D. Geddes: Plasmon light scattering in biology and medicine: New sensing approaches, visions and perspectives, Curr. Opin. Chem. Biol. **9**(5), 538–544 (2005)

9.542 C. Yu, J. Irudayaraj: Quantitative evaluation of sensitivity and selectivity of multiplex nanoSPR biosensor assays, Biophys. J. **93**(10), 3684–3692 (2007)

9.543 C. Yu, H. Nakshatri, J. Irudayaraj: Identity profiling of cell surface markers by multiplex gold nanorod probes, Nano Lett. **7**(8), 2300–2306 (2007)

9.544 X.-J. Huang, C.-C. Li, B. Gu, J.-H. Kim, S.-O. Cho, Y.-K. Choi: Controlled molecularly mediated assembly of gold nanooctahedra for a glucose biosensor, J. Phys. Chem. C **112**(10), 3605–3611 (2008)

9.545 M.-C. Daniel, D. Astruc: Gold nanoparticles: Assembly, supramolecular chemistry, quantum-size-related properties, and applications toward biology, catalysis, and nanotechnology, Chem. Rev. **104**(1), 293–346 (2004)

9.546 Q. Wei, K. Hirota, K. Tajima, K. Hashimoto: Design and synthesis of TiO_2 nanorod assemblies and their application for photovoltaic devices, Chem. Mater. **18**(21), 5080–5087 (2006)

9.547 J. Xiaohui, W. Feng, K. Varutt, T. Hori, A. Fujii, M. Ozaki: Fabrication of oriented ZnO nanopillar self-assemblies and their application for photovoltaic devices, Nanotechnology **19**(43), 435706 (2008)

9.548 V. Dhas, S. Muduli, W. Lee, S. Han, S. Ogale: Enhanced conversion efficiency in dye-sensitized solar cells based on zno bifunctional nanoflowers loaded with gold nanoparticles, Appl. Phys. Lett. **93**(24), 243108 (2008)

9.549 E. Pedrueza, J.L. Valdés, V. Chirvony, R. Abargues, J. Hernández-Saz, M. Herrera, S.I. Molina, J.P. Martínez-Pastor: Novel method of preparation of gold-nanoparticle-doped TiO_2 and SiO_2 plasmonic thin films: Optical characterization and comparison with Maxwell–Garnett modeling, Adv. Funct. Mater. **21**(18), 3502–3507 (2011)

9.550 J. Chen, Y. Zou, Y. Li, X. Zhou, J. Zhang, X. Li, X. Xiao, Y. Lin: Improving the photoelectrochemical performance of polythiophene sensitized TiO_2 electrode by modification with gold nanoparticles, Chem. Phys. Lett. **460**(1–3), 168–172 (2008)

9.551 T. Hasobe, H. Imahori, P.V. Kamat, S. Fukuzumi: Quaternary self-organization of porphyrin and fullerene units by clusterization with gold nanoparticles on SnO_2 electrodes for organic solar cells, J. Am. Chem. Soc. **125**(49), 14962–14963 (2003)

9.552 S. Yamada, T. Tasaki, T. Akiyama, N. Terasaki, S. Nitahara: Gold nanoparticle–porphyrin self-assembled multistructures for photoelectric conversion, Thin Solid Films **438/439**(0), 70–74 (2003)

9.553 K. Kim, D.L. Carroll: Roles of Au and Ag nanoparticles in efficiency enhancement of poly(3-octylthiophene)/C_{60} bulk heterojunction photovoltaic devices, Appl. Phys. Lett. **87**(20), 203113 (2005)

9.554 D. Derkacs, S.H. Lim, P. Matheu, W. Mar, E.T. Yu: Improved performance of amorphous silicon solar cells via scattering from surface plasmon polaritons in nearby metallic nanoparticles, Appl. Phys. Lett. **89**(9), 093103 (2006)

9.555 S.W. Tong, C.F. Zhang, C.Y. Jiang, G. Liu, Q.D. Ling, E.T. Kang, D.S.H. Chan, C. Zhu: Improvement in the hole collection of polymer solar cells by utilizing gold nanoparticle buffer layer, Chem. Phys. Lett. **453**(1–3), 73–76 (2008)

9.556 J. Yang, J. You, C.-C. Chen, W.-C. Hsu, H.-R. Tan, X.W. Zhang, Z. Hong, Y. Yang: Plasmonic polymer tandem solar cell, Am. Chem. Soc. Nano **5**(8), 6210–6217 (2011)

9.557 M.D. Brown, T. Suteewong, R.S.S. Kumar, V. D'Innocenzo, A. Petrozza, M.M. Lee, U. Wiesner, H.J. Snaith: Plasmonic dye-sensitized solar cells using core–shell metal–insulator nanoparticles, Nano Lett. **11**(2), 438–445 (2010)

9.558 H.B. Yildiz, R. Tel-Vered, I. Willner: Solar cells with enhanced photocurrent efficiencies using oligoaniline-crosslinked Au/CdS nanoparticles arrays on electrodes, Adv. Funct. Mater. **18**(21), 3497–3505 (2008)

9.559 K. Ishikawa, C.-J. Wen, K. Yamada, T. Okubo: The photocurrent of dye-sensitized solar cells enhanced by the surface plasmon resonance, J. Chem. Eng. Jpn. **37**(5), 645–649 (2004)

9.560 B. Rand, P. Peumans, S. Forrest: Long-range absorption enhancement in organic tandem thin-film

solar cells containing silver nanoclusters, J. Appl. Phys. **96**(12), 7519 (2004)
9.561 A.P. Demchenko, M.A.H. Muhammed, T. Pradeep: Luminescent quantum clusters of gold as bio-labels, Springer Ser. Fluoresc. **9**, 333–353 (2010)
9.562 J. Zheng, P.R. Nicovich, R.M. Dickson: Highly fluorescent noble-metal quantum dots, Annu. Rev. Phys. Chem. **58**, 409–431 (2007)
9.563 M.A.H. Muhammed, P.K. Verma, S.K. Pal, A. Retnakumari, M. Koyakutty, S. Nair, T. Pradeep: Luminescent quantum clusters of gold in bulk by albumin-induced core etching of nanoparticles: Metal ion sensing, metal-enhanced luminescence, and biolabeling, Chemistry **16**(33), 10103–10112 (2010)
9.564 E.S. Shibu, T. Pradeep: Quantum clusters in cavities: Trapped Au_{15} in cyclodextrins, Chem. Mater. **23**(4), 989–999 (2011)
9.565 E.S. Shibu, M.A.H. Muhammed, T. Tsukuda, T. Pradeep: Ligand exchange of $Au_{25}SG_{18}$ leading to functionalized gold clusters: Spectroscopy, kinetics, and luminescence, J. Phys. Chem. C **112**(32), 12168–12176 (2008)
9.566 P.L. Xavier, K. Chaudhari, P.K. Verma, S.K. Pal, T. Pradeep: Luminescent quantum clusters of gold in transferrin family protein, lactoferrin exhibiting FRET, Nanoscale **2**(12), 2769–2776 (2010)
9.567 K. Chaudhari, P.L. Xavier, T. Pradeep: Understanding the evolution of luminescent gold quantum clusters in protein templates, Am. Chem. Soc. Nano **5**(11), 8816–8827 (2011)
9.568 M.A.H. Muhammed, P.K. Verma, S.K. Pal, R.C.A. Kumar, S. Paul, R.V. Omkumar, T. Pradeep: Bright, NIR-emitting Au_{23} from Au_{25}: Characterization and applications including biolabeling, Chemistry **15**(39), 10110–10120 (2009)
9.569 C.-C. Huang, Z. Yang, K.-H. Lee, H.-T. Chang: Synthesis of highly fluorescent gold nanoparticles for sensing mercury(II), Angew. Chem. **119**(36), 6948–6952 (2007)
9.570 I. Diez, R.H.A. Ras: Fluorescent silver nanoclusters, Nanoscale **3**(5), 1963–1970 (2011)
9.571 G.A. Ozin, H. Huber: Cryophotoclustering techniques for synthesizing very small, naked silver clusters Ag_n of known size (where $n = 2–5$). The molecular metal cluster-bulk metal particle interface, Inorg. Chem. **17**(1), 155–163 (1978)
9.572 W. Harbich, S. Fedrigo, J. Buttet: The optical absorption spectra of small silver clusters ($n = 5–11$) embedded in argon matrices, Chem. Phys. Lett. **195**(5-6), 613–617 (1992)
9.573 W. Schulze, I. Rabin, G. Ertl: Formation of light-emitting Ag_2 and Ag_3 species in the course of condensation of Ag atoms with Ar, ChemPhysChem **5**(3), 403–407 (2004)
9.574 A.D. Stevens, M.C.R. Symons: Spectroscopic studies of silver(0) centres formed radiolytically in water-ethanol solvents at 4 and 77 K, J. Chem. Soc. Faraday Trans. I **85**(6), 1439–1450 (1989)
9.575 S. Liu, F. Lu, J.-J. Zhu: Highly fluorescent Ag nanoclusters: Microwave-assisted green synthesis and Cr^{3+} sensing, Chem. Commun. **47**(9), 2661–2663 (2011)
9.576 M. Treguer, F. Rocco, G. Lelong, A. Le Nestour, T. Cardinal, A. Maali, B. Lounis: Fluorescent silver oligomeric clusters and colloidal particles, Solid State Sci. **7**(7), 812–818 (2005)
9.577 H. Xu, K.S. Suslick: Sonochemical synthesis of highly fluorescent Ag nanoclusters, Am. Chem. Soc. Nano **4**(6), 3209–3214 (2010)
9.578 H. Liu, X. Zhang, X. Wu, L. Jiang, C. Burda, J.-J. Zhu: Rapid sonochemical synthesis of highly luminescent non-toxic AuNCs and Au@AgNCs and Cu(II) sensing, Chem. Commun. **47**(14), 4237–4239 (2011)
9.579 T.U.B. Rao, B. Nataraju, T. Pradeep: Ag_9 quantum cluster through a solid-state route, J. Am. Chem. Soc. **132**(46), 16304–16307 (2010)
9.580 C. Shao, B. Yuan, H. Wang, Q. Zhou, Y. Li, Y. Guan, Z. Deng: Eggshell membrane as a multimodal solid state platform for generating fluorescent metal nanoclusters, J. Mater. Chem. **21**(9), 2863–2866 (2011)
9.581 Z. Huang, F. Pu, D. Hu, C. Wang, J. Ren, X. Qu: Site-specific DNA-programmed growth of fluorescent and functional silver nanoclusters, Chemistry **17**(13), 3774–3780 (2011)
9.582 W. Guo, J. Yuan, Q. Dong, E. Wang: Highly sequence-dependent formation of fluorescent silver nanoclusters in hybridized DNA duplexes for single nucleotide mutation identification, J. Am. Chem. Soc. **132**(3), 932–934 (2009)
9.583 A. Ledo-Suárez, J. Rivas, C.F. Rodríguez-Abreu, M.J. Rodríguez, E. Pastor, A. Hernández-Creus, S.B. Oseroff, M.A. López-Quintela: Facile synthesis of stable subnanosized silver clusters in microemulsions, Angew. Chem. Int. Ed. **46**(46), 8823–8827 (2007)
9.584 J. Zhang, S. Xu, E. Kumacheva: Photogeneration of fluorescent silver nanoclusters in polymer microgels, Adv. Mater. **17**(19), 2336–2340 (2005)
9.585 K.V. Mrudula, T.U. Bhaskara Rao, T. Pradeep: Interfacial synthesis of luminescent 7 kDa silver clusters, J. Mater. Chem. **19**(25), 4335–4342 (2009)
9.586 T.U. Bhaskara Rao, T. Pradeep: Luminescent Ag_7 and Ag_8 clusters by interfacial synthesis, Angew. Chem. Int. Ed. **49**(23), 3925–3929 (2010)
9.587 H. Xu, K.S. Suslick: Water-soluble fluorescent silver nanoclusters, Adv. Mater. **22**(10), 1078–1082 (2010)
9.588 J. Zheng, R.M. Dickson: Individual water-soluble dendrimer-encapsulated silver nanodot fluorescence, J. Am. Chem. Soc. **124**(47), 13982–13983 (2002)
9.589 B.G. Ershov, A. Henglein: Time-resolved investigation of early processes in the reduction of Ag^+ on polyacrylate in aqueous solution, J. Phys. Chem. B **102**(52), 10667–10671 (1998)
9.590 Z. Shen, H. Duan, H. Frey: Water-soluble fluorescent Ag nanoclusters obtained from multiarm

star poly(acrylic acid) as "molecular hydrogel" templates, Adv. Mater. **19**(3), 349–352 (2007)
9.591 N. Cathcart, V. Kitaev: Silver nanoclusters: Single-stage scaleable synthesis of monodisperse species and their chirooptical properties, J. Phys. Chem. C **114**(38), 16010–16017 (2010)
9.592 B. Adhikari, A. Banerjee: Facile synthesis of water-soluble fluorescent silver nanoclusters and Hg^{II} sensing, Chem. Mater. **22**(15), 4364–4371 (2010)
9.593 C.I. Richards, S. Choi, J.-C. Hsiang, Y. Antoku, T. Vosch, A. Bongiorno, Y.-L. Tzeng, R.M. Dickson: Oligonucleotide-stabilized Ag nanocluster fluorophores, J. Am. Chem. Soc. **130**(15), 5038–5039 (2008)
9.594 J.T. Petty, J. Zheng, N.V. Hud, R.M. Dickson: DNA-templated Ag nanocluster formation, J. Am. Chem. Soc. **126**(16), 5207–5212 (2004)
9.595 C.I. Richards, J.-C. Hsiang, D. Senapati, S. Patel, J. Yu, T. Vosch, R.M. Dickson: Optically modulated fluorophores for selective fluorescence signal recovery, J. Am. Chem. Soc. **131**(13), 4619–4621 (2009)
9.596 C.M. Ritchie, K.R. Johnsen, J.R. Kiser, Y. Antoku, R.M. Dickson, J.T. Petty: Ag nanocluster formation using a cytosine oligonucleotide template, J. Phys. Chem. C **111**(1), 175–181 (2006)
9.597 V. Soto-Verdugo, H. Metiu, E. Gwinn: The properties of small Ag clusters bound to DNA bases, J. Chem. Phys. **132**(19), 195102 (2010)
9.598 E.G. Gwinn, P. O'Neill, A.J. Guerrero, D. Bouwmeester, D.K. Fygenson: Sequence-dependent fluorescence of DNA-hosted silver nanoclusters, Adv. Mater. **20**(2), 279–283 (2008)
9.599 S.S. Narayanan, S.K. Pal: Structural and functional characterization of luminescent silver-protein nanobioconjugates, J. Phys. Chem. C **112**(13), 4874–4879 (2008)
9.600 N. Makarava, A. Parfenov, I.V. Baskakov: Water-soluble hybrid nanoclusters with extra bright and photostable emissions: A new tool for biological imaging, Biophys. J. **89**(1), 572–580 (2005)
9.601 J. Yu, S.A. Patel, R.M. Dickson: In vitro and intracellular production of peptide-encapsulated fluorescent silver nanoclusters, Angew. Chem. Int. Ed. **46**(12), 2028–2030 (2007)
9.602 L. Peyser-Capadona, J. Zheng, J.I. González, T.-H. Lee, S.A. Patel, R.M. Dickson: Nanoparticle-free single molecule anti-Stokes Raman spectroscopy, Phys. Rev. Lett. **94**(5), 058301 (2005)
9.603 B. Adhikari, A. Banerjee: Short-peptide-based hydrogel: A template for the in situ synthesis of fluorescent silver nanoclusters by using sunlight, Chemistry **16**(46), 13698–13705 (2010)
9.604 A. Mathew, P.R. Sajanlal, T. Pradeep: A fifteen atom silver cluster confined in bovine serum albumin, J. Mater. Chem. **21**(30), 11205–11212 (2011)
9.605 L. Dhanalakshmi, T.U.B. Rao, T. Pradeep: Conversion of double layer charge-stabilized Ag@citrate colloids to thiol passivated luminescent quantum clusters, Chem. Commun., 859–861 (2012)
9.606 T. Udayabhaskararao, Y. Sun, N. Goswami, S.K. Pal, K. Balasubramanian, T. Pradeep: Ag_7Au_6: A 13 atom alloy quantum cluster, Angew. Chem. Int. Ed. **51**, 2155–2159 (2012)
9.607 Y. Watanabe: Photosensitivity in phosphate glass doped with Ag^+ upon exposure to near-ultraviolet femtosecond laser pulses, Appl. Phys. Lett. **78**(15), 2125 (2001)
9.608 M. Bellec, A. Royon, K. Bourhis, J. Choi, B. Bousquet, M. Treguer, T. Cardinal, J.-J. Videau, M. Richardson, L. Canioni: 3-D patterning at the nanoscale of fluorescent emitters in glass, J. Phys. Chem. C **114**(37), 15584–15588 (2010)
9.609 E. Maik, R. Klaus, H. Armin, M.T. Dragomir, W. Wilfried, S.E. Reinhard, P. Gianfranco: Photoluminescence of atomic gold and silver particles in soda-lime silicate glasses, Nanotechnology **19**(13), 135701 (2008)
9.610 G.A. Ozin, F. Hugues, S.M. Mattar, D.F. McIntosh: Low nuclearity silver clusters in faujasite-type zeolites: Optical spectroscopy, photochemistry and relationship to the photodimerization of alkanes, J. Phys. Chem. **87**(18), 3445–3450 (1983)
9.611 G. De Cremer, Y. Antoku, M.B.J. Roeffaers, M. Sliwa, J. Van Noyen, S. Smout, J. Hofkens, D.E. De Vos, B.F. Sels, T. Vosch: Photoactivation of silver-exchanged zeolite A, Angew. Chem. Int. Ed. **47**(15), 2813–2816 (2008)
9.612 G. De Cremer, E. Coutiño-Gonzalez, M.B.J. Roeffaers, B. Moens, J. Ollevier, M. Van der Auweraer, R. Schoonheydt, P.A. Jacobs, F.C. De Schryver, J. Hofkens, D.E. De Vos, B.F. Sels, T. Vosch: Characterization of fluorescence in heat-treated silver-exchanged zeolites, J. Am. Chem. Soc. **131**(8), 3049–3056 (2009)
9.613 G. De Cremer, B.F. Sels, J.-I. Hotta, M.B.J. Roeffaers, E. Bartholomeeusen, E. Coutiño-Gonzalez, V. Valtchev, D.E. De Vos, T. Vosch, J. Hofkens: Optical encoding of silver zeolite microcarriers, Adv. Mater. **22**(9), 957–960 (2010)
9.614 C.-A.J. Lin, T.-Y. Yang, C.-H. Lee, S.H. Huang, R.A. Sperling, M. Zanella, J.K. Li, J.-L. Shen, H.-H. Wang, H.-I. Yeh, W.J. Parak, W.H. Chang: Synthesis, characterization, and bioconjugation of fluorescent gold nanoclusters toward biological labeling applications, Am. Chem. Soc. Nano **3**(2), 395–401 (2009)
9.615 R. Archana, S. Sonali, M. Deepthy, R. Prasanth, M. Habeeb, P. Thalappil, N. Shantikumar, K. Manzoor: Molecular-receptor-specific, non-toxic, near-infrared-emitting Au cluster-protein nanoconjugates for targeted cancer imaging, Nanotechnology **21**(5), 055103 (2010)
9.616 Y. Zhu, H. Qian, M. Zhu, R. Jin: Thiolate-protected Au_n nanoclusters as catalysts for selective oxidation

and hydrogenation processes, Adv. Mater. **22**(17), 1915–1920 (2010)

9.617 A. Leelavathi, T.U.B. Rao, T. Pradeep: Supported quantum clusters of silver as enhanced catalysts for reduction, Nanoscale Res. Lett. **6**, 123 (2011)

9.618 A. Mohanty, N. Garg, R. Jin: A universal approach to the synthesis of noble metal nanodendrites and their catalytic properties, Angew. Chem. Int. Ed. **49**(29), 4962–4966 (2010)

9.619 I. Chakraborty, T.U.B. Rao, T. Pradeep: Luminescent sub-nanometer clusters for metal ion sensing: A new direction in nanosensors, J. Hazard. Mater. **211/212**, 396–403 (2012)

9.620 T.S. Sreeprasad, M.S. Maliyekkal, K. Deepti, K. Chaudhari, P.L. Xavier, T. Pradeep: Transparent, luminescent, antibacterial and patternable film forming composites of graphene oxide/reduced graphene oxide, ACS Appl. Mater. Interfaces **3**(7), 2643–2654 (2011)